

# **Polymeric nanocapsules as versatile platform for the development of new dendritic cell- directed nanovaccines**

## **Dissertation**

zur Erlangung des Grades eines

'Doctor rerum naturalium (Dr. rer. nat.)' der Fachbereiche:

08 – Physik, Mathematik und Informatik,

09 – Chemie, Pharmazie und Geowissenschaften,

10 – Biologie,

Universitätsmedizin

der Johannes Gutenberg-Universität

verfasst und vorgelegt von

David Paßlick

geboren am 12.10.1987

in Ochtrup

Max Planck Graduate Center mit der Johannes Gutenberg-Universität

Mainz

angefertigt an der Hautklinik, Universitätsmedizin Mainz

Mainz, 2018

From the Department of Dermatology, University Medical Center, Mainz & the  
Department of Physical Chemistry of Polymers, Max Planck Institute for Polymer Research

**Doctoral Committee:**

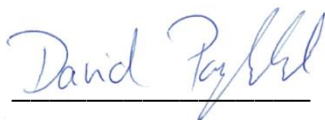
Advisor:

Co-Advisor:

Tag der mündlichen Prüfung: 14.11.2018

# Declaration

I hereby declare that I wrote the dissertation submitted without any unauthorized external assistance and used only sources acknowledged in the work. All textual passages which are appropriated verbatim or paraphrased from published and unpublished texts as well as information obtained from oral sources are duly indicated and listed in accordance with bibliographical rules. In carrying out this research, I complied with the rules of standard scientific practice as formulated in the statutes of Johannes Gutenberg-University Mainz to insure standard scientific practice.

A handwritten signature in blue ink that reads "David Paßlick". The signature is written in a cursive style and is positioned above a horizontal line.

(David Paßlick)

Mainz, 31<sup>st</sup> August, 2018



# Abstract

Therapeutic vaccination against tumor diseases remains a major challenge in immune therapy. The effective activation of dendritic cells by a combination of distinctly acting adjuvants and antigens is essential for success. While conventional vaccine formulations lack the efficiency to trigger sufficient T cell responses in a therapeutic tumor treatment, nanovaccines may offer unique properties to tackle that challenge.

In this doctoral thesis, we report the use of polymeric nanocapsules as a versatile platform for the development of new dendritic cell-directed nanovaccines. Those nanocarriers are characterized by a high biocompatibility and modifiability, low cytotoxicity as well as by a large loading capacity for active substances. The resulting nanovaccine comprises a shell consisting of protein antigen and allows an efficient loading with superadditively acting combinations of adjuvants, even when their corresponding receptors are located intracellularly. Furthermore, the capsule surface can be modified with stealth components to increase blood circulation time, allows the functional encapsulation of small interfering RNA and can also be equipped with specific antibodies to substantially increase dendritic cell targeting.

Initially, we identified the combination of resiquimod and muramyl dipeptide to exert a superadditive stimulatory potential on dendritic cells. This adjuvant combination maintains its superadditive character and stimulates murine dendritic cells more effectively when encapsulated in dextran nanoparticles than when applied directly. At the same time, nanocapsules, consisting of the model antigen ovalbumin, were evaluated as a suitable antigen source for the induction of antigen-specific T cell responses. Subsequently, the aforementioned adjuvant combination was encapsulated in these ovalbumin-based nanocapsules to generate a nanocarrier comprising antigen and superadditive adjuvant combination. Its immunostimulatory potential for dendritic cell stimulation was extensively tested by i) measuring the expression of co-stimulatory markers, ii) the secretion of pro-inflammatory cytokines, iii) the upregulation of immunologically relevant genes on RNA level by transcriptome sequencing, and iv) the capability of accordingly pre-treated dendritic cells to mediate antigen-specific T cell responses. The created nanocapsule,

including antigen and adjuvants, triggered strong dendritic cell stimulation and potent antigen-specific T cell proliferation. Moreover, numerous relevant genes were massively upregulated upon treatment.

The second step was to equip the protein-based nanocapsule with stealth components to increase its blood circulation time and to reduce unspecific cell interaction. Thereby, a special focus was set on the influence of the molecular weight of the used components as well as on the shielding density and the mass density of the modification. It turned out that such a modification can significantly reduce cellular interaction but is highly dependent on molecular weight, shielding and mass density of the used stealth component as well as on the protein environment.

To establish small interfering RNA and targeting moieties in our portfolio of available modifications for polymeric nanocapsules, we switched to a similar, antigen-independent polymeric nanocapsule made of hydroxyethyl starch. Regarding small interfering RNA, we showed that the synthesized nanocapsules were capable of transporting them into dendritic cells and to release them resulting in a functional activity. In terms of targeting, a surface modification with targeting antibodies significantly increased the nanocapsule binding by dendritic cells.

Since the introduced protein-based type of nanocapsule provides the option to replace ovalbumin, for instance, by a tumor-related antigen, it also allows a further optimization for personalized tumor treatment by employing a patient's tumor-specific antigen. In combination with the demonstrated advantages and available modifications, polymeric nanocapsules as presented here constitute a promising platform for the design and generation of new, innovative nanovaccines for tumor treatment.

# Zusammenfassung

Die therapeutische Impfung gegen Tumorerkrankungen stellt bis heute eine große Herausforderung der Immuntherapie dar. Die Aktivierung von dendritischen Zellen durch die kombinierte Gabe von gezielt wirkenden Adjuvantien und Antigenen ist dabei essentiell. Konventionelle Vakzine sind im Falle einer therapeutischen Tumorbehandlung häufig nicht effizient genug um eine ausreichend starke T-Zellantworten zu induzieren. Demgegenüber weisen Nanovakzine spezielle Eigenschaften auf, die eine therapeutische Vakzinverwendung ermöglichen bzw. erleichtern könnten.

In der vorliegenden Doktorarbeit wird die Verwendung von polymeren Nanokapseln als vielseitige Plattform für die Entwicklung neuartiger Nanovakzine beschrieben. Diese Kapseln zeichnen sich vor allem durch eine hohe Biokompatibilität und Modifizierbarkeit, eine geringe Zytotoxizität, sowie durch eine große Ladungskapazität für biologisch aktive Substanzen aus. Das resultierende Nanovakzin weist eine Hülle aus Proteinantigen auf und erlaubt die effiziente Beladung mit superadditiv wirkenden Adjuvanzkombinationen, selbst wenn sich deren Rezeptoren intrazellulär befinden. Zudem kann die Kapseloberfläche mit ‚Stealth‘-Molekülen modifiziert werden, wodurch die Blutzirkulationszeit erhöht wird. Ebenso ermöglicht dieses System die funktionale Verkapselung von small interfering RNA zur Immunmodulation und die Anbindung von Antikörpern zur verstärkten Adressierung von dendritischen Zellen.

Zu Beginn wurde die Kombination der Adjuvantien Resiquimod und Muramyl-Dipeptid als superadditiv für die Stimulation von dendritischen Zellen identifiziert. Es zeigte sich, dass die stimulierenden Eigenschaften dieser Kombination durch Partikulierung in Dextran-basierte Nanopartikel im Vergleich zur solublen Applikation noch gesteigert werden konnten. Gleichzeitig wurde die Verwendung von Nanokapseln, die aus dem Modellantigen Ovalbumin bestanden, als geeignete Antigenquelle zur Einleitung antigenspezifischer T-Zell-Antworten etabliert. Um ein vollständiges Nanovakzin zu generieren, das sowohl Antigen als auch eine superadditive Adjuvanzkombination beinhaltet, wurde die zuvor genannte Adjuvanzkombination in diese Antigenkapseln integriert. Das resultierende immunstimulatorische Potential dieser Kapseln wurde anhand i) der Expression

kostimulatorischer Marker, ii) der Sekretion proinflammatorischer Zytokine, iii) der Aufregulation immunologisch relevanter Gene auf RNA-Ebene durch Transkriptom-Sequenzierung und iv) der Fähigkeit entsprechend vorbehandelter dendritischer Zellen zur Induktion antigenspezifischer T-Zell-Antworten untersucht. Die generierte Nanokapsel, welche sowohl Antigen als auch Adjuvantien enthielt, induzierte eine potente Stimulation dendritischer Zellen und eine starke Proliferation antigenspezifischer T-Zellen. Zudem wurden unter Gabe der Nanokapseln zahlreiche relevante Gene stark aufreguliert.

In einem zweiten Schritt wurden diese proteinbasierten Nanokapseln mit ‚Stealth‘-Komponenten ausgestattet um ihre Blutzirkulationsdauer zu erhöhen und um die unspezifische Interaktion mit Zellen zu reduzieren. Dabei wurde ein spezieller Fokus auf den Einfluss des Molekulargewichts der verwendeten Komponenten sowie auf die Beschichtungs- und Massendichte der Modifikation gesetzt. Es zeigte sich, dass solche eine Modifikation die Interaktion der Nanokapseln mit Zellen signifikant reduzieren kann, der resultierende Effekt allerdings stark von den genannten Einflüssen sowie dem vorherrschenden Proteinmilieu abhängt.

Um die Verkapselung von small interfering RNA und die Kopplung von Antikörpern für polymere Nanokapseln zu etablieren, wurden Nanokapseln aus Hydroxyethylstärke verwendet. Bezüglich small interfering RNA, konnte gezeigt werden, dass die synthetisierten Nanokapseln geeignet waren diese in dendritische Zellen zu transportieren und dort freizusetzen. Die resultierende funktionale Aktivität konnte gemessen werden. In Bezug auf die Adressierung von dendritischen Zellen, konnte eine Oberflächenmodifikation mit spezifischen Antikörpern die Nanokapselbindung durch dendritische Zellen signifikant erhöhen.

Da das präsentierte proteinbasierte Nanokapselsystem die Option bietet, das Ovalbumin durch beispielsweise ein tumorassoziiertes Antigen zu ersetzen, kann es durch die Verwendung von patientenspezifischen Tumorantigenen weiter in Richtung personalisierte Tumorthherapie optimiert werden. Zusammen mit den hier aufgezeigten Vorteilen und möglichen Modifikationen, stellen polymere Nanokapseln eine vielversprechende Plattform für die Synthese von neuartigen, innovativen Nanovakzinen für die therapeutische Tumorbehandlung dar.



# Table of contents

<b>Declaration .....</b>	<b>I</b>
<b>Abstract .....</b>	<b>III</b>
<b>Table of contents.....</b>	<b>VII</b>
<b>1. Introduction.....</b>	<b>1</b>
1.1 Dendritic cells .....	3
1.1.1 Dendritic cell maturation.....	7
1.1.2 Induction of adaptive immune responses .....	15
1.2 Nanovaccines for tumor treatment .....	17
1.3 Thesis objectives .....	24
<b>2. Material.....</b>	<b>26</b>
2.1 Laboratory equipment .....	26
2.2 Reagents .....	28
2.3 Buffers, solutions, media.....	31
2.4 Consumables .....	33
2.5 Antibodies .....	34
2.6 Nanoparticles.....	35
2.7 Kits .....	37
2.8 Software .....	37
<b>3. Methods.....</b>	<b>38</b>
3.1 Nanoparticles synthesis / characterization .....	38
3.1.1 Dextran nanoparticles (Dex-NPs) .....	38
3.1.2 Ovalbumin nanocapsules (OVA-NCs).....	39
3.1.2.1 Alternative cross-linking of OVA-NCs .....	41
3.1.2.2 PEGylation of OVA-NCs .....	41
3.1.3 Hydroxyethyl starch nanocapsules (HES-NCs).....	42
3.1.3.1 PEGylation of HES-NCs .....	43
3.1.3.2 Antibody-modification of HES-NCs .....	43
3.2 Mice.....	45
3.3 Primary immune cells.....	45

3.3.1	Generation of bone marrow-derived dendritic cells.....	45
3.3.2	Isolation of spleen cells .....	46
3.3.3	Isolation of OT-I/OT-II T cells .....	46
3.4	Cell lines.....	47
3.4.1	Generation of DC2.4-mCMV by lentiviral transduction .....	47
3.5	<i>In vitro</i> cell culture .....	48
3.5.1	Dendritic cell stimulation assays.....	48
3.5.2	Nanoparticle interaction assays.....	48
3.5.3	Dendritic cell co-culture with T cells.....	49
3.5.4	Luciferase knockdown assay.....	50
3.5.5	Nanoparticle binding with spleen cells .....	50
3.6	Flow cytometry .....	50
3.6.1	Cell surface staining.....	52
3.6.2	Viability measurement .....	53
3.7	Cytokine measurement via cytometric bead array .....	55
3.8	Confocal laser scanning microscopy.....	56
3.8.1	Membrane / cell core staining .....	58
3.8.2	Nanoparticle detection.....	58
3.9	T cell proliferation assay .....	59
3.10	Transcriptome analysis.....	59
3.10.1	RNA isolation.....	59
3.10.2	RNA sequencing.....	60
3.10.3	Quantification of NGS data .....	60
3.10.4	Pathway analysis .....	61
3.10.5	Real-time polymerase chain reaction .....	62
3.11	Endotoxin quantification .....	63
3.12	Statistical analysis .....	63
<b>4.</b>	<b>Results .....</b>	<b>64</b>
4.1	One nanocarrier for DC-directed T cell stimulation .....	64
4.1.1	Potent NLR and TLR ligands as adjuvants for DC stimulation.....	64
4.1.2	Identification of (L18-)MDP + R848 as superadditive combination .....	66
4.1.3	Dual-adjuvant loaded Dex-NPs.....	71

4.1.3.1	Superadditive DC stimulation with adjuvant-loaded Dex-NPs .....	74
4.1.4	OVA-NCs as antigen delivery system .....	78
4.1.4.1	Binding/degradation of OVA-NCs by DCs .....	79
4.1.4.2	NC-derived peptides for DC-directed T cell stimulation.....	83
4.1.5	Adjuvant-loaded Dex-NPs + OVA-NCs .....	85
4.1.6	Adjuvant-loaded OVA-NCs combining adjuvant and antigen .....	87
4.1.6.1	Superadditive DC stimulation with adjuvant-loaded OVA-NCs.....	88
4.1.6.2	T cell stimulation with adjuvant-loaded OVA-NCs .....	91
4.1.7	Transcriptome analysis of stimulated DC .....	93
4.1.8	Spleen cell interaction with dual-adjuvant OVA-NCs.....	103
4.1.9	Alternative cross-linking method for protein nanocapsules.....	104
4.2	PEG shielding of nanocarriers.....	106
4.2.1	Influence of PEG molecular weight.....	107
4.2.2	Influence of PEGylation density .....	109
4.2.3	Relevance of mass density .....	110
4.3	Gene silencing with siRNA-loaded nanocarriers .....	112
4.3.1	Luciferase knockdown with siRNA-loaded HES-NCs .....	114
4.4	Nanocarrier-mediated DC targeting .....	117
4.4.1	DC-SIGN targeting with antibody-modified HES-NCs .....	117
<b>5.</b>	<b>Discussion.....</b>	<b>121</b>
5.1	DC-directed T cell stimulation with nanovaccine.....	121
5.2	OVA-NC shielding with PEG .....	136
5.3	Gene knockdown with siRNA-loaded HES-NCs.....	139
5.4	DC targeting with HES-NCs .....	142
<b>6.</b>	<b>Summary .....</b>	<b>145</b>
<b>7.</b>	<b>References .....</b>	<b>147</b>
<b>8.</b>	<b>Appendix.....</b>	<b>189</b>
8.1	Supplementary data .....	189
8.2	List of Figures .....	205
8.3	List of Tables.....	207
8.4	List of Abbreviations.....	208
<b>9.</b>	<b>Acknowledgments .....</b>	<b>212</b>



# 1. Introduction

Every single day the human body is exposed to numerous threats such as pathogenic bacteria or viruses. However, we stay remarkably healthy. Millions of years of evolution have driven the development of today's human immune system, a highly complex interplay between specialized organs, cells and molecules, to handle these daily challenges of survival. But nonetheless, despite its high level of efficiency, the human immune system is not able to eliminate every single biohazard. Numerous pathogens, such as poliovirus or the bacterium *Clostridium tetani*, can cause severe or even life-threatening diseases. A common and powerful method to provide a long-lasting immunity against such pathogens is vaccination. The application of a vaccine trains the immune system how the actual pathogen looks like to be prepared for a potential invasion.

A typical vaccine consists of the two basic components antigen and adjuvant. The antigen is a pathogen-related protein or peptide, responsible for mediating pathogen recognition. The adjuvant triggers an antigen-independent immune stimulation, which is required for an effective vaccination effect. After injection, the combination of both components evokes the induction of an antigen-specific immune reaction and thereby the differentiation of B and T cells into long-living memory cells. This mechanism represents the generation of an immunological memory for the used antigens. Upon renewed contact with the same pathogen, the immune system can immediately eliminate the invader. Dendritic cells (DCs) are the key mediators of that underlying immunization process. Thanks to comprehensive vaccination programs, several dreadful diseases, such as rabies or smallpox, were massively reduced or even eradicated. However, the applicability of common vaccine formulations is limited.

In 2014, the World Health Organization (WHO) published the latest World Cancer Report. Accordingly, approximately 14 million people are diagnosed with cancer each year. This number is expected to increase to 24 million by 2035 [1]. A particularly dangerous and rather common representative is the malignant melanoma. Of the numerous variations of skin cancer, it is by far the deadliest and most aggressive form. Compared to other tumors, melanomas show a high tendency to metastasize. Thereby, secondary tumors can frequently

## *INTRODUCTION*

be found in the lung, the liver, the lymph nodes or the brain. The treatment of malignant melanoma is highly dependent on the cancer stage, but usually comprises surgical removal or chemo- and radiation therapy. Also immunotherapy has gained increasing importance. The use of checkpoint inhibitors as well as BRAF and MEK inhibitors has revolutionized melanoma treatment [2]. But still the cancer is often diagnosed too late. A sufficient treatment or even a complete cure cannot be guaranteed.

Therapeutic vaccination constitutes a promising approach for melanoma treatment. The induction of a tumor-directed immune response could potentially eliminate the primary tumor as well as the metastases. Moreover, the rapid development in commercial protein production and genome sequencing allows the use of tailor-made tumor-related antigens for personalized therapy. Nonetheless, common vaccine formulations turned out to be too weak to provide sufficient therapeutic efficacy against already existing melanomas [3]. An interesting and highly up-to-date idea to enhance vaccination efficiency for melanoma treatment is to improve or even re-invent the basic principle of vaccination by means of polymer chemistry providing a source of new, innovative nano-scaled vaccines (nanovaccine). For that reason, our main objective was to develop an optimized DC-directed nanovaccine for melanoma treatment.

## 1.1 Dendritic cells

DCs are members of the innate immune system. This immune cell population was first described by Paul Langerhans in 1868 [4] and its function discovered by Steinman *et al.* in 1973 [5]. DCs are present in all organs and tissues (e.g. skin, lung, intestines) as well as in lymphoid tissue and the blood [6]. As part of the first defense line of the body against invading pathogens, they constitutively sample their environment for pathogens and abnormal cells by endocytosis of soluble and particulate matter. Moreover, they are essentially involved in the development and maintenance of peripheral tolerance under homeostatic conditions. Internalized proteins are degraded into peptides and loaded onto major histocompatibility complex (MHC) molecules of type I (MHC-I) and II (MHC-II). Upon maturation and migration to lymphoid tissues, MHC-peptide complexes are presented by DCs to T cells to trigger antigen-specific T cell activation and proliferation [7]. Therefore, DCs belong to the group of professional antigen-presenting cells (APCs), also including macrophages and B cells. Due to their enormous potential to trigger such antigen-specific adaptive immune responses, DCs are the key players in vaccination approaches.

Since DCs are relatively short-lived cells, their precursors are continuously produced in the bone marrow [8]. Like other leukocytes, DCs develop from bone marrow-derived hematopoietic stem cells (HSC). Thereby, DCs can originate from either a common myeloid (CMP) or a common lymphoid (CLP) progenitor [6]. Monocyte and DC lineages share a common progenitor, hereafter referred to as monocyte and dendritic cell progenitor (MoDP), which develops from CMP [9]. These two cell types diverge upon MoDP differentiation into either monocytes (MO) or committed DC progenitors (CDP) in the bone marrow. CDP give rise to pre-DCs, which migrate to lymphoid and non-lymphoid tissues. There, they differentiate into immature DCs and form two important DC subpopulations, namely lymphoid-resident and migratory DCs [10], regulated by growth factor Flt3L [11, 12] (Figure 1). These DCs of myeloid origin are often described as conventional DCs (cDCs). It has also been shown that monocytes can differentiate into DCs (moDCs) during inflammation [13], independent of Flt3L [14]. CLP as well as CDP can develop into interferon-producing cells (IPCs) and further into plasmacytoid DCs (pDCs) [15, 16]. In contrast to cDCs, pDCs leave the bone marrow only after complete development. Then, they circulate in blood and periphery [17].

## INTRODUCTION

Lymphoid-resident DCs include all DC populations which are consistently present in lymphoid tissue, particularly in spleen and lymph nodes. The murine spleen features two major resident DC subsets [18, 19]. One is constituted by  $CD8\alpha^+ CD11b^-$  cDCs (referred to as  $CD8\alpha^+$  cDCs), which are primarily localized in the marginal zone of the spleen [20]. They are predominantly responsible for cross-presentation of antigens [21], IL-12 production and are able to induce IFN- $\gamma$ -producing  $CD4^+$  T helper cells (Th) of type 1 (Th1) and  $CD8^+$  cytotoxic T cells (Tc) of type 1 (Tc1) [22]. These T cell populations are key players in the induction of cellular adaptive immune responses against infected and malignant cells [23]. The other subset is characterized by a lack of  $CD8\alpha$  but the presence of  $CD4$ ,  $CD11b$  [24], referred to as  $CD8\alpha^-$  cDCs. This subset can be found in the red pulp and bridging channels of the spleen. It is particularly important for antigen presentation via MHC-II, the induction of T helper cell type 2 (Th2) responses [25] and, therefore, for humoral adaptive immune responses. Upon activation both DC subsets migrate into the T cell area. pDCs can be found in the spleen as well [18].

Murine migratory DCs, i.e. DCs which are endowed with the capacity to migrate to secondary lymphoid organs upon maturation, are represented by Langerhans cells (LCs), interstitial DCs (intDCs) and TNF and inducible nitric oxide synthase (iNOS) producing DCs (Tip-DCs). These cells originate either from bone marrow-derived pre-DCs or as moDCs from MOs during inflammation (Figure 1) [26-28]. LCs, a DC subset characterized by its expression of Langerin ( $CD207$ ) [29], are present in the epidermis of the skin [30]. IntDCs are a diverse migratory DC population, which is particularly present in the dermis [31], the lamina propria of mucous membranes [32] and other connective tissues [26]. The surface marker composition of intDCs is very complex and highly dependent on the cells' specific function and localization [33]. Prominent representatives are  $CD103^+ CD11b^-$  cDCs, which share their origin and function with the lymphoid-resident  $CD8^+$  cDCs [34, 35]. Tip-DCs, a relatively new DC subset introduced by Serbina et al. [36], can be described as inflammatory DCs with high levels of co-stimulatory molecules and TNF/iNOS upon infections [37]. Tip-DCs are exclusively moDCs [38]. All three migratory DC subsets have in common that they are primarily specialized in pathogen sensing at immature state. But while LCs and intDCs migrate to lymphoid tissue and trigger antigen-specific T cell responses after antigen contact and maturation [39, 40], Tip-DCs react with



## INTRODUCTION

an enhanced production of antimicrobial TNF and iNOS in the spleen but are not essential for T cell priming [36].

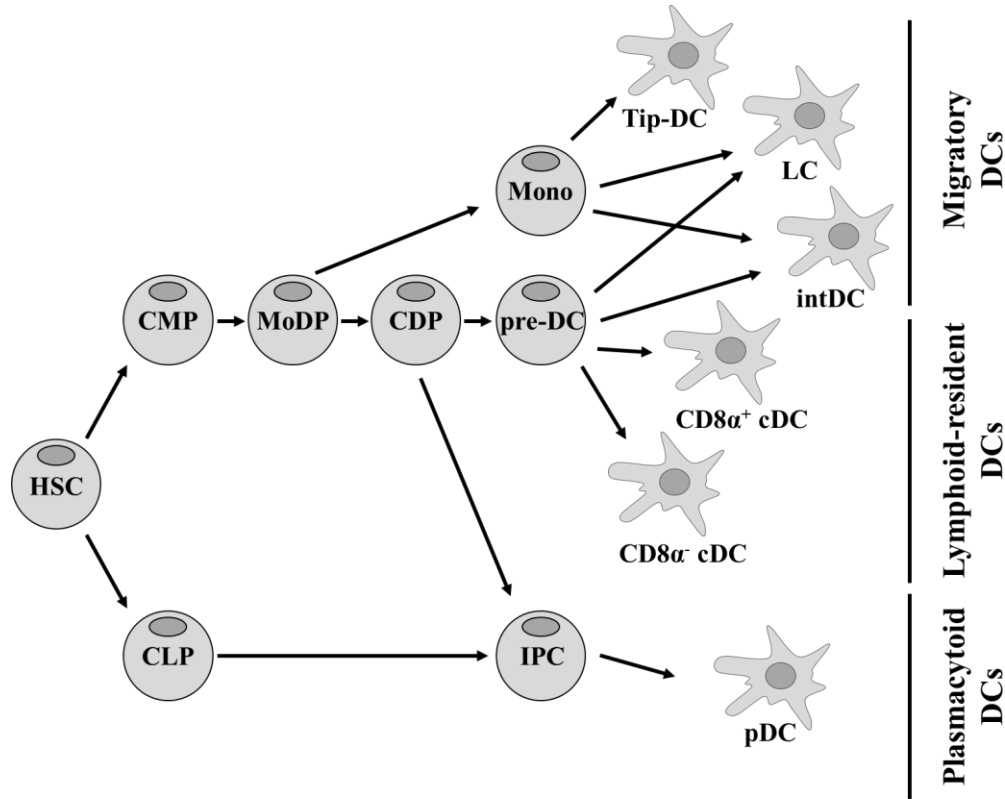


**Figure 1** DC development

DCs development starts with bone marrow-derived HSCs. These differentiate into either CMP or CLP. CMP develops to MoDP. MoDP differentiate either into Mono or CDP. CDP leave the bone marrow as pre-DCs and migrate to lymphoid and non-lymphoid tissue. Subsequently, they differentiate into migratory LCs and intDCs as well as lymphoid-resident CD8 $\alpha^+$  and CD8 $\alpha^-$  cDCs. Upon inflammation, Mono can also differentiate into intDCs and LCs. In addition, Tip-DCs can rise in this way. IPC develop from CLP and CDP as well. After differentiation into pDCs, they leave the bone marrow and circulate in the periphery (adapted from [41]).

A unique DC subset that has either myeloid or lymphoid origin is that of pDCs (Figure 1). These relatively rare circulating DCs are able to secrete high amounts of type 1 IFNs in case of virus recognition [42], underlining their innate importance. Moreover, they are endowed with the feature to present antigens to CD4 $^+$  and CD8 $^+$  T cells [43, 44], albeit less

## INTRODUCTION

effective than cDCs [45]. Indeed, pDCs have been described as essential factors of antiviral immune responses, but have also been identified to be associated with the pathogenesis of several autoimmune diseases [46] as well as with the induction of tolerance [47]. Common markers for pDC identification in mice are CD11c, B220, Siglec-H, BST2 and Ly6C [48].

Since DCs are very rare in tissues, appropriate protocols to produce DCs *in vitro* are required to obtain sufficient amounts. In this study, bone marrow-derived DCs (BMDCs) were generated for experiments with nanovaccines. They constitute a widely used and well-characterized DC test system for immunological approaches [49]. To generate BMDCs, murine bone marrow cells are treated with granulocyte-macrophage colony-stimulating factor (GM-CSF) for approximately one week. BMDCs express CD11c and MHC-II, undergo maturation upon recognition of microbial stimuli and provide the ability to present exogenous antigens to T cells [50]. Usually they are described as DCs with inflammatory phenotype, most comparable to pDCs or moDCs [51]. Nonetheless, BMDCs are not without controversy. It has recently been proposed that BMDC cultures comprise a heterogeneous population of DCs and macrophages [52]. Furthermore, BMDCs generated by Flt3L treatment instead of GM-CSF have been described as phenotypic equivalent to a mixture of murine splenic CD8 $\alpha$ <sup>+</sup> and CD8 $\alpha$ <sup>-</sup> cDCs as well as pDCs, providing a better coverage of the relevant DC subsets *in vivo* [53]. However, BMDC generation with GM-CSF has repeatedly proven to be a suitable and reliable test system for DC studies with nanoparticles [54-57]. As a first step towards a better comparability with the actual *in vivo* situation, we included experiments with murine splenic DCs.

Furthermore, the murine DC cell line DC2.4, which is based on oncogene-driven immortalization, was used in this study [58]. Since BMDCs are relatively short-lived compared to cell lines and have to be generated *de novo* for each experiment, they are not suitable for long-term culture. To be able to study immune modulation based on RNA interference, we transduced DC2.4 with a target gene and used that subline for knockdown experiments. DC2.4 has been described as cell line with DC morphology and a high expression of DC-specific markers as well as MHC and co-stimulatory molecules. Moreover, the cell line has been reported to be able to present antigens via MHC-I and -II.

## INTRODUCTION

DCs as a linker between innate and adaptive immunity orchestrate and modulate immune responses. As professional APCs, they are very potent in stimulating T cell activation and proliferation by antigen presentation via MHC. But particularly the effective stimulation of T cells, which is essential for vaccination approaches, requires sufficient DC maturation.

### 1.1.1 Dendritic cell maturation

Immature DCs are specialized in the sensing of pathogens and danger signals. Therefore, they are equipped with a huge repertoire of pattern recognition receptors (PRRs) to be able to recognize a large number of potential hazards. These receptors are localized either on the cell surface, within endosomes or in the cytosol to allow a detection of pathogens in different cellular compartments. PRR stimulation is an essential step of DC maturation and usually required for the effective induction of adaptive T cell responses.

Toll-like receptors (TLRs) are the best known and most studied group of PRRs, since they can detect a variety of different PAMPs (pathogen-associated molecular patterns) [59] and DAMPs (damage-associated molecular patterns) [60], such as proteins, lipoproteins and nucleic acids [61, 62]. In human, 10 distinct TLRs are known (TLR1-10), each with its specific set of ligands [63]. In mouse, 13 TLRs have been identified (TLR1-13) to this day [64-66]. TLR1, 2, 4, 5, 6 and 10 are localized on the cell surface, whereas TLR3, 7, 8, 9, 11, 12 and 13 can be found on endosomes. Except TLR3, whose signaling is exclusively dependent on Toll/IL-1 receptor (TIR)-domain-containing adapter-inducing interferon- $\beta$  (TRIF), all TLRs use myeloid differentiation primary response 88 (MYD88) as adapter molecule [67]. Only TLR4 activation triggers both TRIF and MYD88 signaling [68]. The exact mechanism of MYD88 signaling depends on the associated TLR. In principle, it is based on the cytoplasmic association of a TIR domain with MYD88. Upon stimulation, MYD88 recruits and activates the IL-1 receptor-associated kinase 4 (IRAK-4) [69]. After that, IRAK-1 and IRAK-2 can be activated by phosphorylation and bind the ubiquitin protein ligase TNF receptor-associated factor 6 (TRAF6) [70]. TRAF6 can ubiquitinate the I $\kappa$ B kinase (IKK), which leads to the recruitment of TGF- $\beta$ -activated kinase 1 (TAK1) and subsequently to a TAK1-mediated IKK activation by phosphorylation [71]. IKK inactivates the NF- $\kappa$ B inhibitor I $\kappa$ B, triggering NF- $\kappa$ B translocation into the nucleus and the transcription of NF- $\kappa$ B-dependent genes. Furthermore, TAK1 mediates the activation of c-

## INTRODUCTION

Jun N-terminal kinases (JNKs), which induce the MAPK/ERK (mitogen-activated protein kinases/extracellular signal-regulated kinases) signaling pathway resulting in the expression of genes that depend on activator protein 1 (AP-1). In combination, NF- $\kappa$ B and AP-1 mediate DC maturation by increased cytokine secretion and upregulation of adhesion and co-stimulatory molecules [72]. Initially, TRIF is recruited to the intracellular domain of TLRs. There, it interacts with the TANK binding kinase 1 (TBK1) and IKK to mediate the activation of the transcription factor interferon regulatory factor 3 (IRF3) by phosphorylation, finally resulting in DC maturation [73, 74]. Additionally, it has been shown that TLR3-associated TRIF can recruit TRAF6 and TAK1, leading to TAK1 activation and subsequent activation of NF- $\kappa$ B and AP-1 [75] (Figure 2).

Another group of PRRs which has been discussed as promising inducers of DC maturation in the context of immunotherapeutic approaches is constituted by the nucleotide-binding oligomerization domain-like receptors, or NOD-like receptors (NLRs). Like TLRs, NLRs are sensors for PAMPs and DAMPs, and thus regulate innate immune responses [76]. But in contrast to TLRs, they are specialized in sensing cytosolic pathogens, particularly intracellular RNA viruses and bacteria [77, 78]. All NLRs have three domains in common – a NACHT domain, a C-terminal leucine-rich repeat, which is responsible for ligand recognition, and a variable N-terminal domain. Based on the N-terminal domain, NLRs can be divided into four subgroups. The best described subgroup is NLRC, which is characterized by a caspase recruitment domain (CARD). This group also encompasses NOD1 and NOD2, which recognize specific bacteria-derived peptidoglycans [79]. Upon activation, the NACHT domain triggers self-oligomerization, which serves as docking point for signaling molecules [80]. The CARD of NOD1 and NOD2 binds the CARD of the receptor-interacting serine/threonine-protein kinase 2 (RIP2), which evokes RIP2 activation [81]. The activated RIP2 recruits TAK1, which subsequently activates IKK and JNKs [71]. Similar to MYD88 signaling, this triggers the transcription of NF- $\kappa$ B- and AP-1-dependent genes [82] and results in DC maturation (Figure 2).

## INTRODUCTION

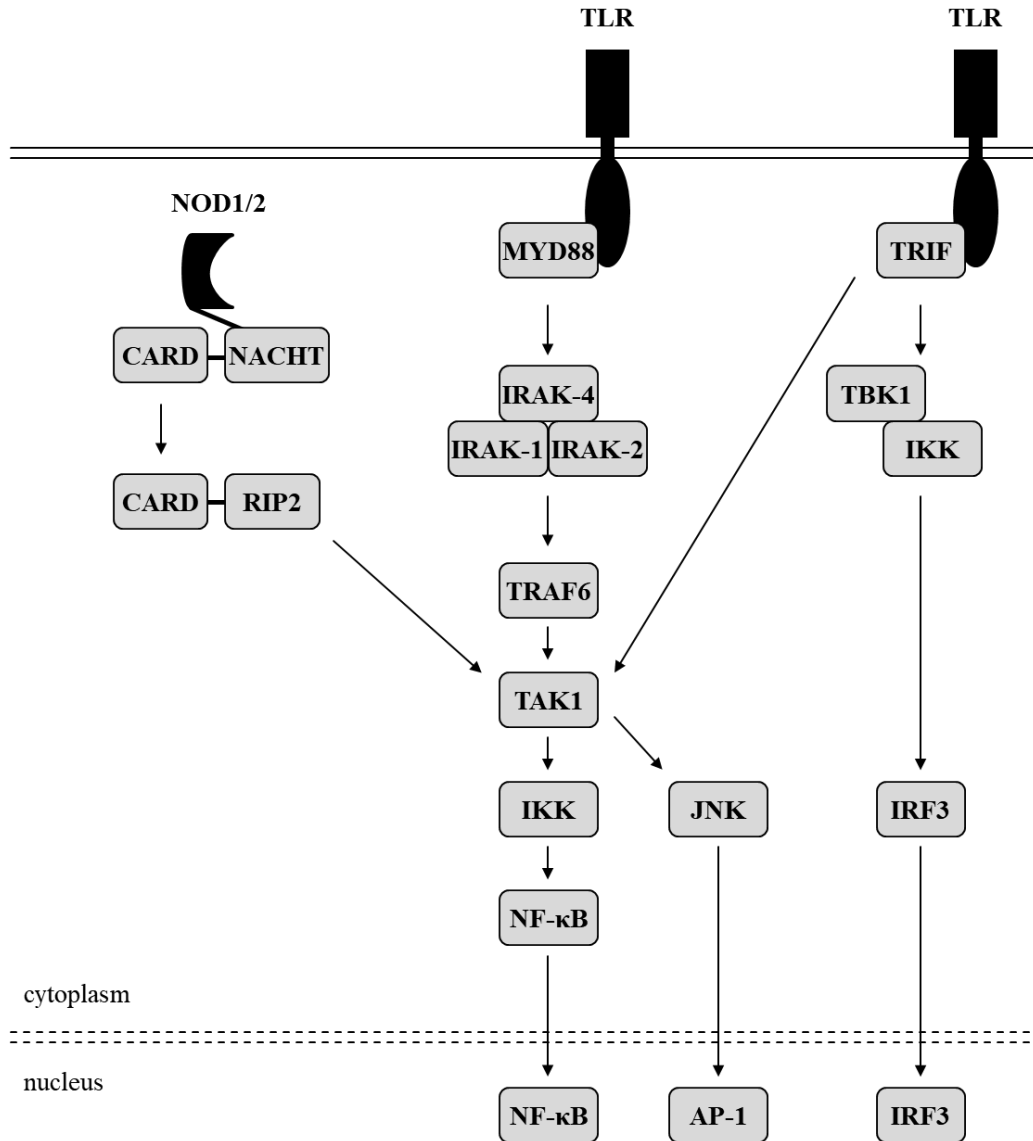


**Figure 2** TLR and NLR signaling

A simplified illustration of the signaling cascades upon activation of NOD1/2 and TLRs in general was created based on literature. MYD88 and TRIF signaling were imaged separately. Arrows that point at boxes in the nucleus indicate the induction of the corresponding transcription factors.

Besides TLRs and NLRs, C-type lectins are a well-described subgroup of PRRs, which are almost exclusively localized on the outer cell membrane. Prominent representatives are CD205 (DEC-205), CD206, also termed mannose receptor (MR), and CD209, which is also named dendritic cell-specific intercellular adhesion molecule-3-grabbing non-integrin (DC-

## INTRODUCTION

SIGN). Moreover, the C-type lectin domain family 7 member A (CLEC7A or Dectin-1) and family 9 member A (CLEC9A) are frequently mentioned C-type lectins. Although C-type lectins are endowed with the capacity for immune stimulation by ligand recognition [83], they seem to be more relevant for antigen capturing and presentation. Several C-type lectins are associated with specific DC subpopulations and are expressed in dependence of the cell's activation state. For instance, DEC-205 is primarily present on CD8 $\alpha$ <sup>+</sup> lymphoid-resident cDCs [26], where it positively correlates with CD8 $\alpha$  expression [84]. Upon DC maturation, it is massively upregulated [85]. Due to these reasons, C-type lectins are popular for the targeting of distinct DC subpopulations.

Sufficient adjuvants in form of PRR ligands are needed to stimulate DCs in order to trigger DC maturation and T cell activation. In this study, one TLR ligand for a cell surface TLR and three specific for different endosomal TLRs were used in comparative assays for DC stimulation. Lipopolysaccharide (LPS), a large molecule that can be found in the outer membrane of gram-negative bacteria, is recognized by the extracellular TLR4 and is commonly seen as a gold standard for DC stimulation. Therefore, it was repeatedly used as positive control in our study. CpG ODN 1826 (CpG), a synthetic oligonucleotide containing unmethylated CpG motifs, is specific for the endosomal TLR9. Unmethylated CpG motifs are present at a higher frequency in bacterial than in mammalian DNA [86]. Since it has been shown in numerous studies that CpG provides a strong immunostimulatory potential [87-89], it was chosen as a promising candidate. Polyinosinic:polycytidylic acid (Poly I:C) is a ligand of the endosomally localized TLR3. It is a synthetic analog of double-stranded RNA, a pattern that is highly associated with viral infections [90]. Due to TRIF signaling upon TLR3 activation, Poly I:C was particularly interesting as an alternative for MYD88-triggering TLR ligands. In addition, resiquimod (R848), a ligand for TLR7 and TLR8, was chosen. R848 is an imidazoquinoline derivative that comprises high antiviral and antitumor activity [91, 92]. The structurally similar component imiquimod has already been approved as topical treatment for basal cell carcinoma [93]. Furthermore, a clinical trial with R848 in combination with the tumor-related antigens glycoprotein 100 (gp100) [94] and melanoma-associated antigen 3 (MAGE-A3) [95] in melanoma patients showed promising results and is currently in phase

## INTRODUCTION

II [96]. Since TLR8 has been determined to be non-functional in mouse [97, 98], TLR7 is most likely responsible for the bioactivity of R848.

Regarding NLRs, different NOD1 and NOD2 ligands were tested for their DC maturation capacity.  $\gamma$ -D-glutamyl-meso-diaminopimelic acid (iE-DAP) is the minimal bioactive motif for NOD1 [99], while muramyl dipeptide (MDP) constitutes the minimal motif for NOD2 [100]. Similar to the aforementioned TLR ligands, different NOD1 and NOD2 ligands have also been reported to trigger DC maturation [101]. Since mutations in the NOD2 gene have been connected with several chronic diseases, such as Crohn's disease [102], an increased research focus was set on that NLR representative [103]. Furthermore, particularly NOD2 ligands have repeatedly been described to modulate TLR-mediated DC maturation [104]. Therefore, MDP as a minimal active motif of NOD2 stimulation was of particular interest. Interestingly, MDP was recognized in 1974 as minimal component responsible for the adjuvanticity of complete Freund's adjuvant [105].

In the present study, differently localized PRRs were addressed with adjuvants (Figure 3a). For the stimulation experiments with adjuvant-loaded nanocarriers, we used R848 and MDP alone or in combination as adjuvants to trigger DC maturation (Figure 3b).

The reason for using different PRR ligands in combination is an immunological phenomenon called stimulatory synergy or superadditive stimulation. It has been reported in numerous studies that the combined application of specific PRR ligands that bind distinct receptors which in turn trigger diverse signaling adaptor molecules significantly enhances their stimulatory capacity [106, 107]. According to Underhill, this is due to an extensive collaboration and cross-talk between all innate immune receptors, including TLRs and NLRs. A single PRR might not be sufficient to mediate of a protective immune response [108].

Figure 2 demonstrates the partially broad overlap of the three depicted signaling pathways triggered by different PRRs and ligands. Therefore, it is conceivable that a simultaneous stimulation of at least two pathways enhances the stimulatory outcome. In the end, an effective DC stimulation triggers an increased expression of the co-stimulatory molecules B7-1 (CD80), B7-2 (CD86) and others as well as the secretion of pro-inflammatory cytokines, such as IL-12. Furthermore, the DC is enabled to leave its current location and to

## INTRODUCTION

migrate to the next draining lymphoid organ. These are signature features of a matured DC and they are highly required for the induction of subsequent T cell responses.

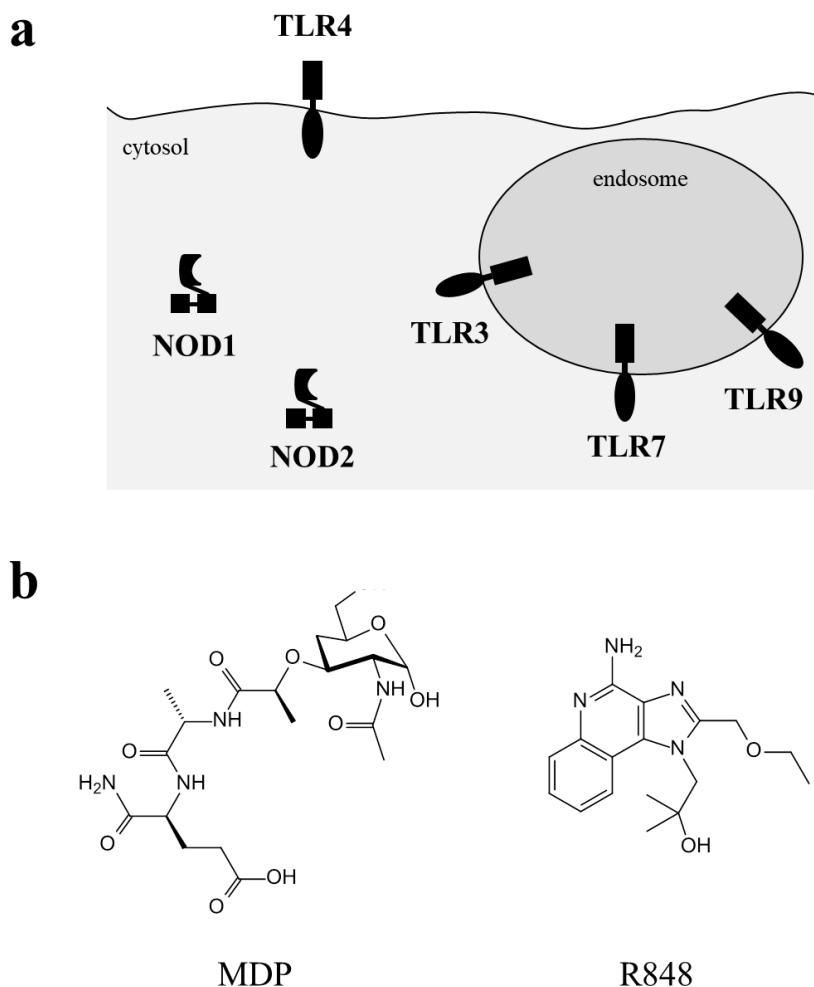


**Figure 3** Project-relevant PRRs and adjuvants

(a) Illustrated is the cellular localization of the project-relevant PRRs, namely TLR3, 4, 7 and 9 as well as NOD1 and NOD2. (b) Structural formulas of the adjuvants MDP and R848 were imaged according to IUPAC nomenclature.

In their function as professional APC, DCs are endowed with ability to capture antigens from the environment, to process them and to present the resulting peptides on MHC molecules [109]. This functionality is the second important parameter of an effective DC



## INTRODUCTION

maturation and is required for the induction of antigen-specific adaptive immune responses. In general, antigen uptake is performed by phagocytosis, macropinocytosis or receptor-mediated endocytosis. Vaccines usually contain antigens that are highly specific for the corresponding pathogen. After antigen recognition, internalization and processing by the DC, the resulting peptides are loaded onto MHC molecules. Due to their exogenous origin, derived peptides are usually loaded onto MHC-II, a molecule that is almost exclusively present on APCs [110]. Non-loaded MHC-II molecules consist of  $\alpha$ - and  $\beta$ -chains, stabilized by the so-called invariant chain (Ii) [111]. Triggered by acidic pH, the invariant chain is digested. Thereafter, the peptide-binding groove of MHC-II is blocked by a class II-associated invariant chain peptide (CLIP) [112]. Subsequently, CLIP is exchanged with an appropriate peptide from the endocytic pathway, followed by a transport of the loaded MHC-II to the cell surface.

In contrast to MHC-II, MHC-I is expressed on almost all body cells. It is responsible for the presentation of endogenous peptides, derived from the degradation of intracellular proteins. This is particularly important for the recognition of intracellular viruses or abnormal/mutated cells [113]. Assembled in the endoplasmic reticulum (ER), MHC-I consists of a heavy chain and a chain called  $\beta$ 2-microglobulin ( $\beta$ 2m). In its non-loaded state, it forms a complex with tapasin (TS), calreticulin (CRT), TAP (transporter associated with antigen processing) and ERp57 (ER-resident protein 57). Triggered by TS [114], TAP mediates the translocation of appropriate peptides from the cytosol into the ER [115]. After peptide loading, MHC-I is also transported to the cell surface via the Golgi apparatus.

Especially in tumor-directed vaccination approaches it is essential that the according antigen is presented via MHC-I and -II. Only in this case, a potent antigen-specific T cell response, comprising Tc1 and Th1 T cells, can be triggered. To enable the presentation of an exogenous antigen via MHC-I, distinct DC populations, for instance lymphoid-resident  $CD8\alpha^+$  cDCs, are endowed with the ability to cross-present (Figure 4). By this, DCs are able to present exogenous antigen peptides simultaneously via MHC-I and -II [116]. Also BMDCs [117] and DC2.4 [58] have been described to provide this specific feature termed cross-presentation.

## INTRODUCTION

Antigen uptake, processing and presentation combined with the upregulation of co-stimulatory molecules like CD80 and CD86 as well as the production of pro-inflammatory cytokines triggered by danger signals reflects DC maturation. In case of LCs, intDCs and pDCs, maturation also mediates their migration to the next secondary lymphoid organ, whereas matured lymphoid-resident DCs migrate to the T cell area within the lymphoid tissue [118]. After arrival, they interact with T cells and stimulate those that recognize the presented MHC-peptide complex.

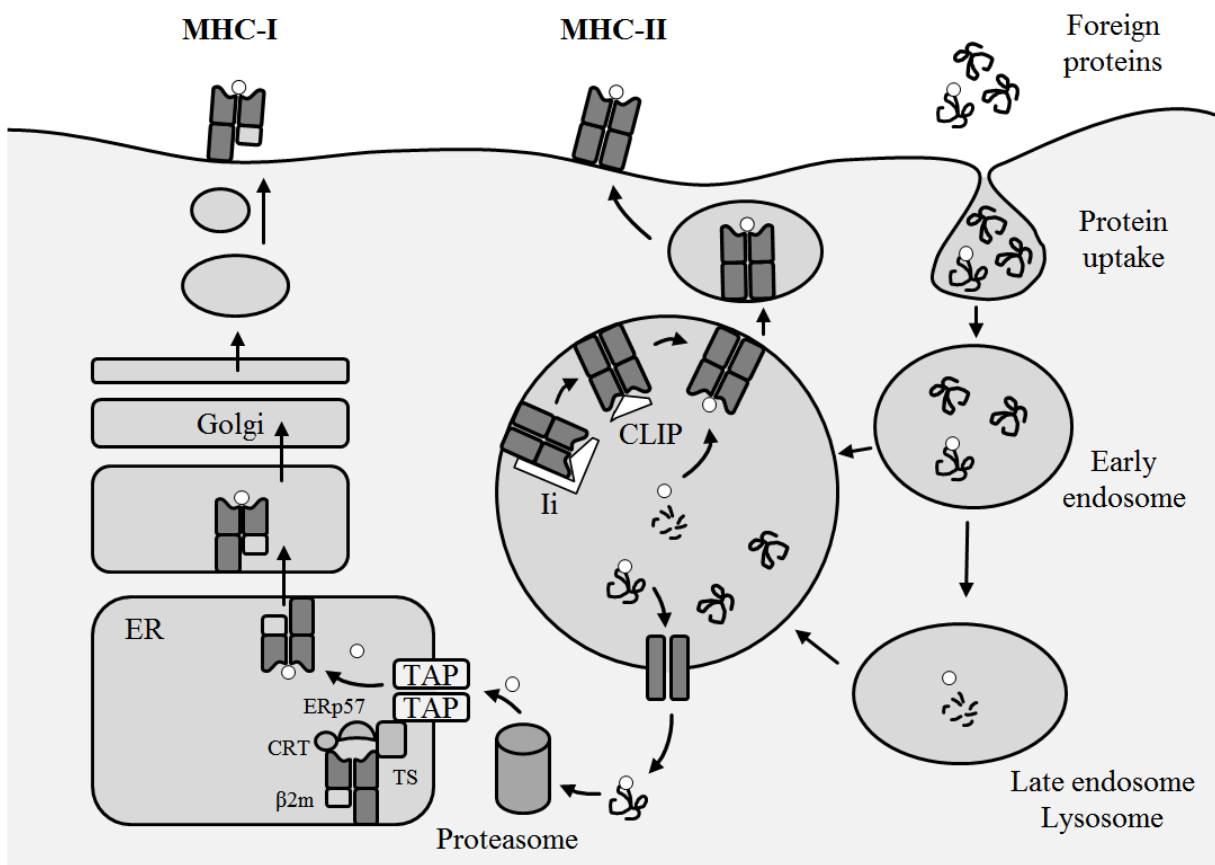


**Figure 4** Cross-presentation

The schematic illustration of cross-presentation in APCs demonstrates the intracellular trafficking of exogenous antigens after internalization. Besides the common MHC-II loading process, DCs with the ability to cross-present provide an additional mechanism that allows the controlled endosomal release of foreign proteins. Upon proteasomal degradation, the protein-derived peptides (white circles) are transported into the ER by TAP and loaded onto MHC-I. As a result, exogenous antigens are presented simultaneously by MHC-I and -II (adapted from [119, 120]).

### 1.1.2 Induction of adaptive immune responses

An effective interaction between DCs and T cells in lymphoid tissue, and subsequent induction of adaptive immune responses, is based on three (or sometimes described as two [121]) required signals [122]. The first one is the recognition of MHC-peptide complexes on DCs by an antigen-specific T cell receptor (TCR). Each TCR contains a unique, highly variable region, which allows the TCR to recognize a specific antigenic MHC-peptide complex among numerous other irrelevant complexes with an enormous specificity and sensitivity [123]. Each TCR is associated with either CD4 or CD8 $\alpha$  receptors. CD4 recognizes MHC-II and thus enables the interaction between the TCR and MHC-II. In contrast, CD8 $\alpha$  specifically binds MHC-I, mediating the interaction between the TCR and MHC-I [124]. Upon activation, naïve CD4<sup>+</sup> T cells differentiate towards one of the several known Th lineages (Th1, Th2, Th type 17 (Th17) and induced regulatory T cells (iTreg)), whereas CD8 $\alpha$ <sup>+</sup> T cells usually become Tc1. Tc type 2 (Tc2) and type 17 (Tc17) are rarely described subsets with partially unknown and controversially discussed functions [125]. In that context, antigen-specific peptide recognition comprises the first required signal. The second one is the co-stimulation by DC-derived CD80 and CD86. These molecules bind CD28 on T cells. Since CD80 and CD86 are highly expressed on activated DCs, sufficient T cell stimulation is exclusively mediated by those APCs. DC/T cell interaction with an insufficient or without co-stimulation leads to anergy [126] or even apoptosis of the T cell [127]. The polarization of the T cells into their final subtypes is determined by the third signal, namely polarizing mediators like cytokines. Importantly, this signal also contributes essentially to the T cell activation. For instance, the presence of IL-12 during T cell activation triggers the polarization of naïve CD4<sup>+</sup> T cells into Th1 [128]. IL-1 $\beta$  and TNF- $\alpha$  have also been described as Th1-promoting cytokines [129, 130]. In contrast, if IL-4 is present, those T cells preferentially polarize into Th2 [131]. Additionally, some APC surface molecules are known to influence T cell polarization. ICAM-1 (intracellular adhesion molecule 1) has been described to promote Th1 differentiation via interaction with LFA-1 (lymphocyte function-associated antigen 1) [132], whereas OX40L mediates Th2 differentiation by OX40 engagement [133]. Only if all three signals reach the naïve T cell in a sufficient intensity, it becomes fully activated, undergoes clonal expansion and acquires its effector function [134].

## INTRODUCTION

Consequently, the T cell subset composition (or T cell response) upon DC-mediated activation is highly dependent on i) the presented MHC context, ii) the pattern of co-stimulatory receptors and iii) the prevailing cytokine milieu. Activated T cells can be characterized by their cytokine secretion profile, which is also connected to their effector function. Th1 mediate cellular immune responses against intracellular bacteria and viruses, involving the recruitment and activation of phagocytes and antigen-specific Tc1. This is particularly essential for the recognition and killing of tumor cells. Th1 produce predominantly IFN- $\gamma$ , IL-2 and TNF- $\alpha$ . Th2 induce humoral immune responses against extracellular pathogens, which includes the activation of B cells and thus the production of antigen-specific antibodies. Since many tumors are insusceptible to antibodies due to low immunogenicity [135], a Th2-dominated T cell response is usually not preferred in tumor approaches. A typical Th2 response is characterized by increased levels of IL-4, IL-5 and IL-13. In contrast to Th, Tc1, also referred to as cytotoxic T lymphocytes, are able to recognize infected or malignant cells via MHC-I and to directly kill those cells. This T cell subset is particularly interesting for tumor vaccination approaches since tumor-specific Tc1 cells can potentially fight the corresponding tumor directly. However, this strategy strongly depends on the tumor accessibility and the tumor microenvironment. Similar to Th1, a differentiation of CD8 $\alpha^+$  T cells into Tc1 can be detected by increased levels of IFN- $\gamma$ .

Due to their specific effector function, a Tc1/Th1-dominated T cell response has been described to be highly beneficial for tumor treatment [136]. Antigen-specific Tc1 can directly fight the tumor cells, while Th1 attract phagocytes and enhance the Tc1 response. In contrast, a Th2-biased response has turned out to be less efficient in most tumor diseases [137]. For example, Aspord *et al.* have reported that Th2 heavily infiltrate breast and pancreatic cancer tissue, where they accelerate the tumor growth by IL-13 production [138]. Moreover, it has been shown that B cell-derived tumor-binding IgG can promote tumor progression by inducing regulatory macrophages and mast cell-derived release of proangiogenic factors [139, 140].

## 1.2 Nanovaccines for tumor treatment

In 1980, smallpox was declared as eradicated by the WHO. It was the first disease to have been fought globally. This was achieved through collaborations between numerous countries which included systematic vaccination and outbreak recording [141]. This breakthrough was preceded by a long suffering history (earliest clinical evidence from 1500 B.C. [142]) with 300-500 million deaths only in the 20th century [143]. The smallpox case exemplifies the exceptional potential of vaccines to treat and control diseases that were considered as untreatable. Since its first use, vaccination has had an enormous impact on public health.

First generation vaccines, as used for smallpox vaccination, basically consisted of live-attenuated or whole-pathogen preparations [144, 145], which needed no additional stimulation in form of an adjuvant. While several of these formulations are still in use today, the treatment of some groups of diseases requires much higher vaccination specificity and efficiency. Neoplastic diseases or intracellular infections can be controlled only insufficiently or not at all with such formulations. Furthermore, the risk of reversion to virulence or incomplete virus/bacteria inactivation is omnipresent [144]. Hence, modern vaccines (second generation) have changed fundamentally. Recombination technologies allow the production of purified, highly specific antigens, and systematic combination of multiple antigens potentially enables the treatment of even complex diseases. Despite better safety profiles and higher specificity, purified antigens are frequently less immunogenic and lack PAMPs due to removal of pathogenic contaminations [146]. Therefore, adjuvants are needed to induce a sufficient immune response. Besides the traditional stimulants, aluminum salts (alum) [147] and Freud's adjuvant [148], which have been intensively used for more 90 years [149], numerous synthetic and biological molecules were identified as new immunostimulants. These substances act as PAMPs and are recognized by PRRs to induce innate immune responses. Over time, it turned out that the type of vaccine adjuvant essentially influences the character of an elicited immune response [150]. However, since almost all adjuvants feature harmful side effects, it was attempted to keep the required amounts as low as possible.

## INTRODUCTION

A vaccine is usually administered prophylactically. It yields a DC-directed adaptive immune response intended to subsequently lead to eradication of the relevant pathogen in case of an infection. Ideally, it triggers the generation of antigen-specific memory B and T cells and thus mediates a life-long protection. In case of tumor diseases, it is a totally different situation. With the exception of the HPV (human papillomavirus) vaccine [151], which protects against the trigger of cervical cancer, prophylactic vaccination against tumors is insufficient due to their tremendous complexity and variability combined with a quite low immunogenicity. Regarding antigens, it is virtually impossible to find one that is, for instance, present on melanomas in general. Furthermore, therapeutic vaccination is not less complex. While it is possible nowadays to identify and synthesize individual antigens specific for an existing tumor, therapeutic vaccines have to induce very strong antigen-specific T cell responses that are potent enough to compete with an already established tumor disease [152]. This is rarely successful. An effective antitumor response also requires a specific immune cell composition (see 1.1.2) and therefore a suitable adjuvant. Moreover, several tumor forms are immunologically isolated. In addition, many tumors create an immunosuppressive microenvironment, which further impedes an effective intervention [153]. Another fundamental problem is that many vaccine formulations suffer from poor immunogenicity [154].

T cell therapy with chimeric antigen receptors (CARs) [155] as well as the use of several checkpoint inhibitors to break T cell suppression [156] have been shown to enhance antitumor responses, thereby underlining the importance of T cells for tumor rejection. However, the majority of patients do not develop a sufficient tumor-specific Tc1 response. Therefore, new ideas are urgently needed to enable tumor treatment by vaccination.

Nanovaccines, i.e. nanoparticle (NP)-based vaccine formulations, represent a new strategy for therapeutic tumor treatment and offer the opportunity to deal with some of these problems. Similar to a common vaccine, nanovaccines include all components that are required for an effective antigen-specific immune stimulation. But in contrast, the vaccine components are usually bound or encapsulated to/in a nanocarrier in adjustable concentrations and close proximity to each other and are thereby co-delivered to the same target cells. Frequently, these nanocarriers provide a shielding of the active substances against extracellular degradation or clearance processes. Therefore, nanovaccines enable a

## INTRODUCTION

protected transport and in addition also allow the use of components that are usually not suitable for vaccines due to insufficient pharmacokinetics or solubility. Under optimal conditions, the encapsulated antigen/adjuvant combination is delivered to the DC. In this way, high local concentrations of those substances are achieved [157], which may provide increased activation and antigen presentation, potentially resulting in enhanced antigen-specific T cell responses. Furthermore, the nanocarrier surface can be modified in numerous ways to increase blood circulation time and selectivity for APCs as well as to reduce unspecific uptake or protein adsorption.

An important parameter of nanovaccine design is the carrier material [158]. Thereby, three major classes of nanocarriers can be defined according to their material, namely inorganic, liposomes, and polymeric [159]. Immunostimulatory complexes, virus-like particles and self-assembled proteins are three additional but less frequently used classes of nanocarriers [160]. NPs consisting of inorganic materials such as gold, carbon or silver, are widely used for biomedical applications [161] and have also been investigated intensively for nanovaccine approaches [160]. For example, it has been reported that gold NPs associated with the tumor antigen extra domain B can induce an antigen-specific T cell response against the murine breast cancer cell line 4T1 *in vivo*, whereas the application of soluble antigen failed [162]. Most inorganic types of NPs provide a high modifiability and are readily internalized by APCs but are controversially discussed regarding solubility, biocompatibility and long-term toxicity [163-165]. Liposomes, another promising platform for nanovaccines, are spherical carriers with at least one phospholipid bilayer. Common exemplary lipids for liposome synthesis are DOTAP (N-(2,3-dioleoyloxy-1-propyl)trimethylammonium methyl sulfate), DOPE (1,2-dioleoyl-sn-glycero-3-phosphoethanolamine) and PC (phosphatidylcholine) [166]. Besides excellent biocompatible properties, liposomes provide high modifiability due to the option to alter the phospholipid composition [167, 168]. Indeed, it has been shown that antigens conjugated to [169] as well as encapsulated in [170] liposomes are able to induce CD8<sup>+</sup> T cell responses. Furthermore, several liposomal formulations have already been approved as delivery system by the Food and Drug Administration (FDA) [171]. However, although liposomes are usable for the encapsulation of diverse substances due to their amphiphilic character, many liposomal formulations suffer from a low stability and insufficient loading

## INTRODUCTION

capacities [172, 173]. Polymeric NPs are also a widely used and extensively studied class of nanocarriers. They are either prepared by dispersion of preformed polymers or by polymerization of monomers [174]. Various methods are available for their synthesis, such as solvent evaporation, dialysis, micro- or miniemulsion. Likewise, numerous base materials can be used for polymeric NPs. Typical representatives are PLA (poly lactic acid) [175], PLGA (poly lactic-co-glycolic acid) [176] and PS (polystyrene) [177]. Dependent on the synthesis process and the used base material, polymeric NPs can provide a high biocompatibility and loading capacity combined with an enormous modifiability.

The physicochemical properties of the synthesized NP do also determine their suitability to serve as nanovaccine. Regarding surface charge, cationic NPs have been described to be more toxic for phagocytic cells than anionic ones *in vitro*. This is most likely due to direct NP penetration into the negatively charged membrane causing physical damage as well as to NP-induced production of reactive oxygen species (ROS) resulting in increased oxidative stress [178-181]. In contrast, isolated APCs internalize anionic NPs much easier than cationic [182, 183]. However, the impact of surface charge cannot be predicted sufficiently *in vivo* since adsorbing proteins in blood or tissue can alter the NP's surface properties. Nonetheless, a negative surface charge is usually preferred for nanovaccines. For successful nanovaccine design the NP size is a further important parameter. It should be optimized to enter the secondary lymphoid organs as efficient as possible. NPs smaller than 3-5 nm do not reach the lymph nodes due to a rapid renal clearance [184]. If NPs are bigger than that but smaller than 200 nm, they have been described to drain the lymph nodes in a DC-independent manner [185]. NPs with a size of more than 200 nm are usually internalized by APCs at the NP injection site and are transported to the lymph nodes [186]. Finally, the size of a nanovaccine has to be adjusted to the preferred mechanism to reach lymphoid tissue. However, the NPs should bear a size sufficient to prevent fast clearance by the kidney but not too big to be taken up.

To induce a sufficient adaptive immune response against a tumor disease, the NP-delivered antigen has to be presented via MHC-II and due to cross-presentation also via MHC-I. Therefore, it is necessary that the antigen that is delivered to the DC reaches the cytosol and is degraded by the proteasome (see Figure 4). Several strategies have been established to trigger an endosomal release of antigen. For example, NPs with a high buffering capacity



## INTRODUCTION

may be designed to mediate endosomal rupture by the proton sponge effect. By the influx of ions and water into the endosome the osmotic pressure is increased, potentially resulting in compartment rupture [187]. The use of such a NP combined with an antigen can induce increased levels of antigen-specific CD8<sup>+</sup> T cells [188].

As outlined in 1.1.1, a sufficient DC maturation, associated with upregulation of co-stimulatory molecules and secretion of pro-inflammatory cytokines, is also an essential parameter for the success of a nanovaccine to trigger anti-tumor responses. One option is to use a nanocarrier system that stimulates the DCs based on its intrinsic immunostimulatory activity. In this regard, iron oxide NPs have been reported to stimulate CD86 expression and the secretion of IL-1 $\beta$ , IL-6, TNF- $\alpha$  and IL-12 in DCs [189]. Furthermore, it has recently been shown by Afroz *et al.* that antigen-loaded zinc oxide NPs can mediate the expansion of antigen-specific CD4<sup>+</sup> and CD8<sup>+</sup> T cells in the absence of any adjuvant [190]. However, the more common option is to co-deliver adjuvants. The adjuvant is either chemically conjugated on or encapsulated in the NP, based on synthesis, structure and chemical properties. In the context of therapeutic melanoma treatment, adjuvants that trigger Tc1/Th1-directed T cell responses are preferred for nanovaccine generation. Since it is well-known that the commonly used adjuvant alum, which can be found in vaccines against diphtheria-tetanus-pertussis, HPV or hepatitis, triggers a strong Th2 response [147], it is not suitable for nanovaccines intended to treat melanoma. NPs enable the encapsulation of adjuvants, which can result in an enhanced delivery and a stronger stimulatory capacity. In this context, the potential of R848 in nanovaccines to provoke potent T cell responses has been reported in several studies [191-193]. Due to its relatively weak stimulatory potential alone, MDP was rarely used for nanovaccines [194, 195] but has shown superadditive potential particularly in combination with other adjuvants [196]. In the end, the chosen adjuvant has to be compatible with the nanovaccine synthesis.

A special feature of most NPs is their high modifiability. Surface modifications can essentially alter NP's properties with regard to their cellular binding characteristics. Typical surface modifications are the coupling of polyethylene glycol (PEG) to minimize unwanted unspecific cell binding, and targeting moieties to facilitate recognition by target cells as outlined below.

## INTRODUCTION

Nanoparticulate formulations for *in vivo* applications often suffer from low blood circulation time associated with massive protein adsorption and unspecific interaction with cells, mainly of the mononuclear phagocyte system (MPS) [197], resulting in a fast and usually unwanted clearance [198]. A surface modification of NPs with PEG, also called PEGylation, reduces unspecific NP interactions with proteins and cells [199], which is also described as ‘stealth effect’. Consequently, PEGylation prolongs the NP circulation time and thus enhances the specificity of a potential targeting moiety. Furthermore, PEGylation can increase the nanocarriers’ stability [200] and decreases liver accumulation [201]. Moreover, PEG is low priced, versatile and FDA approved for diverse applications [202]. In the pharmaceutical industry, it represents the gold standard for stealth polymers to tackle the mentioned problems, and has been used for decades [203]. In theory, a NP modification with PEG chains counteracts hydrophobic and electrophilic interactions between NPs and plasma proteins or cells [201, 204], and increases the NP solubility in buffer and serum due to the hydrophilic ethylene glycol repeats [205, 206]. Besides the use of PEGylated NPs as delivery system for cytostatics for direct tumor therapy [207, 208], such NPs have also been applied as nanovaccines [209, 210]. The actual stealth properties of a NP are determined by numerous factors, such as the molecular weight (MW) of the used PEG and the PEGylation density.

Substances that actively bind target structures on cells are called targeting moieties. The cell targeting is mediated by either receptor ligands or antibodies. Such a modification can be used in nanovaccine approaches to specifically address DCs and thus to support nanovaccine efficiency. A stronger DC association can result in a stronger uptake and thereupon in a more efficient antigen delivery and DC stimulation. Regarding receptor ligand targeting, it has, for instance, been shown by Carrillo-Conde *et al.* that a NP surface functionalization with mannose significantly increases the DC uptake by targeting MR and DC-SIGN [211]. Another study has reported that a NP surface modification with CpG facilitates DC targeting [212]. Besides its function as immunostimulant, CpG was revealed to be recognized by DEC-205 [213]. The coupling of DC-directed antibodies to NP’s surface can also substantially increase DC targeting. Saluja *et al.* were able to show that DC targeting with DEC-205-specific antibodies on PLGA NPs leads to enhanced cross-presentation of co-delivered melanoma-associated antigens [214]. Moreover, it has also

## INTRODUCTION

been reported for CD40, DC-SIGN and CD11c that a targeting via NP-coupled antibodies triggers the induction of efficient CD8<sup>+</sup> T cell responses [215, 216]. In general, surface modifications of nanovaccines with DC-directed targeting moieties, such as receptor ligands or antibodies, are able to enhance the vaccination efficacy via an improved delivery to DCs. Furthermore, the increase in cell specificity also reduces the unspecific uptake by unwanted cell types. For these reasons, this kind of modification has qualified as promising strategy for optimized nanovaccines [217].

A further promising but rather rarely used immunomodulatory modification of nanovaccines is the encapsulation of small interfering RNA (siRNA). These small RNA molecules bind complementary sequences on the target cell's mRNA and thus inhibit the expression of the corresponding sequence or gene. In case of nanovaccines, the effective delivery of siRNA into DCs could be exploited to inhibit immunosuppressive mechanisms. As a result, accordingly treated DCs would show enhanced immunostimulatory properties. It has been demonstrated for polypeptide micelles that the combined delivery of Poly I:C, tumor antigen and STAT3 siRNA could overcome the activation-resistant state of tumor-associated DCs, resulting in a stronger antitumor response [218].

For the application of nanocarriers in vaccination approaches, they have to fulfil certain criteria. It is essential that the carrier material is biocompatible and degradable without any toxic byproducts. Many polymers that were tested for these approaches are biocompatible but lack the latter requirement [219, 220]. Components, such as the well-known protein ovalbumin (OVA), the FDA approved starch derivative hydroxyethyl starch (HES) as well as the polysaccharide dextran (Dex) offer crucial benefits compared with the most completely synthetic materials since almost all body cells have the capacity to process and degrade them. This advantage qualifies OVA, HES and Dex to be promising base materials for degradable polymeric NPs [221-225] or possibly even nanovaccines.

Polymeric nanocapsules (NCs), which are usually hollow carriers with a liquid core, constitute a special form of NPs. They enable the protection of the payload from external influences. Furthermore, certain stimuli, such as pH, redox potential or temperature, can be used to trigger the payload release [226-230]. A common method to synthesize nanocapsules is the polymerization at droplet's interface in miniemulsion [231].

### 1.3 Thesis objectives

The main objective of this study was to develop a DC-directed nanocapsule-based platform for the optimized design of nanovaccines that may allow therapeutic treatment of the malignant melanoma. To achieve this, the project was separated into four sections, each of them dealing with a specific challenge.

The first section was focused on the integration of the two main components of a vaccine, namely antigen and adjuvant, in one functional nanocapsule. Therefore, we initially planned to search for an appropriate stimulatory adjuvant combination. We decided to scan for TLR/NLR ligand combinations that exclusively target intracellular PRRs and may provide synergistic stimulatory properties on BMDCs, since those adjuvants are particularly interesting for the delivery by nanocapsules. Promising candidate combinations should then be encapsulated in Dex-based NPs to check whether the encapsulation preserves the stimulatory synergy. The encapsulation should also increase delivery and enhance the combination's stimulatory capacity. To focus on antigenicity, we wanted to analyze the suitability of already described OVA-based polymeric NCs to serve as an antigen source for DC-mediated OVA-specific T cell stimulation. To fuse both vaccine requirements, we thereafter planned to transfer the identified adjuvant combination into the OVA-based NCs to finally obtain our dual-function nanocapsule. The suitability of this nanocapsule to trigger BMDC-mediated OVA-specific T cell responses *in vitro* should then be assessed sufficiently. In addition, it was planned to examine the stimulatory effect of the nanovaccine on BMDCs by transcriptome analysis. As a first important step towards an *in vivo* application, the nanocapsules should be tested on primary spleen cells to identify preferred target cells. At last, we wanted to evaluate an alternative synthesis method for adjuvant-loaded protein-based nanocapsules providing better biocompatibility.

An optimization of the nanovaccine's stealth properties was the objective of the second project section. We planned to modify the surface of the OVA-based NCs with PEG to substantially reduce unspecific interactions with proteins and cells and to increase their blood circulation time. After successful modification, the impact of the PEG size, the PEGylation density and the PEG mass density on the interaction between BMDCs and OVA-based NCs should be assessed by detailed binding assays. To mimic the *in vivo*

## *INTRODUCTION*

situation, the assays were performed under different serum conditions. In the end, it should be possible to give a recommendation how to reach the maximum stealth effect with PEG on protein-based NCs.

The additional encapsulation of siRNA into nanocapsules constitutes a promising option to further modulate the triggered immune reaction. Consequently, the third project section dealt with the objective to evaluate siRNA as a nanocapsule payload to modulate gene expression. Therefore, the suitability of siRNA-loaded PEGylated HES-based NCs as an antigen-independent polymeric nanocapsule system to knockdown gene expression in transduced DC2.4 should be assessed in detail exemplified by the expression of firefly luciferase. A sufficient gene knockdown would indicate a successful cargo release and also an endosomal release.

In the last section, we planned to add a targeting moiety in form of a DC-SIGN-directed antibody to the surface of the HES-based NC to actively address DCs and to potentially increase NC uptake and cargo release. For this, it was intended to study the interaction between DC2.4 and such modified NC to see whether a DC-SIGN targeting strategy improves the NC's properties, for example regarding siRNA-mediated gene knockdown.

Since OVA- and HES-based NCs feature a comparable modifiability, the results of the last two sections should easily be transferred to the adjuvant-loaded protein-based nanocapsules from the first two sections. In this way, we would be able to create a versatile platform for the development of new nanovaccines for the treatment of cancer, including the malignant melanoma.

## 2. Material

### 2.1 Laboratory equipment

Equipment	Model	Manufacturer
Biological safety cabinet	LaminAir HB 2448	Heraeus, Hanau, Germany
Biological safety cabinet	Herasafe HS18	Heraeus, Hanau, Germany
Cell counting chamber	Neubauer Improved	LO - Laboroptik, Lancing, UK
Cell harvester	Mach 3	Tomtec, Hamden, USA
Centrifuge	Sigma 3 K-30	Sigma, Osterode am Harz, Germany
Centrifuge	Multifuge 1 L-R	Heraeus, Hanau, Germany
Centrifuge	Megafuge 40R	Heraeus, Hanau, Germany
Centrifuge	Multifuge X3R	Heraeus, Hanau, Germany
Centrifuge	Sigma 1-14	Sigma, Osterode am Harz, Germany
Centrifuge	5417 C	Eppendorf, Hamburg, Germany
CO <sub>2</sub> Incubator	CB 210	Binder, Tuttlingen, Germany
Electrophoresis power supply	EPS 3500 XL	Pharmacia Biotech, Uppsala, Sweden
Electrophoresis unit	VARIA	Roth, Karlsruhe, Germany
Flow cytometer	BD FACS Canto II	BD Biosciences, Heidelberg, Germany
Flow cytometer	Attune NxT	Thermo Fisher Scientific, Waltham, USA
Gel documentation system	Fusion SL	Vilber Lourmat, Marne-la-Vallée, France
Laser scanning microscope	LSM 710	Carl Zeiss, Oberkochen, Germany
Liquid scintillation counter	1205 Betaplate	LKB Wallac, Turku, Finland
Microplate reader	Infinite M200 Pro	Tecan, Männedorf, Switzerland
Microplate reader	Centro LB 960	Berthold Technologies, Bad Wildbad, Germany
Microplate reader	MRX TC Revelation	Dynex, Cantilly, USA
Microscope	NanoSight LM10	Malvern Instruments, Herrenberg, Germany
Microscope	CH2	Olympus, Tokyo, Japan
Microscope, inverse	FE.2915	Euromex, Arnhem, Netherlands
Microscope, inverse	CK2	Olympus, Tokyo, Japan
Microwave	Micromat 15	AEG, Nürnberg, Germany
Motric pipette filler	Pipetus standard	Hirschmann, Eberstadt, Germany
NMR spectrometer	Avance 300	Bruker, Billerica, USA
Real-Time PCR System	CFX96	Bio-Rad, Hercules, USA
Scanning electron microscope	1530 Gemini LEO	Carl Zeiss, Oberkochen, Germany
Submicron particle sizer	Nicomp 380	Nicomp, Port Ritchey, USA
Thermomixer / heat block	5436	Eppendorf, Hamburg, Germany
Transmission electron microscope	JEM-1400Flash	Jeol, Freising, Germany
Ultrasonic bath	Sonorex RK 102	Bandelin, Berlin, Germany

*MATERIAL*

Ultrasonic bath	Sonorex RK 52 H	Bandelin, Berlin, Germany
Ultrasonic homogenisator	Sonopuls HD 2070	Bandelin, Berlin, Germany
Ultrasonic homogenisator	Sonifier W-450-Digital	Branson Ultrasonics, Danbury, USA
UV-Vis spectrophotometer	Lambda 16	Perkin Elmer, Waltham, USA
UV-Vis spectrophotometer	NanoDrop 2000	Thermo Fisher Scientific, Waltham, USA
UV-Vis spectrophotometer	NanoDrop 8000	Thermo Fisher Scientific, Waltham, USA
Vortex mixer	444-1372	VWR, Radnor, USA
Water bath	1083	GFL, Burgwedel, Germany
Zetasizer	Zetasizer Nano Range	Malvern Instruments, Herrenberg, Germany

**Table 1** Laboratory equipment

## 2.2 Reagents

Reagent	Manufacturer
[Methyl- <sup>3</sup> H] thymidine	Perkin Elmer, Waltham, USA
1,6-hexanediol dipropiolate (HDDP)	Sigma-Aldrich, Deisenhofen, Germany
2,2'-(ethylenebis(oxy))bisacetic acid	Merck Millipore, Darmstadt, Germany
2,2'-(ethylenedioxy)bis(ethylamine)	Sigma-Aldrich, Deisenhofen, Germany
2,4-toluene diisocyanate (TDI)	Sigma-Aldrich, Deisenhofen, Germany
2-azido-1-ethylamine	Sigma-Aldrich, Deisenhofen, Germany
4-(2-phenyl-2H-tetrazol-5-yl)benzoic acid (TET) [232, 233]	Max Planck Institute for Polymer Research, Mainz, Germany
4',6-diamidino-2-phenylindole (DAPI)	Sigma-Aldrich, Deisenhofen, Germany
7-Aminoactinomycin D (7AAD)	BD Biosciences, Heidelberg, Germany
Acetic acid (99 %)	Sigma-Aldrich, Deisenhofen, Germany
Acetone	VWR, Radnor, USA
Acetone	Sigma-Aldrich, Deisenhofen, Germany
Agarose	Roth, Karlsruhe, Germany
Alexa Fluor 647 (AF647) Annexin V	Biolegend, San Diego, USA
AllStars Negative Control siRNA (AF647-labeled)	Qiagen, Hilden, Germany
Ammonium chloride (NH <sub>4</sub> Cl)	Sigma-Aldrich, Deisenhofen, Germany
Aqua Ampuwa, sterile (H <sub>2</sub> O <sub>st</sub> )	Fresenius Kabi, Bad Homburg vor der Höhe, Germany
Boric acid	Sigma-Aldrich, Deisenhofen, Germany
CellMask Orange	Thermo Fisher Scientific, Waltham, USA
Cy5-labeled oligonucleotide with the sequence Cy5-CCA CTC CTT TCC AGA AAA CT-3' (Cy5-Oligo)	IBA, Göttingen, Germany
Cyclohexane (HPLC grade)	VWR, Radnor, USA
Dextran, 9-11 kilodaltons (kDa)	Sigma-Aldrich, Deisenhofen, Germany
Dibenzocyclooctyne-PEG4-N-hydroxysuccinimidyl ester (DBCO-PEG4-NHS)	Jena Bioscience, Jena, Germany
Dichloromethane (DCM)	Sigma-Aldrich, Deisenhofen, Germany
Diethyl ether	Sigma-Aldrich, Deisenhofen, Germany
Dimethyl sulfoxide (DMSO)	Sigma-Aldrich, Deisenhofen, Germany
Dimethylformamide (DMF)	Sigma-Aldrich, Deisenhofen, Germany
Dinorbornene (DN)	Max Planck Institute for Polymer Research, Mainz, Germany
D-mannosamine	Sigma-Aldrich, Deisenhofen, Germany
DMSO	Thermo Fisher Scientific, Waltham, USA
DQ OVA (OVA-DQ)	Molecular Probes, Eugene, USA
Ethanol (≥ 99.8 %)	Sigma-Aldrich, Deisenhofen, Germany
Ethylenediaminetetraacetic acid disodium salt dehydrate (EDTA-Na <sub>2</sub> )	Sigma-Aldrich, Deisenhofen, Germany
Fluorescamine	Sigma-Aldrich, Deisenhofen, Germany
HES (200 kg/mol, degree of	Fresenius Kabi, Bad Homburg vor der Höhe, Germany



*MATERIAL*

substitution: 0.5)	
Human serum albumin (HSA)	Sigma-Aldrich, Deisenhofen, Germany
Isocyanate PEG <sub>2000</sub> (2000 g/mol)	Nanocs, New York, USA
Isocyanate PEG <sub>3400</sub> (3400 g/mol)	Nanocs, New York, USA
Isocyanate PEG <sub>5000</sub> (5000 g/mol)	Nanocs, New York, USA
Isocyanate PEG <sub>5000</sub> -isocyanate	Nanocs, New York, USA
L-glutamine	Sigma-Aldrich, Deisenhofen, Germany
Lipofectamine	Thermo Fisher Scientific, Waltham, USA
Luciferase GL2 Duplex siRNA	GE Healthcare Life Sciences, Freiburg, Germany
NHS-PEG4-azide	Sigma-Aldrich, Deisenhofen, Germany
O-(2-aminoethyl)-O'-(2-azidoethyl)pentaethylene glycol (Azido-PEG-amine)	Sigma-Aldrich, Deisenhofen, Germany
OVA (grade VI)	Sigma-Aldrich, Deisenhofen, Germany
Paraformaldehyde (PFA)	Sigma-Aldrich, Deisenhofen, Germany
Penicillin	Sigma-Aldrich, Deisenhofen, Germany
pGreenFire1-mCMV (EF1 $\alpha$ -puro) Lentivector	System Biosciences, Palo Alto, USA
Poly((ethylene-co-butylene)-b-(ethylene oxide) (P((E/B)-b-EO)) [234]	Max Planck Institute for Polymer Research, Mainz, Germany
Polyvinyl alcohol (PVA)	Sigma-Aldrich, Deisenhofen, Germany
Potassium bicarbonate (KHCO <sub>3</sub> )	Sigma-Aldrich, Deisenhofen, Germany
Potassium chloride (KCl)	Sigma-Aldrich, Deisenhofen, Germany
SDS	Sigma-Aldrich, Deisenhofen, Germany
Sodium chloride (NaCl)	Sigma-Aldrich, Deisenhofen, Germany
Sodium dodecyl sulfate (SDS)	Alfa Aesar, Heysham, UK
Streptomycin	Sigma-Aldrich, Deisenhofen, Germany
Terralin Liquid	Schülke & Mayr, Norderstedt, Germany
Toluene	Sigma-Aldrich, Deisenhofen, Germany
Triethylamine (TEA)	Sigma-Aldrich, Deisenhofen, Germany
Triphosgene	Sigma-Aldrich, Deisenhofen, Germany
Tris	Roth, Karlsruhe, Germany
Trypan blue	Sigma-Aldrich, Deisenhofen, Germany
Trypsin	Thermo Fisher Scientific, Waltham, USA
$\beta$ -Mercaptoethanol	Roth, Karlsruhe, Germany

**Table 2** Reagents and substances

## MATERIAL

### NOD1 ligands:

iE-DAP	Invivogen, Toulouse, France
Lauroyl group-modified iE-DAP (C12-iE-DAP)	Invivogen, Toulouse, France
L-Alanine-modified iE-DAP (Tri-DAP)	Invivogen, Toulouse, France

### NOD2 ligands:

MDP	Invivogen, Toulouse, France
Fluorescein (FITC)-labeled MDP (MDP-FITC)	Invivogen, Toulouse, France
Stearoyl group-modified MDP (L18-MDP)	Invivogen, Toulouse, France
Murabutide	Invivogen, Toulouse, France

### TLR ligands:

R848	Invivogen, Toulouse, France
CpG	Invivogen, Toulouse, France
Poly I:C (high molecular weight)	Invivogen, Toulouse, France
LPS	Invivogen, Toulouse, France

**Table 3** PRR ligands

## 2.3 Buffers, solutions, media

Name	Manufacturer / Formulation
Eagle's Minimum Essential Medium (EMEM)	Sigma Aldrich, Deisenhofen, Germany
Fetal calf serum (FCS)	Sigma Aldrich, Deisenhofen, Germany
Hank's Balanced Salt Solution (HBSS)	Thermo Fisher Scientific, Waltham, USA
Iscove's Modified Dulbecco's Medium (IMDM)	Sigma Aldrich, Deisenhofen, Germany
Phosphate-buffered Saline (PBS)	Sigma Aldrich, Deisenhofen, Germany
GM-CSF	Derived from X63.Ag8-653 myeloma cells stably transfected with murine GM-CSF expression construct [235]
Murine serum (mS)	Department of Dermatology, University Medical Center, Mainz, Germany
Human serum (hS)	Blood Transfusion Center, University Medical Center, Mainz, Germany
Human plasma (hP)	Blood Transfusion Center, University Medical Center, Mainz, Germany
2.4G2 blocking solution	PBS + CD16/CD32 antibodies (1:50)
50x TAE (pH 8.5)	2 M Tris 1 M Acetic acid 0.05 M EDTA-Na <sub>2</sub>
BMDC culture medium	IMDM + 5 % FCS + 50 µM β-mercaptoethanol + 2 mM L-glutamine + 100 U/ml penicillin + 100 µg/ml streptomycin + 5 % GM-CSF
Cell line medium	IMDM + 5 % FCS + 50 µM β-mercaptoethanol + 100 U/ml penicillin + 100 µg/ml streptomycin
Cytometric bead array (CBA) buffer	PBS + 1 % FCS
Fixation buffer	PBS + 0.7 % PFA
Flow cytometry buffer	PBS + 2 % FCS
Lysis buffer (pH 7.4)	155 mM NH <sub>4</sub> Cl 10 mM KHCO <sub>3</sub> 100 µM EDTA-Na <sub>2</sub>
Passive Lysis Buffer 5X	Promega, Madison, USA
PBS-EDTA	PBS + 2 mM EDTA-Na <sub>2</sub>
PEG-it Virus Precipitation Solution	System Biosciences, Palo Alto, USA
Staining Buffer	Promega, Madison, USA
T cell isolation buffer	EMEM + 2 % FCS + 100 U/ml penicillin + 100 µg/ml streptomycin

*MATERIAL*

Test medium / spleen cell medium	IMDM + 5 % FCS + 50 $\mu$ M $\beta$ -mercaptoethanol + 2 mM L-Glutamine + 100 U/ml penicillin + 100 $\mu$ g/ml streptomycin
Washing buffer	IMDM + 5 % FCS + 50 $\mu$ M $\beta$ -mercaptoethanol

**Table 4** Buffers, solutions, media

## 2.4 Consumables

Consumable	Manufacturer
µ-Slide 8 well chambered coverslips	Ibidi, Planegg, Germany
1 ml tips	Starlab, Hamburg, Germany
10/20 µl tips	Starlab, Hamburg, Germany
12 well suspension culture plates	Greiner Bio-One, Frickenhausen, Germany
200 µl tips	Starlab, Hamburg, Germany
24 well suspension culture plates	Greiner Bio-One, Frickenhausen, Germany
24 well tissue culture plates	Greiner Bio-One, Frickenhausen, Germany
48 well tissue culture plates	Greiner Bio-One, Frickenhausen, Germany
6 well suspension culture plates	Greiner Bio-One, Frickenhausen, Germany
6 well tissue culture plates	Greiner Bio-One, Frickenhausen, Germany
96 well tissue culture plates	Greiner Bio-One, Frickenhausen, Germany
Aluminum foil	Roth, Karlsruhe, Germany
Cell culture flasks 175 cm <sup>2</sup>	Greiner Bio-One, Frickenhausen, Germany
Cell culture flasks 25 cm <sup>2</sup>	Greiner Bio-One, Frickenhausen, Germany
Cell culture flasks 75 cm <sup>2</sup>	Greiner Bio-One, Frickenhausen, Germany
Cell strainer 40 µm	Greiner Bio-One, Frickenhausen, Germany
Cell strainer 70 µm	Greiner Bio-One, Frickenhausen, Germany
Centrifugal filter (100 kDa)	Merck Millipore, Darmstadt, Germany
Centrifuge tubes 15 ml	Greiner Bio-One, Frickenhausen, Germany
Centrifuge tubes 50 ml	Greiner Bio-One, Frickenhausen, Germany
Disposable syringes 1 ml	Braun, Melsungen, Germany
Disposable syringes 20 ml	BD Biosciences, Heidelberg, Germany
Glass fiber filters	Perkin Elmer, Waltham, USA
Microcentrifuge tubes 0.5 ml	Roth, Karlsruhe, Germany
Microcentrifuge tubes 1.5 ml	Eppendorf, Hamburg, Germany
Microcentrifuge tubes 2 ml	Eppendorf, Hamburg, Germany
Needles 20G x 1 1/2", 0.9 x 40	BD Biosciences, Heidelberg, Germany
Needles 25G x 5/8", 0.5 x 16	Braun, Melsungen, Germany
Nylon wool	Kisker Biotech, Steinfurt, Germany
Petri dishes Ø 94 mm	Greiner Bio-One, Frickenhausen, Germany
Polystyrene tubes 5 ml, round-bottom	Corning Inc., Corning, USA
Serological pipette 10 ml	Greiner Bio-One, Frickenhausen, Germany
Serological pipette 25 ml	Greiner Bio-One, Frickenhausen, Germany
Serological pipette 5 ml	Greiner Bio-One, Frickenhausen, Germany
Serological pipette 50 ml	Greiner Bio-One, Frickenhausen, Germany
Syringe filter, 0.22 µm	Merck Millipore, Darmstadt, Germany

**Table 5** Consumables

*MATERIAL*

## 2.5 Antibodies

Epitope	Reactivity	Label	Clone	Conc. [mg/ml]	Per sample [μl]	Manufacturer
CD11c	hamster - anti-mouse	Allophycocyanin (APC <sub>f</sub> )	N418	0.2	0.125	eBioscience, San Diego, USA
	hamster - anti-mouse	FITC	N418	0.5		eBioscience, San Diego, USA
	hamster - anti-mouse	Phycoerythrin (PE)/cyanine 7 (PE-Cy7)	N418	0.2	0.2	eBioscience, San Diego, USA
CD16/CD32	rat - anti-mouse	-	2.4G2	0.268	0.5	Department of Dermatology, University Medical Center, Mainz, Germany
CD19	rat - anti-mouse	PE	1D3	0.2	0.2	BD Biosciences, Heidelberg, Germany
	rat - anti-mouse	APC <sub>f</sub> /cyanine 7 (APC <sub>f</sub> -Cy7)	1D3	0.2	0.2	BD Biosciences, Heidelberg, Germany
CD209	rat - anti-mouse	-	LWC06	0.5	(see 3.1.3.2)	eBioscience, San Diego, USA
CD3e	hamster - anti-mouse	PE-Cy7	145-2C11	0.25	0.2	eBioscience, San Diego, USA
	hamster - anti-mouse	PE/cyanine 5 (PE-Cy5)	145-2C11	0.25	0.2	eBioscience, San Diego, USA
CD68	rat - anti-mouse	PE	FA-11	0.5	0.2	Biologend, San Diego, USA
CD80	hamster - anti-mouse	FITC	16-10A1	0.25	0.5	eBioscience, San Diego, USA
	hamster - anti-mouse	PE	16-10A1	0.3	0.2	BD Biosciences, Heidelberg, Germany
CD86	rat - anti-mouse	FITC	GL-1	0.5	0.5	eBioscience, San Diego, USA
	rat - anti-mouse	PE	GL-1	0.25	0.2	eBioscience, San Diego, USA
	rat - anti-mouse	PE-Cy7	GL-1	0.2	0.2	eBioscience, San Diego, USA
MHC class II I-A/IE	rat - anti-mouse	eFluor450	M5/114.15.2	0.5	0.2	eBioscience, San Diego, USA

**Table 6** Antibodies

## 2.6 Nanoparticles

Name	Modifications	Manufacturer
Dex-blank	-	AG Wich
Dex-MDP	MDP	AG Wich
Dex-R848	R848	AG Wich
Dex-MDP/R848	MDP + R848	AG Wich

Encapsulation measurements:

Dex-MDP-FITC	MDP-FITC	AG Wich
Dex-MDP-FITC/R848	MDP-FITC + R848	AG Wich

**Table 7** Dextran-based NPs used for experiments

Name	Modifications	Cross-linker	Manufacturer
OVA-NC	Cy5-Oligo	TDI	AK Landfester
OVA-DQ-NC	Cy5-Oligo, OVA-DQ	TDI	AK Landfester
OVA-MDP-NC	Cy5-Oligo, MDP	TDI	AK Landfester
OVA-R848-NC	Cy5-Oligo, R848	TDI	AK Landfester
OVA-MDP/R848-NC	Cy5-Oligo, MDP + R848	TDI	AK Landfester

Encapsulation measurements:

OVA-MDP-Alexa 488-NC	Cy5-Oligo, MDP-Alexa 488	TDI	AK Landfester
OVA-MDP-Alexa 488/R848-NC	Cy5-Oligo, MDP-Alexa 488 + R848	TDI	AK Landfester

Alternative cross-linking:

OT-DN-R848-NC	Cy5-Oligo, R848, OVA-based	TET / DN	AK Landfester
HT-DN-R848-NC	Cy5-Oligo, R848, HSA-based	TET / DN	AK Landfester

**Table 8** Protein-based NCs used for stimulation experiments

Name	Modifications	Manufacturer
OVA-PEG <sub>2000</sub> (2.47)	Cy5-Oligo, 2.47 PEG / cm <sup>2</sup>	AK Landfester
OVA-PEG <sub>2000</sub> (0.54)	Cy5-Oligo, 0.54 PEG / cm <sup>2</sup>	AK Landfester
OVA-PEG <sub>2000</sub> (0.18)	Cy5-Oligo, 0.18 PEG / cm <sup>2</sup>	AK Landfester
OVA-PEG <sub>3400</sub> (0.83)	Cy5-Oligo, 0.83 PEG / cm <sup>2</sup>	AK Landfester
OVA-PEG <sub>3400</sub> (0.22)	Cy5-Oligo, 0.22 PEG / cm <sup>2</sup>	AK Landfester
OVA-PEG <sub>5000</sub> (0.19)	Cy5-Oligo, 0.19 PEG / cm <sup>2</sup>	AK Landfester

**Table 9** PEGylated and antibody-modified OVA-NCs used for experiments

*MATERIAL*

<b>Name</b>	<b>Modifications</b>	<b>Manufacturer</b>
HES-NC	Cy5-Oligo	AK Landfester
HES-siRNA-NC	Cy5-Oligo, luciferase-siRNA	AK Landfester
HES-control-NC	control-siRNA (AF647)	AK Landfester
HES-PEG-NC	Cy5-Oligo, PEG	AK Landfester
HES-PEG-siRNA-NC	Cy5-Oligo, PEG, luciferase-siRNA	AK Landfester
HES-PEG-control-NC	PEG, control-siRNA (AF647)	AK Landfester

Targeting experiments:

HES-PEG-siRNA-DC-SIGN-NC	Cy5-Oligo, PEG, luciferase-siRNA, $\alpha$ DC-SIGN antibody	AK Landfester
HES-PEG-control-DC-SIGN-NC	PEG, control-siRNA (AF647), $\alpha$ DC-SIGN antibody	AK Landfester

**Table 10** HES-NC used for experiments



## 2.7 Kits

Kit	Application	Manufacturer
Alexa Fluor 488 5-SDP ester Labeling kit	Fluorescent labeling	Thermo Fisher Scientific, Waltham, USA
CBA Flex Set (IL-1 $\beta$ , IL-5, IL-6, IL-10, IL-12p70, IFN- $\gamma$ , TNF- $\alpha$ )	Cytokine measurement	BD Biosciences, Heidelberg, Germany
iScript cDNA Synthesis Kit	cDNA synthesis	Bio-Rad, Hercules, USA
Luciferase Assay System	Firefly luciferase measurement	Promega, Madison, USA
Pierce LAL (Limulus amoebocyte lysate) Chromogenic Endotoxin Quantitation Kit	Endotoxin measurement	Thermo Fisher Scientific, Waltham, USA
RNeasy Mini Kit	RNA isolation	Qiagen, Hilden, Germany

**Table 11** Commercial kits

## 2.8 Software

Software	Application	Manufacturer
Attune NxT software 2.6	Cytometric measurement / analysis	Thermo Fisher Scientific, Waltham, USA
BD FACSDiva 8.0	Cytometric measurement	BD Biosciences, Heidelberg, Germany
CFX Manager	Real-time PCR analysis	Bio-Rad, Hercules, USA
Database for Annotation, Visualization and Integrated Discovery (DAVID) 6.8	Bioinformatic resources and functional annotation tool	Leidos Biomedical Research, Reston, USA
FlowJo 7.6.5	Cytometric analysis	FlowJo, Ashland, USA
Geneious R8.0	Next-generation sequencing analysis	Biomatters, Auckland, New Zealand
ImageJ 1.5	Image analysis	NIH, Bethesda, USA
MestReNova 9.0.1	NMR spectroscopy	Mestrelab, Santiago de Compostela, Spain
MikroWin 2000	Microplate reader analysis	Labsis, Neunkirchen-Seelscheid, Germany
NTA software 3.0	Nanoparticle tracking analysis	Malvern Instruments, Herrenberg, Germany
Prism 5.01	Statistical analysis	GraphPad Software, La Jolla, USA
ZEN 2009	Image analysis	Carl Zeiss, Oberkochen, Germany

**Table 12** Software

## 3. Methods

### 3.1 Nanoparticles synthesis / characterization

#### 3.1.1 Dextran nanoparticles (Dex-NPs)

Spermine-functionalized and acetalated Dex (Sp-Ac-Dex, based on dextran 9-11 kDa) was synthesized as described by Fréchet *et al.* [236]. Sp-Ac-Dex particles were prepared using a double emulsion method, using a probe sonicator. For this, 10 mg Sp-Ac-Dex was dissolved in 800  $\mu$ l DCM and 100  $\mu$ l PBS or 70  $\mu$ g R848/MDP in 100  $\mu$ l PBS was added for the first sonication step of 10 s. In this way, four different dextran-based NPs were generated, empty, MDP-loaded, R848-loaded and MDP/R848-loaded ones. Then 4 ml PVA solution (3 wt% in PBS, 13-27 kDa, 87-89 % partially hydrolyzed) was added and the secondary water-in-oil-in-water emulsion was performed by sonication for 20 s. The resulting double emulsion was stirred overnight to remove all DCM by evaporation. Dex-NPs were purified by ultracentrifugation (45,000 x g, 20 min, 20 °C) and washed with H<sub>2</sub>O<sub>st</sub> (pH 8). Before lyophilization, 100  $\mu$ l of PVA solution (0.3 wt% in H<sub>2</sub>O<sub>st</sub>, pH 8) was added as cryoprotectant. The particle yield based on the initial Sp-Ac-Dex material was at 45 %.

The size of the Dex-NPs was determined by nanoparticle tracking analysis (NTA) with a NanoSight LM 10 microscope equipped with a green laser ( $\lambda = 532$  nm) and a sCMOS camera. All Dex-NP samples were measured after sonification for 20 s at concentrations of approximately 2  $\mu$ g per ml in PBS (purified through a 0.22  $\mu$ m filter). Dex-NP movements were recorded as videos of 30 s at 25 °C. The size calculation was performed with NTA software.

To quantify the encapsulated adjuvants, two additional particles were synthesized, including fluorescent MDP-FITC instead of MDP (Dex-MDP-FITC and Dex-MDP-FITC/R848). All particles (10 mg per ml) were initially dissolved in 0.3 M acetate buffer (pH 5) and incubated for 24 h. The MDP content was analyzed by using MDP-FITC ( $\lambda_{\text{ex}} = 495$  nm,  $\lambda_{\text{em}} = 525$  nm). R848 was measured by means of its own fluorescent properties ( $\lambda_{\text{ex}} = 260$  nm,  $\lambda_{\text{em}} = 360$  nm). The quantification was performed by fluorescent spectroscopy.

## METHODS

The concentration of encapsulated MDP-FITC and R848 was calculated with a calibration curve in the range of 0.0625 to 10 µg/ml. By these results, it was also possible to conclude the actual concentration of encapsulated non-labeled MDP in the other Dex-NP. In the experimental part of this work, Dex-MDP-FITC and Dex-MDP-FITC/R848 were exclusively used to analyze the binding/uptake of Dex-NPs by BMDCs. For DC stimulation assays, Dex-NPs containing non-fluorescent MDP were used to prevent problems due to potential functional differences between MDP and MDP-FITC.

Before use in cell culture, the Dex-NPs were dissolved in endotoxin-free water and adjusted to 1 mg/ml. The synthesis and chemical characterization of the Dex-NPs were performed by ... (Institute of Pharmacy and Biochemistry, Johannes Gutenberg-University, Mainz, Germany, group of ...).

### 3.1.2 Ovalbumin nanocapsules (OVA-NCs)

OVA-NCs were synthesized by an inverse miniemulsion process as previously described [237]. Briefly, 50 mg ovalbumin was dissolved together with 7.14 mg NaCl in 500 µl H<sub>2</sub>O<sub>st</sub>. 13 nmol Cy5-Oligo were added to the aqueous phase. Next, 35.8 mg of the surfactant P((E/B)-b-EO) were dissolved in 7.5 g of cyclohexane and added to the aqueous phase under stirring (500 rpm). The pre-emulsion was homogenized by ultrasonication. Separately, 10.7 mg P((E/B)-b-EO) were dissolved in 5 g of cyclohexane and 2 mg of the cross-linker TDI was added to the solution. This mixture was added dropwise to the obtained miniemulsion and the reaction was allowed to proceed for 24 h at 25 °C. Afterwards, excess of surfactant was removed from the obtained nanocapsules by repetitive centrifugation (3743 x g, 30 min, RT) and replacement of the supernatant with fresh cyclohexane. For the nanocapsule transfer to water, 600 µl of the dispersion from cyclohexane were added dropwise to 5 ml of a 0.1 wt% aqueous SDS solution placed in an ultrasound bath during transfer. The sample was stirred with an open cap overnight to evaporate cyclohexane. Subsequently, excess of SDS was removed via four centrifugation steps replacing the supernatant with H<sub>2</sub>O<sub>st</sub>. For loading of the nanocapsules with MDP and R848 respectively, 70 µl R848 (10 mg/ml in DMSO) and 250 µl MDP (10 mg/ml in H<sub>2</sub>O<sub>st</sub>) were used and the amount of water was reduced accordingly to maintain 500 µl of total

## METHODS

volume. In this way, four different OVA-NCs were generated, empty, MDP-loaded, R848-loaded and MDP/R848-loaded ones.

The sonication was performed for 3 min at 70 % amplitude with a pulse regime of 20 s sonication and 10 s pauses in between. Visual characterization of the OVA-NCs via transmission electron microscopy (TEM) was performed with an accelerating voltage of 120 kV and via scanning electron microscopy (SEM) with 170 V. 20  $\mu$ l of diluted NC dispersion was dropped either onto a 300 mesh carbon-coated copper grid (for TEM) or onto a silica wafer (for SEM) allowing drying under ambient conditions. Dynamic light scattering (DLS) was used to determine the average size and size distribution of the NCs. The measurements were performed at 25 °C using a submicron particle sizer at an angle of 90 °. Zeta potential of the capsules was measured in 10<sup>-3</sup> M KCl solution at pH 6.8 and 25 °C with a Zetasizer.

To determine adjuvant (MDP and R848) encapsulation, we modified MDP with an Alexa Fluor 488 5-SDP ester (MDP-Alexa 488), following the manufacturer's instructions, prior to capsule synthesis. For encapsulation measurement, two additional OVA-NCs were synthesized, including fluorescent MDP-Alexa 488 instead of MDP (OVA-MDP-Alexa 488-NCs and OVA-MDP-Alexa 488/R848-NCs). After synthesis, the supernatants of all nanocapsule dispersions were separated from the capsules by using a centrifugal filter with molecular weight cut-off of 100 kDa (3743 x g, 30 min, RT). The residue pellets of OVA-NCs were redispersed into 2 mg/ml of trypsin in PBS buffer and incubated for 24 h. The content of MDP-Alexa 488 was measured by using a microplate reader ( $\lambda_{\text{ex}} = 498$  nm,  $\lambda_{\text{em}} = 519$  nm) and calculated with a calibration curve in the range of 0.34 to 2.26  $\mu$ g/ml. The concentration of R848 was analyzed by measuring its characteristic absorbance at  $\lambda = 325$  nm by using UV-Vis spectroscopy and calculated with a calibration curve in the range of 0.01 to 1 mg/ml. MDP-Alexa 488 was exclusively used for encapsulation measurements. For stimulation assays with OVA-NCs, unmodified MDP was encapsulated.

OVA-DQ containing OVA-NCs, which were used to detect the nanocapsule degradation, were synthesized by adding 300  $\mu$ l of a DQ ovalbumin solution in PBS (1 mg/ml) to the aqueous phase during the synthesis process as described above. OVA-DQ describes OVA molecules which are heavily labeled with BODIPY FL fluorochrome, leading to a strong

## METHODS

quenching effect. Upon degradation of the OVA-DQ to peptides, the quenching effect is relieved. The fluorescence of the single, dye-labeled peptides can be measured ( $\lambda_{\text{ex}} = 505$  nm,  $\lambda_{\text{em}} = 515$  nm).

### 3.1.2.1 Alternative cross-linking of OVA-NCs

To optimize the properties of protein nanocapsules (such as cargo release, biocompatibility) and to avoid highly reactive isocyanates (e.g. TDI), we additionally tested a different cross-linking chemistry (bioorthogonal tetrazole-ene cycloaddition instead of TDI). For that purpose, a new batch of protein nanocapsules based on OVA and HSA respectively, was synthesized [238], in which the relatively unspecific cross-linker TDI was replaced by a combination of TET (conjugated to OVA (OT) and HSA (HT)) and DN (as cross-linker). This synthesis method is one of the fastest bioorthogonal reactions, is performed under ambient conditions and does not require any metal catalysts. Furthermore, it is triggered by UV light. To assess the suitability of these capsules as drug delivery system, the adjuvant R848 was encapsulated into OVA-based as well as in HSA-based nanocapsules.

### 3.1.2.2 PEGylation of OVA-NCs

To equip OVA-NCs with isocyanate PEG, the synthesis process was slightly modified. Instead of 2 mg TDI, 11.4 mg TDI was used for the cross-linking. After removing excessive surfactant by repetitive centrifugation (3,743 x g, 30 min, RT) and redispersion in cyclohexane, 2.5 ml cyclohexane was added into 2.5 ml of OVA-NC dispersion at 25 °C. 800  $\mu$ l of acetone solution of isocyanate PEG (PEG<sub>2000</sub>, PEG<sub>3400</sub> and PEG<sub>5000</sub>) at various concentrations was added dropwise into the capsule dispersion. The reaction was allowed to proceed for 4 h, and centrifuged for 30 min (3,743 x g, RT) afterwards to remove non-coupled PEG. The precipitate was redispersed in 600  $\mu$ l of cyclohexane. The final transfer into aqueous medium was performed similar to that of the non-PEGylated OVA-NCs.

<sup>1</sup>H-NMR spectroscopy was used to determine the number of PEG chains coupled to OVA-NCs. A glass capillary tube containing 5 % of DCM in deuterated DCM was used as a constant internal reference for all samples. The PEGylated OVA-NC dispersion was freeze-dried, re-dissolved in H<sub>2</sub>O<sub>st</sub>, and set for NMR measurement inside a second glass vial with the internal reference. Integration of the resonance corresponding to PEG units (at 3.5 ppm) was compared with the resonance of DCM (at 5.5 ppm) to quantify the amount of PEG

## METHODS

chains in the dispersion. The number of capsules in the dispersion could be calculated through the solid content, the average diameter of the capsules, and the polymer to water ratio in the capsule, by assuming that the density of the shell was  $1 \text{ g/cm}^3$ .  $^1\text{H-NMR}$  spectra were measured at 300 MHz with deuterated water as solvent and processed with the MestReNova software.

The synthesis and chemical characterization of all protein-based NCs were performed by ... (Max Planck Institute for Polymer Research, Mainz, Germany, group of ...).

### 3.1.3 Hydroxyethyl starch nanocapsules (HES-NCs)

The first step to generate PEGylated HES-NCs was to synthesize 1,2-bis(2-isocyanatoethoxy)ethane (hereafter referred to as diisocyanate). To do so, 4.5 g of 2,2'-(ethylenedioxy)bis(ethylamine) was dissolved together with 5.2 g of TEA in 8 ml of DCM, and added dropwise into a solution of 3 g of triphosgene in 30 ml of DCM, while the latter was cooled to  $4 \text{ }^\circ\text{C}$ . After finishing the addition, the system was kept at  $4 \text{ }^\circ\text{C}$  for 20 min, then at RT for 1 h, followed by refluxing at  $50 \text{ }^\circ\text{C}$  for 2 h. The solvent was then removed in vacuum, and the product extracted by diethyl ether. The product was checked by NMR and used without further purification in the next step.

1,500 mg of 2-azido-1-ethylamine was dissolved in 2 ml of diethyl ether, and added at a speed of 2 ml/h by a syringe pump into the diisocyanate solution to synthesize 1-(2-azidoethyl)-3-(2-(2-(2-isocyanatoethoxy)ethoxy)ethyl)urea. This specific product can be used to functionalize HES with an azide group at RT without any catalyst. After the addition, the solvent was removed at reduced pressure. The product was checked by infrared spectroscopy (IR), redissolved in DMF without further purifications and subsequently added dropwise into a solution of 500 mg of HES (with a theoretical degree of substitution of 3) in 6 ml DMF. The reaction was allowed to proceed for 48 h, and the product was purified by dialysis against  $\text{H}_2\text{O}_{\text{st}}$  in a dialyzing tube with a molecular weight cut-off of 14 kDa, while the solution was freeze dried to obtain 520 mg of product (azide-HES) afterwards.

To synthesize siRNA-loaded HES-NCs, 50 mg of azide-HES, 20 nmol of siRNA (Luciferase GL2 Duplex siRNA or AF647-labeled AllStars Negative Control siRNA) and

## METHODS

10 nmol of Cy5-Oligo were dissolved in 460  $\mu\text{l}$   $\text{H}_2\text{O}_{\text{st}}$  as the aqueous phase, while 70  $\mu\text{g}$  of P((E/B)-b-EO) was dissolved in a mixture of 5 g cyclohexane and 2 g toluene (oil phase). The water phase was shaken gently at 40 °C for 3 h to ensure the complete solvation of azide-HES. Afterwards, it was mixed with the oil phase, stirred magnetically at 200 rpm for 30 min, followed by ultrasonication at 70 % amplitude for 3 min with a pulse of 20 s on and 10 s off at 0 °C. 80 mg of HDDP was dissolved together with 20 mg P((E/B)-b-EO) in 800  $\mu\text{l}$  of toluene and added into the system after sonication. The whole system was magnetically stirred at 500 rpm for 5 days, while the temperature was kept at 50 °C.

The encapsulation efficiency of HES-NCs was measured based on the release of the model drug D-mannosamine. A fluorogenic reaction between that substance and fluorescamine was used to quantify the drug release. Both empty and D-mannosamine-loaded HES-NCs were prepared and transferred into water. A standard working function of fluorescamine and D-mannosamine was established, while the same concentration of empty capsules was added in all the stock solutions of D-mannosamine. The water dispersion of D-mannosamine-loaded capsules was tested under the same conditions, to measure free D-mannosamine that was released from the HES-NCs.

### 3.1.3.1 PEGylation of HES-NCs

For a typical coupling reaction, 2 ml of the HES-NC dispersion was centrifuged at 4,000 rpm for 30 min to remove the excess of surfactant. The upper phase was discarded, while the precipitate was redispersed in 2.5 g of cyclohexane by pipetting up and down. Either 16 mg of isocyanate PEG<sub>5000</sub> or isocyanate-PEG<sub>5000</sub>-isocyanate was dissolved in 0.63 g (800  $\mu\text{l}$ ) of acetone and added dropwise into the capsule dispersion, which was magnetically stirred at 500 rpm. The reaction was allowed to proceed for 5 h, and centrifuged at 4,000 rpm afterwards to remove non-coupled PEG. The precipitate was redispersed in 400  $\mu\text{l}$  of cyclohexane and used for further steps.

### 3.1.3.2 Antibody-modification of HES-NCs

A 0.1 wt% SDS solution was prepared and filtered (0.2  $\mu\text{m}$  pore size). 5 ml of this SDS solution was gently shaken in a sonication bath, while nanocapsules (from 2 ml of the prepared dispersion) were redispersed in 400  $\mu\text{l}$  of cyclohexane and added slowly. Then the whole dispersion was magnetically stirred with 1,000 rpm at RT overnight in an open vial

## METHODS

to allow evaporation of the cyclohexane. The obtained dispersion was ultrafiltrated by a centrifugal filter with a molecular weight cut-off of 100 kDa in order to remove the excess of SDS.

To obtain azide-functionalized antibodies, 0.4 mg of anti-DC-SIGN antibodies were dissolved in 400  $\mu\text{l}$  of PBS buffer, and the pH was adjusted to  $7.60 \pm 0.05$ . A stock solution of  $1.16 \times 10^{-3}$  mg of NHS-PEG4-azide in DMSO was added, which was 3.7 mol equivalent to the antibody. The reaction was allowed to proceed for 1 h, while the excess of NHS-PEG4-azide was removed by dialyzing.

500  $\mu\text{l}$  of 0.8 M boric acid solution was added to 5 ml of the HES-NC dispersion with a solid content of 0.1 wt%. The pH of the solution was adjusted to 8.3 and different amounts of DBCO-PEG4-NHS (prepared as a stock solution of 1 mg in 1ml DMSO) were added. The reaction was allowed to proceed for 4 h, uncoupled DBCO was removed by ultrafiltration. Coupled DBCO was quantified by a fluorogenic reaction with anthracene azide. Azide-functionalized anti-DC-SIGN antibodies were added with a 1:1 molar ratio to the coupled DBCO. The general two-step procedure to modify HES-NCs with antibodies is summarized in Figure 5.

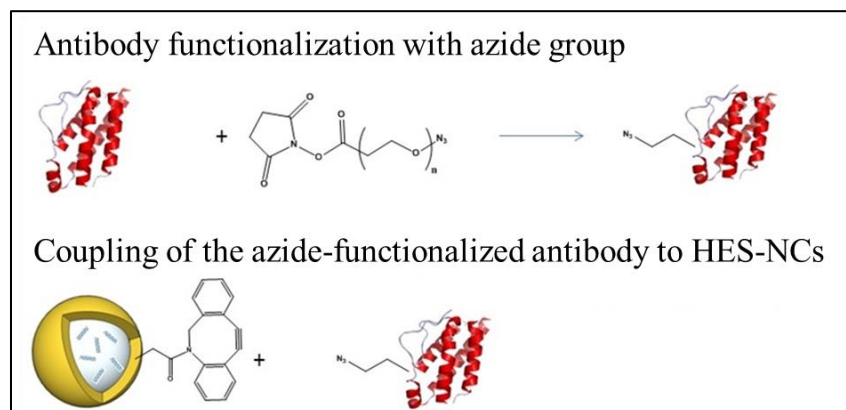


**Figure 5** Antibody-modification of HES-NCs

Surface modification of HES-NCs with antibodies is based on two major steps. The first one is the initial functionalization of the antibody with an azide group by NHS-PEG4-azide. The second step includes the coupling of the azide-functionalized antibody to the DBCO-functionalized HES-NC (adapted from [239]).



## METHODS

The synthesis and chemical characterization of all HES-NC formulations were performed by ... (Max Planck Institute for Polymer Research, Mainz, Germany, group of ...).

### 3.2 Mice

Wildtype C57BL/6 and transgenic OT-I and OT-II (both C57BL/6 background) mice were bred and maintained in the Translational Animal Research Center of the University Medical Center Mainz under pathogen-free conditions on a standard diet. The recommendations of the Guide for the Care and Use of Laboratory Animals by the National Institutes of Health were followed. CD8<sup>+</sup> OT-I T cells recognize OVA<sub>257-264</sub> peptides in the context of H-2K<sup>b</sup>, and CD4<sup>+</sup> OT-II T cells are specific for OVA<sub>323-339</sub> peptide in the context of H-2 I-A<sup>b</sup> and I-A<sup>d</sup> [240].

### 3.3 Primary immune cells

All primary immune cells were obtained from mice. They were grown and treated in specific cell culture media and maintained at 37 °C and 10 % CO<sub>2</sub>. In all experiments the cells were handled under sterile conditions.

#### 3.3.1 Generation of bone marrow-derived dendritic cells

BMDCs were differentiated from bone marrow progenitors of 8- to 10-week old C57BL/6 mice as described by Bros *et al.* [241]. Initially, the mice were sacrificed by cervical dislocation and cleaned with ethanol. Both femur and tibia bones as well as the os ilium were removed by carefully peeling off the fur from the knee joint up to the back and dissecting the legs. BM cells were obtained by flushing the isolated bones with washing buffer. Potential bone fragments were removed with a cell strainer. Following centrifugation (300 x g, 10 min, 4 °C), the cell pellet was resuspended in 1 ml lysis buffer (pH 7.4) to eliminate erythrocyte contamination via osmotic shock. After stopping the lysis by adding 49 ml washing buffer, the cells were centrifuged again as described before. The cells were then counted with a Neubauer chamber and the cell concentration adjusted to 2 x 10<sup>6</sup> BM cell per ml. To analyze stimulation assays (see 3.5.1) and nanoparticle interaction assays (see 3.5.2) via flow cytometry, the BM cells were seeded in 12 well suspension culture plates with BMDC culture medium (2 x 10<sup>5</sup> cells / 1.25 ml) and cultured at 37 °C and 10 % CO<sub>2</sub>. At day 3, 500 µl of the same medium was added into each well. On day 6, 1

## METHODS

ml of the old medium was replaced with 1 ml fresh medium per well. On day 7, the BMDC differentiation was complete and the cells were treated directly in the well. For the other DC assays, the BM cells were seeded on petri dishes ( $2 \times 10^6$  cells / 10 ml). On day 3 and 6, additional 5 ml of BMDC culture medium was added into these dishes. Aliquots of non-adherent and loosely adherent BMDCs were harvested on day 7 of culture, centrifuged ( $300 \times g$ , 10 min, RT), counted and reseeded in wells of 6 well (for transcriptome analysis, see 3.10), 24 well (for T cell proliferation assays, see 3.5.3 and 3.9) as well as 48 well (for cytometric bead arrays, see 3.5.1 and 3.7, and confocal microscopy analysis, see 3.5.2 and 3.8) tissue culture plates in BMDC culture medium.

### 3.3.2 Isolation of spleen cells

Spleen cells were isolated from spleens of C57BL/6 mice. To do this, the animal was first sacrificed by cervical dislocation and cleaned with ethanol to sterilize the area of interest, namely the left lower back. After making an incision of 1-2 cm through the skin and the peritoneal wall, the spleen was grasped with a curved forceps and gently pulled out. Redundant connective tissue was removed and spleen cells were isolated by carefully grinding the spleen through a cell strainer into spleen cell medium. Next, the cells were centrifuged ( $300 \times g$ , 10 min,  $4^\circ\text{C}$ ) and remaining erythrocytes were lysed by adding 1ml of lysis buffer (pH 7.4) to the cell pellet for 1 min. After stopping the lysis with 49 ml of spleen cell medium, the splenocyte suspension was centrifuged again and counted. For treatment (see 3.5.5), the freshly isolated spleen cells were then seeded on 24 well suspension culture plates in a volume of 1 ml spleen cell medium per well ( $1 \times 10^6$  cells/ml).

### 3.3.3 Isolation of OT-I/OT-II T cells

To isolate T cells from transgenic OT-I and OT-II mice, splenocytes of the corresponding animals were obtained as described in the previous section and transferred to 1 ml T cell isolation buffer. The resulting suspension was passed over nylon wool columns to enrich T cells and to get rid of unwanted immune cells. To do so, each column was placed in a 50 ml centrifuge tube and equilibrated with 20 ml T cell isolation buffer for 45 min at  $37^\circ\text{C}$  in the water bath. Afterwards, the buffer was removed and the column was washed twice with 10 ml of fresh pre-warmed buffer. The spleen cell suspension was dripped centrally onto the

## METHODS

column, followed by adding additional 500 µl of buffer. Afterwards, the tube including the column was closed, transferred to the water bath and incubated for 45 min at 37 °C again. The T cells were eluted with 20 ml of T cell isolation buffer, centrifuged (300 x g, 10 min, 4 °C) and counted in 2 ml test medium. Finally, the T cells were ready for co-culture experiments (see 3.5.3).

### 3.4 Cell lines

Human HEK293T [242] and murine DC2.4 [58, 243] were grown in cell line medium. Cells were maintained at 37 °C and 10 % CO<sub>2</sub>, and were handled under sterile conditions.

#### 3.4.1 Generation of DC2.4-mCMV by lentiviral transduction

HEK293T cells were co-transfected with a lentiviral vector encoding destabilized luciferase and the green fluorescent protein (GFP) 2 from the copepod *Pontellina plumata* (copGFP) under control of a minimal CMV (mCMV) promoter and a puromycin resistance gene driven by the EF1 promoter (pGreenFire1-mCMV+EF1 $\alpha$ -puro), and helper plasmids (pCMV-dR8.91, pMD2.G) to generate replication-deficient HIV1-based VSV-G pseudotyped lentiviral particles as described [244]. Supernatants harvested 2 and 3 days later were pooled, and lentiviral particles were concentrated 100-fold as recommended by the manufacturer. DC2.4 cells ( $5 \times 10^5$  cells in 1 ml) were seeded into 6-well tissue culture plates, and were transduced with 50 µl of lentiviral particle solution. After 2 days, puromycin (2 µg/ml) was added to select puromycin-resistant DC2.4 (DC2.4-mCMV). The generated cell line was grown under continuous puromycin selection and aliquots of DC2.4-mCMV were stored in liquid nitrogen. The components and the protocol for the lentiviral transduction were kindly provided by ... (Department of Dermatology, University Medical Center, Mainz).

Prior to experiments with this cell line, required amounts of aliquots were thawed and transferred to 10 ml cell line medium each supplemented with 2 µg/ml puromycin (in 25 cm<sup>2</sup> cell culture flask). After a few days, the culture medium, containing floating (dead) cells, was discarded. Attached cells were detached by adding 5 ml of PBS-EDTA for 3 min. The resulting suspension was centrifuged (300 x g, 10 min, RT). Afterwards, the pellet was resuspended in 15 ml fresh cell line medium and the cell suspension was transferred into a

## METHODS

75 cm<sup>2</sup> cell culture flask (+ 2 µg/ml puromycin). At a confluency of approximately 80 %, medium was discarded and the cells were detached by adding 5 ml PBS-EDTA again for 3 min. After centrifugation, the pellet was dissolved in 5 ml of fresh cell line medium. 100 µl of this suspension was added to a new 75 cm<sup>2</sup> flask with 14.5 ml cell line medium (+ 2 µg/ml puromycin). The mentioned process of detaching and reseeding was repeated each time the confluency reaches 80 % again. After approximately the third passage the cells can be used for experiments. Between each n of an experiment were at least three passages.

### **3.5 *In vitro* cell culture**

#### **3.5.1 Dendritic cell stimulation assays**

The stimulatory effect of different adjuvants and adjuvant combinations was determined via flow cytometry (expression of co-stimulatory molecules) as well as cytometric bead array (secretion of cytokines). For the former, BMDCs on day 7 of differentiation were treated with specific adjuvants and adjuvant-loaded nanocarriers (in 12 well suspension culture plates, see 3.3.1) as indicated in the figure legends for 24 h. All non-encapsulated substances were dissolved (supplied lyophilized) in endotoxin-free water and applied to the cells under sterile conditions. After incubation, cells were harvested and transferred into polystyrene tubes for cytometric analysis (see 3.6).

To measure adjuvant-triggered cytokine secretion, day 7 BMDCs were seeded in 48 well tissue culture plates (1 x 10<sup>6</sup> cells in 1 ml BMDC culture medium per well, see 3.3.1) and treated with different amounts of adjuvants, adjuvant combinations and adjuvant-loaded nanocarriers (indicated in the figure legends) for 24 h. Afterwards, supernatants were collected and secreted cytokines measured via cytometric bead array (see 3.7).

#### **3.5.2 Nanoparticle interaction assays**

The interaction of BMDCs with nanoparticulate formulations was assessed by applying defined amounts of NPs to the cells and, after incubation, subsequent analysis of NP binding, uptake and degradation based on NP's fluorescent label. For cytometric analysis (see 3.6), cells were treated in 1 ml BMDC culture medium in 12 well suspension culture plates (see 3.3.1) and collected in polystyrene tubes after expiration of the incubation times

## METHODS

as indicated in the figure legends. Similar to the BMDC assays, the interaction of DC2.4-mCMV (see 3.4.1) with variously modified HES-NC was analyzed by incubating the cell line with those nanocapsules. To measure the interaction via flow cytometry,  $3 \times 10^5$  cells per sample were treated with certain amounts of HES-NC for 24 h. After that, cells were collected in polystyrene tubes for cytometric analysis.

Cellular interaction with NPs was also analyzed via confocal microscopy (see 3.8). Therefore, BMDCs ( $3 \times 10^5$  cells in 400  $\mu$ l BMDC culture medium) as well as DC2.4-mCMV ( $3 \times 10^5$  cells in 400  $\mu$ l cell line medium) were treated with NPs in 48 well tissue culture plates (see 3.3.1) as indicated. Afterwards, the samples were stained, transferred to chambered coverslips and imaged.

To assess the influence of endocytosis on NP uptake, the interaction assays for flow cytometry and confocal microscopy were partly performed at 4 °C. Energy-dependent engulfing processes, such as clathrin- or caveolae-dependent endocytosis, can be slowed down by reducing the temperature [245]. At 4 °C these processes are almost completely inhibited. A reduced fluorescence signal at 4 °C indicates a reduced cellular uptake of NPs.

Required quantities of NPs were calculated on the basis of known stock concentrations. Before use, NP formulations were checked for turbidity and suspended sediment. Suspicious samples were rejected. Additionally, all NP formulations were tested for potential endotoxin contaminations by LAL assay (see 3.11). In accordance with recommendations of the FDA, an endotoxin concentration of 0.5 EU/ml was used as permitted maximum [246].

### **3.5.3 Dendritic cell co-culture with T cells**

To measure the capacity of BMDCs, treated with protein nanocapsules, to trigger proliferation of antigen-specific T cells,  $10^6$  cells were incubated with the different OVA-NCs or soluble OVA as control in 24 well tissue culture plates for 12 h. Afterwards, some samples were stimulated with LPS (100 ng/ml) or Dex-NPs as indicated. After 6 h of additional incubation, all BMDC samples were harvested and thoroughly washed. Splenic OT-I and OT-II T cells (see 3.3.3) were co-cultured with serially diluted BMDCs (starting with  $10^4$ ) in triplicates in a volume of 0.2 ml of test medium on 96 well tissue culture plates

## METHODS

for four days. Co-culture supernatants were collected for T cell cytokine measurement (see 3.7). T cell proliferation was assessed as genomic incorporation of [Methyl-<sup>3</sup>H] thymidine (see 3.9).

### 3.5.4 Luciferase knockdown assay

To determine the efficiency of HES-NC to transport functional siRNA into DC2.4-mCMV, luciferase-specific siRNA (Luciferase GL2 Duplex, not labeled) and non-coding siRNA (AllStars Negative Control, AF647-labeled) respectively, were encapsulated into HES-NC (see 3.1.3). DC2.4-mCMV cells were seeded onto 24 well tissue culture plates (1 x 10<sup>5</sup> cells in 1 ml per well) 24 h prior to HES-NC treatment. The medium was replaced with 500 µl fresh medium per well. Afterwards, the siRNA-loaded HES-NC (300 µg/ml) were added to the cells in triplicates. As positive control, cells were transfected with luciferase-specific siRNA (5 pmol per well) via lipofectamine, according the manufacturer's instructions. After incubation for 24 h, the cells were lysed with Passive Lysis Buffer and luciferase activity was measured with a Centro LB 960 Microplate Reader and the MikroWin 2000 software.

### 3.5.5 Nanoparticle binding with spleen cells

The interaction of splenocytes with NPs was assessed by seeding freshly isolated spleen cells (see 3.3.2) on 24 well suspension culture plates in a volume of 1 ml spleen cell medium. Spleen cells were treated with adjuvant-loaded OVA-NCs as indicated in the figure legends. Cellular binding by DCs, macrophages, B and T cells was assessed by measuring the resulting frequencies of NC-positive cells in flow cytometry. Additionally, DCs and macrophages were tested for their activation status. To prepare the samples for the subsequent cytometric analysis (see 3.6), they were collected in polystyrene tubes.

## 3.6 Flow cytometry

Flow cytometry describes a laser-based biophysical method to identify cell populations and to analyze them distinctly. This high-throughput machinery enables the quantification of thousands of cells and particles in real time on the basis of their size, granularity and biomarker expression. For this purpose, the flow cytometer is equipped with a flow cell and

## METHODS

a complex composition of lasers, optical modules, mirrors, bandpass filters and detectors. This setup is complemented by a computer system for raw data acquisition (Figure 6).

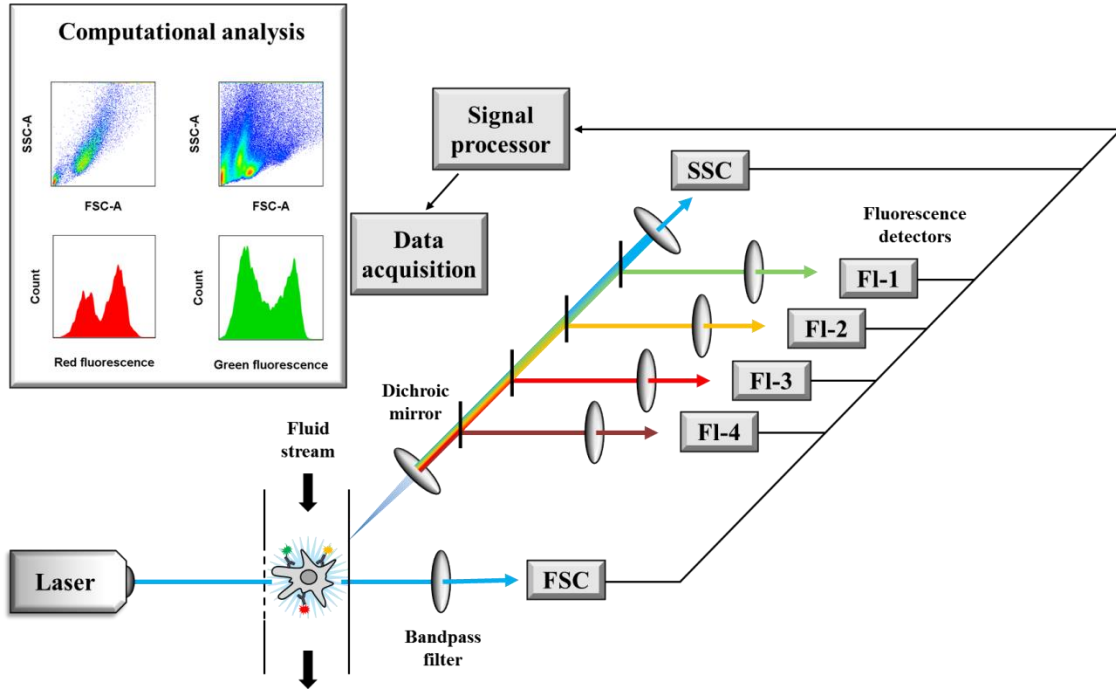


**Figure 6** Schematic illustration of a flow cytometer

Cells in the laminar fluid stream are exposed to distinct laser wavelengths. As a result, cell-associated fluorochromes are excited and emit fluorescence. By a complex arrangement of mirrors and filters, the different emissions are guided to their corresponding detectors. Resulting signals are processed and flow cytometric raw data is acquired for further analysis.

The scattering and emission of optical signals is used to differentiate cells. If a sample is inserted into the flow cytometer, the containing cells are guided by a laminar fluid stream through a capillary and pass specific optical modules one by one. There, the cells are exposed to lasers of defined wave lengths. The beam of one laser (488 nm) is scattered by the size and granularity of the cell and the resulting scattered light is detected. Thereby, the forward scatter (FSC) results from the cell size (measurable as area FSC-A, height FSC-H, and width FSC-W), the side scatter (SSC) is based on the cell granularity (measurable as area SSC-A, height SSC-H and width SSC-W). These two parameters enable a first

## METHODS

differentiation of cell populations by their size and granularity. Moreover, distinct cell subpopulations can be identified by staining characteristic biomarkers with fluorochrome-labeled antibodies or ligands prior to cytometric analysis. Cellular interaction with NPs can be analyzed by using fluorescent-labeled nanocarriers and measuring the proportion of cells positive for the corresponding fluorescence. Excited by defined laser wavelengths, the fluorochromes emit fluorescence that is sensed by detectors. In this way, cells can be classified into biomarker/NP positive and negative. By the use of selected laser, filter and detector combinations, it is possible to analyze various biomarkers in parallel. However, it is essential to ensure that the absorption and emission spectra of the fluorochromes do not overlap. Otherwise, a compensation of the corresponding fluorochromes is necessary.

In this thesis, the flow cytometry was used as an essential tool to investigate the interaction of immune cells with different nanoparticulate system and to examine if the used nanocarriers fulfil their intended immunological effect. Moreover, the capacities of various adjuvants and adjuvant combinations to induce an increased expression of the co-stimulatory molecules CD80 and CD86 was assessed, among others, by this method.

### 3.6.1 Cell surface staining

For flow cytometric analysis, cellular surface biomarkers were stained by initially centrifuging (300 x g, 10 min, 4 °C) the samples in polystyrene tubes and discarding the supernatants. Cell pellets were resuspended in 1ml pre-cooled staining buffer per sample and centrifuged again (300 x g, 10 min, 4 °C). Afterwards, the pellets were resuspended and 25 µl of 2.4G2 solution (0.268 mg/ml, 1:100 in staining buffer) was added to each sample and incubated for 15 min at RT to block Fc receptor-mediated staining. The final staining step was performed by applying 50 µl of a prepared master mix (labeled antibodies in staining buffer, diluted according to 2.5) to each sample. The samples were incubated for 30 min at 4 °C and the staining was stopped by adding 1 ml of staining buffer per sample. Remaining antibodies were removed by washing the samples once with 1 ml staining buffer each as described above. Finally, each sample was resuspended in 500 µl fixation buffer.

The samples were measured with the two flow cytometers FACS Canto II (equipped with the FACSDiva software) and the Attune NxT (equipped with the Attune NxT software). All measurements of a project section were done with the same device. Cell characterization



## METHODS

and subpopulation definition were performed by the use of gating strategies, systematical procedures to visually partition the initial population by the means of size, granularity, biomarker expression and nanocarrier signals step by step. For each specific question, an individual gating strategy was prepared. Each strategy served as template for all following experiments with the corresponding NP. For spectral compensation, unstained controls and single-stained samples were prepared in parallel. Cell doublets, so cell agglomerates that can potentially give false positive results, were excluded when indicated.

In this way, it was possible to i) identify specific cell populations (Table 13), ii) analyze BMDC activation levels (by CD80 and CD86 expression) and iii) measure NP binding/uptake/degradation by different immune cell types (with NP-specific fluorescence signals) very precisely. Flow cytometric data was finally processed with the FlowJo software. The gating strategies used in this thesis were attached in the Supplementary Data (see 8.1).

<b>Cell population</b>	<b>Identification markers</b>
DCs / BMDCs	CD11c <sup>+</sup> , MHC-II <sup>+</sup>
Macrophages	CD68 <sup>+</sup> , MHC-II <sup>+</sup>
B cells	CD19 <sup>+</sup> , MHC-II <sup>+</sup>
T cells	CD3 <sup>+</sup> , MHC-II <sup>-</sup>

**Table 13** Identification of cell populations in flow cytometry

### 3.6.2 Viability measurement

Cellular viability is an additional parameter that can be measured by flow cytometry. For that purpose, ether fluorescent-labeled molecules that bind apoptosis/necrosis markers or fluorescent substances that intercalate into DNA are usually used to detect dying or dead cells. Viability of NP-treated immune cells ( $1 \times 10^6$  cells/ml) was assessed by incubating the cells with at least the highest NP concentrations used in the experiments (OVA-NCs: 150  $\mu\text{g/ml}$ ; Dex-NPs: 100  $\mu\text{g/ml}$ ; HES-NCs: 300  $\mu\text{g/ml}$ ) for 24 h (see 3.5.2). Untreated cells as well as cells treated with soluble adjuvants were analyzed for comparison. As

## METHODS

positive control, cells were supplemented with 10 vol-% DMSO. Subsequently, samples were harvested and transferred to polystyrene tubes. 1 ml of HBSS was added to each sample, followed by centrifugation (300 x g, 10 min, 4 °C). The supernatants were discarded. Afterwards, the cells were treated with Alexa Fluor 647-labeled Annexin V (0.3 µl in 50 µl HBSS per sample) to stain surface-exposed phosphatidylserine of apoptotic cells, and 7AAD (2.5 µl in 50 µl HBSS per sample) to identify necrotic/late apoptotic cells. Similar to trypan blue, 7AAD is able to intercalate into chromosomal DNA of dying cells. The samples were mixed and incubated for 15 min at RT. After adding 300 µl HBSS to each sample, they were stored on ice till measurement. The ratios of apoptotic as well as necrotic/late apoptotic cells were determined via flow cytometry by plotting the signals of Annexin V against the signals of 7AAD. Cells negative for both Annexin V and 7AAD were defined as living. By additionally measuring the frequencies of early apoptotic (Annexin V<sup>+</sup> 7AAD<sup>-</sup>), necrotic (Annexin V<sup>-</sup> 7AAD<sup>+</sup>) and double-positive late apoptotic/necrotic (Annexin V<sup>+</sup> 7AAD<sup>+</sup>) cells, the cytotoxicity of a nanoparticulate formulation for a distinct cell type was finally evaluated (Figure 7).

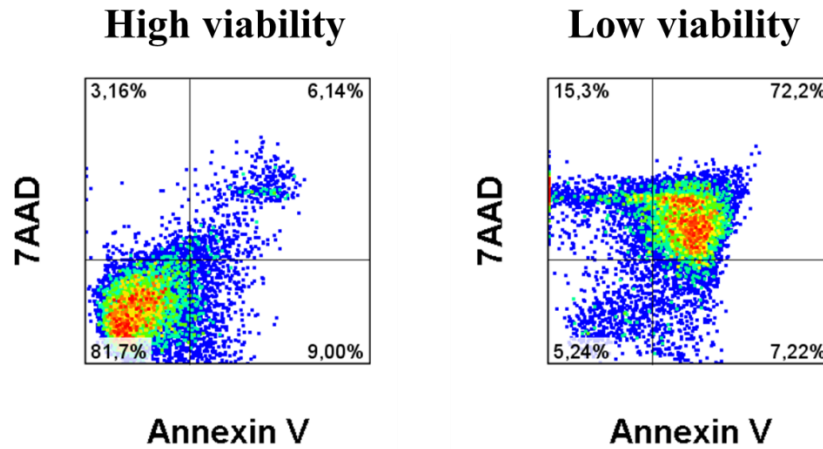


**Figure 7** Viability measurement via 7AAD/Annexin V double staining

Representative dot plots show cell samples with high (left) and low (right) viability after undergoing viability staining with 7AAD and Annexin V. The displayed percentages in the four sections indicate to what proportion the cells are viable (Annexin V<sup>-</sup> 7AAD<sup>-</sup>), early apoptotic (Annexin V<sup>+</sup> 7AAD<sup>-</sup>), necrotic (Annexin V<sup>-</sup> 7AAD<sup>+</sup>) or late apoptotic/necrotic (Annexin V<sup>+</sup> 7AAD<sup>+</sup>).

### 3.7 Cytokine measurement via cytometric bead array

In addition to the expression of cell surface markers, the secretion of pro- and anti-inflammatory cytokines is also an important parameter to characterize an immunological reaction. Distinct cytokine patterns enable conclusions to be drawn on the type of immune response. For instance, certain cytokines are markers for defined T cell subsets. An increased secretion of one of these cytokines can indicate the presence of a specific T cell subset, associated with its unique features. Furthermore, cytokine concentrations can be used to assess the strength and efficiency of an immune response and also to detect immune suppression.

The basic principle of CBA is to catch free cytokines with beads (capture-beads) which were modified with cytokine-specific antibodies and a precisely defined amount of two different fluorochromes (APC<sub>f</sub>/APC<sub>f</sub>-Cy7). As a result, each cytokine-specific bead has its own fluorescent fingerprint to be distinguishable from the others. After adding fluorescent-labeled detection antibodies (PE, detection-antibodies), which are all labeled to the same extent and specific for other epitopes of the cytokines, the bead-bound cytokines are ready for quantification via flow cytometer.

Cytokine levels in BMDC culture medium and BMDC/T cell co-culture supernatants were measured by cytometric bead array (Table 14), following the manufacturer's instructions. After treatment, samples were centrifuged (300 x g, 10 min, 4 °C) and supernatants were collected and frozen till bead analysis. Samples for testing were then thawed. In parallel, master mixes for capture-beads and detection-antibodies as well as a cytokine standard dilution series (from 0 to 10,000 pg/ml) were prepared. To capture the cytokines, 10 µl of each sample was mixed with 10 µl of capture-beads master mix (0.2 µl of each required bead filled up with CBA buffer to 10 µl in total). After 1 h incubation in the dark at RT, 10 µl of detection-antibodies master mix (0.2 µl of each required antibody filled up with CBA buffer to 10 µl in total) was added to each sample. The samples were incubated again for 1 h under the same conditions and washed once with 1 ml CBA buffer. Afterwards, the samples were resuspended in 100 µl CBA buffer and had to be measured within an hour.

Source	Quantified cytokines
BMDCs	IL-1 $\beta$ , IL-6, IL-10, IL-12, TNF- $\alpha$
BMDC/T cell co-culture	IFN- $\gamma$ , IL-5, IL-10

**Table 14** Cytokines quantified via cytometric bead array

### 3.8 Confocal laser scanning microscopy

For visual clarification of biological and medical questions, various microscopic methods are available. In contrast to the commonly used conventional light microscopy, fluorescence microscopy enables the detection of single molecules or low-molecular structures, such as proteins or specific chromosomal regions, on the basis of fluorescence emissions. Therefore, targets of interest are tagged with fluorescence-labeled target-specific antibodies or substances. Alternatively, the sequence of a fluorescent protein (e.g. GFP) can be integrated into a specific locus in the DNA (under the control of a present promoter) to detect the protein distribution all over the cell. After excitation of the fluorescent components with distinct laser wavelengths, the resulting emissions can be detected and visualized with a combination of detection and processing units. Similar to flow cytometry, it is possible to detect a number of fluorescent sources simultaneously as long as their emission spectra do not overlap. However, resolution and contrast of the common fluorescence microscopy is technically limited. It is not possible to determine the exact spatial position of a signal. Especially when you investigate the interaction of immune cells with nanoparticulate formulations, it is essential to know if and to what extent NPs are bound and taken up by cells. Flow cytometry enables to differentiate between fluorescence positive and negative cells, but it lacks distinctive features of extra- and intracellular signals. Intracellular localization of NPs allows a prediction of the particles' intracellular fate.

A precise three-dimensional analysis of distribution and localization of fluorescence signals (such as labeled NPs) can be achieved by confocal laser scanning microscopy (CLSM), an advanced fluorescence-based imaging technique for increased resolution and contrast. By the use of a spatial pinhole, it is possible to detect light derived exclusively from the focus plane, while emitted light from planes above and below (out-of-focus background) is

## METHODS

effectively excluded. Thus, the resolution and the contrast of the focus plane are increased. To reconstruct the three-dimensional fluorescence distribution in a sample and, thereby, analyze the spatial localization of a specific fluorescence source, a series of multiple images (optical sections) of different planes of a sample are capture this way (Figure 6).

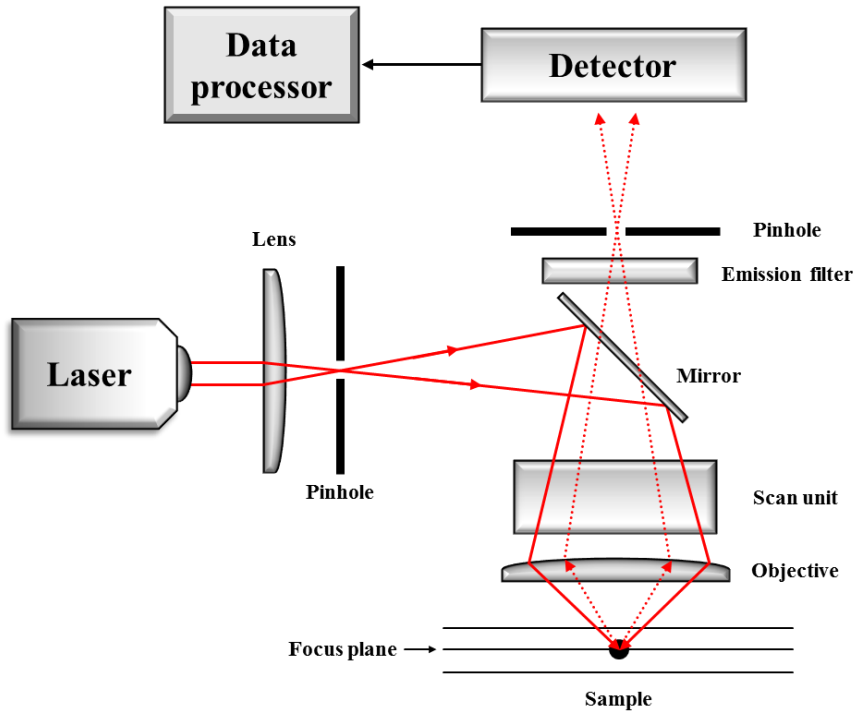


**Figure 8** Light path in a confocal laser scanning microscope

Laser light, which is initially focused by lens and pinhole, is directed through the objective to the sample planes by galvanometric mirrors. Emission from the focus plane is guided through objective, emission filters and adjustable pinhole and reaches emission detectors. Resulting data is transmitted to the data processor for visualization.

Due to these properties, the CLSM is a suitable method to study the interaction of immune cells with nanomaterials. Otherwise, it is difficult to evaluate if a NP is actually taken up. Accordingly, it perfectly complements the spectrum of methods to assess the interaction in its entirety.

## METHODS

In this study, CLSM was used to analyze the cellular uptake and fate of specific NPs in DCs. Therefore, NPs used for CLSM were all labeled with an appropriate fluorochrome. Apart from the evaluation of NP uptake and localization, CLSM was also used to detect intracellular degradation of OVA-NCs in BMDCs by visualizing the fluorescence emission resulting from the cleavage of OVA-DQ (see 3.1.2). Furthermore, the intracellular localization of dye-labeled siRNA released from HES-NC was performed with DC2.4mCMV. All samples were imaged with a LSM 710 in cooperation with ... (I. Medical Clinic, University Medical Center, Mainz, Germany). Images were processed and analyzed with ImageJ and ZEN software.

### 3.8.1 Membrane / cell core staining

To visualize plasma membrane and cell core, the 48 well plates containing the samples were centrifuged (300 x g, 8 min, RT). The supernatants were discarded and cells were redispersed with 200  $\mu$ l PBS per well. After two additional centrifugation (300 x g, 8 min, RT) and redispersion (200  $\mu$ l PBS per well) steps, 2  $\mu$ l of a DAPI solution (1:100 dilution of a 10 mg/ml stock) was added to each sample to stain cell cores. Samples were incubated in the dark at RT for 45 min. Then the washing procedure (mentioned above) was repeated two times. Before imaging, each sample was mixed with 1  $\mu$ l CellMask Orange (1:50 dilution of stock) to stain the plasma membrane and transferred to chambered coverslips. DAPI ( $\lambda_{\text{ex}} = 358$  nm,  $\lambda_{\text{em}} = 461$  nm) and CellMask Orange ( $\lambda_{\text{ex}} = 554$  nm,  $\lambda_{\text{em}} = 567$  nm) were detected and visualized on the basis of their fluorescent properties. In this way, it was possible to image plasma membranes and cell cores and thus to reconstruct the three-dimensional cell proportions.

### 3.8.2 Nanoparticle detection

The interaction analysis of cells with NPs via fluorescence microscopy requires NP localization in relation to cellular compartments. To be able to detect NPs in CLSM, they have to be modified with a fluorochrome. In this study, either Cy5-Oligo (directly encapsulated,  $\lambda_{\text{ex}} = 649$  nm,  $\lambda_{\text{em}} = 670$  nm) or AF647 (covalently bound to encapsulated siRNA) were used to visualize the NPs. In combination with membrane and cell core staining (see 3.8.1), the NP distribution over the cell can be determined very precisely. Additionally, it enables a differentiation between membrane bound and internalized NPs.

### 3.9 T cell proliferation assay

T cell proliferation in BMDC co-culture with OT-I/OT-II T cells (see 3.5.3) was measured by genomic incorporation of [Methyl-<sup>3</sup>H] thymidine (0.25 µCi/well), added for the last 16 h of culture. Cells were harvested and transferred to glass fiber filters. The retained radioactivity of the methyl tritium was assessed quantified with a liquid scintillation counter.

### 3.10 Transcriptome analysis

To analyze the transcriptome, so the totality of all RNA molecules, of BMDCs treated with MDP/R848-loaded OVA-NCs, the next-generation sequencing (NGS) method RNA-Seq (also called “whole transcriptome shotgun sequencing”) was performed. With this method one is able to visualize the RNA composition and quantity of a single cell or a cell population at a defined time point [247]. In general, RNA-Seq is divided into three steps: i) Fragmentation and purification of the isolated RNA, ii) converting RNA into complementary DNA (cDNA) and adding sequencing adapters (cDNA library) and finally iii) sequencing of the prepared library. In the subsequent bioinformatic data analysis, the sequencing results are aligned to reference genomes to identify and quantify abundant RNAs. The NGS experiments in this thesis were performed and analyzed together with ... (Max Planck Institute for Polymer Research, Mainz, Germany, group of ...).

#### 3.10.1 RNA isolation

For RNA isolation, BMDCs ( $2 \times 10^6$  cells in 1 ml per well) were seeded into 6-well suspension culture plates in BMDC culture medium. 24 h later, cells were treated with MDP/R848-loaded OVA-NCs as well as empty OVA-NCs (both 75 µg/ml, see 3.1.2) in biological triplicates for 1, 2 and 4 hours. Untreated BMDCs were used as negative control. The three time points of each sample were pooled afterwards. The total RNA of the samples was extracted with the RNeasy Mini Kit, following the manufacturer’s instructions. The RNA quality was controlled by agarose gel electrophoresis, RNA quantity photometrically with a NanoDrop 8000. Then, the total RNA was transferred to StarSEQ (Mainz, Germany) to do additional quality and quantity tests and, subsequently, to perform the RNA-Seq.

## METHODS

### 3.10.2 RNA sequencing

RNA-Seq was performed by StarSEQ. For that reason, the transferred samples were checked regarding RNA quality and quantity. Afterwards, mRNA was isolated from the total RNA, among other things, to get rid of ribosomal RNA. After cDNA library preparation, the samples were sequenced by an Illumina NextSeq 500 (Illumina, San Diego, USA). In total, 25 million paired-end reads (150 nucleotides (nt) per read) were created per sample (3.75 giga base pairs (Gbp) per sample). Data were obtained in the .fastq format.

### 3.10.3 Quantification of NGS data

The received RNA-Seq data were quantified by using the Geneious software. Initially, the .fastq files were imported. Low quality nucleotides were trimmed off (cutoff = 10 base pairs) and paired-end reads were assembled. The murine reference genome (mus musculus, C57BL/6) was obtained by the National Center for Biotechnology Information (NCBI) in the .fasta format (GCF\_000001635.26\_GRCm38.p6\_genomic.fna) and annotations were added in .gff format (GCF\_000001635.26\_GRCm38.p6\_genomic.gff). The pre-processed data sets were aligned against the reference sequence including all 21 chromosomes and also mitochondrial DNA. The same alignment settings were used for all samples (Table 15).

Setting	Mode
Sensitivity	Custom
Fine tuning	Iterate 2 times
Trim sequences	Do not trim
Map multiple best matches	Randomly
Allow gaps	Yes
Maximum gaps per read	3 %
Maximum gap size	5,000
Minimum overlap	No
Word length	24
Index word length	14
Ignore words repeated more than	8 times
Maximum mismatches per read	10 %
Maximum ambiguity	4
Accurately map reads with errors to repeat regions	No



## METHODS

Use paired read distances to improve assembly	Yes
Search more thoroughly for poor matching reads	No
Only map paired reads which match nearby	No

**Table 15** Settings for RNA-Seq quantification with the Geneious software.

With the help of the Geneious software, sequence overlaps were quantified and the final transcripts per kilobase million (TPM) values for all detectable genes were calculated and exported to Excel. The subsequent pathway analysis was based on these values. The quantification of the NGS raw data and the corresponding setting evaluation were performed by ....

### 3.10.4 Pathway analysis

Pathway analysis enables the identification of cellular signaling pathways which are associated with a list of genes. To generate lists of upregulated genes, the TPM mean values of the biological duplicates were calculated initially. By dividing the TPM mean values of each gene of one sample (numerator) by the TPM mean values of another sample (denominator), the mean enrichment scores for each gene were determined. A positive mean enrichment score indicates a gene, that is stronger expressed in the numerator sample than in the denominator sample. Consequently, dividing the TPM mean values of a sample of interest by the ones of a control sample provides a mean enrichment score for every gene in this sample comparison. For instance, an enrichment score of 5 means a five times higher expression of the specific gene.

For every sample combination, a gene list, comprising genes that showed a mean enrichment score of at least 2, was generated. These lists were uploaded to online software DAVID Bioinformatics Resources 6.8 into the Functional Annotation Tool with the identifier "OFFICIAL\_GENE\_SYMBOL". By means of the KEGG pathway database, the gene lists were aligned to prominent signaling pathways. Finally, the software generates a chart showing all relevant signaling pathways and the number of associated genes.

## METHODS

### 3.10.5 Real-time polymerase chain reaction

To be able to check the RNA-Seq results with a different method, the RNA samples were also analyzed by quantitative real-time polymerase chain reaction (qPCR). Therefore, qPCR primers for several genes (upregulated, downregulated and balanced) were designed for the amplification of ~200 bp DNA fragments. The RNA samples were initially transcribed into cDNA by a cDNA Synthesis Kit according to the manufacturer's instructions. Subsequently, the primers were mixed with SYBR Green and cDNA templates (Table 16) and transferred to the real-time system CFX96 for cyclic amplification and measurement of SYBR Green dye. The qPCR procedure followed a defined protocol (Table 17). SYBR Green fluorescence was recorded after each round of amplification and afterwards for the determination of a melt curve, supported by the CFX manager software.

Substance	Amount
iQ SYBR Green Supermix	10 $\mu$ l
F-Primer	1 $\mu$ l
R-Primer	1 $\mu$ l
cDNA template	3-100 ng
Nuclease-free water	To 20 $\mu$ l

**Table 16** Composition of the qPCR mixture

Finally, gene expression was calculated by using the  $\Delta\Delta C_t$  method [248]. GAPDH was used as a reference gene. The melt curve was analyzed carefully for successful amplification of target DNA fragments.

Step	Temperature / °C	Length	Count	
1	Equilibrium	50	2 min	1 x
2	Initial Denaturation	95	10 min	1 x
3	Denaturation	95	15 sec	40 x
	Annealing	Variable (52-62)	30 sec	
	Elongation	72	30 sec	
4	Final Elongation	72	10 min	1 x
5	Equilibrium	50	5 sec	1 x
6	Melt curve determination	50-95	-	1 x
7	Storage	4	$\infty$	$\infty$

**Table 17** qPCR protocol

### **3.11 Endotoxin quantification**

Before use, all NP formulations were checked for endotoxin contaminations. Therefore, aliquots of the corresponding formulations were prepared, matching the final working concentrations of the cellular assays. The measurement was done with the Pierce LAL Chromogenic Endotoxin Quantitation Kit, following the manufacturer's instructions. Briefly, a series of endotoxin standards in the range of 0.1 to 1 EU/ml was prepared. Endotoxin free water was used as negative control. Standards, samples of interest and negative control were transferred to a 96 well tissue culture plate (50  $\mu$ l per sample) in duplicates. 50  $\mu$ l of LAL reagent was added to each well. The plate was incubated for 10 min at 37 °C. Subsequently, 100  $\mu$ l of chromogenic substrate solution was applied to each sample. After additional 6 min of incubation at 37 °C, the reaction was stopped by adding 100  $\mu$ l of stop reagent (25 % acetic acid) to each well. The absorbance was measured at 405-410 nm on a microplate reader. The average absorbance of the negative control was subtracted from the average absorbance of all standards and samples. A standard curve was generated by plotting the resulting absorbance of the endotoxin standards in Excel. This curve was used to quantify the samples endotoxin contaminations. Thereby, the coefficient of determination,  $R^2$ , had to be  $\geq 0.98$ . In accordance with recommendations of the FDA, an endotoxin concentration of 0.5 EU/ml was used as permitted maximum [246].

### **3.12 Statistical analysis**

Data are presented as means  $\pm$  SD (standard deviation) of the values. Data were analyzed by applying Student's t test using GraphPad Prism. A p value of less than 0.05 was considered to be statistically significant.

## 4. Results

### 4.1 One nanocarrier for DC-directed T cell stimulation

An essential objective of this project was to generate and evaluate a nanocarrier that combines the two main components of a vaccine, antigen and adjuvant in an effective manner. Therefore, an adjuvant combination that showed stimulatory synergies for BMDCs was identified first. Next, this combination was encapsulated in Dex-NPs and thoroughly tested to be sure that it maintains its effects. Afterwards, OVA-NCs were evaluated as an antigen delivery system for BMDCs to mediate OVA-specific T cell proliferation. To align these two approaches, the adjuvant combination was encapsulated into OVA-NCs to generate a nanocarrier that has both properties. To check if adjuvant-loaded OVA-NCs featured the intended functionality, the capsules' effect on BMDCs in the context of DC maturation and DC-mediated OVA-specific T cell stimulation was assessed. To understand the interplay between BMDCs and adjuvant-loaded OVA-NCs in more detail and on a deeper analysis level, the transcriptome of accordingly treated BMDCs was analyzed by RNA-Seq. Interaction assays with spleen cells were additionally performed to test, which splenic immune cell population showed a preference to bind OVA-NCs. Finally, a different cross-linking method for OVA-NCs was evaluated as a potential alternative for the controversially discussed cross-linker TDI.

#### 4.1.1 Potent NLR and TLR ligands as adjuvants for DC stimulation

Adjuvant-mediated immune stimulation is one of the key factors of an effective vaccination. But the underlying mechanisms are versatile. A first step to realize an effective nanovaccine was to identify a suitable adjuvant combination. It is well-known, that some combinations provide stimulatory synergies, which may enable a reduction of the required adjuvant doses and thus weaker side effects.

One project idea was to target differently localized intracellular PRRs addressing in particular a combination of a NLR and a TLR. Since the effects of NLR ligands were less predictable due to their poor membrane penetrability and the cytosomal receptor localization, six NLR ligands (according to the manufacturer's recommendations) were

## RESULTS

initially tested in different concentrations for their BMDC stimulatory effect based on the expression of co-stimulatory molecules (Figure 9). Three ligands were specific for NOD1 and three for NOD2. The analysis was performed via flow cytometry and based on the attached gating strategy (see Figure S 1).

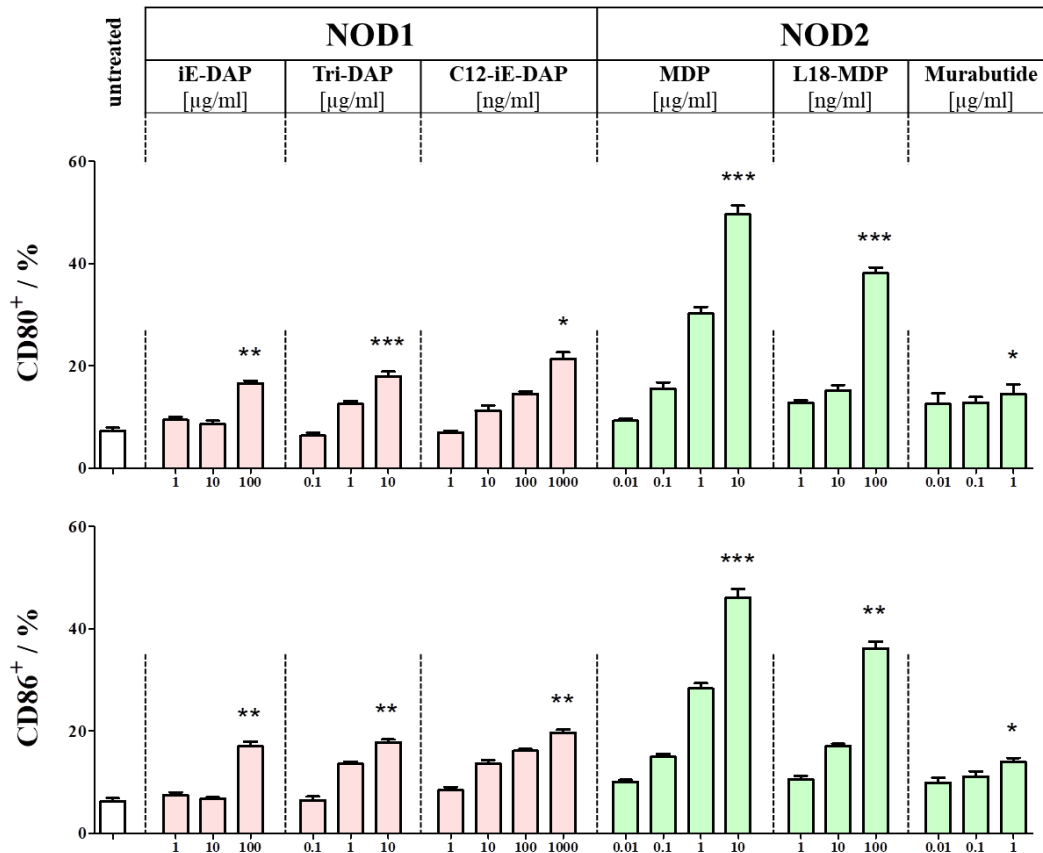


**Figure 9** Stimulatory effects of NLR ligands on CD80 and CD86 expression in BMDC

BMDCs ( $2 \times 10^5$  cells/ml) were treated with three NOD1 and three NOD2 ligands. The adjuvants were applied as indicated for 24 h. Frequencies of CD80 and CD86 in  $CD11c^+/MHC-II^+$  BMDCs after *in vitro* stimulation were measured by flow cytometry (mean  $\pm$  SD; n=3). \*p < 0.05, \*\*p < 0.01, \*\*\*p < 0.001, sample versus (vs.) untreated.

The results indicated that all tested NLR ligands exert a detectable dose-dependent stimulatory effect on BMDCs. Particularly the highest concentrations of each adjuvant

## RESULTS

induced a significantly increased expression of CD80 and CD86 after an incubation of 24 h. The NOD2 ligands MDP and L18-MDP turned out to be the most potent BMDC stimulators in the setup, whereas Murabutide, a synthetic derivative of MDP, evoked the weakest stimulation. Since L18-MDP, a stearyl group-modified MDP, showed the strongest stimulatory effect on BMDCs, this NLR ligand was chosen to be tested for potential synergies when combined with TLR ligands. Thereby, L18-MDP served as an effective representative of MDP, since it carries the minimal NOD2 motif and shows good membrane penetrability due to its hydrophobicity. To identify synergistic or rather superadditive NLR/TLR combinations with L18-MDP, three commonly used TLR ligands, which are specific for endosomal TLRs, were picked for experimental setup: Poly I:C (engages TLR3), R848 (TLR7/8) and CpG (TLR9).

### 4.1.2 Identification of (L18-)MDP + R848 as superadditive combination

To assess potential superadditive stimulatory effects, BMDCs were treated with L18-MDP in combination with either the TLR3 ligand Poly I:C, the TLR7 ligand R848, or the TLR9 ligand CpG for 24 h. All substances were applied simultaneously into the corresponding samples. The stimulatory capacities of these agents were evaluated on the basis of the expression of co-stimulatory molecules (via flow cytometry) and the secretion of pro-inflammatory cytokines (via cytometric bead array). For cytometric measurements, all adjuvants were used in three concentrations as indicated in the figure legends. The analysis was done as shown in the gating strategy (see Figure S 1). To assess the induction of cytokine secretion, the highest concentration of each adjuvant was used.

The measurement of CD80 and CD86 expression after administration of those adjuvants revealed diverse patterns of superadditive cooperation. Especially, the combined application of L18-MDP with Poly I:C and R848, respectively, showed increased stimulatory effects compared with the single adjuvant ones. This was particularly the case when focusing on the mean fluorescence intensities (MFIs) of CD86 (also by those of CD80 but weaker). There it seemed that the combination of 100 ng/ml of L18-MDP with either 1 µg/ml Poly I:C or 100 ng/ml R848 induced a significantly higher CD86 expression than the addition of the single agents. In this context it was remarkable that Poly I:C alone did not induce a detectable stimulation, whereas it exerted superadditive stimulatory effects

## RESULTS

when combined with L18-MDP. In contrast, R848 triggered CD80 and CD86 upregulation in a dose-dependent manner. Moreover, when applied in combination with L18-MDP this effect was even more enhanced (Figure 10). CpG as potent TLR9 ligand showed no relevant superadditive cooperation with L18-MDP in this setup. Increases in CD80/CD86 expression of L18-MDP (100 ng/ml) treated BMDCs by additional administration of CpG (5-500 ng/ml) were consistently non-significant (ns).

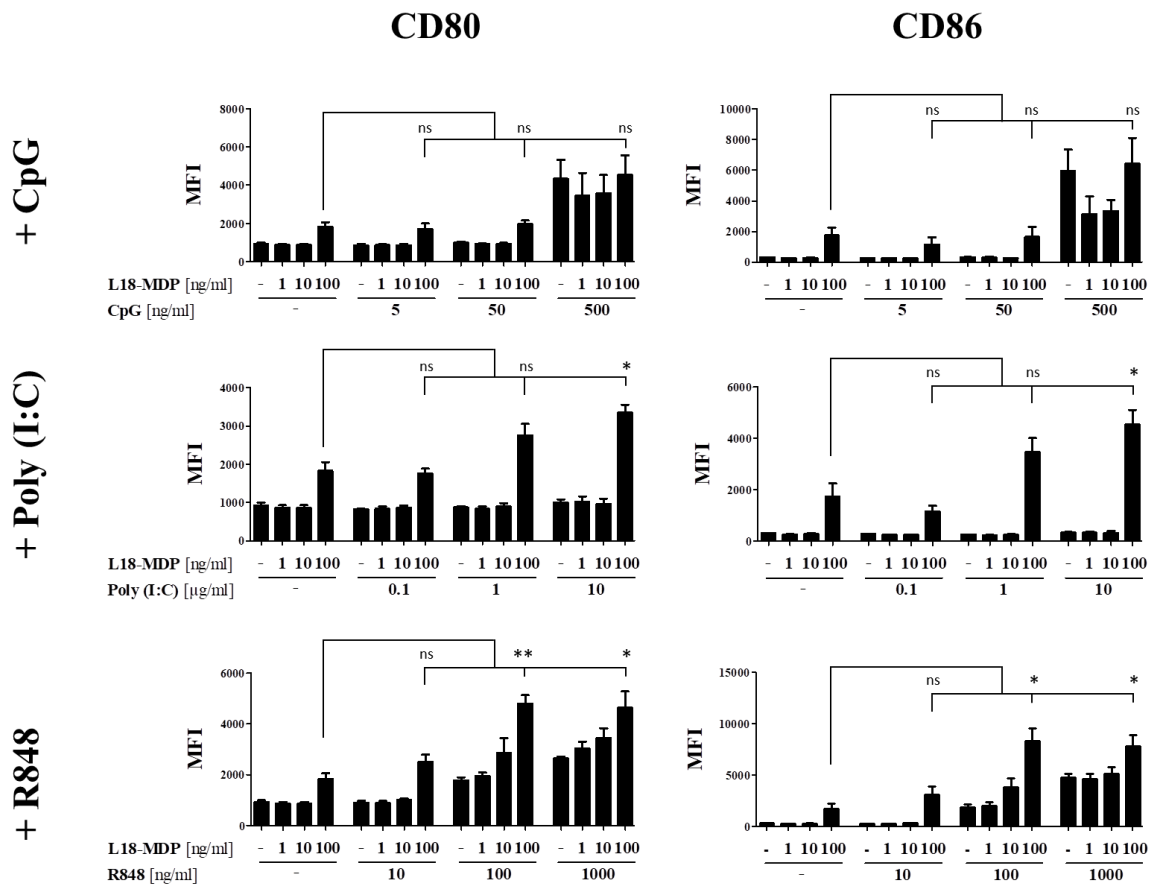


**Figure 10** Identification of superadditive TLR/NLR ligand combinations by MFIs

BMDCs ( $2 \times 10^5$  cells/ml) were analyzed for CD80 and CD86 expression after 24 h treatment with different TLR ligands and L18-MDP, alone or in combination as indicated, via flow cytometry. CpG (5-500 ng/ml), Poly I:C (0.1-10  $\mu$ g/ml) and R848 (10-1000 ng/ml) were applied simultaneously to L18-MDP (1-100 ng/ml). Identification of possible superadditive effects was done on the basis of MFIs (mean  $\pm$  SD;  $n=3$ ). \* $p < 0.05$ , \*\* $p < 0.01$ . Data and figure published in the Journal of Controlled Release [249].

## RESULTS

In contrast to the MFIs, CD80 and CD86 frequencies did not enable a comprehensive differentiation between differentially stimulated BMDCs (see Figure S 2). Accordingly, the final assessment of superadditive effects was based on the MFI results.

Potential superadditive effects regarding the induction of cytokine secretion were analyzed by cytometric bead array. Therefore, the supernatants of adjuvant-treated samples were collected and analyzed for cytokines. The resulting cytokine patterns allowed drawing conclusions about the stimulatory capacity of the corresponding adjuvants, the pro- or anti-inflammatory character of stimulation, and the theoretical phenotype of a subsequent stimulation-associated T cell polarization. IL-1 $\beta$ , IL-6, IL-12 and TNF- $\alpha$ , as prominent pro-inflammatory markers of DC stimulation, as well as IL-10, a typical anti-inflammatory cytokine, were selected for analysis. The cytokine secretion induced by L18-MDP alone was consistently low, partly comparable to that of the untreated control. However, when combined with CpG, Poly I:C or R848, significantly increased concentrations of IL-6, TNF- $\alpha$  and IL-12 were detectable. Nonetheless, the overall IL-12 levels were very low. As in the flow cytometric analysis, the stimulatory effect of Poly I:C alone was marginal. The secretion of IL-1 $\beta$  was clearly enhanced after treatment with the combination L18-MDP + R848. The other two combinations did not reveal such an effect. Measurements of the anti-inflammatory cytokine IL-10 showed superadditive effects in case of L18-MDP combined with Poly I:C or R848 (Figure 11). LPS was used as a well-established positive control.

Since R848 turned out to be the most promising partner for L18-MDP to achieve a sufficient stimulation, the experimental focus was placed on this combination. In both flow cytometric analysis of co-stimulatory receptor expression and measurement of pro- and anti-inflammatory cytokine secretion, this combination evoked the strongest superadditive effects on BMDCs. The results for L18-MDP and R848 were summarized in one figure (Figure 12).



## RESULTS

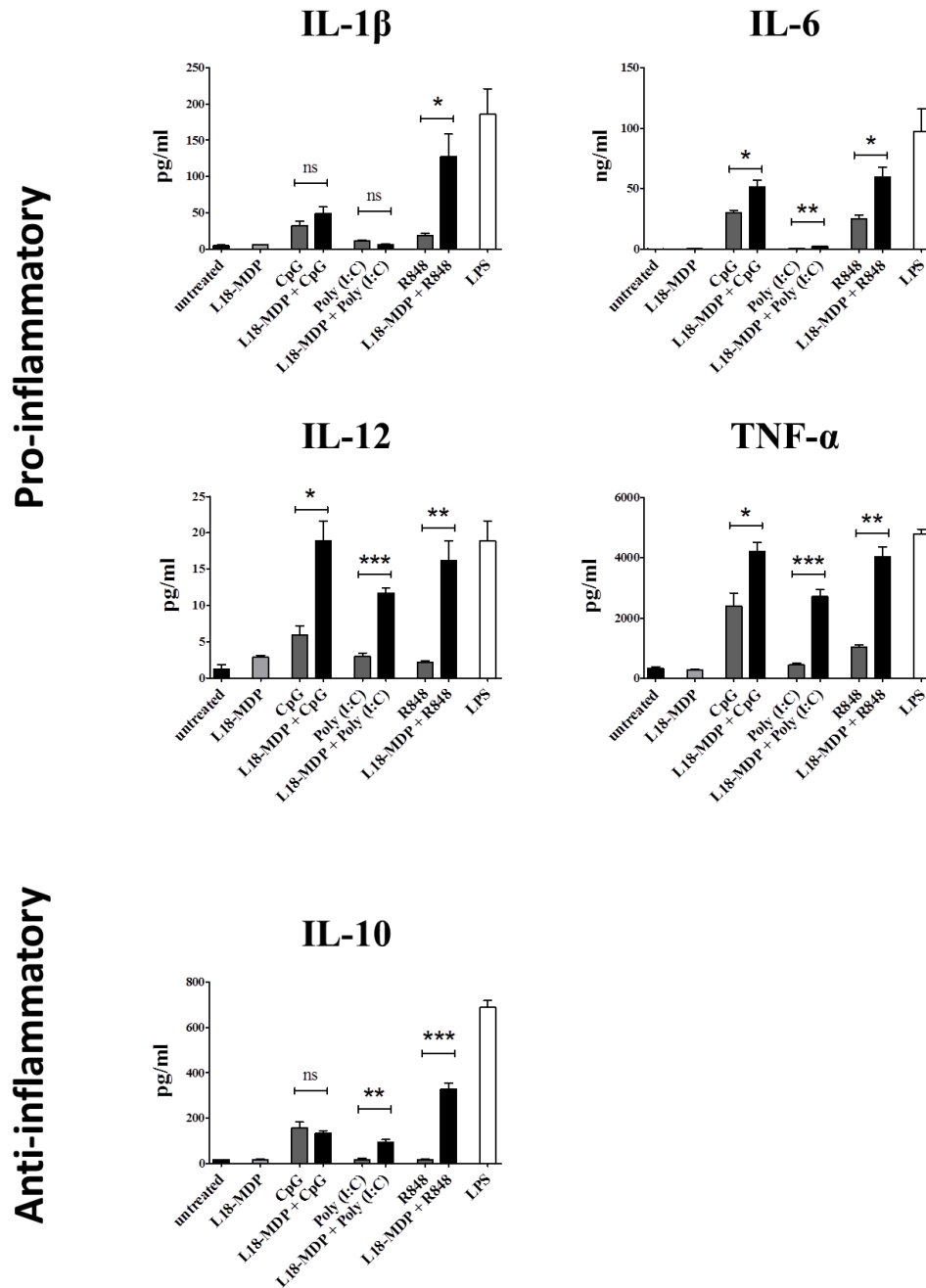


**Figure 11** Cytokine profiles after treatment with soluble TLR/NLR ligand combinations

Cytokine (pro-inflammatory: IL-1 $\beta$ , IL-6, IL-12, TNF- $\alpha$ , anti-inflammatory: IL-10) concentrations in supernatants of BMDCs ( $1 \times 10^6$  cells/ml) treated with the NOD2 ligand L18-MDP (100 ng/ml) in combination with the TLR ligands CpG (500 ng/ml), Poly I:C (10  $\mu$ g/ml) or R848 (100 ng/ml) for 24 h were assessed by cytometric bead array. Untreated as well as LPS-treated (100 ng/ml) BMDCs were used as control (mean  $\pm$  SD; n=3). \*p < 0.05, \*\*p < 0.01, \*\*\*p < 0.001. Data and figure published in the Journal of Controlled Release [249].

## RESULTS

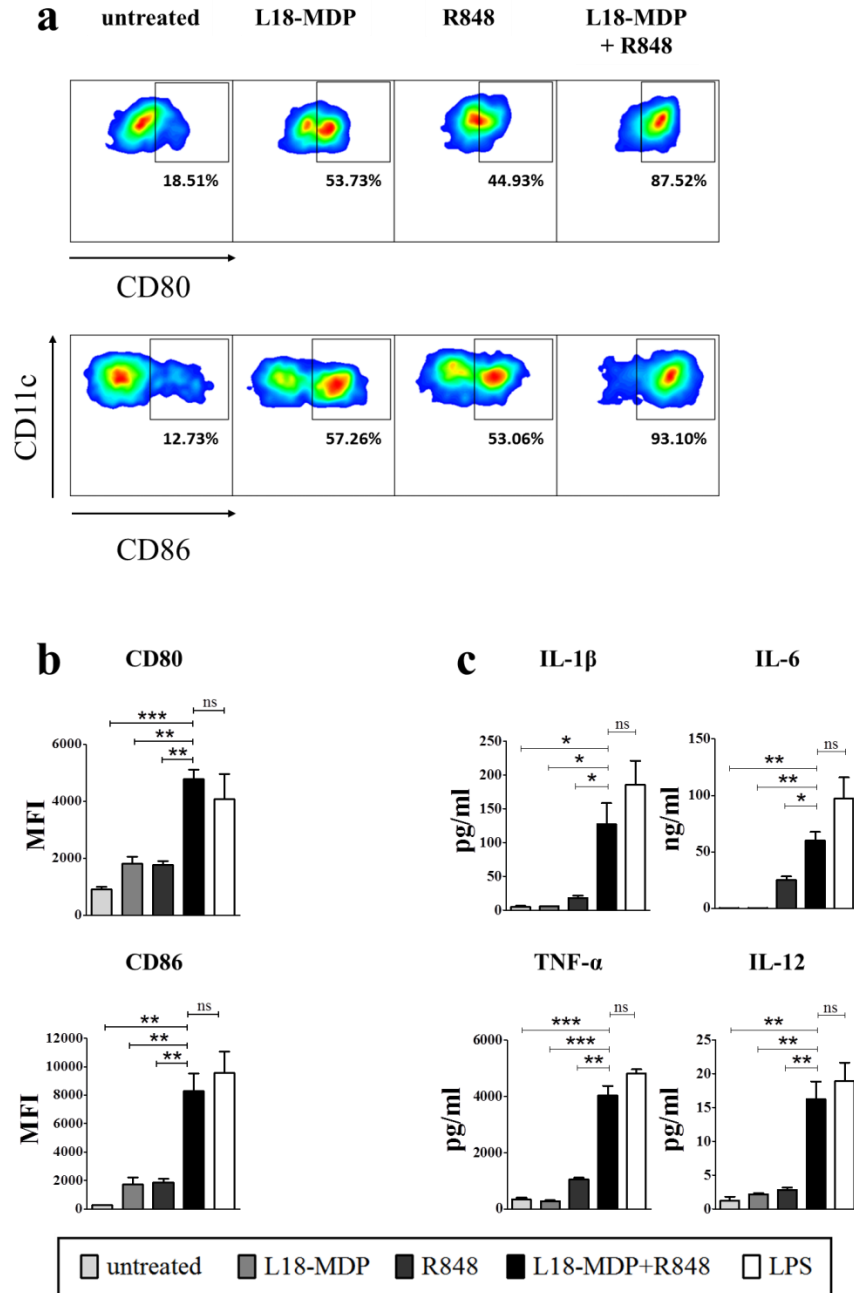


**Figure 12** Superadditive BMDC stimulation with L18-MDP + R848

BMDCs treated with L18-MDP (100 ng/ml) and R848 (100 ng/ml) for 24 h, were analyzed for maturation by flow cytometry and cytometric bead array. (a) Frequencies of CD80 and CD86 expression in CD11c<sup>+</sup>/MHC-II<sup>+</sup> BMDC after stimulation are indicated. Shown graphs are representative of three independent experiments each. (b) Quantification of CD80 and CD86 expression of differently treated BMDC. Data show the MFIs. (c) Cytokine contents in supernatants of L18-MDP/R848-treated BMDCs were assessed (mean  $\pm$  SD; n=3). LPS (100 ng/ml) was used as positive control. \*p < 0.05, \*\*p < 0.01, \*\*\*p < 0.001. Data and figure published in the Journal of Controlled Release [249].

### 4.1.3 Dual-adjuvant loaded Dex-NPs

A next step was to synthesize and evaluate a nano-sized delivery system i) to transport the identified adjuvant combination into BMDCs as effective as possible and ii) to release the adjuvants intracellularly for subsequent receptor engagement. Due to its better suitability for nanoparticle synthesis, MDP was used instead of L18-MDP. In the following experimental sections the combination MDP + R848 constitutes the combination of choice.

Acetal-modified Dex-NPs are a well-established drug delivery system used in different biomedical approaches and described in numerous publications. They are known to be a suitable carrier for a variety of substances and provide biocompatible properties at the same time. To test if these NPs are a suitable system for the delivery of MDP and R848 into BMDCs, four different Dex-NP variants were synthesized (see 3.1.1). Empty Dex-NPs (Dex-blank) were used as control to exclude unwanted effects induced by the Dex-NPs itself. Two variants were loaded with either MDP (Dex-MDP) or R848 (Dex-R848) alone to study the effect of the encapsulated single adjuvants. To examine whether the superadditive effect of MDP and R848 was preserved when encapsulated in Dex-NP, one variant was loaded with MDP + R848 (Dex-MDP/R848) in almost equimolar amounts (equal MDP/R848 concentrations as in Dex-MDP and Dex-R848).

First, the generated Dex-NPs were characterized in detail. The diameter of the prepared Dex-NPs was on average 150 nm as determined by NTA (Figure S 3, Table S 1). For the single adjuvant particles (Dex-MDP and Dex-R848), the adjuvant loading was determined to be 1.34 nmol MDP and 1.26 nmol R848 per mg particle material, respectively. Regarding Dex-MDP/R848, the measurements revealed comparable payloads with 1.38 nmol MDP and 1.29 nmol R848 per mg particle material (Table S 2).

To ensure a sufficient NP quality and purity and to exclude cytotoxic effects on DCs, all Dex-NP formulations were initially checked for three relevant parameters: i) endotoxin contaminations, ii) binding properties and iii) cytotoxic effects. Endotoxin contaminations in NP formulations can induce DC stimulation. To avoid this potential source of errors, endotoxin concentrations in Dex-NP formulations were determined by LAL assay (see 3.11). The binding of Dex-NPs by BMDCs was visualized by incubating those with Dex-NPs including MDP-FITC. The frequencies of MDP-FITC<sup>+</sup> BMDCs were assessed in a

## RESULTS

nanoparticle interaction assay (see 3.5.2) by flow cytometry (see Figure S 1). NPs itself as well as their individual components are potential sources for cytotoxicity. To rule out that the synthesized Dex-NPs were toxic for DCs, the viability of BMDCs treated with different concentrations of adjuvant-loaded Dex-NP was analyzed by 7AAD/Annexin V double staining (see 3.6.2). Cells treated with the soluble adjuvant counterparts were used as a control.

The quality tests for endotoxins showed no relevant contaminations according to the FDA recommendations (maximum 0.5 EU/ml). In all samples the endotoxin concentrations were below the permitted maximum, even lower than that of sterile PBS which was used as control (Figure 13a). Unwanted stimulatory effects due to endotoxins could therefore be excluded in case of Dex-NPs. The interaction analysis of BMDCs with Dex-NPs on the basis of MDP-FITC revealed a dose-dependent binding. The frequencies of MDP-FITC<sup>+</sup> BMDCs were thereby highly comparable for both NPs, Dex-MDP-FITC and Dex-MDP-FITC/R848 (Figure 13b), indicating a high degree of comparability across the Dex-NP formulations. Regarding NP cytotoxicity, no notable effect of the used Dex-NPs on BMDC viability was detectable. Compared with the positive control (10 vol-% DMSO), the viability of all Dex-NP samples was as high as in the untreated sample. Only the highest concentration of Dex-MDP (100 µg/ml) as well as soluble R848 (100 ng/ml) showed a slightly toxic effect on BMDCs as reflected by minimal increases in apoptotic and necrotic cells respectively (Figure 13c).

## RESULTS

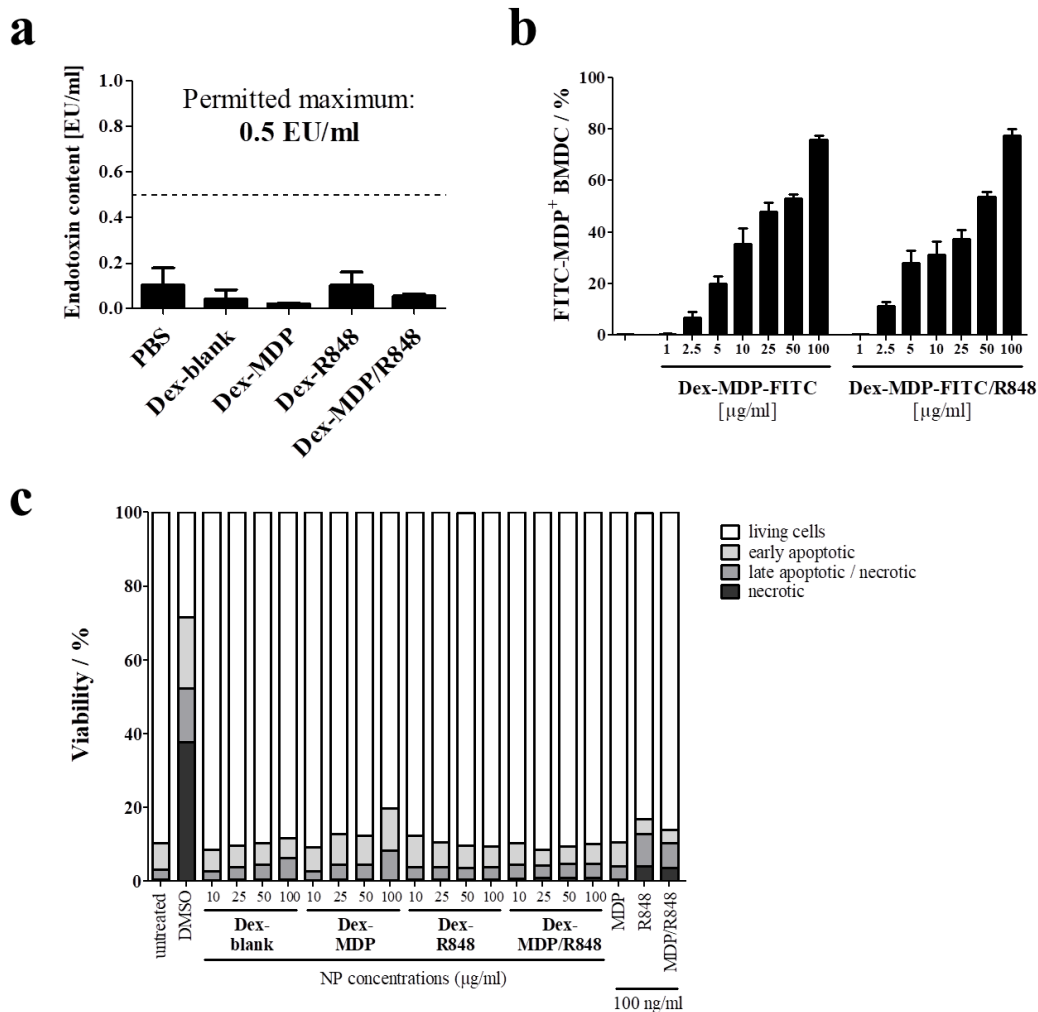


**Figure 13** Quality tests for Dex-NP formulations

Dex-NPs were tested to exclude endotoxin contaminations and cytotoxic effects on BMDCs. In addition, their binding by BMDCs was analyzed. (a) Endotoxin concentrations in Dex-NP formulations were assessed by LAL assay (n=2, two independent NP batches). (b) BMDCs ( $2 \times 10^5$  cells/ml) were treated with Dex-MDP-FITC and Dex-MDP-FITC/R848 (1-100  $\mu\text{g/ml}$ ). Binding of these NPs was measured based on MDP-FITC<sup>+</sup> cells (mean  $\pm$  SD; n=2). (c) To measure cytotoxicity of adjuvant-loaded Dex-NPs, BMDCs ( $1 \times 10^6$  cells/ml) were incubated with increasing concentrations (10-100  $\mu\text{g/ml}$ ) for 24 h. Viability was determined by 7AAD/Annexin V staining and was visualized as classification into living, early apoptotic, late apoptotic/necrotic and necrotic cells. Cytotoxicity of soluble MDP and R848 (100 ng/ml) was analyzed for comparison. 10 vol-% DMSO was used as positive control. Figure 13b and c as well as corresponding data published in the Journal of Controlled Release [249].

## RESULTS

### 4.1.3.1 Superadditive DC stimulation with adjuvant-loaded Dex-NPs

To evolve their stimulatory potential, MDP as well as R848 have to cross the plasma membrane. After entering the cell, it is essential that these agents reach specific intracellular compartments to be recognized by associated PRRs. Endocytosis is usually responsible for that transport into the cell. A drug delivery system such as Dex-NPs can also mediate and even enhance this trans-membrane transfer to induce a much more potent stimulation. NP loading capacity, transport efficiency, intracellular release and fate as well as drug quantity are examples of crucial factors influencing the overall system's efficacy.

To validate the potential of MDP/R848-loaded Dex-NPs to stimulate BMDCs, we measured the CD80 and CD86 expression after 24 h incubation testing different concentrations (1-100  $\mu\text{g/ml}$ ) of the established adjuvant-loaded Dex-NPs (see Figure S 1). Dex-blank NPs were included in the analysis to exclude stimulatory effects of the carrier itself. As an internal control, some BMDC samples were treated with soluble MDP (sMDP), soluble R848 (sR848) or both in combination. In these experiments, the concentrations of soluble adjuvants were equimolar to the encapsulated ones (see Table S 2). Dex-blank evoked no effect on the CD80 and CD86 expression of BMDCs, whereas LPS, used as an internal positive control, induced a strong upregulation of both co-stimulatory receptors (Figure 14). As expected, treatment of BMDCs with sMDP, which is unable to penetrate cell membranes, did not induce any stimulatory effect regarding CD80 and CD86, while sR848 stimulated BMDCs. The combination of sMDP and sR848 did not reveal any advantages compared with R848 alone here. Dex-MDP induced an increase in CD80 and CD86 expression in a dose-dependent manner. At the highest concentration applied, Dex-MDP stimulated BMDCs significantly better than equimolar amounts of sMDP. Compared to LPS, Dex-R848 mediated moderate BMDC stimulation, though stronger than that of sR848 in case of CD86. Only half the amount of Dex-R848 was thereby needed to reach the maximal stimulatory effect. Furthermore, Dex-MDP/R848 exhibited the strongest stimulatory effect on CD80/CD86 expression, even higher than exerted by the soluble combination.

## RESULTS

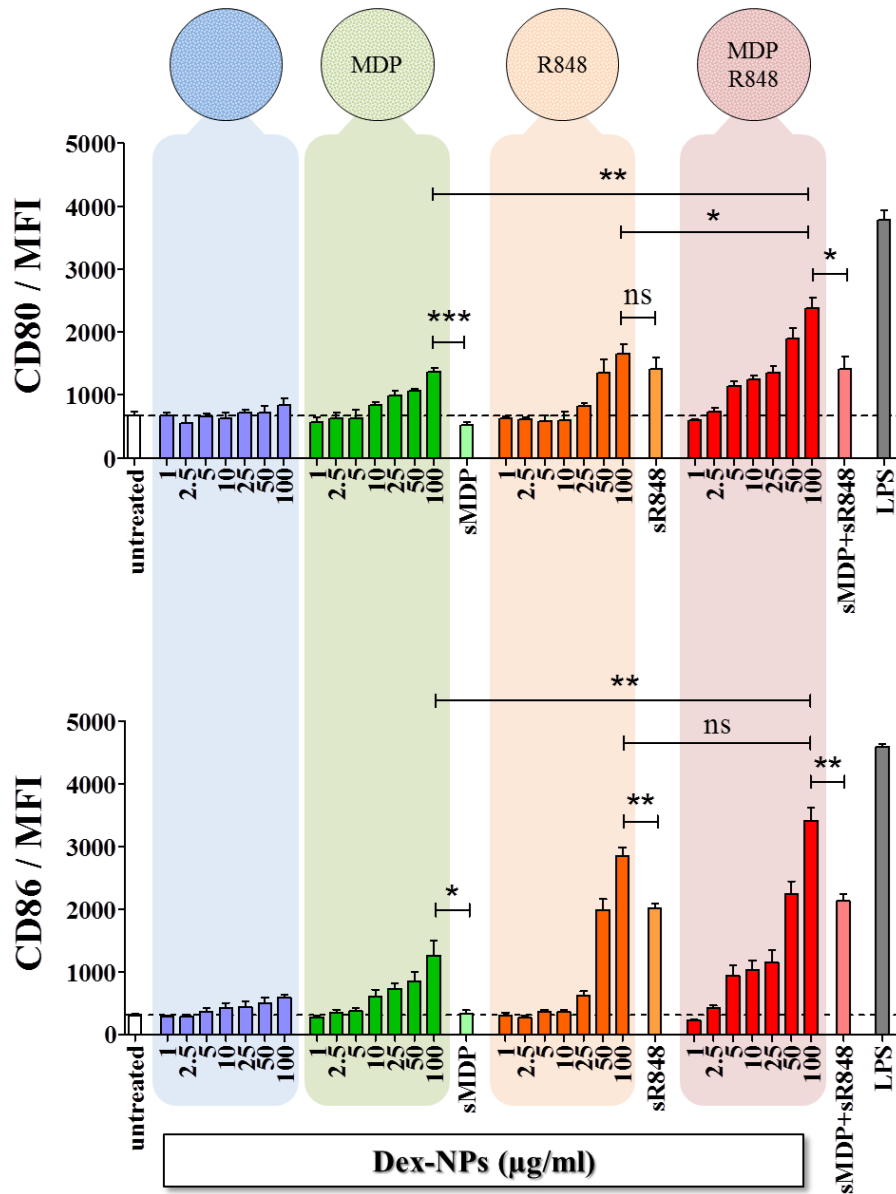


**Figure 14** BMDC stimulation with adjuvant-loaded Dex-NPs

BMDCs ( $2 \times 10^5$  cells/ml) were treated with Dex-blank (blue), Dex-MDP (green), Dex-R848 (orange) or Dex-MDP/R848 (red) as indicated for 24 h. For comparison, equimolar amounts of sMDP (66 ng/ml) and sR848 (44 ng/ml) alone or in combination were also used as stimulants. LPS (100 ng/ml) treated BMDCs served as positive control. Surface expression of CD80 and CD86 on differently treated BMDCs was measured by flow cytometry based on MFIs. Dashed lines indicate expression levels of the untreated control (mean  $\pm$  SD; n=3). \* $p < 0.05$ , \*\* $p < 0.01$ , \*\*\* $p < 0.001$ . Data and figure published in the Journal of Controlled Release [249].

## RESULTS

As already described in 4.1.2, the release of pro-inflammatory cytokines was used as an additional parameter to assess the stimulatory capacity of adjuvant-loaded Dex-NPs to activate BMDCs. Therefore, the supernatants of differentially treated BMDCs were checked for IL-1 $\beta$ , IL-6, TNF- $\alpha$  and IL-12. Dex-MDP/R848 induced a strong secretion of the first three mentioned cytokines in a superadditive manner compared to the single-adjuvant carrying Dex-NPs (Figure 15). BMDCs treated with the soluble combination at equimolar amounts showed highly comparable cytokine levels. In general, the concentrations of IL-12, an essential cytokine for Th1 differentiation, were again very low and close to the detection limit.

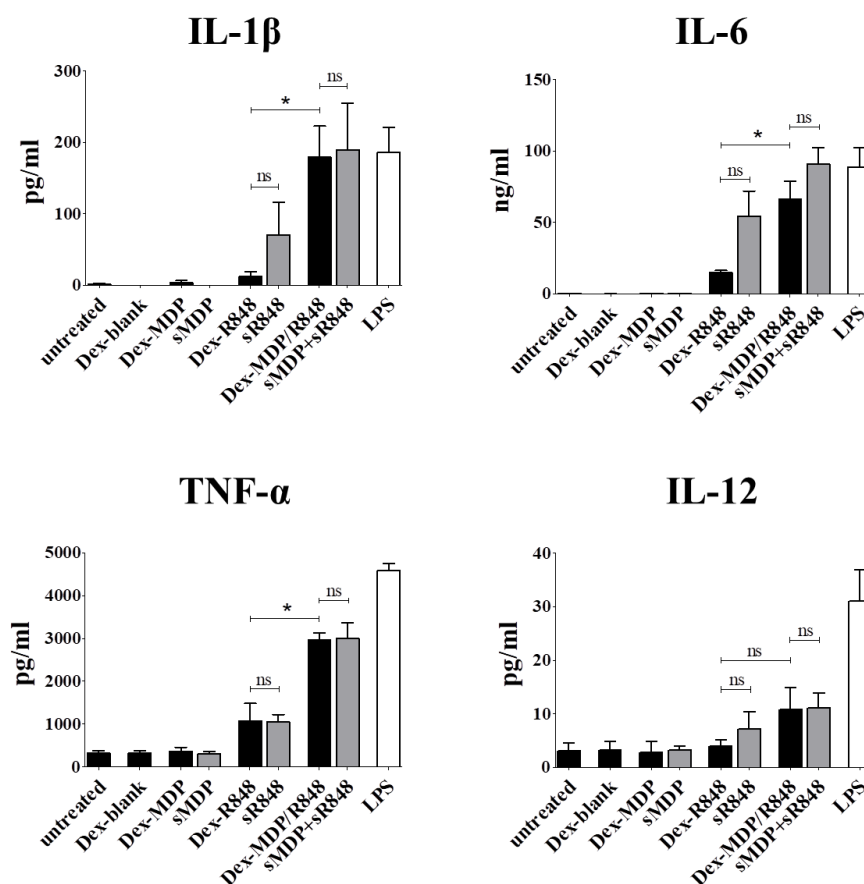


**Figure 15** Cytokine secretion triggered by adjuvant-loaded Dex-NPs

Cytokine contents in supernatants of BMDCs ( $1 \times 10^6$  cells/ml) treated with adjuvant-loaded Dex-NPs (100  $\mu$ g/ml) or equimolar amounts of soluble adjuvant (sMDP: 66 ng/ml, sR848: 44 ng/ml) for 24 h were analyzed by CBA. LPS treated BMDCs were used as positive control (mean  $\pm$  SD; n=3). \*p < 0.05. Data and figure published in the Journal of Controlled Release [249].



## RESULTS

Potential leakage of encapsulated adjuvants was ruled out by treating BMDCs with Dex-NP supernatants for 24 h and measuring the expression of CD80 and CD86. In contrast to treatment with adjuvant-loaded Dex-NPs, none of the supernatants of the different Dex-NP formulations induced any significant upregulation of the markers. Only in case of CD86, the supernatants of the adjuvant-loaded Dex-NPs induced a very slight increase which was weaker than that induced by the empty Dex-NPs (Figure 16).

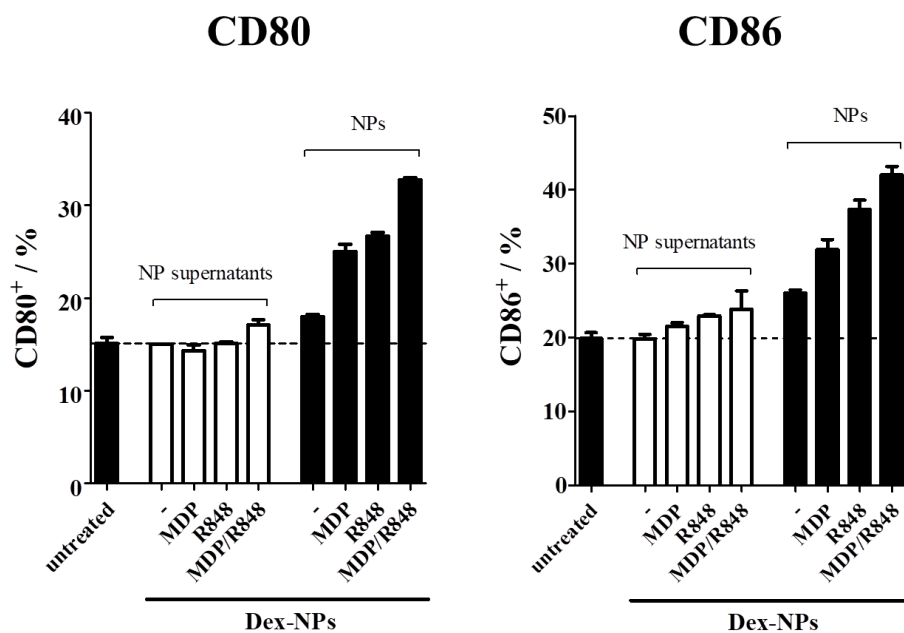


**Figure 16** Biological activity of Dex-NPs' supernatants

To detect potential free adjuvants (MDP, R848) in the Dex-NP formulations, BMDCs ( $2 \times 10^5$  cells/ml) were treated with the different types of Dex-NPs (100  $\mu$ g/ml) or with the corresponding volumes of their supernatants for 24 h. Afterwards, the frequencies of CD80- and CD86-positive BMDCs were measured by flow cytometry. The results are displayed relative to the untreated control (dashed line, mean  $\pm$  SD; n=2). Data and figure published in the Journal of Controlled Release [249].

## RESULTS

### 4.1.4 OVA-NCs as antigen delivery system

Apart from adjuvants for stimulation, a nanovaccine usually requires a target-specific antigen. Polymeric nanocapsules with an aqueous core and a shell consisting of OVA protein, which was cross-linked with TDI in an inverse miniemulsion process, were used for this task. To test if these OVA-NCs are a suitable antigen delivery system for DCs and can serve as antigen source to mediate OVA-specific T cell responses, the interaction of BMDCs with OVA-NCs was analyzed. For that purpose, unmodified OVA-NCs (OVA-blank-NC) were synthesized and characterized in detail. Cy5-Oligo (hereinafter called Cy5) was encapsulated to be able to detect the NCs (see 3.1.2). The diameter of the OVA-NCs was approximately 250 nm in cyclohexane. In water the size increased by about 90 nm. The zeta potential was -26 mV (Table S 3). The capsules morphology was visualized by SEM and TEM images (Figure 17).

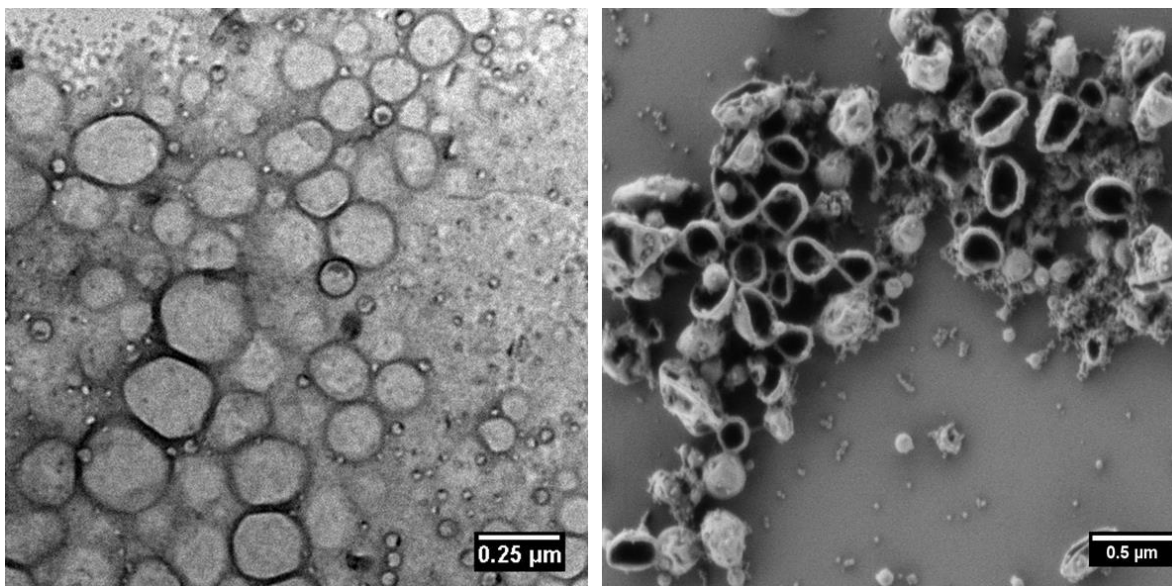


**Figure 17** Visualization of OVA-NC morphology

The morphology of OVA-NCs was microscopically visualized by SEM (left) and TEM (right). Indicated scale bars illustrate NC sizes. Figure published in the *Journal of Controlled Release* [249].

## RESULTS

To detect intracellular NC degradation, a slightly different type of capsule was generated. To this end, OVA-DQ was incorporated into the NC shell in addition to the unmodified OVA (OVA-DQ-NC, see 3.1.2). Enzymatic degradation of OVA-DQ induces detectable fluorescence emission, which was utilized to measure and visualize OVA-NC degradation.

Initially, both synthesized OVA-NCs (OVA-blank-NC, OVA-DQ-NC) were routinely checked for endotoxin contaminations and potential cytotoxic effects. All tested OVA-NC batches were almost free of endotoxins and the measured concentrations were consistently under 0.5 EU/ml (Figure S 4a). Referring to cytotoxicity, OVA-blank-NCs were well-tolerated by BMDCs. Although the frequencies of living cells inversely correlated with increasing NC concentration, they were always over 70 %. At a concentration of 150  $\mu\text{g}$  OVA-DQ-NC per ml, approximately 20 % of all cells were defined as necrotic (Figure S 4b). Since these NCs were exclusively used for degradation analysis and OVA-DQ was not incorporated in further capsules, the moderate cytotoxicity of OVA-DQ-NCs was tolerated.

### 4.1.4.1 Binding/degradation of OVA-NCs by DCs

A protein antigen has to be taken up by the DC to be available for intracellular degradation and subsequent MHC loading. To do so, the cell binds the antigen and internalizes it via endocytosis and macropinocytosis. In case of NCs, it is essential to know whether the DC is able to recognize and bind it. Those interactions are highly dependent on the NC's material and properties, such as hydrophobicity and zeta potential. Low interaction potentially results in low uptake and a lack of antigen presentation. Missing or insufficient antigen-presentation impedes antigen-specific immune responses, which are indispensable for vaccinations. For this reason, the binding of OVA-blank-NCs by BMDCs was analyzed by flow cytometry (based on Cy5 emission). Antigen-presentation also requires degradation of internalized proteins. To prove OVA-NCs' intracellular degradation, BMDCs were incubated with OVA-DQ-NCs and the emission derived from OVA-DQ degradation was measured by flow cytometry as well. Cytometric analysis of binding and degradation followed a specific gating strategy (Figure S 5).

To verify the cellular binding of OVA-NCs, BMDCs were treated with different amounts of OVA-blank-NCs (37.5-150  $\mu\text{g}/\text{ml}$ ). The cytometric analysis showed that after an incubation time of 24 h almost all BMDCs were positive for OVA-NCs (Cy5<sup>+</sup> cells).

## RESULTS

Nonetheless, the MFIs revealed dose-dependent capsule binding. The higher the NC concentration, the higher was the resulting Cy5 intensity (Figure 18a). By measuring Cy5 intensities and frequencies at different incubation time points, it turned out that BMDCs bound OVA-NCs also in a time-dependent manner. Although nearly all BMDCs were Cy5<sup>+</sup> after 0.5 h already, the MFIs showed a constant increase over time (Figure 18b).

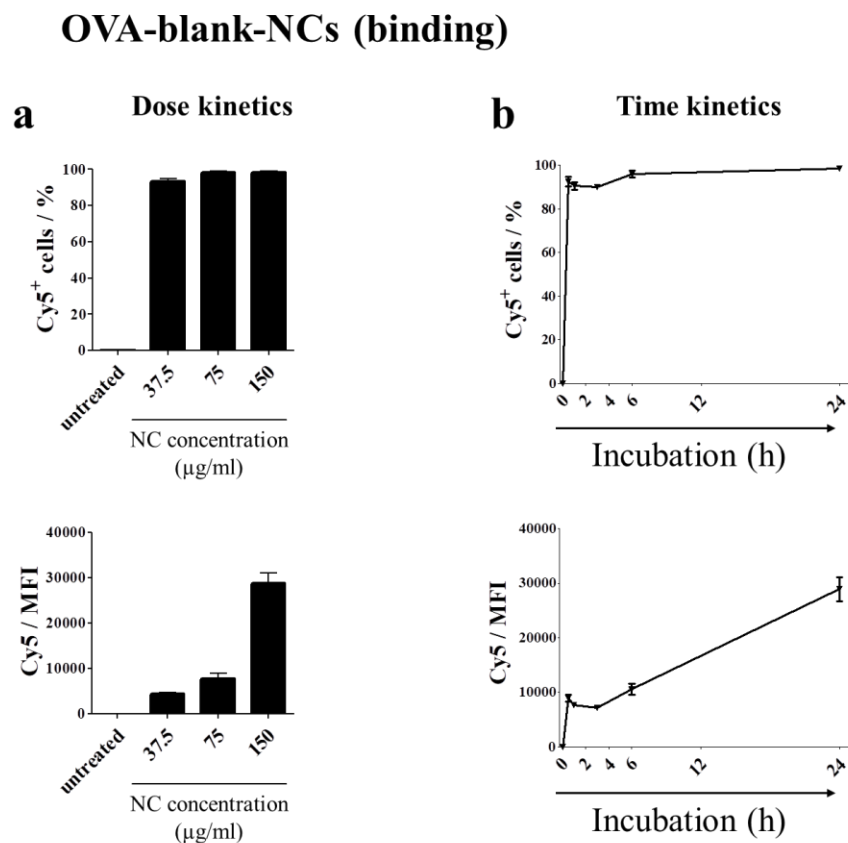


**Figure 18** Cellular binding of OVA-NCs by BMDCs

For binding analysis, BMDCs ( $2 \times 10^5$  cells/ml) were incubated with OVA-blank-NCs (labeled with Cy5). Frequencies of Cy5<sup>+</sup> cells and MFIs were collected by flow cytometry. (a) To test for dose-dependency, cells were incubated with different NC concentrations (37.5-100 µg/ml) for 24 h (n=3). (b) Time-dependency was examined by treating cells with OVA-blank-NCs (100 µg/ml) for indicated periods of time (0.5-24 h, mean  $\pm$  SD; n=4). Data and figure published in the Journal of Controlled Release [249].

## RESULTS

Similarly, the intracellular degradation of OVA-NCs was examined by means of OVA-DQ-NCs. For this, BMDCs were treated either with different concentrations of OVA-DQ-NCs for 24 h or with 100  $\mu\text{g}/\text{ml}$  of those NCs for various periods of time, as indicated. The fluorescence emission derived from degraded OVA-DQ proteins was measured by flow cytometry. As shown in Figure 19, OVA-DQ-NCs were degraded by BMDCs in a dose- and time-dependent manner. Increasing NC concentrations (Figure 19a) and incubation times (Figure 19b) increased the frequencies of degradation<sup>+</sup> cells and corresponding emission intensities.

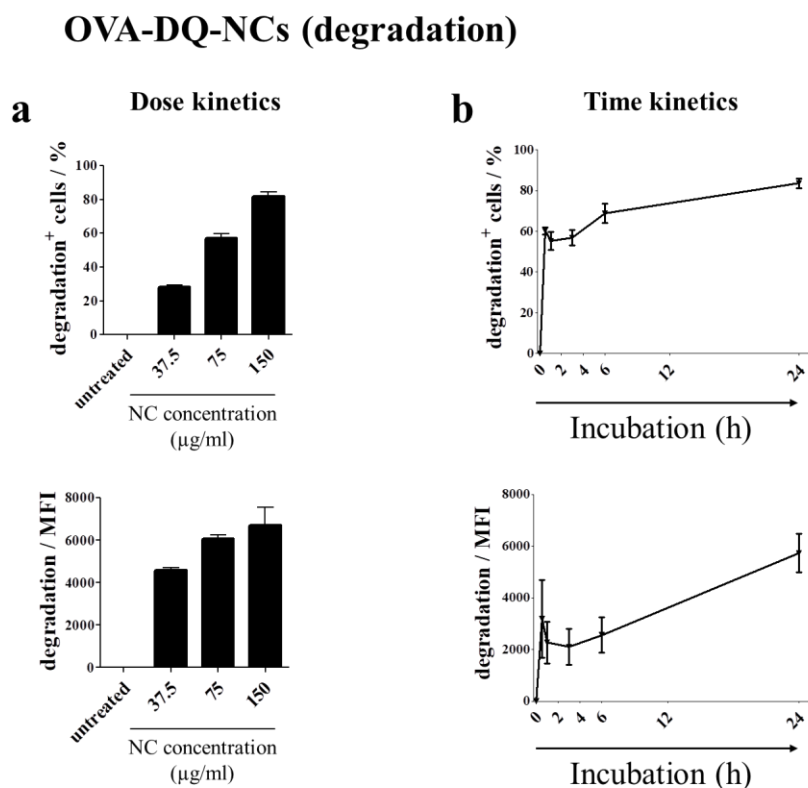


**Figure 19** Degradation of OVA-NCs by BMDCs

To detect OVA-NC degradation, BMDCs ( $2 \times 10^5$  cells/ml) were incubated with OVA-DQ-NCs. Frequencies of OVA-DQ<sup>+</sup> cells and MFIs were collected by flow cytometry. (a) To test for dose-dependent degradation, cells were incubated with different NC concentrations (37.5-100  $\mu\text{g}/\text{ml}$ ) for 24 h (n=3). (b) Time-dependent degradation was examined by treating cells with OVA-DQ-NCs (100  $\mu\text{g}/\text{ml}$ ) for indicated periods of time (0.5-24 h, mean  $\pm$  SD; n=4). Data and figure published in the Journal of Controlled Release [249].

## RESULTS

Additionally, confocal images of BMDCs treated with OVA-DQ-NCs at 4 and 37 °C, respectively, for 3 h (as outlined in 3.5.2) revealed temperature-dependent degradation of OVA-NCs. Thereby, CLSM (see 3.8) enabled the visualization of intracellular NC degradation. Upon cleavage of OVA-DQ to peptides, the included quenching property was relieved. The fluorescence of the single, dye-labeled peptides was imaged in combination with CellMask Orange used to visualize plasma membranes and DAPI which stained cell nuclei. This combination allowed a precise localization of OVA-DQ degradation signals (as exemplarily shown in Figure S 6). During analysis, not a single degradation signal was detectable extracellularly regardless of incubation temperature.

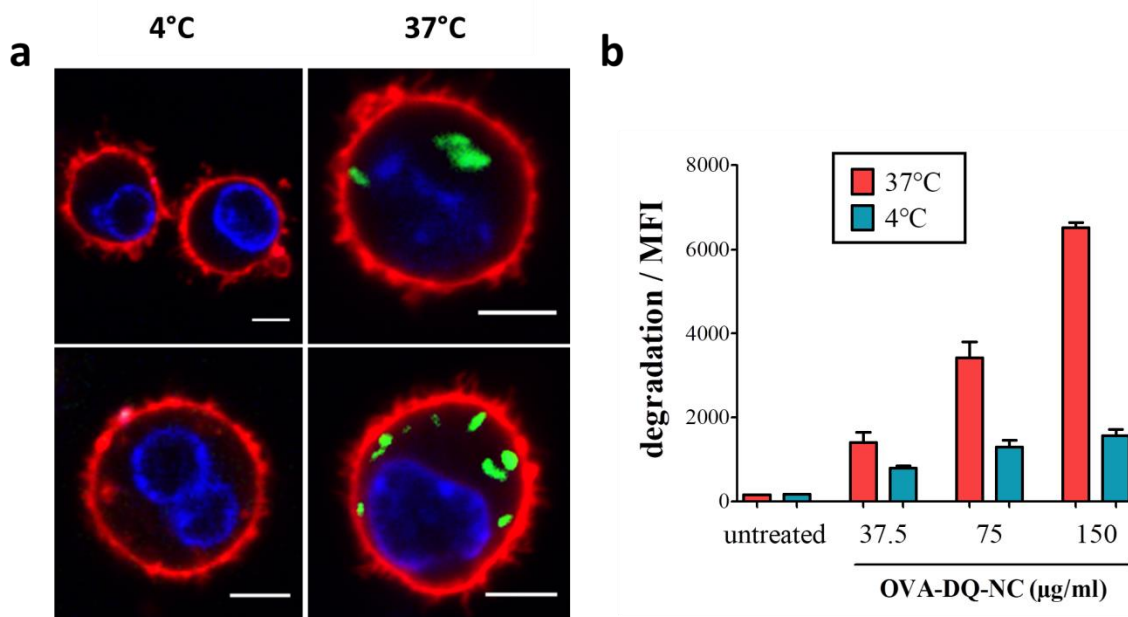


**Figure 20** Temperature-dependent OVA-NC degradation

Intracellular degradation of OVA-DQ-NC was analyzed by CLSM and flow cytometry. (a) Representative confocal images of BMDCs ( $7.5 \times 10^5$  cells/ml) treated with OVA-DQ-NCs (100 µg/ml) at 4 and 37 °C respectively for 3 h. Cell membranes were stained with CellMask Orange (red), nuclei with DAPI (blue). OVA-DQ degradation was detected by its characteristic fluorescent emission (green). Scale bars represent 5 µm. (b) BMDCs ( $2 \times 10^5$  cells/ml) were analyzed for OVA-DQ degradation at 4 and 37 °C after incubation with OVA-DQ-NCs (37.5-150 µg/ml) for 24 h. Resulting MFIs were measured by flow cytometry (mean  $\pm$  SD; n=2). Data and figure published in the Journal of Controlled Release [249].

## RESULTS

Clearly visible signals with the characteristic fluorescent properties of OVA-DQ-derived peptides were observed intracellularly after 3 h at 37 °C, while at 4 °C such signals did not appear at all (Figure 20a). This temperature-dependency was confirmed by flow cytometry. After incubating BMDCs with OVA-DQ-NC for 24 h in parallel assays at 4 and 37 °C, the low-temperature samples showed only weak degradation signals in flow cytometry, while the BMDCs treated under physiological conditions showed a strong, dose-dependent increase in degradation emission (Figure 20b).

### 4.1.4.2 NC-derived peptides for DC-directed T cell stimulation

Next, we aimed to demonstrate that OVA-NCs can be used to trigger antigen-directed immune reactions. The availability of degraded OVA from OVA-NCs, serving as antigen source, was analyzed using OVA peptide-specific transgenic OT-I (CD8<sup>+</sup>) and OT-II (CD4<sup>+</sup>) primary T cells (see 3.2 and 3.3.3). OT-I T cells recognize a specific OVA peptide in the context of MHC-I, while OT-II T cells are specific for a distinct OVA peptide presented on MHC-II. These T cell populations are commonly used test systems for measuring the efficiency of OVA peptide presentation via MHC-I and -II. Since antigen presentation via both MHC-I and -II can be essential for vaccination approaches, the suitability of OVA-NCs as an antigen source for BMDC-mediated T cell stimulation was analyzed with both two T cell systems. The assessment was carried out by DC-mediated T cell proliferation (see 3.5.3), measured by [Methyl-<sup>3</sup>H] thymidine incorporation (see 3.9).

Aliquots of BMDCs pre-incubated with OVA-blank-NCs at different concentrations for 24 h induced a moderate OT-I proliferation in case of the highest dose (100 µg/ml), and a dose-correlating proliferation of OT-II T cells was observed (Figure 21, left panel). Concomitant stimulation of OVA-blank-NC pre-treated BMDCs with LPS (100 ng/ml) resulted in an increased proliferation of CD8<sup>+</sup> and CD4<sup>+</sup> T cells (Figure 21, right panel), particularly at the highest dose of OVA-NCs applied.

RESULTS

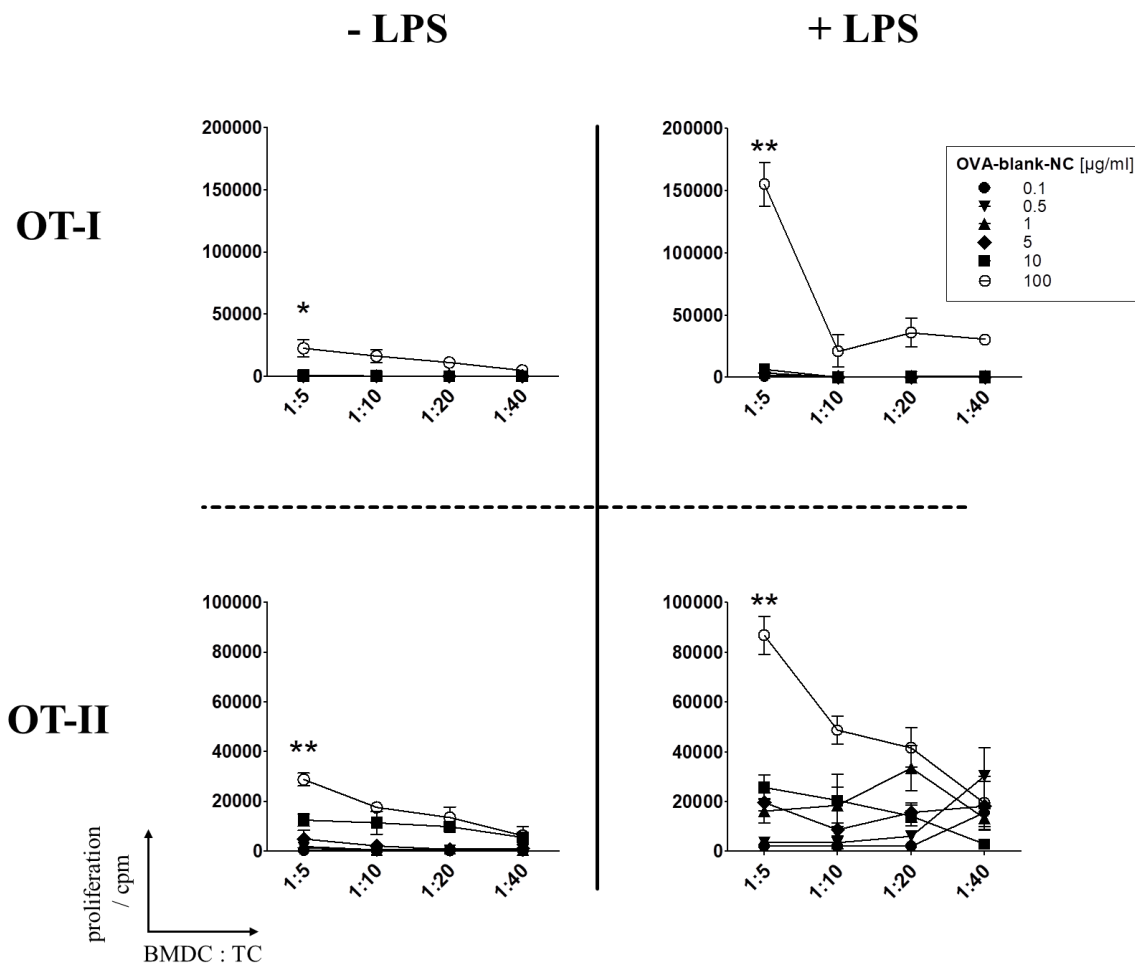


**Figure 21** OVA-NC-mediated T cell proliferation

BMDCs ( $1 \times 10^6$  cells/ml) were incubated with OVA-blank-NCs (1-100  $\mu\text{g/ml}$ ) for 24 h. Aliquots were co-treated with LPS (100 ng/ml). Titrated numbers of pre-treated BMDCs (starting with  $10^5$  cells) were co-cultured with OVA peptide-specific OT-I ( $\text{CD8}^+$ ) and OT-II ( $\text{CD4}^+$ ) T cells (each  $5 \times 10^5$  cells) in triplicates in 96 well plates. T cell proliferation was measured in counts per minute (cpm) by  $^3\text{H}$ -thymidine incorporation, applied after three days of BMDC/T cell co-culture for 16 h (mean  $\pm$  SD;  $n=3$ ). \* $p < 0.05$ , \*\* $p < 0.01$ , OVA-blank-NCs (100  $\mu\text{g/ml}$ ) vs. OVA-blank-NCs (10  $\mu\text{g/ml}$ ). Data and figure published in the Journal of Controlled Release [249].



#### 4.1.5 Adjuvant-loaded Dex-NPs + OVA-NCs

The question arose, whether both nanocarrier systems – Dex-MDP/R848 for adjuvant delivery and OVA-NCs as antigen source – could work together to mediate OVA-specific T cell proliferation. Consequently, a combined application of the two evaluated systems was tested. To do this, BMDCs were co-treated with OVA-blank-NCs + Dex-MDP/R848, again followed by a co-culture with OT-I and OT-II T cells. Those BMDCs, which received a pre-treatment with Dex-MDP/R848 and OVA-blank-NCs, initiated the strongest proliferation of OT-I as well as OT-II T cells compared to samples treated with one of either type of nanocarriers only (Figure 22).

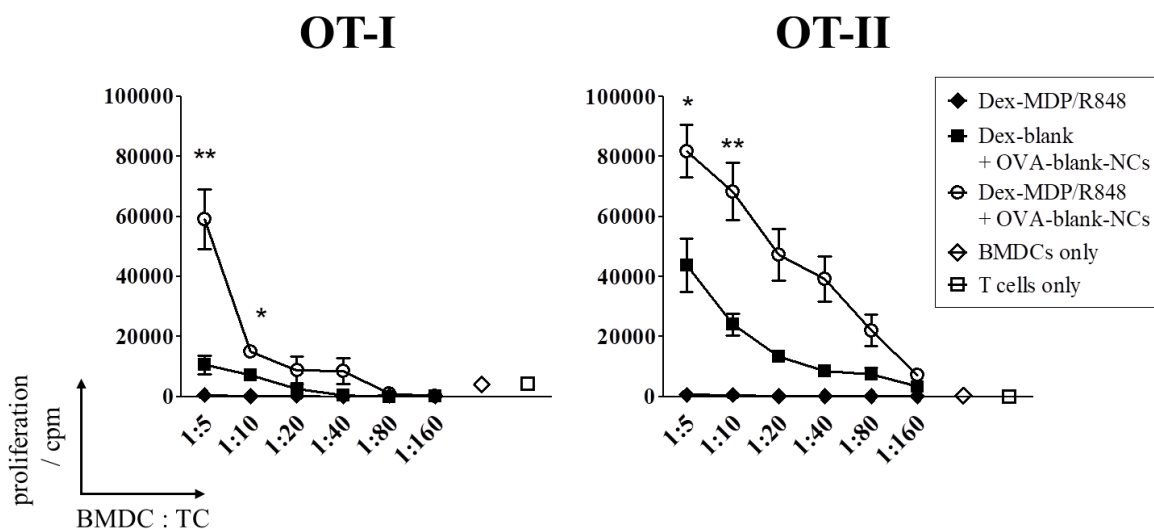


**Figure 22** T cell proliferation triggered by nanocarrier combination

BMDCs ( $1 \times 10^6$  cells/ml) were treated with Dex-blank, Dex-MDP/R848 and OVA-blank-NCs (each 100  $\mu\text{g/ml}$ ) in the indicated combinations for 24 h. Titrated numbers of pre-treated BMDCs (starting with  $10^5$  cells) were co-cultured with OVA peptide-specific OT-I ( $\text{CD8}^+$ ) and OT-II ( $\text{CD4}^+$ ) T cells (each  $5 \times 10^5$  cells) in triplicates in 96 well plates. T cell proliferation was measured in cpm by  $^3\text{H}$ -thymidine incorporation, applied after three days of BMDC/T cell co-culture for 16 h. Proliferation of BMDCs and T cells without further treatment was used as control (mean  $\pm$  SD;  $n=3$ ). \* $p < 0.05$ , \*\* $p < 0.01$ , Dex-MDP/R848 + OVA-blank-NCs vs. Dex-blank + OVA-blank-NCs. Data and figure published in the Journal of Controlled Release [249].

## RESULTS

Especially in case of OT-II proliferation, Dex-MDP/R848 enhanced the T cell stimulatory capacity of OVA-blank-NC-treated BMDCs (Figure 22, left). BMDCs co-treated with OVA-blank-NCs + Dex-blank also induced T cell proliferation, although to a lower extent. As expected, the administration of Dex-MDP/R848 alone did not trigger any proliferation of OT-I and OT-II T cells. The individual proliferation signals of BMDCs, OT-I and OT-II T cells without any further treatment were assessed as controls.

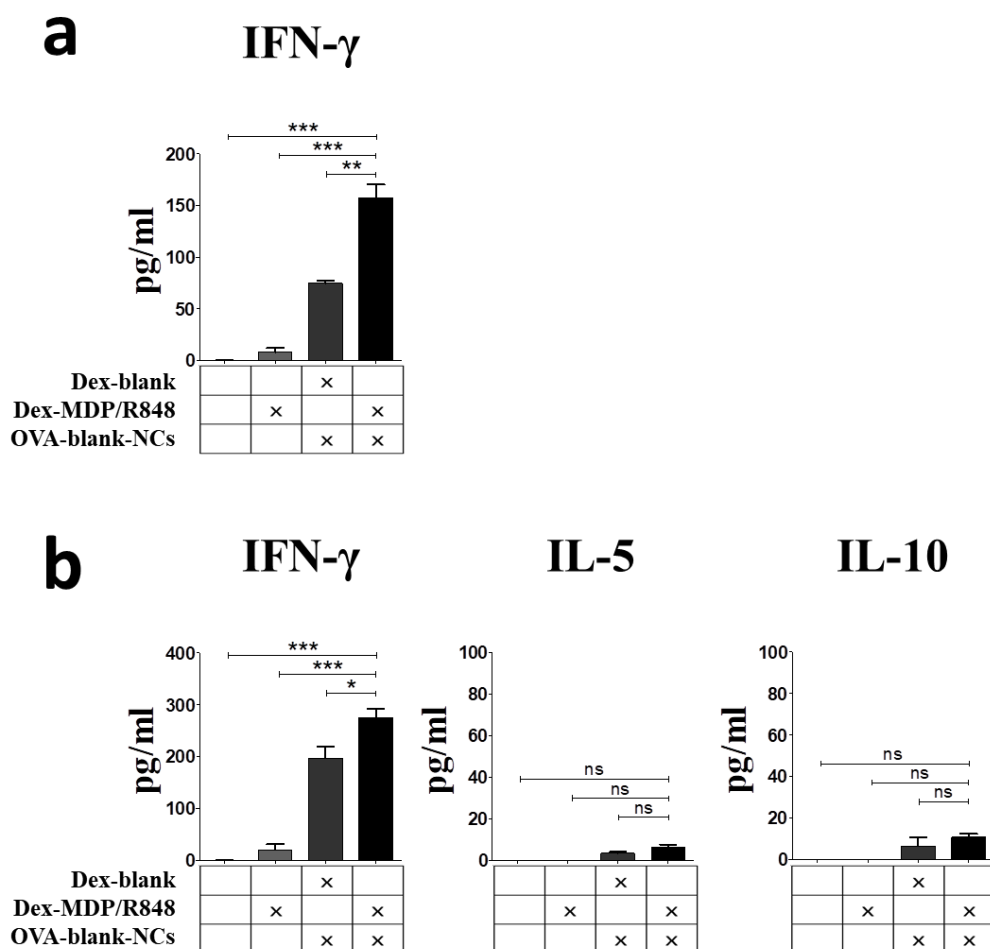


**Figure 23** Cytokine secretion triggered by nanocarrier combination

BMDCs ( $1 \times 10^6$  cells/ml) were treated with Dex-blank, Dex-MDP/R848 and OVA-blank-NCs (each 100  $\mu\text{g/ml}$ ) in the indicated combinations for 24 h. After three days of co-culture with (a) OT-I and (b) OT-II T cells, supernatants were collected, and characteristic cytokines (IFN- $\gamma$ , IL-5, IL-10) were measured by CBA (mean  $\pm$  SD, n=3). \* $p < 0.05$ , \*\* $p < 0.01$ , \*\*\* $p < 0.001$ . Data and figure published in the Journal of Controlled Release [249].

## RESULTS

To characterize the observed induction of OVA-specific T cell stimulation in more detail, cytokine contents in the corresponding BMDC/T cell co-culture supernatants were measured by CBA. The results showed significantly increased levels of the Tc1/Th1 marker cytokine IFN- $\gamma$  in samples containing BMDCs pre-treated with Dex-MDP/R848 in combination with OVA-blank-NCs co-cultured with OT-I (Figure 23a) as well as OT-II (Figure 23b) T cells. In contrast, an expression of the Th2 marker IL-5 and dual Th2/Treg marker IL-10 was barely detectable in any culture supernatant.

### 4.1.6 Adjuvant-loaded OVA-NCs combining adjuvant and antigen

As an important next step to generate a nanocarrier combining the two main requirements of a vaccine, namely adjuvanticity and antigen delivery, the evaluated adjuvant combination MDP + R848 was integrated into OVA-NCs. The resulting nanocapsule offers a degradable protein shell, usable as antigen source, and at the same time protects the adjuvant combination due to complete encapsulation and an aqueous capsule core. Energy-dependent degradation of the OVA-NCs ensures intracellular release of the encapsulated adjuvants. Similar to the experiments with adjuvant-loaded Dex-NPs, a new batch of OVA-NCs including four different variants was synthesized for the following experiments: empty OVA-NCs (OVA-blank-NCs), MDP-loaded OVA-NCs (OVA-MDP-NCs), R848-loaded OVA-NCs (OVA-R848-NCs) and MDP/R848-loaded ones (OVA-MDP/R848-NCs). Additionally, Cy5 was co-encapsulated in all variants to enable NC detection via flow cytometry. The diameter of the capsules was determined by DLS. On average it was about 290 nm in cyclohexane. In water the size increased to approximately 360 nm. The zeta potential was roughly -29 mV (Table S 3).

These nanocarrier formulations were routinely checked for endotoxin contaminations. As described in 4.1.3, such contaminations are a potential source for unintended BMDC stimulation. All tested formulations were almost free of endotoxins (Figure S 4a). Also, cytotoxicity of the OVA-NC variants was analyzed by 7AAD/Annexin V staining. As exemplarily shown in Figure S 4c, no relevant cytotoxicity of the adjuvant-loaded OVA-NCs was detectable. For the single adjuvant capsules (OVA-MDP-NCs and OVA-R848-NCs), the adjuvant loading was determined to be 7.78 nmol MDP and 3.16 nmol R848 per mg capsule material, respectively. Regarding OVA-MDP/R848-NCs, the measurements

## RESULTS

revealed comparable payloads of 7.14 nmol MDP and 2.85 nmol R848 per mg capsule material (Table S 4).

### 4.1.6.1 Superadditive DC stimulation with adjuvant-loaded OVA-NCs

To assess the potential of adjuvant-loaded OVA-NCs to stimulate BMDCs and to analyze how efficient OVA-NCs transferred MDP and R848 to their intracellular PRRs, BMDCs were treated with all four OVA-NC variants (mentioned above) for 24 h. The resulting expression of the surface markers CD80 and CD86 was measured by flow cytometry (see Figure S 1) once again compared to equimolar amounts of soluble adjuvants (see Table S 4). OVA-blank-NCs, OVA-MDP-NCs as well as sMDP showed no stimulatory effect on BMDCs in this experimental setup, while OVA-R848-NCs at the two highest concentrations (50 and 100  $\mu\text{g/ml}$ ) and the corresponding amounts of sR848 induced a comparable, moderate upregulation of both surface markers. Compared to the single adjuvant carrying OVA-NCs, the co-delivery of MDP + R848 in OVA-NCs (OVA-MDP/R848-NCs) increased the expression of CD80 and CD86 in a superadditive manner. In contrast to BMDCs treated with OVA-MDP- or OVA-R848-NCs, significantly higher MFIs for both markers were detectable after administration of OVA-MDP/R848-NCs, especially in case of 50 and 100  $\mu\text{g/ml}$  NCs (Figure 24). In this context, the combined application of sMDP and sR848 did not show any advantages compared to OVA-MDP/R848-NCs. The stimulatory effect of the dual-adjuvant OVA-NCs was similar to that of LPS, our positive control, and stronger than that of the corresponding Dex-NP formulation (see Figure 14).

The efficiency of MDP/R848-loaded OVA-NCs to stimulate BMDCs was also analyzed with a focus on stimulation-induced cytokine secretion. The supernatants of BMDCs, treated with the four different types of OVA-NCs for 24 h, were checked for IL-1 $\beta$ , IL-6, TNF- $\alpha$  and IL-12 secretion. MDP- as well as R848-loaded OVA-NCs did not induce any remarkable cytokine secretion. The only exception was a moderate increase in IL-1 $\beta$  upon OVA-R848-NC treatment. In contrast to that, OVA-MDP/R848-NCs triggered the secretion of high amounts of IL-1 $\beta$ , IL-6, TNF- $\alpha$  and IL-12 in BMDCs (Figure 25).

## RESULTS

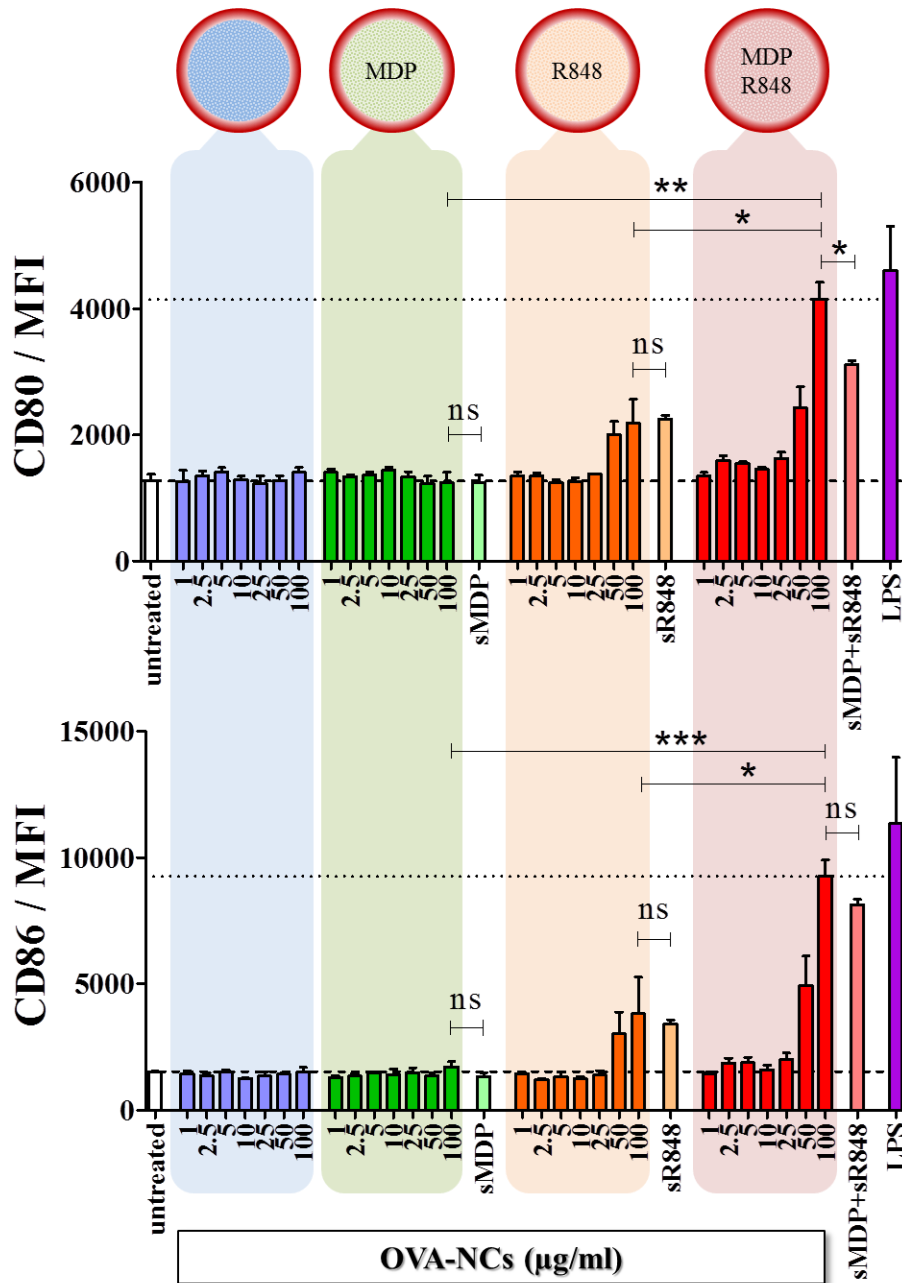


**Figure 24** BMDC stimulation with adjuvant-loaded OVA-NCs

BMDCs ( $2 \times 10^5$  cells/ml) were treated with OVA-blank- (blue), OVA-MDP- (green), OVA-R848 (orange) or OVA-MDP/R848-NCs (red) as indicated for 24 h. For comparison, equimolar amounts of sMDP (383 ng/ml) and sR848 (111 ng/ml) alone or in combination were also used as stimulants. LPS (100 ng/ml) treated BMDCs were used as positive control. Surface expression of CD80 and CD86 on differently treated BMDCs was measured by flow cytometry based on MFIs. Dashed lines indicate expression levels of the untreated control, dotted lines those induced by the highest concentration of OVA-MDP-R848-NCs (mean  $\pm$  SD; n=3). \* $p < 0.05$ , \*\* $p < 0.01$ , \*\*\* $p < 0.001$ . Data and figure published in the Journal of Controlled Release [249].

## RESULTS

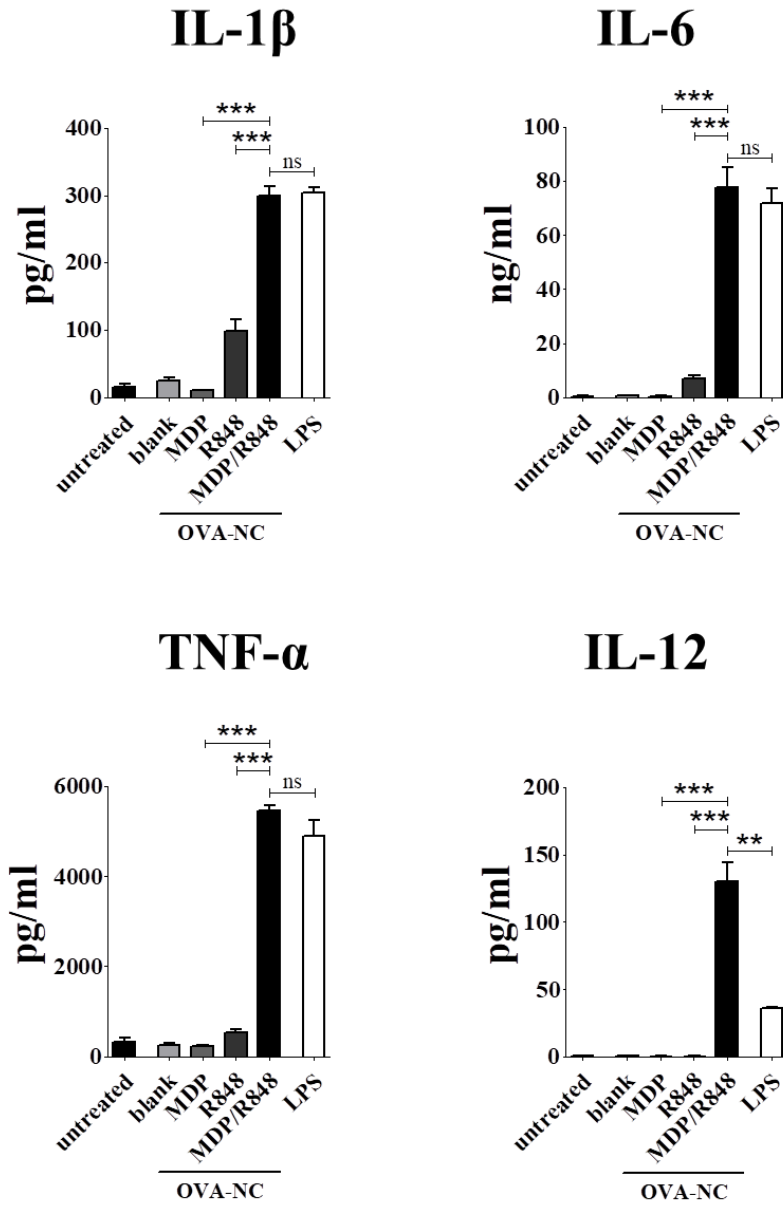


**Figure 25** Cytokine secretion triggered by adjuvant-loaded OVA-NCs

Cytokine contents in supernatants of BMDCs ( $1 \times 10^6$  cells/ml) treated with adjuvant-loaded OVA-NCs (100  $\mu\text{g/ml}$ ) for 24 h were analyzed by CBA. LPS treated BMDCs were used as positive control (mean  $\pm$  SD; n=3).

\*\*p < 0.01, \*\*\*p < 0.001. Data and figure published in the Journal of Controlled Release [249].

## RESULTS

The detected cytokine profile was in general comparable to that of BMDCs treated with Dex-MDP/R848. However, IL-12, an essential cytokine for Th1 promotion, was not detectable in case of Dex-MDP/R848 treatment (see Figure 15). In contrast, IL-12 secretion in BMDCs was strongly induced by OVA-MDP/R848-NCs, and to a significantly higher extent than evoked by LPS. Taken together, the adjuvant combination MDP + R848 encapsulated in OVA-NCs induced a strong Th1-promoting BMDC activation, even stronger than with the use of Dex-NPs.

As a complementary measure, all adjuvant-loaded OVA-NC formulations were checked for potential adjuvant leakage. Therefore, BMDCs were stimulated with these NCs and corresponding volumes of NC supernatants for 24 h. The subsequent analysis of CD80 and CD86 expression showed no relevant upregulation induced by NC supernatants, indicating that the encapsulated adjuvants were tightly sealed in the capsules (Figure S 7).

### 4.1.6.2 T cell stimulation with adjuvant-loaded OVA-NCs

To characterize the suitability of MDP/R848-loaded OVA-NCs to trigger OVA-specific T cell responses, proliferation assays with OT-I (CD8<sup>+</sup>) and OT-II (CD4<sup>+</sup>) T cells were performed based on the adjuvant-loaded OVA-NCs. OVA-blank- as well as OVA-MDP-NCs mediated only a weak OT-I and OT-II proliferation, whereas BMDC pre-treatment with OVA-R848-NC induced a moderate proliferation of OT-I, but not of OT-II T cells. A pre-incubation with OVA-MDP/R848-NCs triggered the strongest proliferation rates of both T cell types (Figure 26a). These results were highly consistent with the stimulation results of the corresponding OVA-NCs on BMDCs (see Figure 24).

To complete the picture, cytokines in the co-culture supernatants were measured by CBA. When stimulated with OVA-MDP/R848-NCs, BMDCs induced significantly increased levels of IFN- $\gamma$  in both T cell systems, while IL-5 and IL-10 concentrations remained on low to moderate levels in the OT-II co-cultures (Figure 26b).

## RESULTS

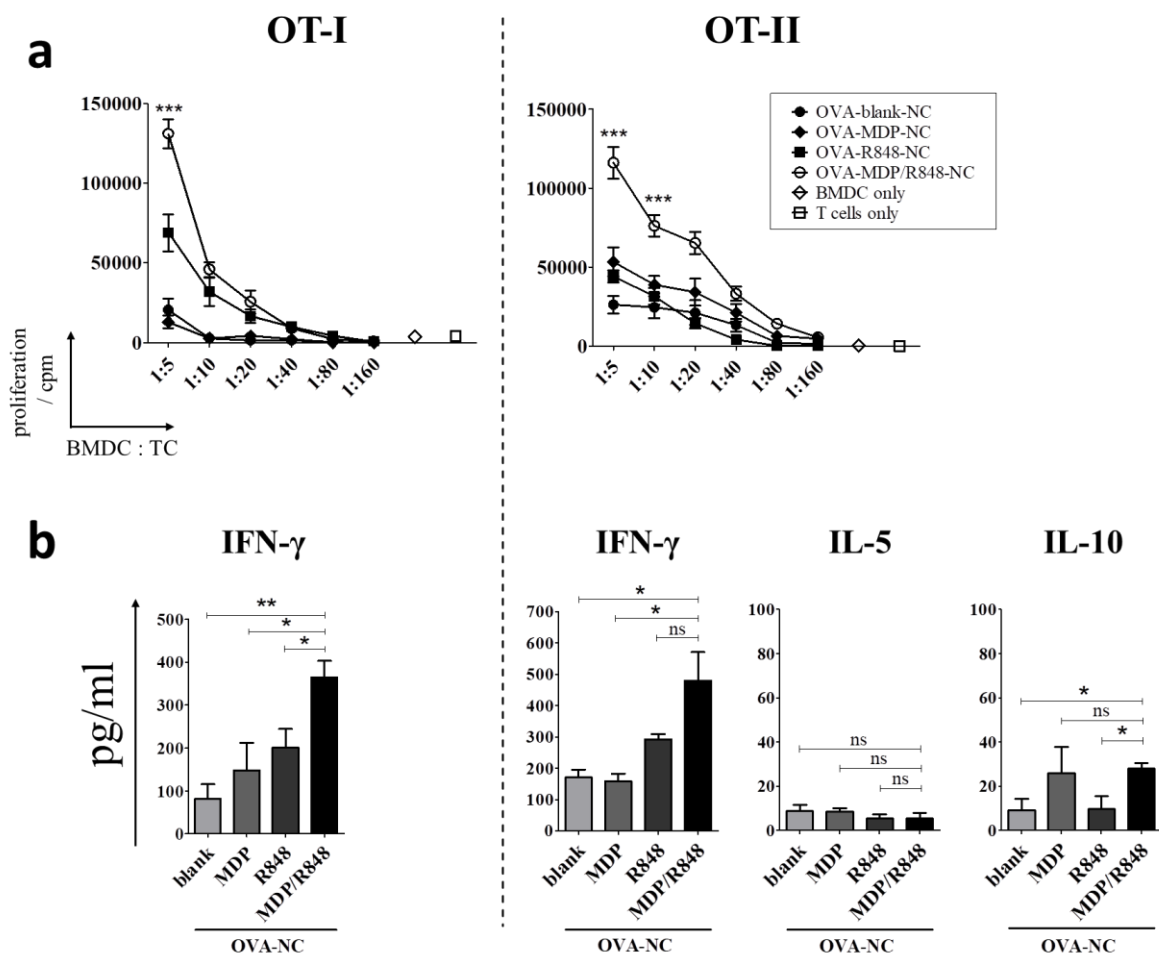


**Figure 26** T cell stimulation induced by adjuvant-loaded OVA-NCs

BMDCs ( $1 \times 10^6$  cells/ml) were incubated with OVA-blank-, OVA-MDP-, OVA-R848- or OVA-MDP/R848-NCs (each  $100 \mu\text{g/ml}$ ) for 24 h. (a) For proliferation measurement, titrated numbers of pre-treated BMDCs (starting with  $10^5$  cells) were co-cultured with OVA peptide-specific OT-I and OT-II T cells (each  $5 \times 10^5$  cells) in triplicates in 96 well plates. Proliferation was recorded in cpm by  $^3\text{H}$ -thymidine incorporation, applied after three days of BMDC/T cell co-culture for 16 h. Proliferation of BMDCs and T cells without treatment was used as control ( $n=3$ ). (b) Supernatants of BMDC/T cell co-culture were collected after 3 days, and cytokines of interest were measured by CBA (mean  $\pm$  SD,  $n=3$ ). \* $p < 0.05$ , \*\* $p < 0.01$ , \*\*\* $p < 0.001$ , OVA-MDP/R848-NC vs. OVA-R848-NC, unless otherwise indicated. Data and figure published in the Journal of Controlled Release [249].



#### 4.1.7 Transcriptome analysis of stimulated DC

Since the actual adjuvant effect might be different on transcriptional level, we analyzed the transcriptome of BMDCs after incubation with 75 µg/ml OVA-MDP/R848-NCs (1, 2 and 4 h pooled). As a control we used OVA-blank-NC-treated and untreated BMDCs. Transcriptome analysis allows a deeper understanding of the cellular processes that were initiated by a nanocarrier and its payload.

First of all, the total RNA of the treated samples was isolated and checked for purity. Therefore, RNA samples were separated by gel electrophoresis. RNA purity in all samples was confirmed by the characteristic 28S and 18S ribosomal RNA (rRNA) bands with a ratio of  $\geq 2$  (Figure S 9). Total RNA quantity was measured by NanoDrop. After transferring the RNA samples to StarSEQ, quality and quantity were checked once again prior to mRNA isolation. Samples with poor quality or low quantity were rejected. By RNA-Seq analysis, a total of 14,531 genes was identified of which numerous were strongly upregulated in the OVA-MDP/R848-NC-treated samples compared to both controls. First of all, the gene list was scanned for genes, which could be assigned to defined categories of interest, such as DC marker genes, cytokines or activation markers. The TPM values (see 3.10.3) of the corresponding genes were analyzed comparatively to identify changes on RNA level triggered by the MDP/R848-loaded OVA-NCs.

Focusing on genes of co-stimulatory molecules, we observed higher TPM values for CD40, CD80, CD83 and CD86 mRNA as well as for OX40L, ICAM-1 and ICOS-L in BMDCs after treatment with OVA-blank-NCs compared to the untreated cells. When treated with OVA-MDP/R848-NCs for the aforementioned short periods of time, the transcript numbers were increased by approximately 50 % as compared with the untreated control (Figure 27a). Regarding cytokines, the empty OVA-NCs induced only a decent increase in the expression of IL-1 $\alpha$ , IL-1 $\beta$ , IL-6, IL-12 $\beta$  and TNF- $\alpha$  mRNA. In contrast to that, the administration of adjuvant-loaded OVA-NCs triggered high numbers of all indicated cytokine mRNAs (Figure 27b).

## RESULTS

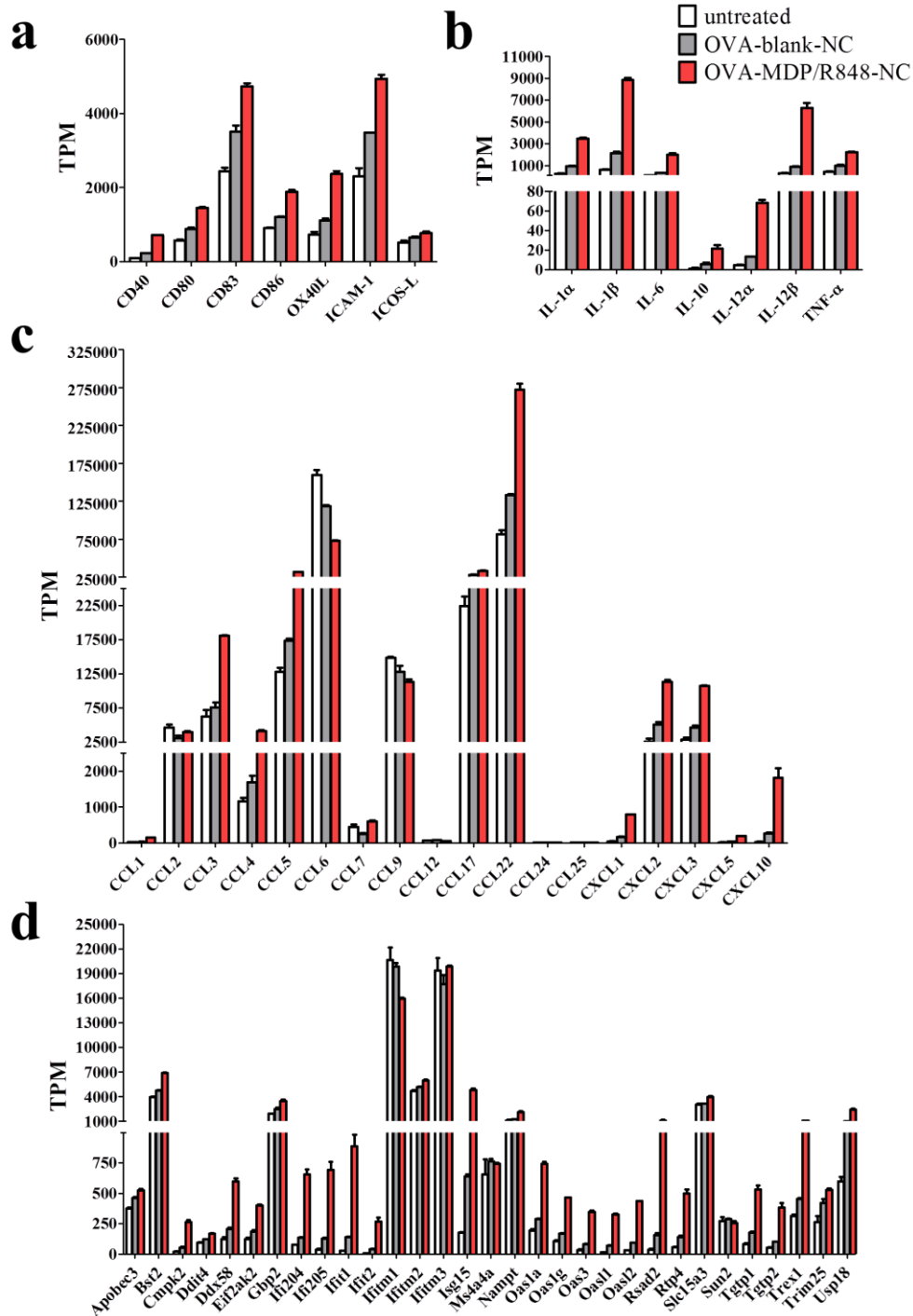


**Figure 27** mRNA expression of BMDCs treated with adjuvant-loaded OVA-NCs

BMDCs ( $2 \times 10^6$  cells/ml) were treated with OVA-blank- or OVA-MDP/R848-NCs (both  $75 \mu\text{g/ml}$ ) for 1, 2 and 4 h. Untreated BMDCs were used as negative control. The three time points of each sample were pooled, mRNA was isolated and RNA-Seq performed. TPM values for BMDC (a) activation markers, (b) cytokines, (c) chemokines and (d) interferon-stimulated genes were calculated (mean  $\pm$  SD; n=2).

## RESULTS

Chemokine mRNA expression in BMDCs was differentially affected by the MDP/R848-loaded capsules. Certain chemokine mRNAs were upregulated, such as CCL3, CCL5, CCL22, CXCL2 and CXCL3, whereas some showed no changes, reductions or were not detectable at all (Figure 27c). Interferon-stimulated gene products are important for an effective immune response. Therefore, we checked the mRNA expression of some members of this gene family. The mRNA levels of all indicated genes were consistently increased by the OVA-MDP/R848-NC treatment as compared to the controls (Figure 27d).

To characterize the influence of MDP/R848-loaded OVA-NCs on BMDCs mRNA expression as detailed as possible, the mRNA levels of further gene groups were analyzed, too. Gene groups in which an altered mRNA expression was not necessarily expected, for instance DC marker genes or TLRs/NLRs, were included in the analysis on purpose. Except some fluctuations and expected changes, the mRNA expression in the PRR and DC marker groups were relatively unaffected (Figure S 10). Expression analysis of important signaling components revealed some upregulated genes associated with MAPK/ERK- (e.g. TRAF6, Figure S 11a), NF- $\kappa$ B (e.g. I $\kappa$ B, Figure S 11b) and IFN-signaling (e.g. IRF7, Figure S 11c).

After calculating the mean enrichment scores (see 3.10.4) of all sample combinations for every gene, the gene list was sorted using these scores. A KEGG-annotated pathway analysis based on the DAVID software with a threshold of 2 (mean enrichment score  $\geq 2$ ) was performed for all sample combinations. So, only genes that were at least upregulated by the factor 2 were included into the analysis. Thereby, fitting genes were assigned to immunologically-relevant signaling pathways to assess the overall impact of OVA-MDP/R848-NCs on mRNA level.

Comparing the untreated control with the OVA-MDP/R848-NC-treated sample, ten relevant signaling pathways were determined of which marker genes were upregulated. All these pathways were connected with essential immunological processes, such as cell-cell-interaction, stimuli response and cell signaling. The number of upregulated genes ranged from 6 regarding NLR signaling (10.7 % of all NLR-associated genes according to DAVID) to 35 associated with cytokine-cytokine receptor interaction (14.3 % of all associated genes). The comparison of the OVA-blank-NC-treated sample with the OVA-

## RESULTS

MDP/R848-NC-treated one revealed reduced but still relatively high numbers of upregulated genes for seven of the analyzed pathways. For three pathways, namely cell adhesion molecules, antigen processing/presentation, and NLR signaling, no upregulated genes were detectable using a threshold of 2. The pathway analysis of the sample combination OVA-blank-NC versus untreated showed a further decrease in the number of upregulated genes. Still 16 genes were associated with cytokine-cytokine receptor interaction (6.5 %), whereas less than 10 genes were assigned to the other pathways. As expected, this time upregulated genes regarding antigen processing/presentation were detectable again (Table 18).

Pathway	Upregulated genes (threshold = 2)		
	OVA-blank-NC / untreated	OVA-MDP/R848-NC / OVA-blank-NC	OVA-MDP/R848-NC / untreated
Cytokine-cytokine receptor interaction	16 (6.5 %)	29 (11.8 %)	35 (14.3 %)
TNF signaling	8 (7.3 %)	15 (13.8 %)	25 (22.9 %)
JAK/STAT signaling	7 (4.8 %)	14 (9.7 %)	21 (14.5 %)
TLR signaling	9 (8.9 %)	12 (11.9 %)	20 (19.8 %)
Chemokine signaling	6 (3.1 %)	14 (7.1 %)	17 (8.7 %)
NF-κB signaling	5 (5.2 %)	11 (11.3 %)	17 (17.5 %)
Cell adhesion molecules	0	0	15 (9.3 %)
MAPK/ERK signaling	0	8 (3.2 %)	13 (5.1 %)
Antigen processing/presentation	4 (4.9 %)	0	9 (11 %)
NLR signaling	0	0	6 (10.7 %)

**Table 18** KEGG-annotated pathway analysis

A KEGG-annotated pathway analysis was performed for BMDCs treated with OVA-blank-NCs and OVA-MDP/R848-NCs respectively (both 75 µg/ml for 1, 2 and 4 h pooled). Untreated BMDCs served as control. A mean enrichment score  $\geq 2$  was used as threshold. The numbers of upregulated genes and the corresponding percentages of the total number of associated genes for all sample combinations were assigned to immunologically-relevant signaling pathways.

## RESULTS

Since the KEGG-annotated pathway analysis indicated remarkable differences in the numbers of upregulated genes in distinct signaling groups of the three sample combinations, heat maps based on mean enrichment scores (n-fold transcripts) of well-described pathway members were generated. Some genes were listed more than once due to their association to several signaling pathways. Heat map analysis of the different signaling pathways revealed distinct genes (mainly key regulators) with increased transcript numbers in every group, whereas many genes were not influenced at all (Figure 28-Figure 30).

To verify the RNA-Seq results with a different method, we picked four upregulated (IL-12 $\beta$ , IRF7, CXCL10 and NOS2), one downregulated (F2RL2) and one slightly downregulated gene (CD11c) and measured the relative copy numbers of those genes in the three mentioned samples by qPCR. The computational analysis of the PCR data showed results similar to those observed with RNA-Seq for all measured genes. Partially, the relative copy numbers were highly comparable (Figure 31, Figure 32). A direct comparison with the results from 4.1.6.1 showed a strong consistency between protein translation and gene transcription of co-stimulatory markers and cytokines induced by OVA-MDP/R848-NCs in BMDCs. All measured markers were upregulated on both analysis levels upon NC treatment (Table 19).

## RESULTS

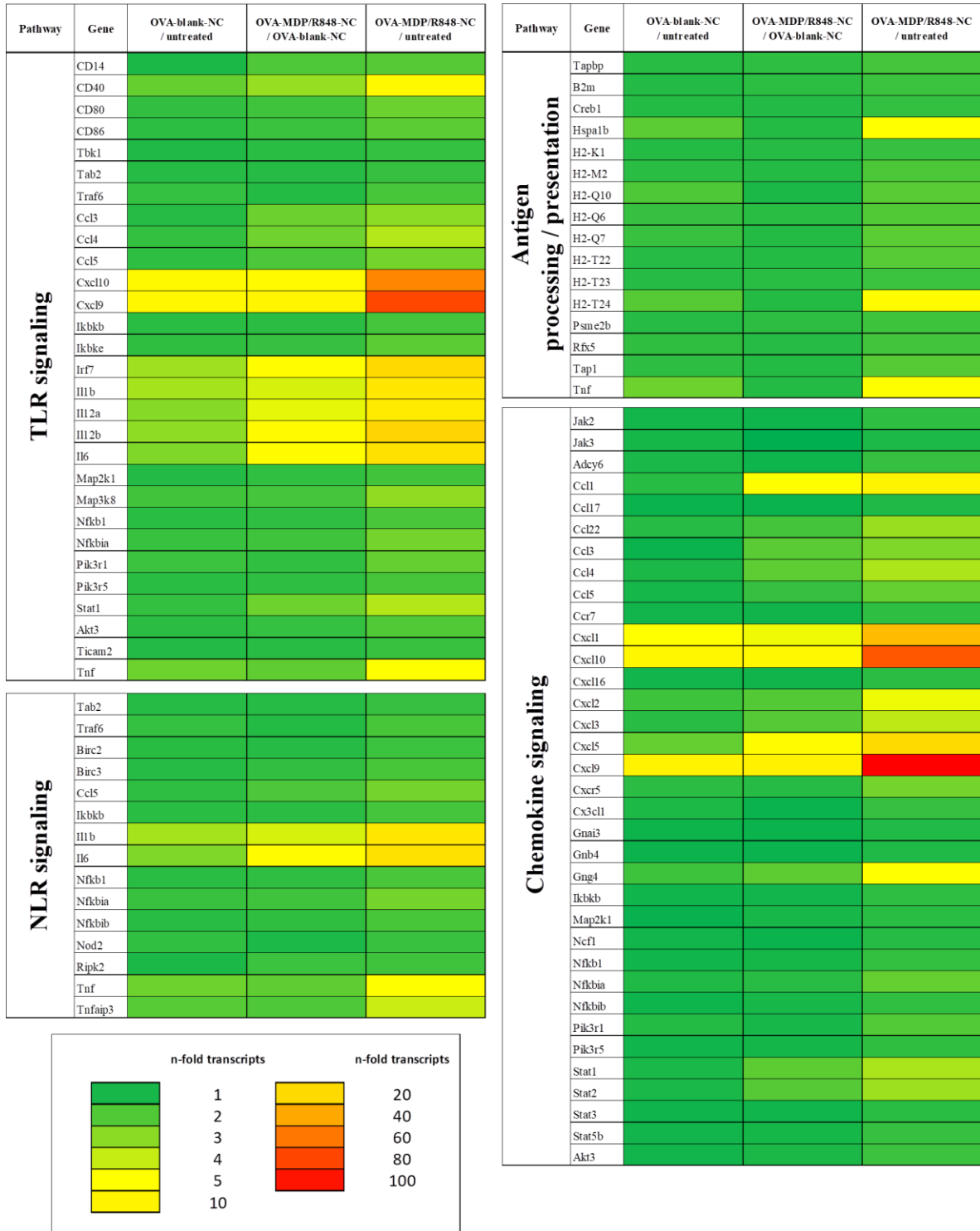


**Figure 28** Heat map based on mRNA mean enrichment scores (part 1)

Based on the calculated mean enrichment scores of the three sample combinations, heat maps for the pathways TLR signaling, NLR signaling, antigen processing/presentation and chemokine signaling were generated. Coloring indicates the n-fold of gene mRNA transcripts in the corresponding combination.

## RESULTS

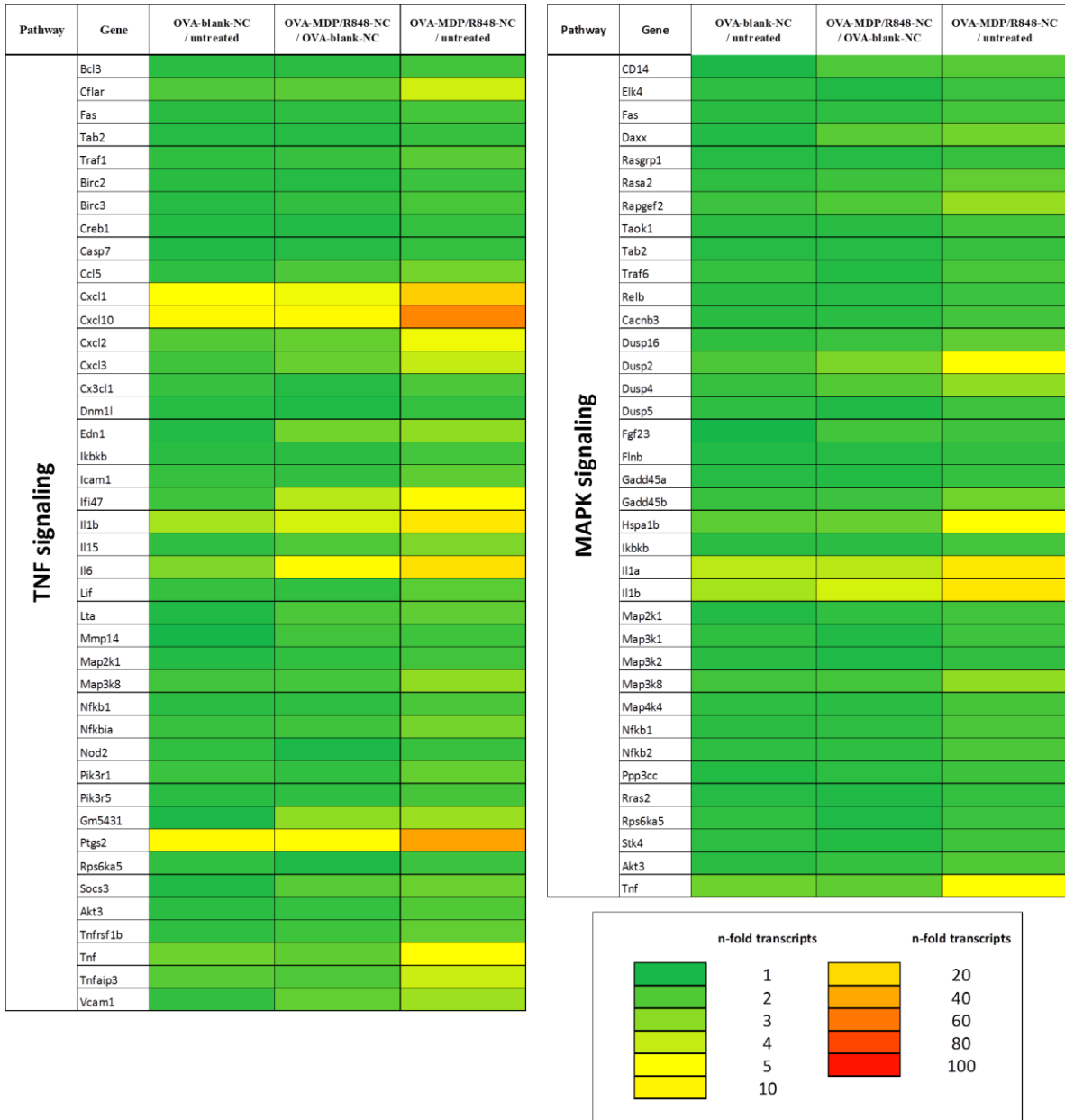


**Figure 29** Heat map based on mRNA mean enrichment scores (part 2)

Based on the calculated mean enrichment scores of the three sample combinations, heat maps for the pathways TNF signaling and MAPK/ERK signaling were generated. Coloring indicates the n-fold of gene mRNA transcripts in the corresponding combination.

## RESULTS

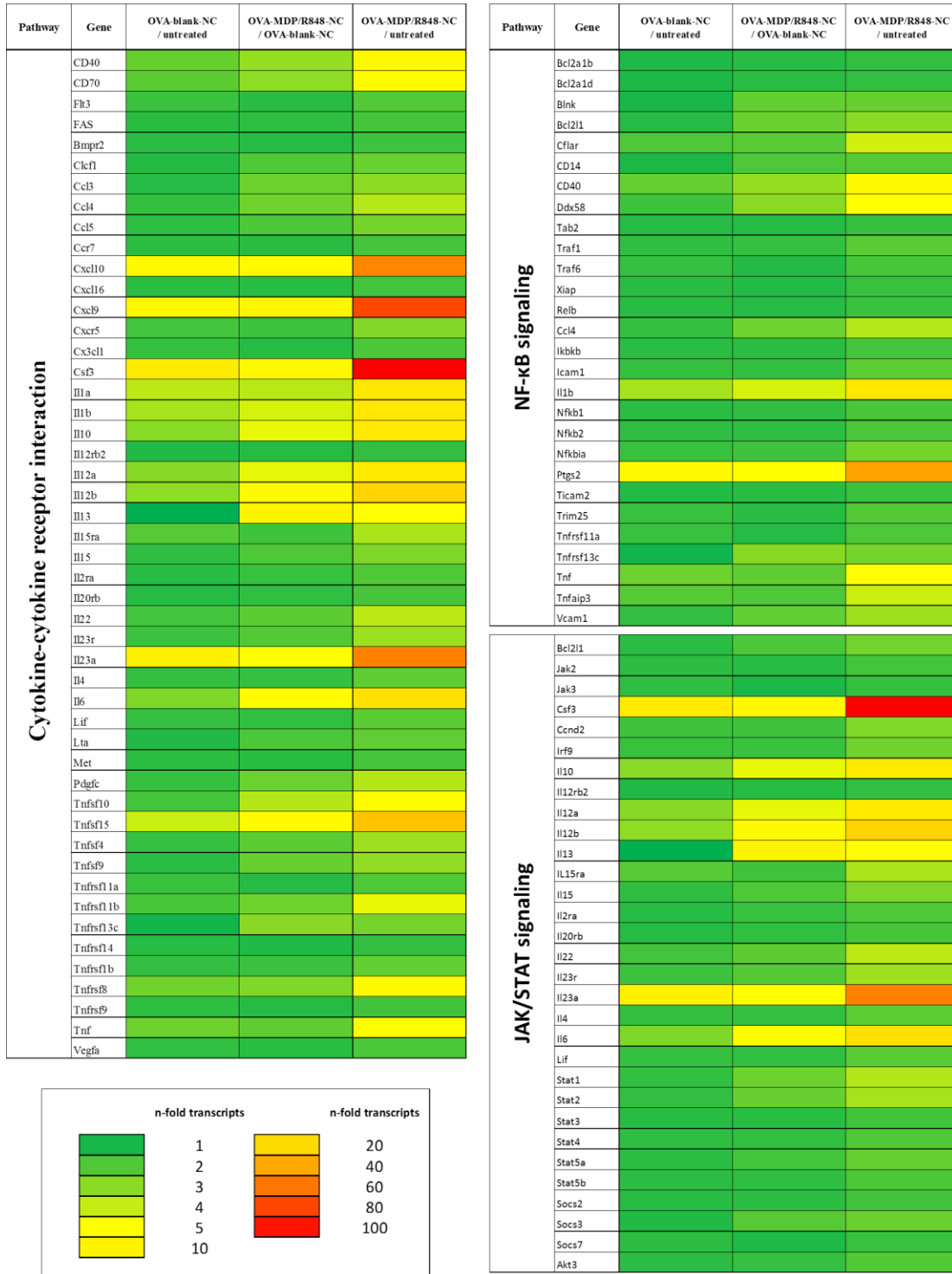


**Figure 30** Heat map based on mRNA mean enrichment scores (part 3)

Based on the calculated mean enrichment scores of the three sample combinations, heat maps for the pathways cytokine-cytokine receptor interaction, NF-κB and JAK/STAT signaling were generated. Coloring indicates the n-fold of gene mRNA transcripts in the corresponding combination.



## RESULTS

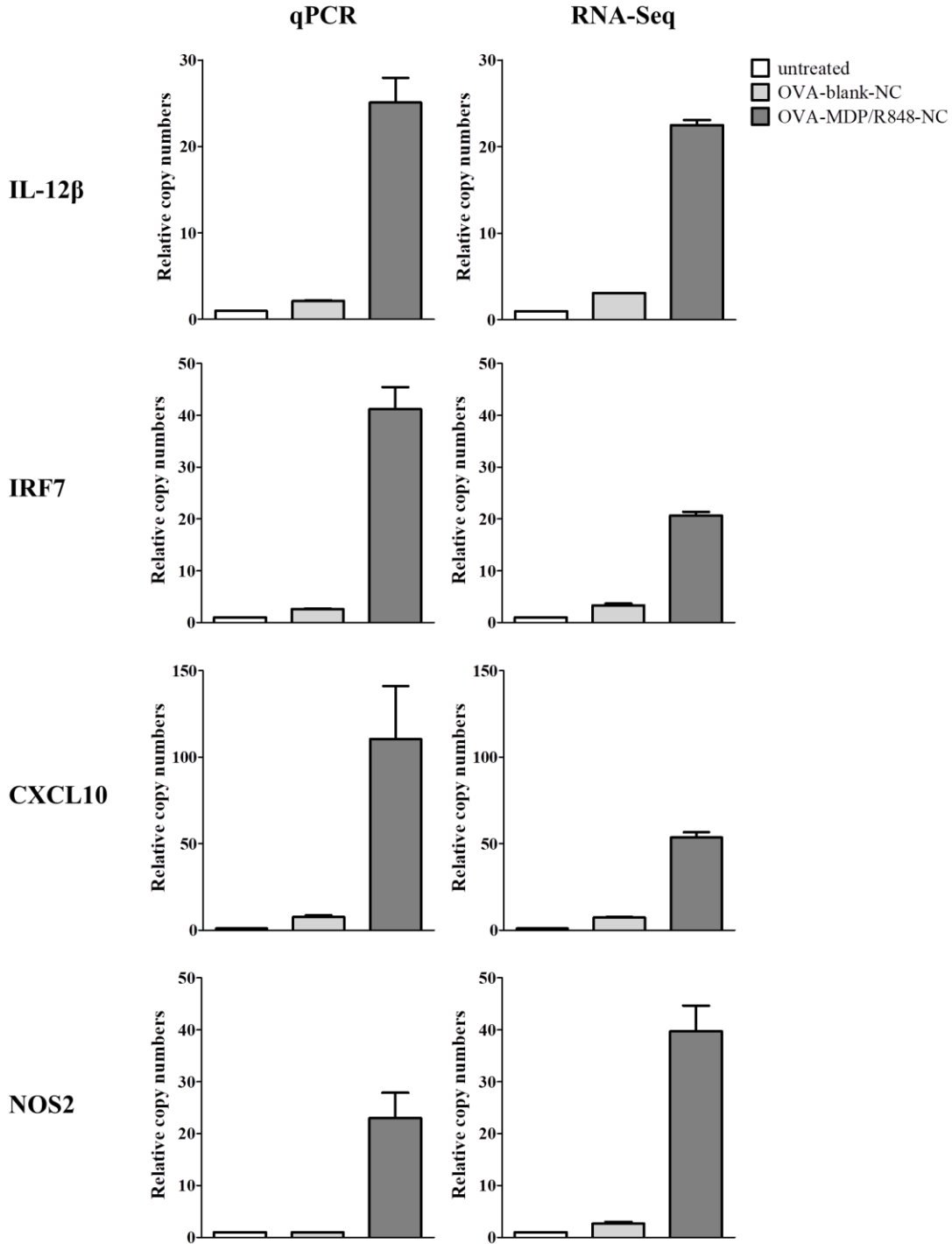


**Figure 31** qPCR and RNA-Seq results for exemplary upregulated genes

To verify the RNA-Seq results for BMDCs treated with MDP/R848-loaded OVA-NCs (75  $\mu$ g/ml, incubation for 1, 2 and 4 h pooled) with a different method, qPCR measurements for exemplary upregulated genes (IL-12 $\beta$ , IRF7, CXCL10 and NOS2) were performed. Relative copy numbers were compared to the corresponding RNA-Seq numbers (mean  $\pm$  SD; n=2).

## RESULTS

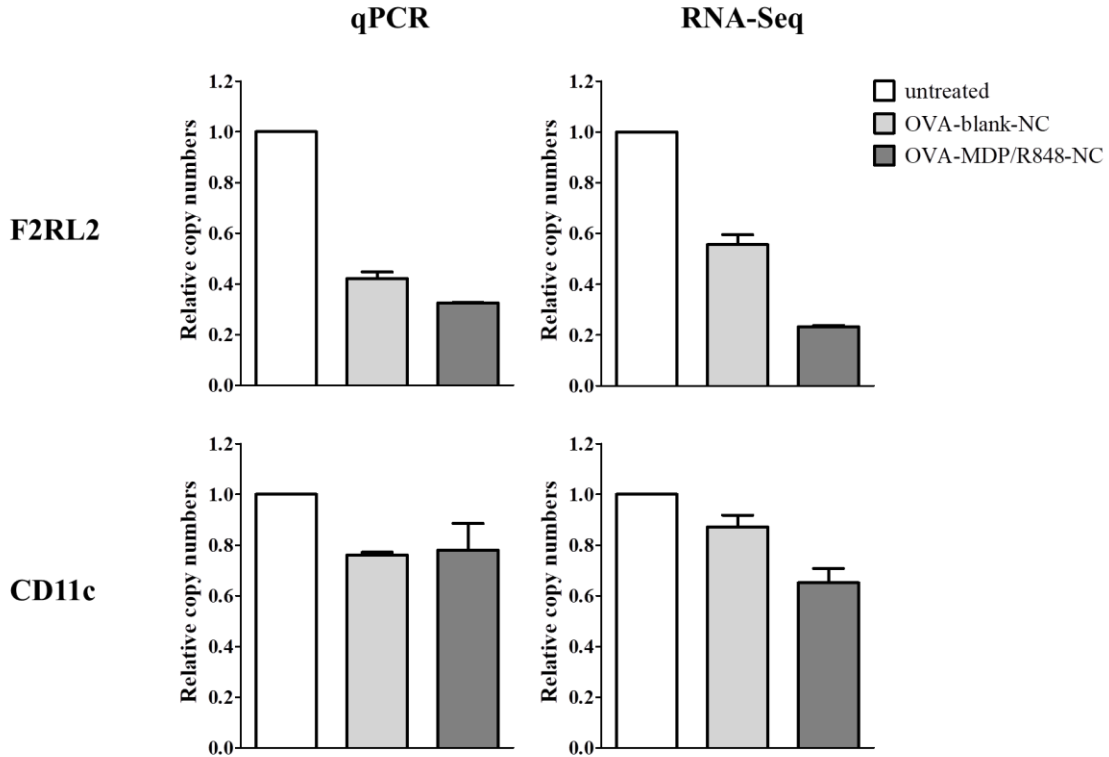


**Figure 32** qPCR and RNA-Seq results for exemplary downregulated/balanced genes

To verify the RNA-Seq results for BMDCs treated with MDP/R848-loaded OVA-NCs (75 µg/ml, incubation for 1, 2 and 4 h pooled) with a different method, qPCR measurements were also performed for exemplary downregulated (F2RL2) and balanced (CD11c) genes. The relative copy numbers from qPCR were blotted next to the corresponding RNA-Seq numbers (mean ± SD; n=2).

Marker	Flow cytometry / CBA	RNA-Seq
<b>CD80</b>	↑↑	↑
<b>CD86</b>	↑↑	↑
<b>IL-1β</b>	↑↑	↑↑
<b>IL-6</b>	↑↑	↑
<b>TNF-α</b>	↑↑	↑
<b>IL-12</b>	↑↑	IL-12α ↑, IL-12β ↑↑

**Table 19** Translational vs. transcriptional effects of OVA-MDP/R848-NCs in BMDCs

### 4.1.8 Spleen cell interaction with dual-adjuvant OVA-NCs

As a first important step towards *in vivo* application of OVA-NC formulations for vaccination approaches, we analyzed the interplay between OVA-NCs (empty as well as adjuvant-loaded) and primary immune cell populations derived from spleen. Since the spleen is a relevant (secondary) lymphoid organ and provides high immune cell yields, spleen cells are an appropriate test system for such an analysis. This complex immune cell mixture contains, among others, DCs, T cells, B cells and macrophages in varying ratios. The cytometric analysis was performed based on a pre-defined gating strategy (Figure S 8).

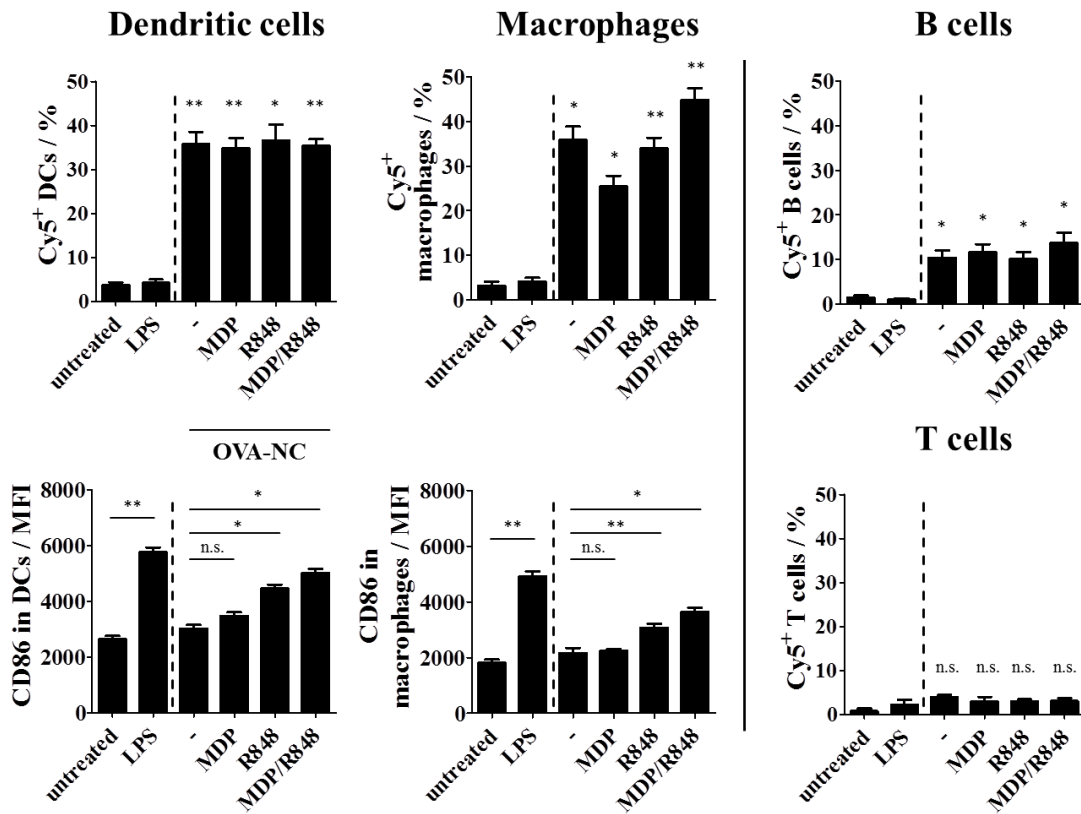


**Figure 33** Spleen cell interaction with adjuvant-loaded OVA-NCs

Isolated spleen cells ( $1 \times 10^6$  cells per sample) were incubated with empty or adjuvant-loaded OVA-NCs (each 100  $\mu\text{g/ml}$ ) for 24 h. Cellular binding by DCs, macrophages, B and T cells was assessed by measuring frequencies of Cy5<sup>+</sup> cells. Activation of DCs and macrophages was analyzed via CD86 expression (MFIs). Untreated and LPS (100 ng/ml) treated cells were used as controls (mean  $\pm$  SD; n=3). \*p < 0.05, \*\*p < 0.01, sample vs. untreated. Data and figure published in the Journal of Controlled Release [249].

## RESULTS

DCs as well as macrophages showed strong OVA-NC binding, whereas their binding by B cells was rather low. T cells did not show any significant binding of OVA-NCs. An influence of encapsulated adjuvants on cellular binding was not detectable. Similarly, all OVA-NC formulations were preferentially bound by DCs and macrophages regardless of any adjuvant payload. The expression of CD86 in DCs and macrophages was significantly increased after treatment with adjuvant-loaded OVA-NCs, and was highest in case of OVA-MDP/R848-NCs (Figure 33). These results were highly comparable to those obtained using BMDCs.

### 4.1.9 Alternative cross-linking method for protein nanocapsules

In case of the previously used OVA-NC formulations, TDI was used as cross-linker to generate a hollow nanocapsule with a protein shell around an aqueous core. This procedure is well-established and robust, but lacks compound selectivity. Since it cannot be excluded that the electrophilic isocyanate also reacts with soluble cargo substances during synthesis, possibly leading to loss of substance functionality, alternative, more selective cross-linking methods for the generation of protein-based nanocapsules were assessed.

One interesting approach for effective drug encapsulation paired with high compound selectivity is the application of bioorthogonal tetrazole-ene cycloaddition (see 3.1.2.1). OVA and HSA were exploited for the preparation of such nanocapsules. To this end, these proteins were modified with TET and cross-linked with DN. To be able to test the new capsule batch for their suitability as drug delivery system, R848 was encapsulated as an active drug. The resulting NCs based on OVA (OT-DN-R848-NCs) and HSA (HT-DN-R848-NCs) showed an average diameter of 287.5 nm in cyclohexane and 303 nm in water due to swelling. Their zeta potential was determined as approximately -33.5 mV (Table S 5). Subsequently, the new capsules were administered to BMDCs for 24 h to check for effective R848 release and resulting stimulation via CD86 expression. BMDCs were also treated with OVA-R848-NCs (TDI cross-linked, as already described) to allow direct comparison between TDI and TET-DN cross-linked capsules. In this context, the same amounts of soluble R848 were used for the synthesis of the different capsule formulations. Cytometric analysis of the CD86 expression of accordingly treated BMDCs showed a strong increase when using 100 µg/ml of either R848-loaded NC, though OT-DN-R848-

## RESULTS

and HT-DN-R848-NCs triggered such an increase at a dose of 10  $\mu\text{g}$  per ml already (Figure 34).

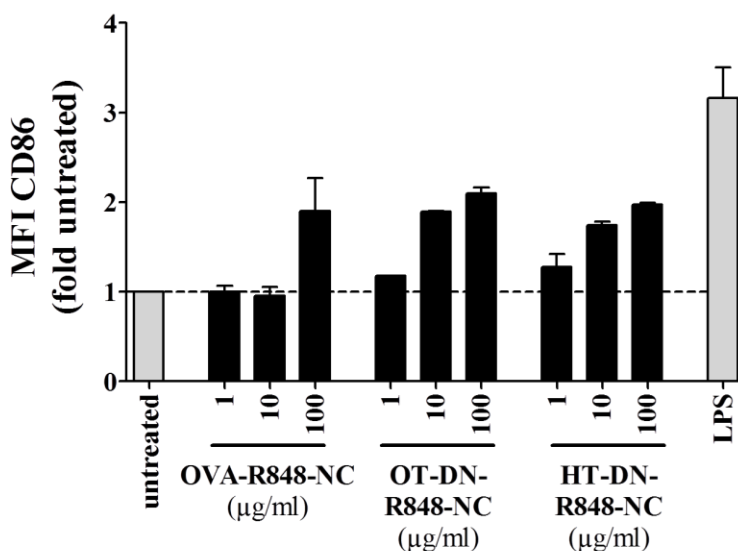


**Figure 34** Comparison of TDI and TET-DN cross-linked nanocapsules

BMDCs ( $2 \times 10^5$  cells/ml) were treated with OVA-R848-NCs, OT-DN-R848-NCs and HT-DN-R848-NCs in indicated concentrations for 24 h. Untreated (dashed line) and LPS-treated (100 ng/ml) BMDCs were used as control. Resulting expression of CD86 was measured by flow cytometry and plotted as fold untreated (mean  $\pm$  SD; n=2). Data published in *Nanoscale Horizons* in a modified version [238].

Similar to TDI cross-linked OVA-NC formulations, a leakage of encapsulated adjuvants could potentially lead to unintended BMDC stimulation here, too. To exclude that, BMDCs were additionally stimulated with corresponding volumes of the NCs supernatants. At all concentrations tested, the NC supernatants did not induce increased expression of CD86 in BMDCs (Figure S 12).

## 4.2 PEG shielding of nanocarriers

Surface modification with PEG is a commonly used and well-described, albeit controversially discussed, method to increase a nanocarriers' blood circulation time (stealth effect). In theory, a shielding with the relatively inert PEG molecules reduces unspecific NP interactions with cells, gives the NP more time to reach its target and thus enhances the specificity of a potential targeting moiety. OVA-NCs offer the opportunity to be modified with PEG chains. Since these capsules were intended to be taken up and processed specifically by DCs, but were also effectively bound by macrophages (see 4.1.8), a reduced unspecific NC interaction by PEGylation might be useful. Additionally, PEG protects the NC against enzymatic degradation and increases its water solubility. All these points would be advantageous regarding *in vivo* application.

To assess if a PEG modification of OVA-based NCs actually reduces unspecific cell interactions, PEGylated OVA-NCs were synthesized (see 3.1.2), varying in MW of the used PEG and in the density of PEGylation. Since it is known that the protein environment can influence the interaction between NPs and cells, binding studies with BMDCs were performed under different protein supplementations. FCS, mS and hS were applied to the samples at defined concentrations. Samples applied without additional serum supplementation were used as control.

Serum of a foreign species might cause unintended rejection reactions when coming in contact with murine BMDCs. To exclude that, BMDCs were incubated with defined amounts (1-10 vol-%) of the different sera in an initial experiment without any NCs. Since complement factors are known to be a potential trigger for increased rejection, BMDCs were also treated with the same protein solutions but heat-inactivated (HI, 30 min, 56 °C). HI is used to inactivate containing complement. The cell viability after a 4 h treatment was used as readout (see 3.6.2). It was shown, that FCS and mS did not mediate increased cell death, neither native nor HI. In contrast, native hS caused a massive reduction in viability of BMDCs. Upon HI, hS lost its cytotoxic properties against BMDCs. To ensure a high level of comparability, FCS, mS and hS were consequently HI before use from then on.

## RESULTS

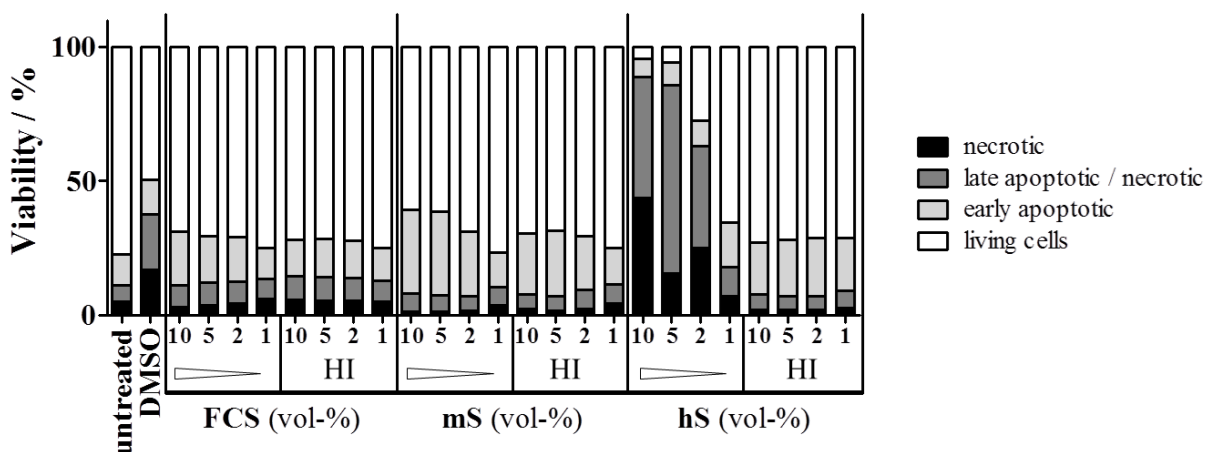


**Figure 35** Cytotoxicity of different sera on murine BMDCs

To check for potential cytotoxicity, BMDCs ( $1 \times 10^6$  cells/ml) were treated with indicated volumes (1-10 vol-%) of FCS, mS and hS (each native and HI) for 4 h. The resulting viability was measured by 7AAD/Annexin V staining. Untreated cells were used as negative, DMSO-treated (10 vol-%) ones as positive control.

### 4.2.1 Influence of PEG molecular weight

PEG is available in various MW (numerically equivalent to atomic mass in Dalton (Da)). To analyze to what extent the MW of the coupled PEG influences the interaction of protein-based NCs with BMDCs, we generated OVA-NCs surface-functionalized with three PEG variants (2000, 3400, 5000 Da), coupled at almost the same density with  $\sim 0.2$  PEG chains per  $\text{nm}^2$  NC (see Table 9). These capsules were tested for their stealth properties on BMDCs compared to non-PEGylated OVA-NCs (OVA-blank-NCs). All NC formulations were applied to the cells simultaneously with the different sera (5 vol-%). After 4 h of incubation, the binding of PEGylated OVA-NCs to BMDCs was assessed by flow cytometry.

It turned out, that the NC modification with the high MW PEG (PEG<sub>5000</sub>) was the most effective one regarding the extent of gained stealth effect followed by the modification with moderate (PEG<sub>3400</sub>) and low MW PEG (PEG<sub>2000</sub>). The increase in MW of the PEG correlated inversely with the resulting Cy5 frequencies and MFIs of such treated BMDCs. Despite the relatively low PEGylation density, a reduced interaction of BMDCs with PEG-

## RESULTS

modified OVA-NCs compared to non-PEGylated ones was still detectable. Regarding protein environment, the results for BMDCs which were supplemented with FCS and mS were highly comparable. Those, which were not treated with serum, showed slightly higher binding of the non-PEGylated and the PEG<sub>2000</sub>-modified OVA-NCs. Cellular binding of the unmodified capsule was further increased when co-applied with hS. The observed binding of OVA-NCs modified with PEG<sub>3400</sub> was consistently between those modified with PEG<sub>2000</sub> and with PEG<sub>5000</sub>. However, the impact of the different sera on OVA-NC interaction with BMDCs was relatively low but particularly detectable on MFI level (Figure 36).

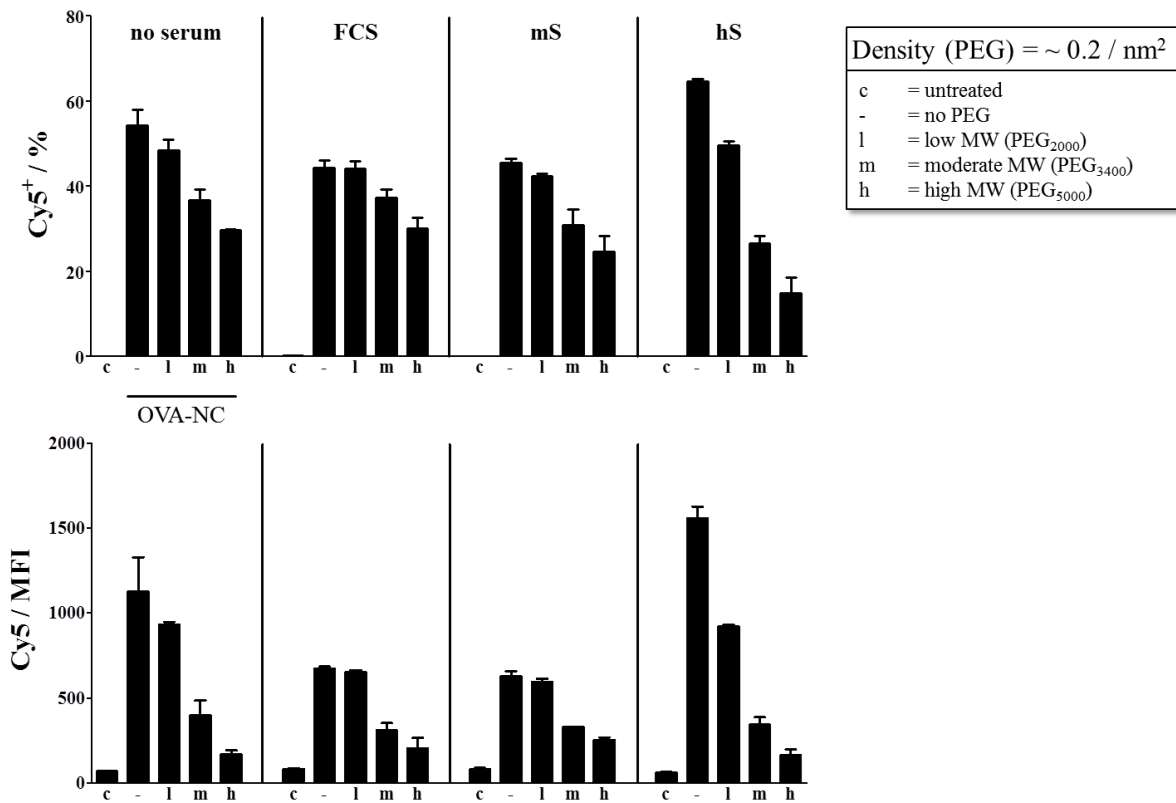


**Figure 36** NCs' stealth effect determined by PEG MW

The interaction of BMDCs with PEGylated OVA-NCs depending on PEG MW was assessed by incubating BMDCs ( $1 \times 10^6$  cells/ml) with capsules that were modified with PEG chains of different MW (2000, 3400, 5000 Da) but in almost the same PEGylation density ( $\sim 0.2 / \text{nm}^2$ ). After 4 h of incubation, the resulting frequencies of NC positive cells and corresponding MFIs were measured by flow cytometry. Cells treated with non-PEGylated OVA-NCs and untreated ones were used as control (mean  $\pm$  SD; n=2).



## RESULTS

### 4.2.2 Influence of PEGylation density

The density of PEG coupling on the NC's surface was another crucial factor to be considered. A PEGylation of high density potentially reduces the surface that is effectively accessible for cellular interaction. To measure the influence of different PEGylation densities on the interplay with BMDCs, OVA-NCs were modified with PEG<sub>2000</sub> at three densities (2.47, 0.54 and 0.18 PEG chains per nm<sup>2</sup>). BMDC interaction with these capsules was analyzed by flow cytometry.

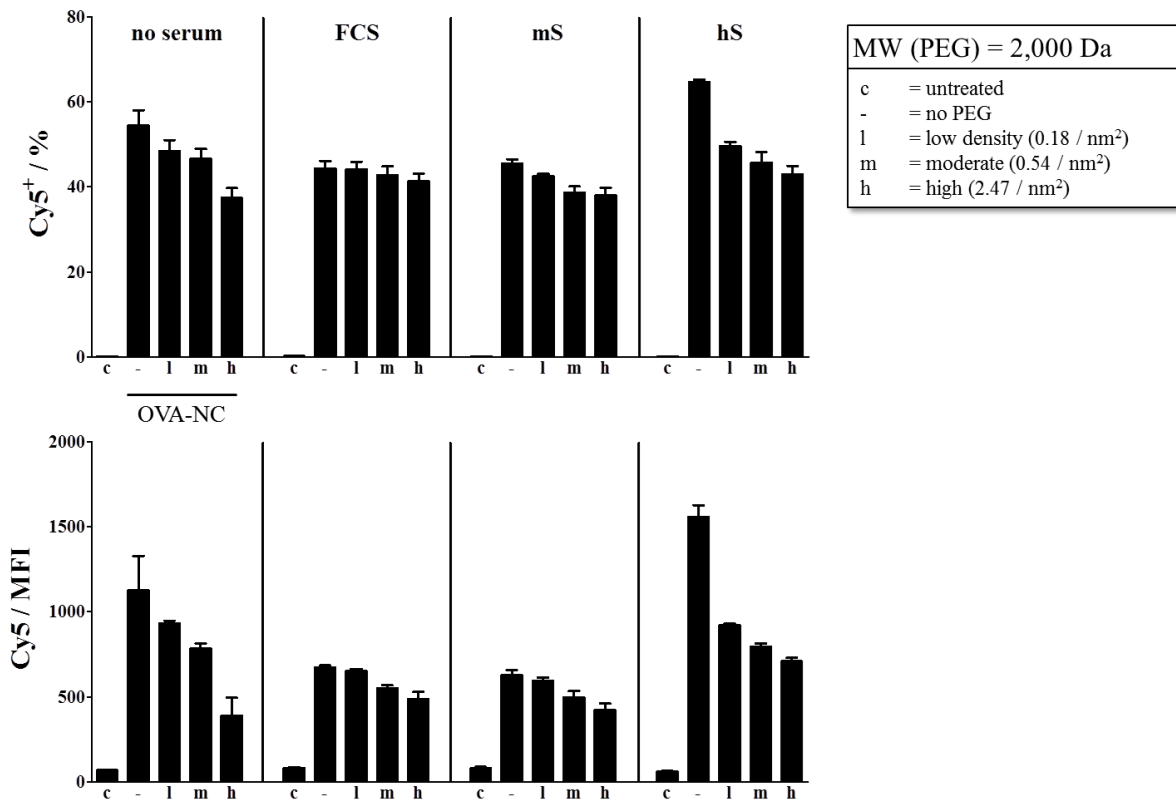


**Figure 37** NCs' stealth effect determined by PEGylation density

The interaction of BMDCs with PEG-modified OVA-NCs depending on PEGylation density was assessed by incubating BMDCs ( $1 \times 10^6$  cells/ml) with capsules that were modified with PEG<sub>2000</sub> in different densities (2.47, 0.54, 0.18 PEG chains per nm<sup>2</sup>). After 4 h of incubation, the resulting frequencies of NC positive cells and corresponding MFIs were measured by flow cytometry. Cells treated with non-PEGylated OVA-NCs and untreated ones were used as control (mean  $\pm$  SD; n=2).

## RESULTS

It was shown that OVA-NCs with the highest surface density of PEG<sub>2000</sub> induced the strongest binding reduction. The lower the PEG density, the weaker was the resulting stealth effect. This tendency was particularly apparent in case of “no serum” and hS supplementation. Upon FCS and mS, these differences were much weaker (Figure 37).

### 4.2.3 Relevance of mass density

Another interesting factor to be considered regarding OVA-NC shielding with PEG was the mass density of NC-coupled PEG chains. Mass density means the atomic mass of PEG per nm<sup>2</sup> of NC surface.

If the stealth effect evoked by PEG was due to the total mass of PEG but independent of the individual PEG chain mass, two OVA-NCs with the same PEG mass density would be expected to bind equally to BMDCs. To test this theory, two OVA-NCs with different PEG chain masses (PEG<sub>2000</sub> / PEG<sub>5000</sub>) and densities (0.54 / 0.19 PEG chains per nm<sup>2</sup>) but almost the same mass density (~ 1,000 Da/nm<sup>2</sup>) were used for experiments.

Although both OVA-NCs exhibited almost the same mass density, the capsule modified with PEG<sub>5000</sub> showed a much stronger binding reduction compared to the non-PEGylated capsules than the PEG<sub>2000</sub>-modified one. The simultaneous administration of serum did not affect this result. The only differences were slightly reduced MFIs for both OVA-NCs upon FCS and mS (Figure 38).

In summary, the strongest stealth effects were achieved by using PEG<sub>5000</sub>, though its density on OVA-NC's surface was always lower than in case of PEG<sub>2000</sub> or PEG<sub>3400</sub>. As exemplified by PEG<sub>2000</sub> modifications, an increased PEG density on NC's surface also increased the resulting stealth effect. Moreover, it turned out that mass density of the coupled PEG played a minor role. A short PEG chain coupled at a high density does not seem to provide advantages over a longer PEG chain coupled in a lower density.

## RESULTS

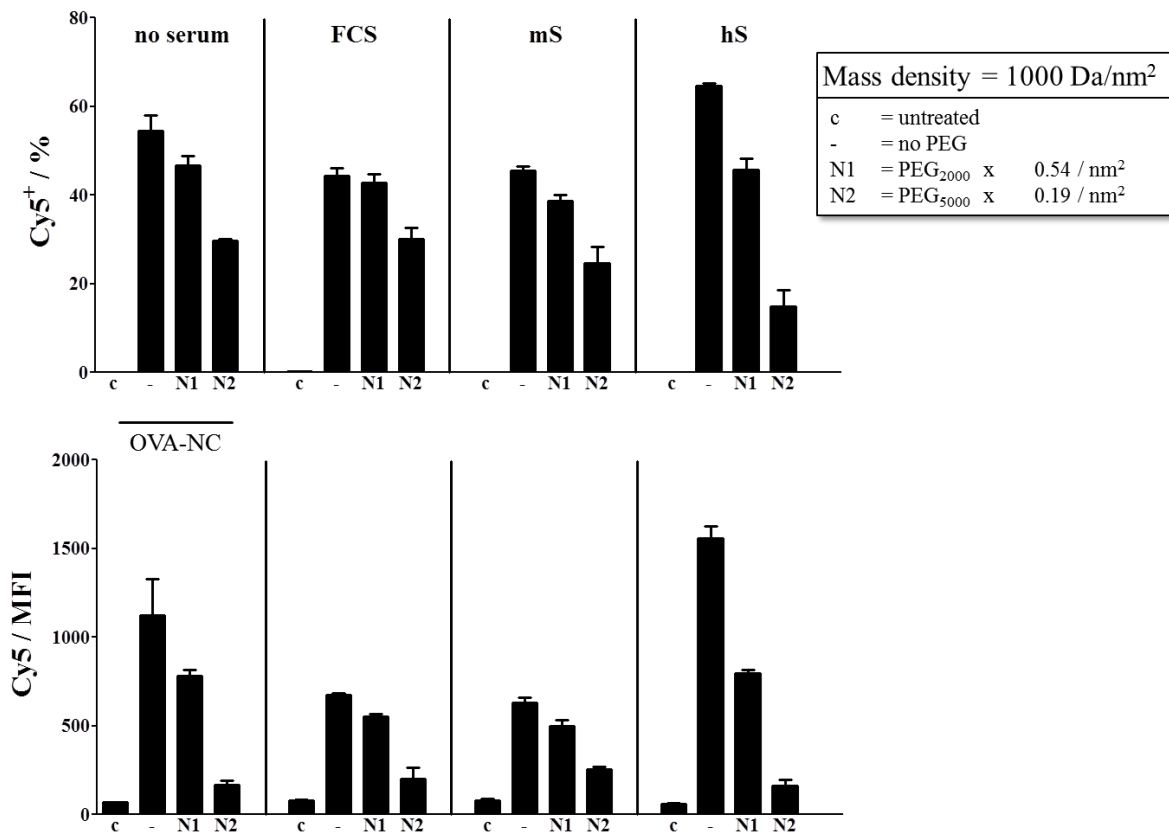


**Figure 38** NCs' stealth effect determined by PEG mass density

BMDC interaction with PEG-modified OVA-NCs depending on mass density was assessed by incubating BMDCs ( $1 \times 10^6$  cells/ml) with capsules of the same mass density but different PEG chain masses and densities. After 4 h of incubation, resulting Cy5 frequencies and MFIs were measured by flow cytometry. Cells treated with non-PEGylated OVA-NCs and untreated ones were used as control (mean  $\pm$  SD; n=2).

### **4.3 Gene silencing with siRNA-loaded nanocarriers**

Another method to influence and control processes of the immune system is the usage of siRNA to precisely knockdown expression of specific genes. These small RNA molecules are integrated into a multiprotein complex, called RNA-induced silencing complex (RISC), after entering the cell. As part of the RISC, the siRNA binds its complementary sequence on the target cell's mRNA and mediates cleavage. In this way, it inhibits the expression of the corresponding sequence or gene. By this approach, the activity of a regulatory gene might be affected to boost or extend a cellular immune response. This procedure, called RNA interference (RNAi), is a very powerful genetic tool, even though it necessarily requires efficient transfer of the siRNA into the cell. In addition, siRNA molecules need constant protection against enzymatic degradation processes mainly mediated by RNases. Nanocapsules with an aqueous core perfectly fulfil those requirements by accommodating the hydrophilic siRNA inside. Therefore, RNAi is a promising concept for nanocapsule-based immune modulation, in particular as an add-on for nanovaccines. The integration of a specific siRNA into an existing nanovaccine provides an additional level of control and fine-tuning.

PEGylated HES-NCs are a well-described drug delivery system that has already been used for diverse biological approaches. For that reason, it was tested whether such modified HES-NCs are a suitable delivery system for siRNA. Since RNA interference is a sensitive and error-prone process, we decided to leave out any antigen source (such as OVA) to be able to assess the siRNA effect as unbiased as possible. In principle, the synthesis was comparable to that of TDI cross-linked OVA-NCs (see 3.1.2). But instead of adjuvants, siRNA (target-specific or negative control) was encapsulated into the HES-NCs. As a siRNA target, the commonly used firefly luciferase reporter gene was chosen. The genetically modified DC cell line DC2.4-mCMV (see 3.4.1), which expresses firefly luciferase at moderate levels, was used as a readout system. The expression of luciferase could be assessed by measuring the bioluminescence after administration of a specific luciferase substrate (see 3.5.4). Additionally, the HES-NCs' surface was modified with PEG<sub>5000</sub> to reduce unspecific uptake.

## RESULTS

First of all, the generated cell line was checked for successful transduction by measuring luciferase and copGFP expression. Bioluminescence measurements of DC2.4-mCMV compared to non-transduced DC2.4 revealed a clearly detectable luciferase activity in the transduced version, whereas the non-transduced cells showed almost no signal (Figure 39a). As a further control, expression of the co-transduced reporter copGFP was visualized by fluorescence microscopy (Figure 39b). To test the bioactivity of the used siRNAs, namely Luciferase GL2 Duplex ( $\alpha$ Luc siRNA) and AF647-labeled AllStars Negative Control siRNA (control siRNA), in the same setup, samples of DC2.4-mCMV were treated with the siRNAs alone or after their complexation with the transfection reagent lipofectamine for 24 h. As expected, siRNA alone, lipofectamine without siRNA as well as lipofectamine plus control siRNA did not reduce the basic bioluminescence of DC2.4-mCMV, whereas the combination of lipofectamine and  $\alpha$ Luc siRNA knocked-down the luciferase signal by approximately 60 % (Figure 39a).

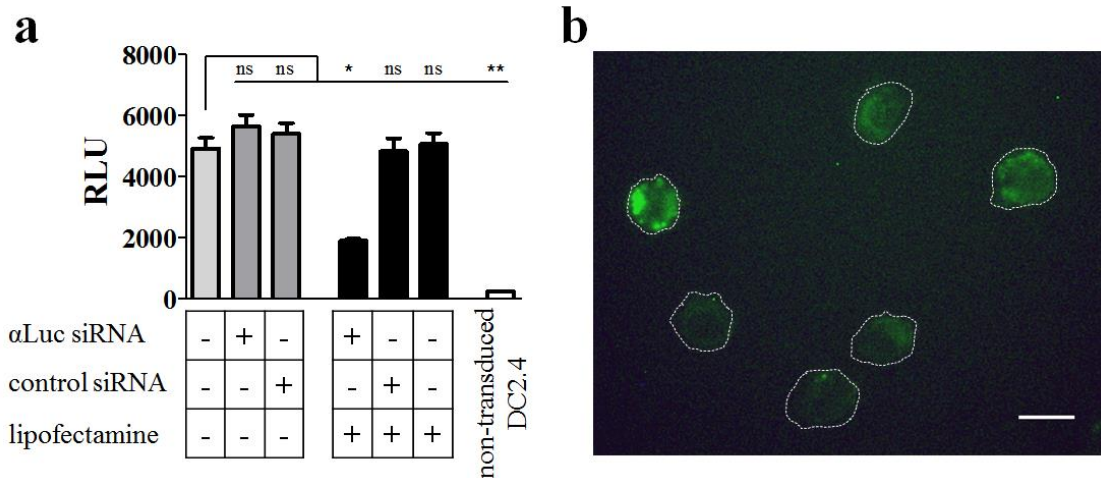


**Figure 39** Transduction and siRNA functionality check

To check for successful transduction of DC2.4 (to DC2.4-mCMV) and to control functionality of the chosen siRNAs ( $\alpha$ Luc siRNA and control siRNA), (a) the corresponding cells ( $1 \times 10^5$  cells/ml, seeded 24 h before) were treated with either soluble siRNA (10 pmol/ml) or complexed with lipofectamine. Untreated DC2.4-mCMV and non-transduced DC2.4 were used as negative control. Luciferase activity was measured in relative light units (RLU) after administration of luciferase substrate (mean  $\pm$  SD; n=3). (b) Transduction was further checked by imaging copGFP expression in DC2.4-mCMV by fluorescence microscopy. Cells are edged by dashed lines (scale bar = 10  $\mu$ m). \*p < 0.05, \*\*p < 0.01.

## RESULTS

### 4.3.1 Luciferase knockdown with siRNA-loaded HES-NCs

First, siRNA-loaded HES-NCs were checked for their size, morphology, encapsulation efficiency as well as for cellular binding and cytotoxicity using DC2.4 cells. For measuring binding of HES-NCs loaded with  $\alpha$ Luc siRNA, Cy5 was co-encapsulated. Cellular interactions of DC2.4-mCMV with HES-NCs containing the control siRNA were assessed by detecting the AF647-label attached to the siRNA. Both fluorochromes have almost the same excitation and emission properties. The diameters of all HES-NC formulations were measured by DLS and determined to be 170 nm on average. Sphere-shaped capsule morphology was imaged by SEM and TEM (Figure 40). The encapsulation efficiency of HES-NCs was assessed by the release of D-mannosamine and turned out to be approximately 70 % (Figure S 13). Binding analysis with DC2.4-mCMV using 300  $\mu$ g/ml HES-NCs, based on a specific gating strategy (Figure S 14), showed a moderate, comparable cell association for both siRNA-loaded HES-NCs of 10-20 %. Despite similar binding frequencies, cells treated with  $\alpha$ Luc siRNA-loaded HES-NCs showed remarkably higher MFIs than cells treated with control siRNA HES-NCs, most likely due to different intensities of the two incorporated fluorochromes (Figure S 15a). The viability of the modified DC cell line was only slightly influenced by the HES-NC formulations (Figure S 15b).

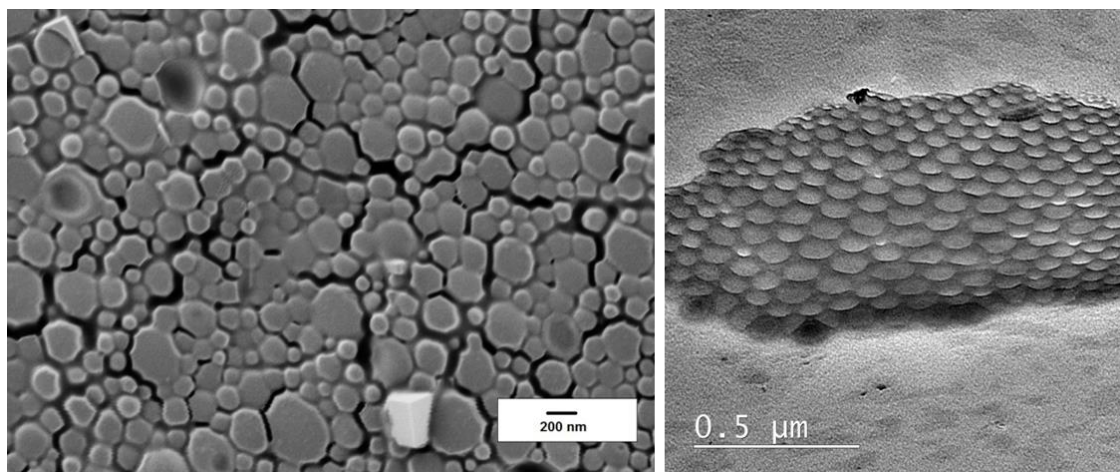


**Figure 40** Visualization of HES-NC morphology

The morphology of HES-NCs was microscopically visualized by SEM (left) and TEM (right). Indicated scale bar illustrates NC size.

## RESULTS

The basic luciferase expression of DC2.4-mCMV was used as readout to assess the suitability of HES-NCs to deliver siRNA into DCs in a functional way to mediate specific gene knockdown. Therefore, DC2.4-mCMV cells were incubated with 300  $\mu\text{g}/\text{ml}$  HES-NCs, containing  $\alpha\text{Luc}$  siRNA and the control siRNA respectively, for 24 h. After that, the remaining luciferase expression was measured. The analysis showed that treatment with HES-NCs loaded with  $\alpha\text{Luc}$  siRNA triggered a significant reduction and an almost complete knockdown of the firefly luciferase activity in DC2.4-mCMV.

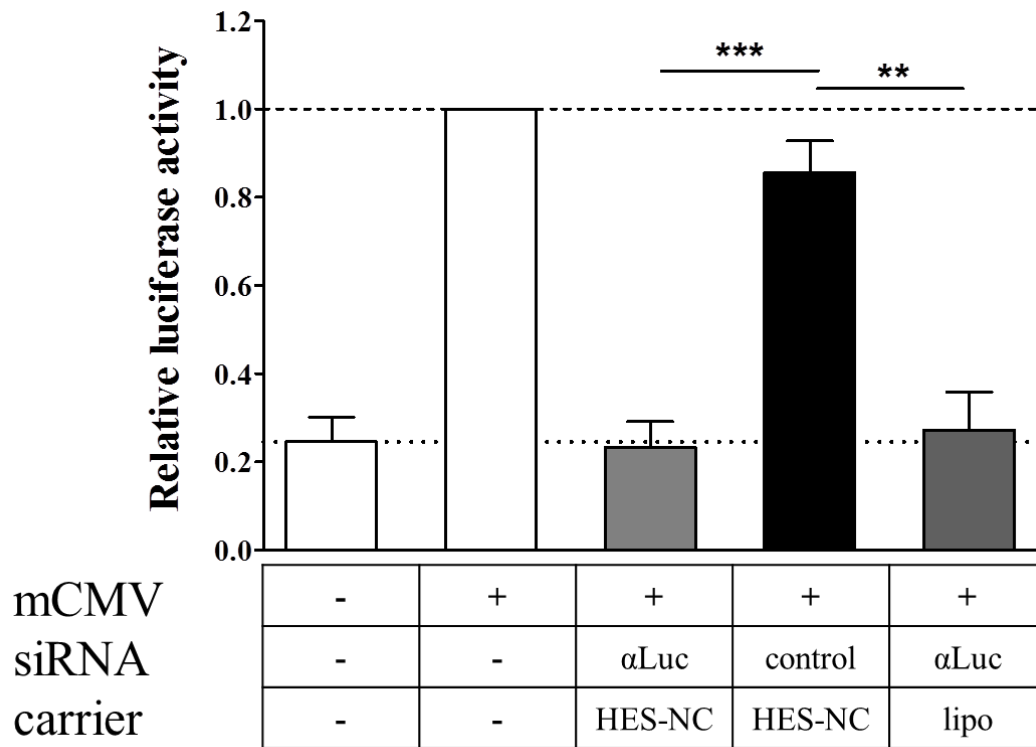


**Figure 41** Luciferase knockdown with siRNA-loaded HES-NCs

Knockdown efficiency of  $\alpha\text{Luc}$  siRNA encapsulated in HES-NCs was assessed. DC2.4-mCMV ( $1 \times 10^5$  cells/ml, seeded 24 h before) were treated with 300  $\mu\text{g}/\text{ml}$  of siRNA-loaded HES-NCs (luciferase-specific or control) for 24 h and the remaining luciferase activity was determined by bioluminescence measurement. Non-transduced DC2.4 cells were used as negative control. As positive control, DC2.4-mCMV cells were transfected with  $\alpha\text{Luc}$  siRNA via lipofectamine (lipo). Results were normalized to untreated DC2.4-mCMV (dashed line). Non-transduced DC2.4 were used as control (dotted line, mean  $\pm$  SD; n=3). \*\*p < 0.01, \*\*\*p < 0.001.

## *RESULTS*

The remaining activity was thereby comparable to the background bioluminescence of non-transduced DC2.4 or the positive control with lipofectamine and  $\alpha$ Luc siRNA. In contrast, HES-NCs loaded with unspecific control siRNA did not induce such an effect. In this case, the luciferase activity was rather comparable with that of untreated DC2.4-mCMV (Figure 41) indicating a high specificity of the used  $\alpha$ Luc siRNA. In summary, HES-NCs are suitable for efficient transport and release of bioactive siRNA concerning DCs.



## 4.4 Nanocarrier-mediated DC targeting

The modification of a NP with antibodies specific for an endocytically/phagocytically active receptor is supposed to increase NP's binding and uptake by a specific cell type. Therefore, cell type specific surface targets are required, that upon binding also mediate internalization of the associated NP, if needed. Especially in case of an *in vivo* application of NPs, the addition of a targeting moiety is frequently recommended [250, 251]. DC-SIGN is a prominent representative of promising DC surface targets. To investigate, whether cell targeting via anti-DC-SIGN antibodies ( $\alpha$ DC-SIGN) is an appropriate way to increase the DC specificity of siRNA-loaded HES-NCs, the surface of the previously described NCs (see 4.3) was additionally modified with  $\alpha$ DC-SIGN. DC2.4-mCMV cells were used as test system, since DC-SIGN is constitutively expressed in that cell line.

### 4.4.1 DC-SIGN targeting with antibody-modified HES-NCs

The newly synthesized HES-NCs modified with antibodies were initially checked for cytotoxicity. A 7AAD/Annexin V double staining of DC2.4-mCMV, which were treated with the antibody-modified HES-NCs, revealed that both NC formulations were non-toxic for the cells. The observed viabilities were comparable to that of untreated cells (Figure S 15b).

The antibody-modified, siRNA-loaded HES-NCs were then checked for their functionality to transfer siRNA into DC2.4 cells. An increased cellular interaction due to DC-SIGN targeting might result in enhanced uptake, higher intracellular siRNA release and eventually a stronger knockdown effect as obtained using non-targeting NCs. Lipofectamine +  $\alpha$ Luc siRNA was used as positive control again. Luciferase activity measurements after 24 h administration of the mentioned NCs confirmed the high efficiency and specificity for the siRNA-loaded, non-targeting HES-NCs. Those loaded with  $\alpha$ Luc siRNA triggered an almost complete knockdown of luciferase activity, whereas the capsules carrying the control siRNA did not. In contrast, a treatment with HES-NCs modified with  $\alpha$ DC-SIGN did not alter luciferase expression (Figure 42).

## RESULTS

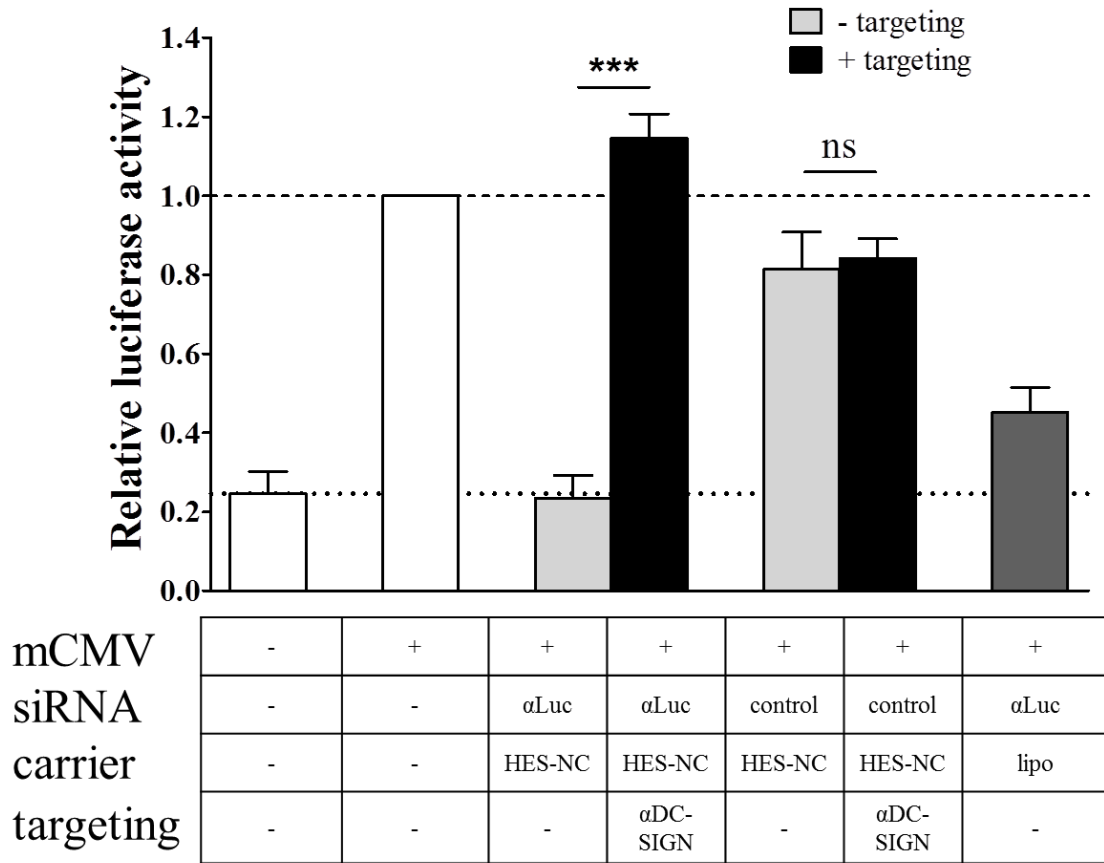


**Figure 42** Luciferase expression upon treatment with targeting HES-NCs

To assess the impact of a  $\alpha$ DC-SIGN modification on the functionality of siRNA-loaded HES-NCs to knockdown a target gene, luciferase-expressing DC2.4-mCMV cells ( $1 \times 10^5$  cells/ml, seeded 24 h before) were treated with the indicated HES-NC formulations ( $\pm$  targeting, each 300  $\mu$ g/ml) for 24 h. The remaining luciferase expression was determined by luciferase activity measurement. Results were normalized to untreated DC2.4-mCMV (dashed line). Non-transduced DC2.4 were used as control (dotted line, mean  $\pm$  SD; n=3). \*\*\*p < 0.001.

Despite the missing knockdown effect, the actual potential of  $\alpha$ DC-SIGN-modified HES-NCs to mediate effective DC targeting was assessed in comparison to the non-modified NCs, focusing on cellular binding by DC2.4-mCMV. Therefore, cells were incubated with the different HES-NCs (loaded with  $\alpha$ Luc or control siRNA,  $\pm$  targeting) and cellular binding was measured by flow cytometry.

## RESULTS

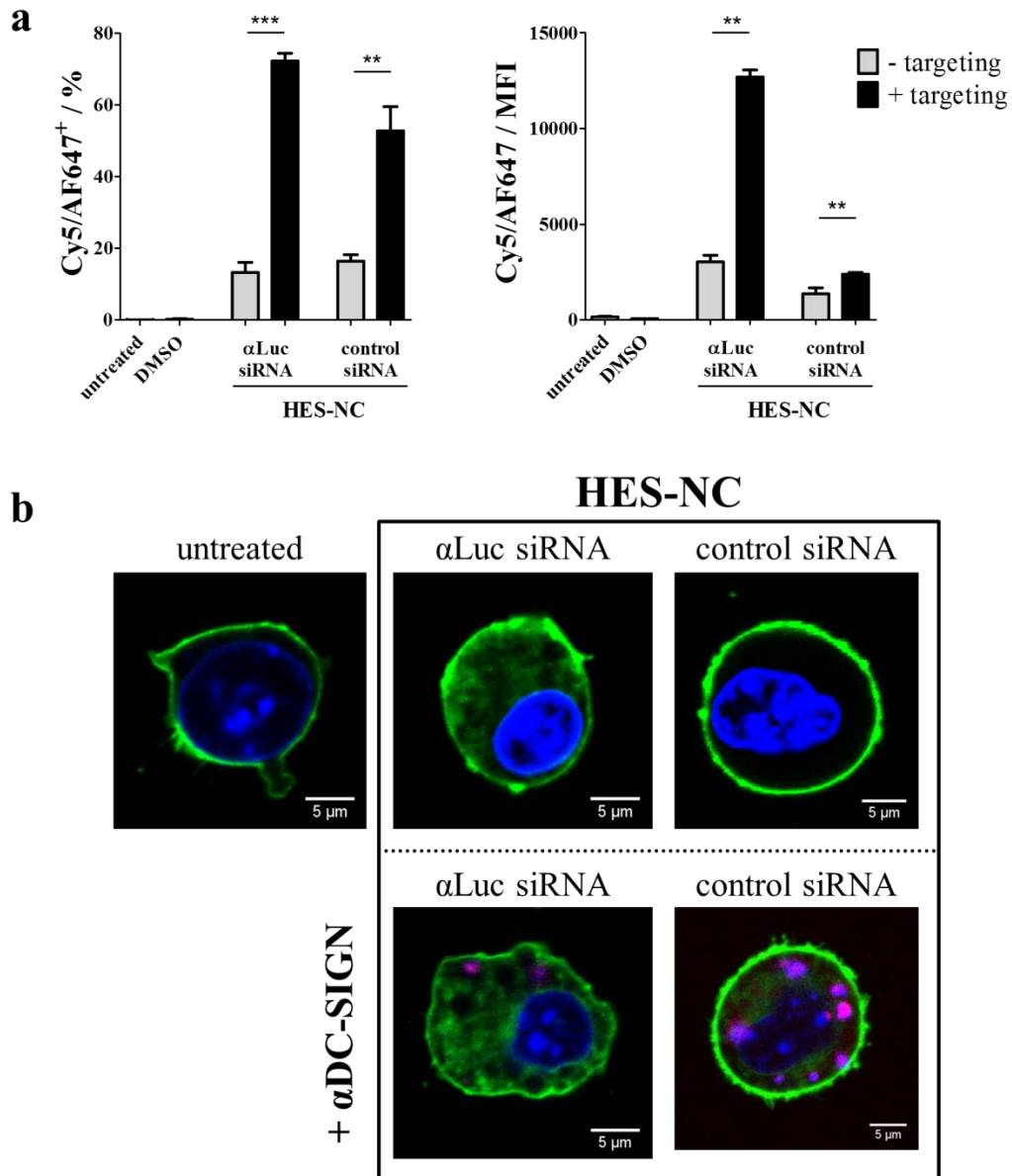


**Figure 43** DC2.4 targeting with αDC-SIGN-modified HES-NCs

The influence of DC-SIGN-directed antibody modification of HES-NCs on the interaction between DC2.4-mCMV and such equipped NCs was assessed by cytometric binding analysis and CLSM. (a) DC2.4-mCMV ( $1 \times 10^5$  cells/ml, seeded 24 h before) were treated with 300  $\mu$ g/ml of antibody-modified (+ targeting) and non-modified (-targeting) siRNA-loaded ( $\alpha$ Luc or control siRNA) HES-NCs for 24 h. Cy5/AF647<sup>+</sup> cells as well as Cy5/AF647 MFIs were measured by flow cytometry (mean  $\pm$  SD; n=6). (b) Cellular uptake of differently-modified HES-NCs into DC2.4-mCMV was microscopically analyzed by CLSM, incubating cells ( $7.5 \times 10^5$  cells/ml) with 100  $\mu$ g per ml of the indicated NCs for 24 h. Cell membranes were stained with CellMask Orange (green), nuclei with DAPI (blue). HES-NCs were detected via Cy5/AF647 label (violet).

## *RESULTS*

It turned out, that those NCs modified with  $\alpha$ DC-SIGN showed significantly increased cell association frequencies and MFIs compared to non-targeting HES-NCs in flow cytometry (Figure 43a). In this context, the frequencies of Cy5/AF647<sup>+</sup> cells mediated by the  $\alpha$ DC-SIGN-modified NCs were comparable, whereas the MFIs of those cells differed most likely due to different fluorescence intensities (see Figure S 15a), as already described in 4.3.1. Nevertheless, the antibody modification significantly enhanced the interaction of HES-NCs with DC2.4 cells, which was also visualized via CLSM. There, the HES-NCs were exclusively detectable when modified with  $\alpha$ DC-SIGN. Without targeting, no intracellular NC signals appeared at all (Figure 43b).

# 5. Discussion

## 5.1 DC-directed T cell stimulation with nanovaccine

About 15 years ago, it was shown for the first time that sets of distinct PRRs can cooperate in a synergistic manner when simultaneously engaged by according ligands [106, 252, 253]. This mechanism potentially allows reducing the amounts of adjuvants in vaccines while still possessing a constant stimulatory potential or to enhance the effect by a cooperative action of more than one adjuvant. Stimulatory synergy has already been described for diverse combinations of TLR ligands, such as CpG plus Poly I:C [254], CpG plus LPS [255] or R848 plus monophosphoryl lipid A (MPLA) [256]. But also some combinations of TLR and NLR ligands have been identified to work in synergistic cooperation [257-259].

The main objective of this work was to develop a nanocarrier that can be used as a nanovaccine for the treatment of melanoma. To do so, the first initial step was to choose an appropriate adjuvant. Such an adjuvant should trigger i) an upregulation of the co-stimulatory molecules CD80 and CD86 as well as ii) an increased secretion of distinct pro-inflammatory cytokines by DCs. Both factors are essential and highly required for DC/T cell interaction and thus for the induction of a tumor-directed adaptive immune response [260]. Particularly in case of tumor diseases, a cellular Tc1/Th1-dominated response has to be the goal [136], since a humoral Th2-biased response has proven to be insufficient in tumor rejection [137]. Recent studies have shown that alum and Freud's adjuvant do not induce a cellular but rather a humoral, antibody-dominated immune response [261-263]. Therefore, a focus was set to establish Th1/Tc1-promoting adjuvants for use in NP formulations. We decided to search for an efficient adjuvant combination of a TLR and a NLR ligand, since a priority objective was to combine adjuvants which are recognized by different intracellular PRRs. Several publications have underlined the therapeutic potential of NLRs for vaccination [76, 264, 265], but less is known about the stimulatory potential and the cross-talk of TLR/NLR ligand combinations [266, 267], particularly when co-delivered by nanocarriers.

## DISCUSSION

In contrast to TLRs, which are localized on the cell surface or in endosomes, NLRs are located in the cytosol. Since the NLR effect was less predictable due to the cytosomal receptor localization and the required endosomal ligand release, we started initial experiments using BMDCs to test to which extent NLR ligands trigger maturation. The cytometric measurements revealed that all tested NLR ligands were capable of inducing increased expression of CD80 and CD86, but L18-MDP, a C18-modified MDP derivative, was by far the strongest (see Figure 9). Consequently, we decided to use L18-MDP for further synergy experiments. Since it carries the NOD2 minimal bioactive motif MDP, displays high membrane penetrability due to its hydrophobicity [268] and was subject of many immunological studies [269-273], it served as an effective representative of all NOD2 ligands.

Afterwards, to identify synergistic combinations, BMDCs were treated with L18-MDP in combination with specific ligands of endosomal TLRs which have been used in vaccination approaches, Poly I:C (TLR3 ligand), R848 (TLR7 ligand) or CpG (TLR9 ligand) [274-277]. Additionally, all combinations trigger different signaling adaptors. NOD2 signaling is based on the recruitment and activation of RIP2, allowing the activation of the NF- $\kappa$ B signaling regulator IKK [278]. In contrast, R848 and CpG are associated with MYD88, the canonical adaptor molecule of TLR signaling [73], whereas Poly I:C recognition by TLR3 triggers the TRIF signaling pathway [279].

The expression of the co-stimulatory molecules CD80 and CD86 upon adjuvant treatment was significantly increased by L18-MDP combined with R848 and Poly I:C respectively. Interestingly, Poly I:C evoked no increase when applied alone (see Figure 10). Regarding cytokine secretion, L18-MDP alone did not induce any variations in the measured concentrations of the pro-inflammatory cytokines IL-1 $\beta$ , IL-6, IL-12 and TNF- $\alpha$ . IL-10 was also not influenced. When applied together with the mentioned TLR ligands, the secretion of IL-6, IL-12 and TNF- $\alpha$  was significantly increased in all combinations compared to the single adjuvant samples. But the secretion of IL-1 $\beta$  was exclusively enhanced by the combination L18-MDP plus R848 (see Figure 11). These results indicated an effective, superadditive DC maturation by the combination of L18-MDP plus R848, since CD80/CD86 expression, as an important requirement of T cell activation [280, 281], the Th1-promoting cytokines IL-1 $\beta$  [129], TNF- $\alpha$  [130], and IL-12 [282] as well as the acute

## DISCUSSION

phase cytokine IL-6 [283] were significantly increased. Our results are in agreement with publications from other groups showing that the combined application of MDP and R848 substantially increased the secretion of pro-inflammatory cytokines in human peripheral blood mononuclear cells [284] and monocyte-derived DCs [285]. In general, combinations of NLR and TLR ligands have been recognized to enhance IL-12 production in APCs and to promote Th1 responses [254, 258, 286, 287]. IL-10, a major anti-inflammatory cytokine, is known to inhibit MHC-II and CD80/CD86 expression as well as the production of pro-inflammatory cytokines in APCs [288]. Furthermore, autocrine IL-10 signaling can block IL-12 production and DC trafficking to the lymph nodes [289, 290]. Therefore, the observed increase in IL-10 production upon treatment with L18-MDP plus R848 has to be taken into account. As just stated, IL-10 is a negative regulator of IL-12. Due to the underlying feedback loop, DC activation associated with an increased production of IL-12 triggers the production of IL-10 in return [291, 292]. For that reason, it was more or less expected to detect elevated IL-10 levels.

Adjuvant application via nanocarriers can increase its immunostimulatory capacity due to higher local concentrations or improved delivery [293-295]. Moreover, several TLR ligand combinations are known to maintain their synergy when applied by a NP [296, 297]. Therefore, we decided to incorporate the identified adjuvant combination into a NP drug delivery system. Dextran-based nanoparticles were chosen, since they have been used for the transport of a variety of substances and provide high biocompatibility [236, 293, 298-300]. Due to L18-MDP's amphiphilic character and the tendency of stearyl derivatives to form micelles [268], L18-MDP was not available for water-based nanoparticle syntheses. Instead, the similar structure MDP was used for encapsulation. In contrast to L18-MDP, MDP requires a vector for effective membrane transfer [301]. Otherwise, ten times higher concentrations of soluble MDP are needed to achieve the effectiveness of L18-MDP (see Figure 9). MDP has been described as a mediator of cellular immune responses when applied by nanocarriers, whereas a soluble application was shown to evoke a primarily humoral response [302].

The quality controls confirmed the suitability of the new synthesized Dex-NPs as a drug delivery system, since the formulations were endotoxin free, non-toxic and were bound by BMDCs in a dose-dependent manner (see Figure 13). The average NP diameter of 150 nm

## DISCUSSION

(see Table S 1) was large enough to limit NP uptake to endocytic active cells [303-305]. According to the literature, NPs of a similar size are potentially taken up via clathrin-mediated (CME) and -independent endocytosis (CIE) pathways [306]. CME is mainly responsible for intracellular signaling, membrane recycling and nutrient uptake [307], whereas CIE pathways are associated with plasma membrane repair and cell polarization [308]. Macropinocytosis, as an actin-driven endocytic process [309], can also be involved in the uptake of NPs [310]. However, most studies analyzing routes of NP uptake reported the involvement of more than one endocytic pathway [311, 312], basically dependent on size [313], shape [314] and charge [179]. Furthermore, it has been described for NPs smaller than 200 nm that they can enter the spleen directly via the lymphatic vessels [186]. The stimulatory potential of single-adjuvant and dual-adjuvant Dex-NPs was directly comparable due to equimolar encapsulation of MDP and R848 (see Table S 2). However, the binding of Dex-NPs by BMDCs was checked by a FITC-label of MDP, but not by direct fluorescence labeling of NPs. In case of an incomplete MDP-FITC encapsulation, it is possible that soluble MDP-FITC was responsible for the binding results. This assumption was partially refuted by the observation that NP supernatants did not induce any stimulation (see Figure 16).

Indeed, the cytometric analysis of BMDCs treated with adjuvant-loaded Dex-NPs showed that all of these induced an increase in CD80 and CD86 expression. While soluble MDP exerted no stimulatory effect, Dex-MDP triggered a dose-dependent moderate stimulation. In comparison, Dex-R848 triggered a higher upregulation of CD80 and CD86. Compared to LPS, Dex-R848 was nonetheless remarkably weaker. This finding might be explained by the fact that LPS signals via MYD88 and TRIF [315], whereas the R848 signaling cascade comprises the MYD88 pathway only. Nevertheless, Dex-R848 mediated a stronger upregulation of CD86, which is more important in the murine system [316, 317], compared to equimolar amounts of soluble R848. Dex-MDP/R848 mediated a significantly stronger expression of CD80 and CD86 than the single adjuvant formulations. The stimulatory potential of these NPs was also illustrated by the cytokine measurements. The secretion of IL-1 $\beta$ , TNF- $\alpha$  and IL-6 by BMDCs was significantly higher upon treatment with Dex-MDP/R848 than in case of Dex-MDP or Dex-R848. However, IL-12, an essential cytokine of Th1 differentiation, was only slightly increased and even close to the detection limit (see



## DISCUSSION

Figure 15). These results confirmed that the adjuvant combination of MDP plus R848 exerts a superadditive stimulatory character when co-delivered by Dex-NPs. As their receptors are localized in the cytosol and endosome, respectively, the results suggest that the adjuvants were released from the NP into the endosome and even managed to escape from there into the cytosol. The concept of TLR/NLR ligand combinations in nanocarriers is relatively new, though MDP and R848 have already been used as single adjuvants in nanovaccines [193, 318]. One of the few exceptions was published by Poecheim *et al.* in 2015, combining MDP and CpG motif rich plasmid DNA in trimethyl chitosan NPs, squalene-in-water and mineral oil-in-water nanoemulsion, respectively. It was shown that the simultaneous targeting of NOD2 and TLR9 significantly enhanced the release of pro-inflammatory cytokines in RAW264.7 macrophages in a synergistic manner [319]. In another interesting approach described by Pavot *et al.* a novel chimeric NOD2/TLR2 ligand, composed of murabutide covalently bound to the TLR2 ligand Pam2C was used [320]. When encapsulated in p24-coated poly(lactic acid) NPs, this adjuvant combination induced a synergistic upregulation of DC maturation markers, co-stimulatory molecules and the secretion of pro-inflammatory cytokines.

Stimulation of DCs needs to be accompanied by delivery of a desired antigen [321]. More recently, a polymeric nanocapsule with a shell consisting of OVA protein cross-linked with TDI was introduced by our group [237]. It was shown that these OVA-NCs were efficiently taken up by human monocyte-derived DCs and degraded intracellularly. Based on these findings, we assumed that OVA-NCs might also be a suitable antigen source for BMDCs to mediate OVA-specific T cell responses in our setting, as already shown in a study with chronic hepatitis B virus antigens [322, 323]. A protein antigen has to be taken up and processed intracellularly by DCs. The resulting peptides are then loaded onto MHC-I and -II, which in turn are transported to the cell surface and present the antigen to the respective T cell population [324].

Compared to Dex-NPs, OVA-NCs are much bigger. Due to an average capsule diameter of approximately 350 nm in water (see Table S 3), macropinocytosis is likely the most prominent endocytic pathway for internalization of OVA-NCs [303, 310, 325, 326]. Since macropinocytosis is closely linked to antigen capture and presentation via MHC-II [327, 328], it is one of the commonly preferred and intended endocytic pathways for antigen-

## DISCUSSION

bearing NPs. Moreover, Manolova *et al.* have reported that NPs bigger than 200 nm are preferentially taken up by APCs at the injection site and are actively transported to the next draining lymph node [186]. To verify cellular binding of OVA-NCs, BMDCs were incubated with those capsules. The results of the cytometric analysis confirmed dose- and time-dependent rapid binding of the capsules by the vast majority of BMDCs. Furthermore, degradation analysis with OVA-DQ-NCs revealed a dose- and time-dependent degradation at 37 °C. In contrast, at 4 °C no degradation signal was detectable in BMDCs. Since endocytic, energy-dependent processes, such as macropinocytosis, are inhibited at 4 °C [245], we concluded that OVA-NCs were taken up by active endocytosis. These observations confirmed an effective internalization and degradation of OVA-NCs in our system. To check for effective presentation of OVA-NC-derived peptides via MHC-I and -II, BMDCs were pre-treated with OVA-blank-NCs, and co-incubated with OVA-reactive OT-I (CD8<sup>+</sup>) and OT-II (CD4<sup>+</sup>) T cells, respectively. An effective OVA peptide presentation on MHC-II was shown by the increased proliferation of CD4<sup>+</sup> T cells upon additional LPS treatment. The detected induction of CD8<sup>+</sup> and CD4<sup>+</sup> T cell proliferation suggested that OVA peptides derived from internalized and degraded OVA-NCs were efficiently presented via MHC-I and -II. BMDCs, pre-treated with OVA-NCs without additional stimulation, triggered a slight proliferation of both T cell populations only. These results indicated that the OVA-NC-derived peptides were not only loaded onto MHC-II but also on MHC-I, allowing cross-presentation and activation of CD8<sup>+</sup> T cells. Usually, MHC-I presents peptides that derived from endogenous proteins [113]. To be able to induce an effective cytotoxic T cell response against a foreign antigen like a virus peptide, specific DC subsets are endowed with the capacity to present antigens from the extracellular environment on MHC-I [116], including BMDCs [117]. Both CD8<sup>+</sup> and CD4<sup>+</sup> T cells are necessary to elicit an effective antitumor response [329]. Activated CD8<sup>+</sup> cytotoxic T cells are able to directly eliminate malignant cells [330], whereas CD4<sup>+</sup> T helper cells are required for the generation and maintenance of CD8<sup>+</sup> T cell responses [331, 332]. Since OVA-NCs triggered both CD4<sup>+</sup> and CD8<sup>+</sup> T cell responses, we focused on these capsules as a reliable antigen source.

Protein-based nanocapsules have been described as drug delivery system in several studies, but primarily for the transport of other substances, such as siRNA or cytostatics [221-223,

## DISCUSSION

333-335]. Thereby, the molding protein was rather used because of its high biocompatibility, low cytotoxicity and its chemical properties, but less because of its antigenicity. In comparison, the idea to use the capsule shell itself as antigen source is quite new. The chemical bonding of the antigen and using it as a capsule material could potentially have made the protein unsuitable to act as an antigen. So it could have been that the degradation of the protein into peptides needed for an effective loading onto MHC molecules would not have been functional anymore. So the question remained whether OVA-NCs could be effectively combined with the aforementioned adjuvant combination.

The first step to answer this question was to combine both nanocarrier systems directly in one approach. Therefore, BMDCs were pre-treated with Dex-MDP/R848 or Dex-blank in combination with OVA-blank-NCs, and co-cultured with OT-I and OT-II T cells. In contrast to the previous experiment, the adjuvant-loaded Dex-NPs replaced LPS in this setup. The combination of MDP/R848-loaded Dex-NPs and OVA-blank-NCs triggered a significantly increased proliferation of both OT-I and OT-II T cells compared to the combination of Dex-blank plus OVA-blank-NCs (see Figure 22). This indicated that the chosen adjuvant combination evoked a suitable stimulation for BMDCs to present the OVA-NC-derived peptides to the T cells in an effective manner. Interestingly, the combination of both empty nanocarriers also mediated a moderate OT-II proliferation. This might be due to the fact that in all experiments a small proportion of BMDCs was in an active state without further stimulation, visible as CD80<sup>+</sup> and CD86<sup>+</sup> cells in the untreated controls. These pre-activated cells could be responsible for the OT-II T cell proliferation without an additional stimulus, since the co-stimulatory molecules CD80 and CD86 were already present and OVA available as antigen. A lack of OT-I proliferation could thereby be explained by insufficient cross-presentation by these cells. Besides that, an OVA-NC mediated stimulation of the BMDCs was taken into account as the trigger. But this option was almost entirely refuted by the finding that empty OVA-NC never evoked any upregulation of CD80 and CD86 (see Figure 24) or pro-inflammatory cytokines (see Figure 25). Additionally, all OVA-NC formulations were almost free of endotoxins (see Figure S 4). Due to the transgenic origin of the employed T cell populations it cannot be excluded that the altered proliferation of OT-II T cells in presence of OVA-NCs without stimulation was due to various sensitivity against OVA itself. In this case, the simple presence of OVA

## DISCUSSION

protein might be sufficient to mediate a moderate OT-II proliferation. This hypothesis was supported by similar results in Figure 21 and Figure 26, where the basic proliferation triggered by OVA-blank-NCs was always stronger for OT-II than for OT-I T cells.

To characterize the induced T cell activation in more detail, we also measured prominent T cell cytokines in the co-culture. OT-I and OT-II T cells that were co-cultured with BMDCs, pre-treated with Dex-MDP/R848 and OVA-blank-NCs, showed significantly increased levels of the Tc1/Th1 marker IFN- $\gamma$  (see Figure 23). IFN- $\gamma$  is a crucial cytokine for innate and adaptive immunity against viral and some bacterial infections [336]. In case of OT-I, it indicated a differentiation towards cytotoxic Tc1 T cells [337]. For OT-II, high IFN- $\gamma$  production reflects an acquired Th1 response [338, 339]. Since Tc1 and Th1 T cells are mediators of cellular immune responses and essential for antitumor reactions, the detected T cell cytokine pattern was in congruence with our requirements for a NP-based melanoma vaccine. In contrast, the Th2 marker IL-5 and the ambiguous Th2/Treg marker IL-10 were not increased. On the basis of these results, we decided to fuse both systems into one functional nanocarrier, including a superadditive adjuvant combination and an antigen source.

Many studies developing nanovaccines conjugate the needed substances (e.g. antigen, adjuvants and fluorochrome) chemically to NP's surface [340-344]. By this, the cell recognizes PAMPs either by extracellular PRRs or after internalization by intercellularly located ones. Subsequently, the antigen is generally cleaved from the NP and thereafter available for processing. However, the NP-coupled molecules are completely exposed to all kinds of enzymatic, chemical and physical processes in the harsh extracellular environment [345]. In case of our NCs, the PRR ligands are in an aqueous core and completely surrounded by a protein shell, in contrast to the antigen which is accessible on the NC's surface. In this way, the ligands are protected from unintended interactions till intracellular release. Thus, it is prevented that the adjuvants stimulate APCs before NC internalization. This is an important advantage since DC maturation reduces their endocytic activity after a strong transient increase [346-348]. Consequently, an early stimulation like by a soluble adjuvant or adjuvants on the surface of a NP could inhibit further NP uptake and thus diminish the final outcome. The same strategy was chosen for the fluorochrome. Although Cy5-Oligo is considered to be relatively unsusceptible to environmental factors like pH, it

## DISCUSSION

was additionally encapsulated into the liquid core to provide stable conditions. A further advantage of the protein-based NCs was that the availability of antigen is directly associated with the payload release. Fast interaction and degradation ensures fast availability of peptides and a quick release of encapsulated adjuvants. Moreover, due to their superior loading capacity and efficiency compared to NCs consisting of synthetic base materials (such as PLGA or PLA) [349], degradation of NCs based on biopolymers like polysaccharides or proteins mediates high local adjuvant concentrations.

It turned out that the adjuvant combination MDP plus R848 also worked when encapsulated in OVA-NCs. The frequencies and MFIs of CD80 and CD86 in BMDCs were significantly increased in a superadditive manner when stimulated with OVA-MDP/R848-NCs compared to the corresponding single-adjuvant capsules and equimolar amounts of soluble adjuvants (see Figure 24). Also the cytokine measurements revealed a strong stimulatory potential. IL-1 $\beta$ , IL-6 and TNF- $\alpha$  levels were significantly higher upon treatment with OVA-MDP/R848-NCs than with the other NCs (see Figure 25). The cytokine profile was thereby comparable with that of BMDCs treated with Dex-MDP/R848. However, IL-12, the essential Th1-promoting cytokine, which was almost undetectable with Dex-NPs, was secreted in high quantities, and to a significantly higher extent than evoked by LPS. As mentioned before, LPS, as a TLR4 ligand, activates MYD88 and TRIF in synergy [315], and therefore is well-accepted as a gold standard to mediate BMDC activation. Altogether, the adjuvant combination MDP plus R848 encapsulated in OVA-NCs induced a stronger Th1-promoting DC activation than in case of Dex-NPs. These remarkable differences to Dex-MDP/R848 might be due to a faster uptake and degradation of the OVA-NCs, resulting in more efficient cargo release, a different uptake route and intracellular trafficking or merely to the higher loading capacity of the NCs. It is also possible that the transfer of MDP into the cytoplasm depends on the nanocarrier type. In this case, the effectiveness of the synergy between NOD2 and TLR7 ligands would be highly dependent on the chosen drug delivery system.

Regarding OVA-specific T cell activation, OVA-MDP/R848-NCs triggered the strongest proliferation rates of OT-I and OT-II T cells (see Figure 26). These results were consistent with the stimulatory effects of the corresponding adjuvant-loaded NC-formulations. Additionally, we observed that BMDCs induced a Tc1/Th1-biased cytokine pattern in the

## DISCUSSION

corresponding T cell population when stimulated with OVA-MDP/R848-NCs as evidenced by significantly increased IFN- $\gamma$  levels, while IL-5 and IL-10 concentrations remained on low to moderate levels. This cytokine pattern largely matched the high activation level of OVA-MDP/R848-NC pre-treated BMDCs and their high expression of Th1-promoting pro-inflammatory cytokines (IL-1 $\beta$ , TNF- $\alpha$ , IL-12).

A totally new approach to characterize the effect of a nanovaccine on DCs is the analysis of the cell transcriptome after administration of the nanovaccine. RNA-Seq allowed us to detect any changes on mRNA level of BMDCs that were mediated by the treatment with OVA-MDP/R848-NCs. The main reason for using this technique was to be able to reconstruct the adjuvant and nanocapsule effects on mRNA level. Since mRNA expression does not consequently result in accordingly regulated protein production [350], RNA-Seq may give a hint for future nanovaccine development to understand how and why a drug delivery system acts in a particular way. RNA-Seq has been used for the analysis of nanoparticle effects in some studies, but those were primarily focused on toxicological effects [351-354]. Furthermore, a few studies have characterized adjuvant effects by this method. Recently, Mathan *et al.* have evaluated protamine-RNA complexes and CpG-P as new adjuvants for dendritic cell immunotherapy by RNA-Seq [355]. To the best of our knowledge is has never been used for the analysis of immune cell interactions with adjuvant-loaded nanocarriers. Due to a lack of appropriate data regarding early alterations in mRNA expression upon NC treatment, we decided to incubate BMDCs with adjuvant-loaded OVA-NC for 1, 2 and 4 hours (based on already used incubation times for transcriptome analysis of stimulated BMDCs according to the Sequence Read Archive, NCBI) and pooled the samples afterwards to capture every mRNA alteration over time in one sample. In the comparative analysis of the transcriptomes of untreated, OVA-blank-NC- and OVA-MDP/R848-NC-treated BMDCs, we were able to detect and identify the mRNAs of 14,531 genes in total, which corresponds to a share of approximately 58 % of the whole mouse genome [356]. Apart from high transcript numbers for the activation markers CD40, CD80, CD83 and CD86 (see Figure 27a), we detected increased mRNA levels for the pro-inflammatory cytokines IL-1 $\alpha$ , IL-1 $\beta$ , IL-6, IL-12 $\beta$  and TNF- $\alpha$  but not for the anti-inflammatory IL-10 (see Figure 27b). These results were highly consistent with the activation and cytokine measurements of BMDCs treated with OVA-MDP/R848-NCs.

## DISCUSSION

Hereby, the upregulation of co-stimulatory markers and Tc1/Th1-promoting cytokines upon MDP/R848 stimulation was detectable on mRNA level. It has already been reported by several studies that DC stimulation with different adjuvants not only triggers increased amounts of co-stimulatory molecules and pro-inflammatory cytokines but also an upregulation of those markers, in particular CD40, CD83, CD86, TNF- $\alpha$ , IL-1 $\beta$  and IL-6, on transcriptional level [357-359]. Moreover, Hotz *et al.* reported in 2016 that BMDC stimulation with R848 for 4 h triggered increased mRNA expression of IL-6, IL-12 $\alpha$  and IL-12 $\beta$  [360]. The increase in transcript numbers of several chemokines (such as CCL3, CCL4, CCL5, CCL22, CXCL1, CXCL2, CXCL3, CXCL10), which are responsible for the recruitment of distinct immune cell types [361], indicates DC maturation (see Figure 27c). In contrast, some chemokines were not influenced or even downregulated. The ability to express specific chemokines differs substantially among different DC subsets [362]. Furthermore, the chemoattractive properties of stimulated DCs seem to be dependent on the corresponding stimulus [358]. Since, as far as we know, nothing has been published about the chemokine transcriptome of DCs (or even BMDCs) stimulated with TLR/NLR ligand combinations so far, there was a lack of sources for comparison. Nonetheless, some similarities indicating a sufficient BMDC activation by OVA-MDP/R848-NCs could be found in literature. The inflammatory chemokines CCL3, CCL4 and CCL5 have been described to be transcriptionally upregulated in human moDCs and murine splenic DCs upon treatment with LPS, TNF- $\alpha$  or CD40 ligand [363-365]. Ross *et al.* have discovered that murine LCs transcribe the T cell attracting CCL22 upon maturation [366]. In case of viral exposure, the chemokines CXCL1, CXCL2 and CXCL3 have been reported to be transcribed by human pDCs and cDCs as part of the first (after 2-4 h) of three distinct chemokine waves [367]. Finally, for CXCL10, an inflammatory chemokine with Th1-attracting properties, it has been shown that it is transcribed by murine lymphoid-resident cDCs upon maturation [368]. Regarding chemokine receptors, we recognized a downregulation of CCR1 and CCR5 mRNA upon treatment with OVA-MDP/R848-NC compared to the controls, whereas the mRNA level of CCR7 was increased (see Figure S 11e). These results were in line with a study from Sallusto *et al.* from 1998, where they showed that human moDCs expressed high levels of CCR7 mRNA after stimulation with LPS or TNF- $\alpha$ , whereas the mRNA levels of CCR1 and CCR5 were decreased by this treatment [369].

## DISCUSSION

The strong BMDC activation was further confirmed by the transcriptional upregulation of numerous interferon-stimulated genes (see Figure 27d), such as RSAD2 (Viperin) and ISG15, which play an emerging role in antiviral immunity [370, 371]. Gene groups in which an altered mRNA expression was not necessarily expected, for instance DC marker genes, or only partially activation-dependent, such as PRR or scavenger receptor genes, were also analyzed. The most transcript numbers in these groups were relatively stable. Nonetheless, several changes in mRNA expression upon treatment with MDP/R848-loaded OVA-NCs were detectable. The observed downregulation of CD11c upon DC stimulation has already been described by Singh-Jasuja *et al.* [372]. Regarding the upregulation of TLR2 and CD14, which is a co-receptor of TLR4, it has been reported that the expression of these PRRs on BMDCs was increased by stimulation [373, 374]. The strong upregulation of SCARA2 (MARCO) after administration of OVA-MDP/R848-NCs was highly consistent with results from Kissick *et al.* showing that the relative MARCO expression in BMDCs is increased upon stimulation with different TLR ligands [375].

To analyze the vast amount of data, we performed a KEGG-annotated pathway analysis to identify signaling pathways that were associated with upregulated genes. The analysis supported our expectations and the previous findings, that immunological relevant pathways were addressed by the adjuvant-loaded OVA-NCs, such as cytokine-cytokine receptor, NF- $\kappa$ B, TLR/NLR and JAK/STAT signaling (see Table 18). These pathways are known to be associated with adjuvant effects and are closely linked to the induction of immune responses [376-380]. In comparison, the results also illustrated that empty OVA-NCs triggered an upregulation of some, but far less, genes that could be assigned to distinct immunologically relevant pathways. Particularly striking, however, was the detection of several genes associated with antigen processing and presentation which were designated as upregulated (mean enrichment score  $\geq 2.0$ ) when comparing the capsule samples to the untreated control. In case of a direct comparison of the two capsule samples, with and without adjuvant cargo, not a single gene of the mentioned pathway showed a mean enrichment score  $\geq 2.0$ . However, more genes associated with that pathway were significantly upregulated when comparing the OVA-MDP/R848-NC sample with the untreated control (=8) than for the corresponding comparison between OVA-blank-NC and that negative control (=4). Consequently, BMDCs reacted to both capsules, but the induced



## DISCUSSION

effect regarding antigen processing and presentation on mRNA level was stronger for the adjuvant-loaded one.

Altogether, the RNA-Seq results demonstrated the induction of many relevant immunological pathways on mRNA level in BMDCs in response to treatment with OVA-MDP/R848-NCs. As expected, genes of co-stimulatory molecules, diverse chemokines and Th1-promoting cytokines were upregulated compared to the negative control and also OVA-NC treatment, though weaker. Several genes, associated with antigen processing and presentation, such as HSPA1B, a gene that represents a protein (HSP70) involved in the proteasome pathway [381], were assigned as upregulated in the OVA-blank-NC sample compared to the untreated control by KEGG-annotated pathway analysis. In contrast, four genes, for instance TAP1, which encodes for the antigen peptide transporter of the same name and is known to be upregulated upon adjuvant-mediated stimulation [382], were found upregulated exclusively when analyzing the OVA-MDP/R848-NC sample against the untreated one. To check the RNA-Seq results for specificity and accuracy, we picked six representative genes (four upregulated, one downregulated and one slightly downregulated) and measured the relative copy numbers also via qPCR. RNA-Seq and qPCR showed similar results for all genes. Compared to the widely used Sanger sequencing, NGS as well as qPCR provide significantly higher but similar analytical sensitivity, specificity and high concordance [383]. Moreover, it has recently been shown that qPCR is a sufficient method to validate RNA-Seq results [384]. Therefore, the qPCR analysis confirmed the RNA-Seq results. Interestingly, the transcriptome of BMDCs has never been deciphered for a study by RNA-Seq, only for selected genes by microarray or qPCR [52, 385]. In contrast, Miller *et al.* have already analyzed the transcriptomes of several murine DC lineage subsets by RNA-Seq [386].

A first important step towards an *in vivo* application of OVA-NC formulations for vaccination purposes was to analyze the interaction of adjuvant-loaded OVA-NCs with primary immune cell populations derived from spleen. In agreement with their profound endocytic activity [387], DCs as well as macrophages showed strong OVA-NC binding, whereas their binding by B cells was rather low. This might be explained by the finding that B cells differ in the capacity to internalize antigens compared to other APCs [388, 389]. T cells, which are known to lack considerable endocytic activity, did not show any

## DISCUSSION

significant binding. Additionally, DCs and macrophages showed a significantly increased expression of CD86 upon treatment with R848- and MDP/R848-loaded OVA-NCs (see Figure 33). These results were highly comparable to the results obtained using BMDCs. Taken together, our analysis confirmed passive targeting of endocytically active primary splenic DCs and macrophages, which constitute only 3-5 % of all splenic immune cells, and their adjuvant-dependent activation. In comparison, T and B cells represent 30-35 % and 45-50 % respectively, of all splenic immune cells. NP size seems to be one of the key factors for passive targeting of nanovaccines and thus determines the resulting immune response [390]. Reddy *et al.* have used pluronic-stabilized polypropylene sulfide NPs (25-100 nm) modified with OVA to passively target lymphoid-resident DCs via the interstitial flow [391]. Moreover, Moon *et al.* have demonstrated the suitability of interbilayer-cross-linked multilamellar vesicles (~ 200 nm) loaded with the malaria antigen VMP001 for passive targeting of lymphoid-resident macrophages and DCs, thereby enhancing the vaccination outcome compared to conventional vaccines [392].

The reactive component TDI has repeatedly been used for the synthesis of nanocapsules by inverse miniemulsion [393, 394] but is rather unselective due to its chemical properties. Unwanted side reactions cannot be excluded. Moreover, it is a highly toxic organic solvent. Although TDI has been reported to be non-toxic in low doses [395] and no cytotoxic effect was detectable in our experiments at all, it is undoubtedly useful to find a functional alternative. Therefore, we tested R848-loaded protein nanocapsules, cross-linked by either TDI or TET-DN, for their stimulatory capacity concerning BMDCs. Compared to TDI, cross-linking with TET-DN provides a much higher selectivity and proceeds at more ambient conditions [233, 396]. Similar to the previously described OVA-NCs cross-linked with TDI, adjuvant leakage of the TET-DN cross-linked ones was excluded by stimulation assays with NC supernatants (see Figure S 12). The average diameter as well as the zeta potential of the new capsules was comparable than that of the TDI cross-linked ones (see Table S 5). Cytometric analysis of CD86 expression upon treatment with these capsules showed similar stimulatory potentials, even though the TET-DN cross-linked NCs were slightly stronger with 10 µg per ml (see Figure 34). The usage of HSA instead of OVA evoked no remarkable differences. These results illustrated that cross-linking with TET-DN represents a good alternative for TDI. Since TET-DN-NCs provided almost the same size

## DISCUSSION

and charge as TDI cross-linked NCs, TET-DN NCs were equally suitable for R848 delivery. Furthermore, they constitute a high selectivity, reducing unspecific, unwanted side reactions.

All findings regarding MDP/R848-loaded protein-based nanocapsules confirmed their potential to serve as an effective nanovaccine for melanoma treatment. They provide a good biocompatibility, protect their cargo, co-deliver antigen and adjuvant in a very effective manner, show a high stimulatory capacity, trigger Tc1/Th1-promoting DC activity and are preferentially bound by primary APCs. In light of the fact that such NCs may be easily modified and the option to replace OVA by any protein or peptide (e.g. a tumor-related protein), qualifies these capsules as an interesting candidate NC platform for nanovaccine approaches.

To test the actual suitability of MDP/R848-loaded OVA-NCs for melanoma treatment *in vivo*, vaccination experiments with the melanoma cell line B16-OVA in mice are planned.

## 5.2 OVA-NC shielding with PEG

Nanovaccines designed for *in vivo* application can be equipped with surface PEG chains to prolong their blood circulation time and to reduce unspecific interactions with cells and proteins. Thereby, an important and critical factor that has to be considered, when planning an *in vivo* application of a nanocarrier, is the adsorption of serum proteins on the particle surface. The formation of such a protein corona usually facilitates unspecific cell uptake [397], mediates a further decrease in circulation time [398] and can also reduce the efficiency of targeting moieties [399]. Even proteins in cell culture media (e.g. components of FCS) are known to adsorb on NPs, thereby changing the actual NP identity [400]. Consequently, a new NP that was PEGylated for *in vivo* application has to be tested for cellular interaction under different protein conditions to understand the impact of different natural protein sources [401].

To further optimize the described OVA-NC and to cover the antigen shell, we decided to modify the NC's surface with PEG. Since many studies give different recommendations regarding the optimal PEG MW and coating density [402], OVA-NCs with three different PEG variants (MW: 2,000, 3,400, 5,000 g/mol) at varying coating densities were synthesized. BMDCs were treated with these capsules under defined protein conditions (no protein, FCS, mS, hS) for 4 h. To exclude the potential problem of complement-mediated cell lysis [403], we incubated BMDCs with the different protein solutions, left untreated or heat-inactivated, for 4 h in an initial experiment and measured the cell viability subsequently. FCS, mS and the no protein condition were not toxic for the cells. In contrast, untreated hS triggered a remarkable cell lysis, whereas heat-inactivated hS did not. This might be due to the mentioned complement-mediated cell lysis by hS components [404]. It is also known that mS constitutes a low intrinsic complement activity [405] compared to hS. However, to ensure a high comparability between the different experimental groups and to prevent unnecessary cell death, we consequently used heat-inactivated protein sources for the PEG experiments in spite of the loss of complement factors. Of course, it has to be noted that heat-inactivation affects the protein corona composition [406] and thus the interaction between cell and NP.

## DISCUSSION

To test to what extent the stealth properties of the PEG-modified OVA-NCs were dependent on PEG MW, we incubated BMDCs with the NCs under different conditions for 4 h and measured the resulting cell association via flow cytometry (see Figure 36). Our findings were in agreement with other publications, showing that an increase in PEG MW prevented the adsorption of blood proteins to NPs [407] and reduced their uptake by MPS [408]. Particularly PEG<sub>5000</sub> has been described to strongly enhance the stealth effect of NPs [408] and to minimize protein adsorption [409]. Interestingly, PEG<sub>2000</sub> has been identified as the minimal PEG MW that is required to exert stealth properties at all [410, 411]. Focusing on coating density, binding of OVA-NCs modified with PEG<sub>2000</sub> at three different densities from 0.18 to 2.47 PEG molecules per nm<sup>2</sup> was assessed. Cytometric analysis revealed a positive correlation between PEGylation density and resulting stealth effect. Again, co-application with hS and without any proteins triggered the strongest reduction of cellular binding (see Figure 37). As already shown by Vonarbourg *et al.* in 2006, PEGylation density is an essential parameter determining the PEG-mediated stealth properties of a nanocarrier [412]. In 2010, Braeckmans *et al.* reported that an increase in PEGylation density on liposomes prevented liposome aggregation [413]. Although an increase in PEG density has been assumed to be advantageous regarding stealth properties, some studies indicated that there is an upper density threshold, above which a further increase does not result in an enhanced stealth effect [414]. Our results perfectly matched the already known facts. However, a density threshold was not detectable in this setup. At last, we analyzed the impact of mass density on the PEG-mediated stealth effect for OVA-NCs. The mass density, or the number of ethylene oxide (base component of PEG) units per nm<sup>2</sup>, is a rarely considered but equally important parameter of nanoparticle studies. It raises the question, whether two PEGylations with the same mass density provide comparable stealth properties. Therefore, BMDCs were treated simultaneously with two PEGylated OVA-NCs with the same mass density, but different PEG MWs (PEG<sub>2000</sub> / PEG<sub>5000</sub>) and coating densities (0.54 / 0.19 PEG chains per nm<sup>2</sup>). The binding assays revealed a stronger stealth effect for the PEG<sub>5000</sub>-modified OVA-NC despite a lower coating density. The absence of protein as well as hS enhanced that difference even further (see Figure 38).

## DISCUSSION

Many studies dealing with nanoparticles and PEG did not consider PEGylation density or, in some cases, even the PEG MW. Here we were able to show that the MW of the used PEG as well as the coating density influences the final stealth properties of protein-based NCs on DCs. Our results suggest a positive correlation between PEG MW and the resulting stealth effect. Also an increase of PEGylation density enhances the NC's stealth properties. The mass density of the coupled PEG plays a minor role, since the mass of the individual PEG chain turned out to be much more relevant than the total PEG mass. In addition, the protein environment can also affect the stealth properties of OVA-NCs and has to be assessed accordingly. In this context, it might be useful to analyze the protein corona composition (e.g. by mass spectrometry) to understand and subsequently be able to predict the interaction between NPs, proteins and even cells. The PEG-mediated stealth effect on OVA-NCs was maintained upon all protein conditions, even when using PEG<sub>2000</sub>. This emphasizes the potential of PEGylated OVA-NCs for *in vivo* approaches. Nevertheless, numerous unpredictable factors remain [415, 416]. Therefore, it would be rather negligent to extrapolate from the *in vitro* to the actual *in vivo* efficiency.

In recent times, the use of PEG as a stealth-mediating component on nanomaterials has frequently been scrutinized [417]. Some studies have criticized the very long clearance time and low biodegradability of PEG [418], others have issued the induction of anti-PEG antibodies on repeated use of PEGylated products [419]. However, PEG represents the best-studied and -characterized stealth component by now and was successfully used in numerous pharmaceuticals. Therefore, it was used in this study and was successfully mounted on the NC surface. Nevertheless, there is a need for alternative components with better stealth properties, higher biocompatibility and lower antigenicity [420].

### 5.3 Gene knockdown with siRNA-loaded HES-NCs

RNAi was recognized for the first time by Ecker *et al.* as a mechanism of gene regulation in transgenic plants in 1986 [421], confirmed by many other reports in the following decade. Based on these observations, Fire *et al.* successfully used double-stranded RNA to inhibit mRNA translation of the gene *unc-22* in *Caenorhabditis elegans* [422]. Since then, RNA silencing was extensively used for genetic manipulation and has become a routine research tool. The use of siRNA allows the targeting of single genes which cannot be reached by conventional drugs, making it particularly attractive for tumor treatment approaches [423]. Therefore, enormous effort has been made for the development of siRNA-based drugs. As of September 2017, approximately 20 clinical trials based on siRNA therapeutics have been initiated [424]. For example, Excellair, a siRNA-based inhibitor of the spleen tyrosine kinase for the treatment of lymphoma [425], is currently in a clinical phase III trial [424]. Regarding immune modulation, it has been shown that the siRNA-mediated silencing of immunosuppressive molecules, such as IL-10RA, in DCs, can enhance the induction of antigen-specific CD8<sup>+</sup> T cell responses [426]. But the use of siRNA for gene manipulation in clinical approaches encounters some tremendous obstacles: i) Target cells need to be transfectable [427], ii) high mRNA turnover rates decrease siRNA efficacy [428], iii) siRNA's polyanionic nature limits passive uptake by cells [429] and iv) siRNA is easily degraded by RNases due to a low chemical stability [430] and a short circulation half-life [431]. Moreover, siRNA can trigger innate immune responses via recognition by PRRs and danger receptors [432]. Therefore, a carrier is needed to protect the siRNA and to shuttle it into the cell and subsequently into the cytosol. Liposomal formulations are most frequently used to transfer siRNA into target cells [433-435]. Especially cationic liposomes are discussed as the most promising carriers regarding siRNA transfection [436]. Commercially available substances like DOTAP complement the anionically charged siRNA due to electrostatic interactions and mediate its effective transfer. Despite that, liposomal formulations have been described to potentially evoke innate immune responses [437] and as rapidly removed from blood stream via MPS [438].

In this context, the delivery of siRNA by polymeric nanocapsules constitutes a promising alternative. As a model system to test the suitability of those NCs to effectively transfer siRNA into cells, we chose PEGylated HES-NCs (see 3.1.3), synthesized by inverse

## DISCUSSION

miniemulsion. They provide a high loading capacity [439], a comparatively long blood circulation time [440-442] and a low tendency to interact with blood proteins [443-445] combined with a good biocompatibility [446] and modifiability [447]. Moreover, the starch derivative HES, which was used as a base component instead of OVA here, is FDA approved for intravenous injection as plasma expander. There has been a long-lasting discussion about side effects of HES in case of sepsis or critical illness [448], starting soon after licensing, which was intensified by three randomized trials [449-451]. However, these risks are only relevant for very high amounts of HES as compared to our envisioned applications. The amount of HES applied by HES-NC administration is significantly lower compared to the use of HES as plasma expander.

The knockdown experiments using the luciferase-expressing subline DC2.4-mCMV and the different types of siRNA-loaded HES-NCs showed a significantly reduced expression of firefly luciferase upon treatment with the  $\alpha$ Luc siRNA-containing HES-NCs. The observed knockdown effect was highly comparable to those of the positive control,  $\alpha$ Luc siRNA transfected by lipo, and the non-transduced DC2.4. These results indicated HES-NC uptake by DC2.4 cells, intracellular cargo release, endosomal escape of the corresponding siRNA molecules and effective interference of the luciferase mRNA. Since it has been reported by Tseng *et al.* that free siRNA is degraded in lysosomes after internalization [452], altered gene expression due to non-encapsulated siRNA was highly unlikely. In general, the physicochemical properties of siRNA like a negative charge and a large molecular weight are unfavorable for cellular uptake [431].

Curiously, the siRNA-loaded HES-NCs were bound by DC2.4-mCMV only at moderate frequencies. Approximately 15 % of all cells were detected as Cy5<sup>+</sup>/AF647<sup>+</sup> in flow cytometry (see Figure S 15). Via CLSM, the HES-NCs were not detectable at all (see Figure 43b). These observations appear incompatible with the knockdown results. An insufficient fluorochrome labeling could not be responsible, since both capsules were labeled differently (free Cy5-Oligo vs. AF647-labeled siRNA) but showed comparable binding frequencies. Furthermore, both types of capsules were detectable via CLSM when modified with a targeting moiety, as discussed in the following section. NC-mediated cytotoxicity did also not explain these contradictory results, since all HES-NC formulations were evaluated as non-toxic at the concentrations applied. A possible explanation for the



## DISCUSSION

relatively low binding frequencies of HES-NCs but almost complete knockdown might be a low level cellular binding and uptake of the HES-NCs below the sensitivity of the flow cytometer. Non-ionic HES is known to reduce cellular interactions of nanoparticulate formulations [444, 453]. Therefore, a moderate binding by DC2.4-mCMV cannot be excluded. Nonetheless, even this low amount of internalized siRNA-loaded HES-NCs might be apparently enough to yield a sufficient knockdown. This theory was supported by the negative knockdown results for the HES-NCs loaded with the control siRNA. Hence, the observed knockdown effect could not be induced by the HES-NC itself. Since HES-NCs provide a high loading capacity, the uptake of a few NCs might be sufficient for a knockdown of the already moderate luciferase expression in DC2.4-mCMV. Another possible explanation is the excretion of HES-NCs or their components by exocytosis, which has been described for numerous other nanoparticulate systems [454]. Since both capsules showed still comparable binding frequencies irrespective of the fluorochrome being either soluble or siRNA-coupled, exocytosis could most likely be excluded as explanation. A further theory is based on a mechanism called 'kiss-and-run'. Originally reported as a form of exocytic vesicle release [455], it has been used as a model to describe non-invasive drug delivery through a 'kiss-and-run' interaction between nanocarrier and cell membrane. Another study has reported the intracellular pharmacokinetics to be the critical factor of siRNA delivery with nano-sized systems [456].

An extended analysis focusing on time-dependent knockdown and binding kinetics might shed new light on the issue of siRNA-loaded HES-NCs for gene knockdown. Once clarified, HES-NCs could potentially be used for the effective transfer of other gene-specific siRNAs. In this regard, it seemed useful to increase HES-NCs uptake by DC2.4-mCMV with a targeting moiety.

## 5.4 DC targeting with HES-NCs

The conjugation of NPs with targeting moieties is a common approach to increase specificity. Such moieties are usually antibodies or receptor-specific ligands like carbohydrates or glycoproteins. A NP modified in this way is intended to be preferentially bound by those cells that express the corresponding moiety counterpart. If NP uptake is desired, receptors that are internalized upon binding are preferable. Regarding the targeting of tumor cells, folate is a prominent and extensively used targeting molecule [457]. The folate receptor is overexpressed on various tumors [458] and can be targeted by conjugating folate or folic acid to NPs [459]. Accordingly equipped carriers, loaded with doxorubicin, have been used for tumor targeting and treatment in numerous studies [460-462]. In case of tumor vaccination approaches, DCs are the intended target cells. A conventional method for DC-based vaccination is to load DCs with tumor antigen *ex vivo* combined with an appropriate stimulation. After reinjection, these DCs are supposed to induce a tumor-specific immune response [250]. A further, less expensive and laborious alternative is the *in vivo* targeting of DCs. Since vaccination requires antigen processing and presentation, internalizing receptors are preferentially addressed. Very interesting and promising DC targets are C-type lectins (for instance DEC-205, MR, CLEC9A and DC-SIGN). Besides their function for cell-cell adhesion, the mentioned members of that group are also associated with pathogen recognition and binding of apoptotic cells [463]. DEC-205 is expressed at high levels on CD8<sup>+</sup> splenic DCs [464], whereas the MR can be found on macrophages and immature DCs [465]. CLEC9A is mainly present on CD8<sup>+</sup> cDCs and pDCs [466]. DC-SIGN, a lectin that is preferentially expressed by immature DCs [467], is a well-described and frequently used candidate for DC targeting in vaccination approaches [468-471]. First of all, it was described to enable the migration of myeloid DCs along the blood endothelium by binding the vascular ligand ICAM-2 [472]. Nonetheless, it also facilitates the interaction between DCs and resting T cells via ICAM-3 [473]. Furthermore, it turned out that DC-SIGN features endocytic activity associated with antigen uptake, as shown for the HIV glycoprotein gp120 by Engering et al. [474], and its engagement can modulate DC maturation [475].

In this work, a targeting of DC-SIGN by  $\alpha$ DC-SIGN antibodies was chosen with the aim to increase the specificity of the siRNA-loaded HES-NCs for DC2.4-mCMV cells. Therefore,

## DISCUSSION

these antibodies were modified with an azide group and were covalently bound to the NC's surface by a DBCO-PEG4-NHS click reaction. DC2.4 cells are particularly suitable for testing DC-SIGN targeting since almost all cells are positive for the marker (in personal communication with Dominika Hobernik, Department of Dermatology, University Medical Center, Mainz). Contrary to our expectations, the modification of HES-NCs with targeting antibodies resulted in strongly elevated binding of HES-NCs to DC2.4 cells, but completely eliminated the  $\alpha$ Luc siRNA-mediated knockdown effect (see Figure 42). At this point, it was not possible to identify the exact underlying reason for that problem. But the antibody modification was basically the only difference between both HES-NCs.

These results could be due to a different uptake route or intracellular trafficking of targeting versus non-targeting HES-NCs. Binding of DC-SIGN mediates clathrin-dependent endocytosis [476]. According to its function as an antigen receptor, internalized DC-SIGN-ligand complexes are rapidly targeted to late endosomal and lysosomal compartments [475], in which the antigens are usually processed for MHC loading. It is possible that this form of intracellular trafficking affected the cytoplasmic release and/or the function of the siRNA, leading to its degradation or impairment of cytosomal release. In comparison, the non-modified HES-NCs were apparently taken up by a more suitable internalization process for siRNA. More probable, however, is an unintended problem regarding the NC synthesis. An unsuccessful degradation of the internalized targeting HES-NCs would explain the distinct signals in CLSM and the lack of luciferase knockdown. The surface modification of HES-NCs with antibodies was, as mentioned, based on a DBCO-PEG4-NHS click reaction. This modification results in a higher shell density and an increased thickness. Most likely, the intracellular degradation processes were not sufficient to break this kind of HES-NC and to release the siRNA cargo. In this case, an optimization of the synthesis process would be necessary to achieve an effective siRNA release combined with targeting.

It should be emphasized that the DC-SIGN targeting with  $\alpha$ DC-SIGN antibodies seems to work for HES-NCs that were synthesized by inverse miniemulsion. It is also conceivable to transfer this modification to adjuvant-loaded OVA-NCs, since both capsule systems are based on similar synthesis processes. With such a modification, the specificity and efficiency of those NCs to stimulate DCs could be further increased. Nonetheless, the

## *DISCUSSION*

actual cause for the contrary results (stronger NC binding, no siRNA bioactivity) should be clarified.

In summary, protein-based nanocapsules combined with the superadditive adjuvant combination MDP/R848 and the options to reduce unspecific interaction by PEGylation and to use tumor-related antigens for the synthesis constitute a promising platform for the development of new nanovaccines. DC-SIGN targeting for increased uptake and siRNA incorporation in a functional manner seem to work as individual modifications but have to be optimized to allow a combined approach.

## 6. Summary

In summary, we demonstrated that the combination of the NOD2 ligand MDP and the TLR7 ligand R848 exerted superadditive stimulatory properties on BMDCs. When encapsulated in Dex-NPs, the stimulatory capacity of co-delivered MDP/R848 on BMDCs was superior to co-application of the components in their soluble form. In addition, OVA-NCs synthesized by inverse miniemulsion were readily internalized and degraded by BMDCs, and constituted an effective antigen delivery system. DCs pre-treated with a combination of MDP/R848-loaded Dex-NPs and OVA-NCs led to a significant increase in the antigen-specific proliferation of CD4<sup>+</sup> and CD8<sup>+</sup> T cells. The transfer of the adjuvant combination into OVA-NCs boosted the T cell stimulatory and Tc1/Th1-promoting activity of BMDCs to an extent that even outperformed the effect of LPS. Transcriptome analysis of such treated BMDCs confirmed these results by revealing an upregulation of numerous genes associated with immunologically relevant signaling pathways. The successful evaluation of an alternative cross-linker for a more selective capsule synthesis and a higher capsule biocompatibility completed these experiments. This first project section demonstrated the suitability of MDP/R848-loaded protein-based nanocapsules to induce effective antigen cross-presentation and to trigger antigen-specific T cell responses. Furthermore, it was shown that OVA-NCs were preferentially bound by DCs and macrophages when applied to splenic immune cells.

To optimize the evaluated OVA-NCs for *in vivo* application, the NC's surface was modified with PEG. It was shown that the PEG MW and density positively correlated with the resulting stealth effect, which describes a reduction of unspecific NP interactions with proteins and cells. Mass density turned out to be less important, since the impact of the individual PEG chain mass was much higher than that of the total PEG mass. The composition of the protein environment slightly affected the NC's stealth properties, though the PEGylation retained its basic functionality upon all conditions.

Next, we tested the suitability of HES-NCs, also synthesized by inverse miniemulsion, as a carrier for siRNA to knockdown gene expression. HES-NCs loaded with  $\alpha$ Luc siRNA turned out to knockdown the expression of firefly luciferase in transduced DC2.4-mCMV

## *SUMMARY*

almost completely, whereas the control siRNA did not show any effect. Nonetheless, the binding frequencies of those capsules were rather low. Therefore, the NCs were modified with  $\alpha$ DC-SIGN antibodies to increase the uptake into DC2.4-mCMV. In this way, the binding frequencies were significantly increased. However, the knockdown effect was no longer present. Further studies are obviously needed to ensure the compatibility of DC-SIGN targeting and siRNA transfer in protein-based nanocapsules.

The new nanovaccine concept introduced in this study has the perspective to allow the development of multi-functionalized nanovaccines for DC-directed immunotherapy. The option to replace the used model antigen OVA by any given protein or peptide, for instance a tumor-related antigen, makes the protein-based nanocapsule system extremely versatile and broadly applicable for vaccination approaches. When loaded with the adjuvant combination MDP plus R848, these capsules can trigger the induction of potent antigen-specific Tc1/Th1-dominated T cell responses. Combined with an alternative cross-linking method with higher selectivity, a PEGylation for longer blood circulation and optional modifications with targeting antibodies and siRNA cargo, our system represents a further step towards an optimized nanovaccine for effective melanoma treatment.

Our system represents a further step towards an optimized nanovaccine for effective melanoma treatment, in particular since it also offers an alternative cross-linking method for better synthesis selectivity, a PEGylation for longer blood circulation and optional modifications with targeting antibodies for increased cell specificity and siRNA for immune modulation.

## 7. References

1. WHO. World cancer report 2014. *International Agency for Research on Cancer*. 2014.
2. Leonardi, G. C.; Falzone, L.; Salemi, R.; Zanghi, A.; Spandidos, D. A.; Mccubrey, J. A.; Candido, S.; Libra, M. Cutaneous melanoma: From pathogenesis to therapy (Review). *Int J Oncol*. 2018; 52(4):1071-1080.
3. Polak, M. E.; Borthwick, N. J.; Jager, M. J.; Cree, I. A. Melanoma vaccines: The problems of local immunosuppression. *Hum Immunol*. 2009; 70(5):331-9.
4. Langerhans, P. Über die Nerven der menschlichen Haut. *Virchows Arch*. 1868; 44:325-337.
5. Steinman, R. M.; Cohn, Z. A. Identification of a novel cell type in peripheral lymphoid organs of mice. I. Morphology, quantitation, tissue distribution. *J Exp Med*. 1973; 137(5):1142-62.
6. Liu, K.; Nussenzweig, M. C. Origin and development of dendritic cells. *Immunol Rev*. 2010; 234(1):45-54.
7. Guermonprez, P.; Valladeau, J.; Zitvogel, L.; Thery, C.; Amigorena, S. Antigen presentation and T cell stimulation by dendritic cells. *Annu Rev Immunol*. 2002; 20:621-67.
8. Chen, M.; Huang, L.; Shabier, Z.; Wang, J. Regulation of the Lifespan in Dendritic Cell Subsets. *Molecular immunology*. 2007; 44(10):2558-2565.
9. Fogg, D. K.; Sibon, C.; Miled, C.; Jung, S.; Aucouturier, P.; Littman, D. R.; Cumano, A.; Geissmann, F. A clonogenic bone marrow progenitor specific for macrophages and dendritic cells. *Science*. 2006; 311(5757):83-7.
10. Liu, K.; Victora, G. D.; Schwickert, T. A.; Guermonprez, P.; Meredith, M. M.; Yao, K.; Chu, F. F.; Randolph, G. J.; Rudensky, A. Y.; Nussenzweig, M. In vivo analysis of dendritic cell development and homeostasis. *Science*. 2009; 324(5925):392-7.
11. Karsunky, H.; Merad, M.; Cozzio, A.; Weissman, I. L.; Manz, M. G. Flt3 Ligand Regulates Dendritic Cell Development from Flt3(+) Lymphoid and Myeloid-committed Progenitors to Flt3(+) Dendritic Cells In Vivo. *The Journal of Experimental Medicine*. 2003; 198(2):305-313.
12. Waskow, C.; Liu, K.; Darrasse-Jèze, G.; Guermonprez, P.; Ginhoux, F.; Merad, M.; Shengelia, T.; Yao, K.; Nussenzweig, M. The receptor tyrosine kinase Flt3 is required for dendritic cell development in peripheral lymphoid tissues. *Nature Immunology*. 2008; 9:676.

## REFERENCES

13. Leon, B.; Lopez-Bravo, M.; Ardavin, C. Monocyte-derived dendritic cells. *Semin Immunol.* 2005; 17(4):313-8.
14. Malissen, B.; Tamoutounour, S.; Henri, S. The origins and functions of dendritic cells and macrophages in the skin. *Nature Reviews Immunology.* 2014; 14:417.
15. Liu, Y.-J. IPC: Professional Type 1 Interferon-Producing Cells and Plasmacytoid Dendritic Cell Precursors. *Annual Review of Immunology.* 2005; 23(1):275-306.
16. Naik, S. H.; Sathe, P.; Park, H. Y.; Metcalf, D.; Proietto, A. I.; Dakic, A.; Carotta, S.; O'keeffe, M.; Bahlo, M.; Papenfuss, A.; Kwak, J. Y.; Wu, L.; Shortman, K. Development of plasmacytoid and conventional dendritic cell subtypes from single precursor cells derived in vitro and in vivo. *Nat Immunol.* 2007; 8(11):1217-26.
17. Swiecki, M.; Colonna, M. The multifaceted biology of plasmacytoid dendritic cells. *Nature reviews Immunology.* 2015; 15(8):471-485.
18. Shortman, K.; Liu, Y. J. Mouse and human dendritic cell subtypes. *Nat Rev Immunol.* 2002; 2(3):151-61.
19. Dudziak, D.; Kamphorst, A. O.; Heidkamp, G. F.; Buchholz, V. R.; Trumfheller, C.; Yamazaki, S.; Cheong, C.; Liu, K.; Lee, H. W.; Park, C. G.; Steinman, R. M.; Nussenzweig, M. C. Differential antigen processing by dendritic cell subsets in vivo. *Science.* 2007; 315(5808):107-11.
20. Idoyaga, J.; Suda, N.; Suda, K.; Park, C. G.; Steinman, R. M. Antibody to Langerin/CD207 localizes large numbers of CD8alpha+ dendritic cells to the marginal zone of mouse spleen. *Proc Natl Acad Sci U S A.* 2009; 106(5):1524-9.
21. Iyoda, T.; Shimoyama, S.; Liu, K.; Omatsu, Y.; Akiyama, Y.; Maeda, Y.; Takahara, K.; Steinman, R. M.; Inaba, K. The CD8+ dendritic cell subset selectively endocytoses dying cells in culture and in vivo. *J Exp Med.* 2002; 195(10):1289-302.
22. Maldonado-Lopez, R.; De Smedt, T.; Michel, P.; Godfroid, J.; Pajak, B.; Heirman, C.; Thielemans, K.; Leo, O.; Urbain, J.; Moser, M. CD8alpha+ and CD8alpha-subclasses of dendritic cells direct the development of distinct T helper cells in vivo. *J Exp Med.* 1999; 189(3):587-92.
23. Chamoto, K.; Kosaka, A.; Tsuji, T.; Matsuzaki, J.; Satoh, T.; Takeshima, T.; Iwakabe, K.; Togashi, Y.; Koda, T.; Nishimura, T. Critical role of the Th1/Tc1 circuit for the generation of tumor-specific CTL during tumor eradication in vivo by Th1-cell therapy 2003. 924-8 p.
24. Bialecki, E.; Macho Fernandez, E.; Ivanov, S.; Paget, C.; Fontaine, J.; Rodriguez, F.; Lebeau, L.; Ehret, C.; Frisch, B.; Trottein, F.; Faveeuw, C. Spleen-Resident CD4+ and CD4- CD8alpha- Dendritic Cell Subsets Differ in Their Ability to Prime Invariant Natural Killer T Lymphocytes. *PLoS One.* 2011; 6(10):e26919.



## REFERENCES

25. Maldonado-Lopez, R.; Maliszewski, C.; Urbain, J.; Moser, M. Cytokines regulate the capacity of CD8alpha(+) and CD8alpha(-) dendritic cells to prime Th1/Th2 cells in vivo. *J Immunol.* 2001; 167(8):4345-50.
26. Merad, M.; Sathe, P.; Helft, J.; Miller, J.; Mortha, A. The Dendritic Cell Lineage: Ontogeny and Function of Dendritic Cells and Their Subsets in the Steady State and the Inflamed Setting. *Annual Review of Immunology.* 2013; 31(1):563-604.
27. Ginhoux, F.; Tacke, F.; Angeli, V.; Bogunovic, M.; Loubreau, M.; Dai, X.-M.; Stanley, E. R.; Randolph, G. J.; Merad, M. Langerhans cells arise from monocytes in vivo. *Nature Immunology.* 2006; 7:265.
28. Seré, K.; Baek, J.-H.; Ober-Blöbaum, J.; Müller-Newen, G.; Tacke, F.; Yokota, Y.; Zenke, M.; Hieronymus, T. Two Distinct Types of Langerhans Cells Populate the Skin during Steady State and Inflammation. *Immunity.* 2012; 37(5):905-916.
29. Takahara, K.; Omatsu, Y.; Yashima, Y.; Maeda, Y.; Tanaka, S.; Iyoda, T.; Clausen, B. E.; Matsubara, K.; Letterio, J.; Steinman, R. M.; Matsuda, Y.; Inaba, K. Identification and expression of mouse Langerin (CD207) in dendritic cells. *Int Immunol.* 2002; 14(5):433-44.
30. Valladeau, J.; Clair-Moninot, V.; Dezutter-Dambuyant, C.; Pin, J. J.; Kissenpfennig, A.; Mattei, M. G.; Ait-Yahia, S.; Bates, E. E.; Malissen, B.; Koch, F.; Fossiez, F.; Romani, N.; Lebecque, S.; Saeland, S. Identification of mouse langerin/CD207 in Langerhans cells and some dendritic cells of lymphoid tissues. *J Immunol.* 2002; 168(2):782-92.
31. Singh, T. P.; Zhang, H. H.; Borek, I.; Wolf, P.; Hedrick, M. N.; Singh, S. P.; Kelsall, B. L.; Clausen, B. E.; Farber, J. M. Monocyte-derived inflammatory Langerhans cells and dermal dendritic cells mediate psoriasis-like inflammation. *Nature Communications.* 2016; 7:13581.
32. Iwasaki, A. Mucosal dendritic cells. *Annu Rev Immunol.* 2007; 25:381-418.
33. Kushwah, R.; Hu, J. Complexity of dendritic cell subsets and their function in the host immune system. *Immunology.* 2011; 133(4):409-419.
34. Del Rio, M. L.; Bernhardt, G.; Rodriguez-Barbosa, J. I.; Forster, R. Development and functional specialization of CD103+ dendritic cells. *Immunol Rev.* 2010; 234(1):268-81.
35. Helft, J.; Ginhoux, F.; Bogunovic, M.; Merad, M. Origin and functional heterogeneity of non-lymphoid tissue dendritic cells in mice. *Immunol Rev.* 2010; 234(1):55-75.

## REFERENCES

36. Serbina, N. V.; Salazar-Mather, T. P.; Biron, C. A.; Kuziel, W. A.; Pamer, E. G. TNF/iNOS-producing dendritic cells mediate innate immune defense against bacterial infection. *Immunity*. 2003; 19(1):59-70.
37. Bosschaerts, T.; Guilliams, M.; Stijlemans, B.; Morias, Y.; Engel, D.; Tacke, F.; Herin, M.; De Baetselier, P.; Beschin, A. Tip-DC development during parasitic infection is regulated by IL-10 and requires CCL2/CCR2, IFN-gamma and MyD88 signaling. *PLoS Pathog*. 2010; 6(8):e1001045.
38. Dominguez, P. M.; Ardavin, C. Differentiation and function of mouse monocyte-derived dendritic cells in steady state and inflammation. *Immunol Rev*. 2010; 234(1):90-104.
39. Mutyambizi, K.; Berger, C. L.; Edelson, R. L. The balance between immunity and tolerance: The role of Langerhans cells. *Cellular and molecular life sciences : CMLS*. 2009; 66(5):831-840.
40. Loser, K.; Beissert, S. Dendritic cells and T cells in the regulation of cutaneous immunity. *Adv Dermatol*. 2007; 23:307-33.
41. Van De Laar, L.; Coffey, P. J.; Woltman, A. M. Regulation of dendritic cell development by GM-CSF: molecular control and implications for immune homeostasis and therapy. *Blood*. 2012; 119(15):3383-3393.
42. Cella, M.; Jarrossay, D.; Facchetti, F.; Alebardi, O.; Nakajima, H.; Lanzavecchia, A.; Colonna, M. Plasmacytoid monocytes migrate to inflamed lymph nodes and produce large amounts of type I interferon. *Nature Medicine*. 1999; 5(8):919-23.
43. Hoeffel, G.; Ripoche, A. C.; Matheoud, D.; Nascimbeni, M.; Escriou, N.; Lebon, P.; Heshmati, F.; Guillet, J. G.; Gannage, M.; Caillat-Zucman, S.; Casartelli, N.; Schwartz, O.; De La Salle, H.; Hanau, D.; Hosmalin, A.; Maranon, C. Antigen crosspresentation by human plasmacytoid dendritic cells. *Immunity*. 2007; 27(3):481-92.
44. Di Pucchio, T.; Chatterjee, B.; Smed-Sorensen, A.; Clayton, S.; Palazzo, A.; Montes, M.; Xue, Y.; Mellman, I.; Banchereau, J.; Connolly, J. E. Direct proteasome-independent cross-presentation of viral antigen by plasmacytoid dendritic cells on major histocompatibility complex class I. *Nat Immunol*. 2008; 9(5):551-7.
45. Villadangos, J. A.; Young, L. Antigen-presentation properties of plasmacytoid dendritic cells. *Immunity*. 2008; 29(3):352-61.
46. Ganguly, D.; Haak, S.; Sisirak, V.; Reizis, B. The role of dendritic cells in autoimmunity. *Nat Rev Immunol*. 2013; 13(8):566-77.

## REFERENCES

47. Gehrie, E.; Van Der Touw, W.; Bromberg, J. S.; Ochando, J. C. Plasmacytoid Dendritic Cells in Tolerance. *Methods in molecular biology (Clifton, NJ)*. 2011; 677:127-147.
48. Swiecki, M.; Colonna, M. Unraveling the functions of plasmacytoid dendritic cells during viral infections, autoimmunity, and tolerance. *Immunological Reviews*. 2010; 234(1):142-162.
49. Inaba, K.; Inaba, M.; Romani, N.; Aya, H.; Deguchi, M.; Ikehara, S.; Muramatsu, S.; Steinman, R. M. Generation of large numbers of dendritic cells from mouse bone marrow cultures supplemented with granulocyte/macrophage colony-stimulating factor. *J Exp Med*. 1992; 176(6):1693-702.
50. Lutz, M. B.; Kukutsch, N.; Ogilvie, A. L.; Rossner, S.; Koch, F.; Romani, N.; Schuler, G. An advanced culture method for generating large quantities of highly pure dendritic cells from mouse bone marrow. *J Immunol Methods*. 1999; 223(1):77-92.
51. Xu, Y.; Zhan, Y.; Lew, A. M.; Naik, S. H.; Kershaw, M. H. Differential development of murine dendritic cells by GM-CSF versus Flt3 ligand has implications for inflammation and trafficking. *J Immunol*. 2007; 179(11):7577-84.
52. Helft, J.; Bottcher, J.; Chakravarty, P.; Zelenay, S.; Huotari, J.; Schraml, B. U.; Goubau, D.; Reis E Sousa, C. GM-CSF Mouse Bone Marrow Cultures Comprise a Heterogeneous Population of CD11c(+)MHCII(+) Macrophages and Dendritic Cells. *Immunity*. 2015; 42(6):1197-211.
53. Naik, S. H.; Proietto, A. I.; Wilson, N. S.; Dakic, A.; Schnorrer, P.; Fuchsberger, M.; Lahoud, M. H.; O'keeffe, M.; Shao, Q. X.; Chen, W. F.; Villadangos, J. A.; Shortman, K.; Wu, L. Cutting edge: generation of splenic CD8+ and CD8- dendritic cell equivalents in Fms-like tyrosine kinase 3 ligand bone marrow cultures. *J Immunol*. 2005; 174(11):6592-7.
54. Kang, K.; Lim, J.-S. Induction of Functional Changes of Dendritic Cells by Silica Nanoparticles. *Immune Network*. 2012; 12(3):104-112.
55. Marzaioli, V.; Gross, C. J.; Weichenmeier, I.; Schmidt-Weber, C. B.; Gutermuth, J.; Gross, O.; Alessandrini, F. Specific Surface Modifications of Silica Nanoparticles Diminish Inflammasome Activation and In Vivo Expression of Selected Inflammatory Genes. *Nanomaterials (Basel)*. 2017; 7(11).
56. Wang, C.; Zhu, W.; Wang, B. Z. Dual-linker gold nanoparticles as adjuvanting carriers for multivalent display of recombinant influenza hemagglutinin trimers and flagellin improve the immunological responses in vivo and in vitro. *Int J Nanomedicine*. 2017; 12:4747-4762.

## REFERENCES

57. Kostadinova, A. I.; Middelburg, J.; Ciulla, M.; Garssen, J.; Hennink, W. E.; Knippels, L. M. J.; Van Nostrum, C. F.; Willemsen, L. E. M. PLGA nanoparticles loaded with beta-lactoglobulin-derived peptides modulate mucosal immunity and may facilitate cow's milk allergy prevention. *European Journal of Pharmacology*. 2018; 818:211-220.
58. Shen, Z.; Reznikoff, G.; Dranoff, G.; Rock, K. L. Cloned dendritic cells can present exogenous antigens on both MHC class I and class II molecules. *J Immunol*. 1997; 158(6):2723-30.
59. Kawai, T.; Akira, S. TLR signaling. *Semin Immunol*. 2007; 19(1):24-32.
60. Matzinger, P. Tolerance, danger, and the extended family. *Annu Rev Immunol*. 1994; 12:991-1045.
61. Medzhitov, R.; Preston-Hurlburt, P.; Janeway, C. A., Jr. A human homologue of the Drosophila Toll protein signals activation of adaptive immunity. *Nature*. 1997; 388(6640):394-7.
62. Yang, R. B.; Mark, M. R.; Gray, A.; Huang, A.; Xie, M. H.; Zhang, M.; Goddard, A.; Wood, W. I.; Gurney, A. L.; Godowski, P. J. Toll-like receptor-2 mediates lipopolysaccharide-induced cellular signalling. *Nature*. 1998; 395(6699):284-8.
63. Brown, J.; Wang, H.; Hajishengallis, G. N.; Martin, M. TLR-signaling networks: an integration of adaptor molecules, kinases, and cross-talk. *J Dent Res*. 2011; 90(4):417-27.
64. Shcheblyakov, D. V.; Logunov, D. Y.; Tukhvatulin, A. I.; Shmarov, M. M.; Naroditsky, B. S.; Gintsburg, A. L. Toll-Like Receptors (TLRs): The Role in Tumor Progression. *Acta Naturae*. 2010; 2(3):21-9.
65. Oldenburg, M.; Kruger, A.; Ferstl, R.; Kaufmann, A.; Nees, G.; Sigmund, A.; Bathke, B.; Lauterbach, H.; Suter, M.; Dreher, S.; Koedel, U.; Akira, S.; Kawai, T.; Buer, J.; Wagner, H.; Bauer, S.; Hochrein, H.; Kirschning, C. J. TLR13 recognizes bacterial 23S rRNA devoid of erythromycin resistance-forming modification. *Science*. 2012; 337(6098):1111-5.
66. Koblansky, A. A.; Jankovic, D.; Oh, H.; Hieny, S.; Sungnak, W.; Mathur, R.; Hayden, M. S.; Akira, S.; Sher, A.; Ghosh, S. Recognition of profilin by Toll-like receptor 12 is critical for host resistance to *Toxoplasma gondii*. *Immunity*. 2013; 38(1):119-30.
67. Deguine, J.; Barton, G. M. MyD88: a central player in innate immune signaling. *F1000Prime Reports*. 2014; 6:97.
68. Iwasaki, A.; Medzhitov, R. Toll-like receptor control of the adaptive immune responses. *Nat Immunol*. 2004; 5(10):987-95.

## REFERENCES

69. Lin, S. C.; Lo, Y. C.; Wu, H. Helical assembly in the MyD88-IRAK4-IRAK2 complex in TLR/IL-1R signalling. *Nature*. 2010; 465(7300):885-90.
70. Li, S.; Strelow, A.; Fontana, E.; Wesche, H. IRAK-4: a novel member of the IRAK family with the properties of an IRAK-kinase. *Nature*. 2002; 415(6877):925-9.
71. Wang, C.; Deng, L.; Hong, M.; Akkaraju, G. R.; Inoue, J.; Chen, Z. J. TAK1 is a ubiquitin-dependent kinase of MKK and IKK. *Nature*. 2001; 412(6844):346-51.
72. Chaudhary, D.; Robinson, S.; Romero, D. L. Recent Advances in the Discovery of Small Molecule Inhibitors of Interleukin-1 Receptor-Associated Kinase 4 (IRAK4) as a Therapeutic Target for Inflammation and Oncology Disorders. *Journal of Medicinal Chemistry*. 2015; 58(1):96-110.
73. Takeda, K.; Akira, S. TLR signaling pathways. *Semin Immunol*. 2004; 16(1):3-9.
74. Ullah, M. O.; Sweet, M. J.; Mansell, A.; Kellie, S.; Kobe, B. TRIF-dependent TLR signaling, its functions in host defense and inflammation, and its potential as a therapeutic target. *J Leukoc Biol*. 2016; 100(1):27-45.
75. Jiang, Z.; Mak, T. W.; Sen, G.; Li, X. Toll-like receptor 3-mediated activation of NF-kappaB and IRF3 diverges at Toll-IL-1 receptor domain-containing adapter inducing IFN-beta. *Proc Natl Acad Sci U S A*. 2004; 101(10):3533-8.
76. Proell, M.; Riedl, S. J.; Fritz, J. H.; Rojas, A. M.; Schwarzenbacher, R. The Nod-like receptor (NLR) family: a tale of similarities and differences. *PLoS One*. 2008; 3(4):e2119.
77. Jensen, S.; Thomsen, A. R. Sensing of RNA Viruses: a Review of Innate Immune Receptors Involved in Recognizing RNA Virus Invasion. *Journal of Virology*. 2012; 86(6):2900-2910.
78. Franchi, L.; Warner, N.; Viani, K.; Nunez, G. Function of Nod-like receptors in microbial recognition and host defense. *Immunol Rev*. 2009; 227(1):106-28.
79. Correa, Ricardo g.; Milutinovic, S.; Reed, John c. Roles of NOD1 (NLRC1) and NOD2 (NLRC2) in innate immunity and inflammatory diseases. *Bioscience Reports*. 2012; 32(6):597-608.
80. Damiano, Jason s.; Oliveira, V.; Welsh, K.; Reed, John c. Heterotypic interactions among NACHT domains: implications for regulation of innate immune responses. *Biochemical Journal*. 2004; 381(Pt 1):213-219.
81. Irving, Aaron t.; Mimuro, H.; Kufer, Thomas a.; Lo, C.; Wheeler, R.; Turner, Lorinda j.; Thomas, Belinda j.; Malosse, C.; Gantier, Michael p.; Casillas, Linda n.; Votta, Bartholomew j.; Bertin, J.; Boneca, Ivo g.; Sasakawa, C.; Philpott, Dana j.; Ferrero, Richard l.; Kaparakis-Liaskos, M. The Immune Receptor NOD1 and

## REFERENCES

- Kinase RIP2 Interact with Bacterial Peptidoglycan on Early Endosomes to Promote Autophagy and Inflammatory Signaling. *Cell Host & Microbe*. 2014; 15(5):623-635.
82. Hasegawa, M.; Fujimoto, Y.; Lucas, P. C.; Nakano, H.; Fukase, K.; Núñez, G.; Inohara, N. A critical role of RICK/RIP2 polyubiquitination in Nod-induced NF- $\kappa$ B activation. *The EMBO Journal*. 2008; 27(2):373-383.
83. Kanazawa, N. Dendritic cell immunoreceptors: C-type lectin receptors for pattern-recognition and signaling on antigen-presenting cells. *J Dermatol Sci*. 2007; 45(2):77-86.
84. Kronin, V.; Wu, L.; Gong, S.; Nussenzweig, M. C.; Shortman, K. DEC-205 as a marker of dendritic cells with regulatory effects on CD8 T cell responses. *Int Immunol*. 2000; 12(5):731-5.
85. Inaba, K.; Swiggard, W. J.; Inaba, M.; Meltzer, J.; Mirza, A.; Sasagawa, T.; Nussenzweig, M. C.; Steinman, R. M. Tissue distribution of the DEC-205 protein that is detected by the monoclonal antibody NLDC-145. I. Expression on dendritic cells and other subsets of mouse leukocytes. *Cell Immunol*. 1995; 163(1):148-56.
86. Krieg, A. M. CpG motifs in bacterial DNA and their immune effects. *Annu Rev Immunol*. 2002; 20:709-60.
87. Jahrsdörfer, B.; Weiner, G. J. CpG oligodeoxynucleotides as immunotherapy in cancer. *Update on cancer therapeutics*. 2008; 3(1):27-32.
88. Lou, Y.; Liu, C.; Lizee, G.; Peng, W.; Xu, C.; Ye, Y.; Rabinovich, B. A.; Hailemichael, Y.; Gelbard, A.; Zhou, D.; Overwijk, W. W.; Hwu, P. Antitumor activity mediated by CpG: the route of administration is critical. *J Immunother*. 2011; 34(3):279-88.
89. Ong, M. L.; Wikstrom, M. E.; Fleming, P.; Estcourt, M. J.; Hertzog, P. J.; Hill, G. R.; Andoniou, C. E.; Degli-Esposti, M. A. CpG pretreatment enhances antiviral T-cell immunity against cytomegalovirus. *Blood*. 2013; 122(1):55-60.
90. Vercammen, E.; Staal, J.; Beyaert, R. Sensing of Viral Infection and Activation of Innate Immunity by Toll-Like Receptor 3. *Clinical Microbiology Reviews*. 2008; 21(1):13-25.
91. Chi, H.; Li, C.; Zhao, F. S.; Zhang, L.; Ng, T. B.; Jin, G.; Sha, O. Anti-tumor Activity of Toll-Like Receptor 7 Agonists. *Frontiers in Pharmacology*. 2017; 8:304.
92. Hemmi, H.; Kaisho, T.; Takeuchi, O.; Sato, S.; Sanjo, H.; Hoshino, K.; Horiuchi, T.; Tomizawa, H.; Takeda, K.; Akira, S. Small anti-viral compounds activate

## REFERENCES

- immune cells via the TLR7 MyD88-dependent signaling pathway. *Nat Immunol.* 2002; 3(2):196-200.
93. Hanna, E.; Abadi, R.; Abbas, O. Imiquimod in dermatology: an overview. *Int J Dermatol.* 2016; 55(8):831-44.
94. Bakker, A. B.; Schreurs, M. W.; De Boer, A. J.; Kawakami, Y.; Rosenberg, S. A.; Adema, G. J.; Figdor, C. G. Melanocyte lineage-specific antigen gp100 is recognized by melanoma-derived tumor-infiltrating lymphocytes. *J Exp Med.* 1994; 179(3):1005-9.
95. Van Den Eynde, B. J.; Van Der Bruggen, P. T cell defined tumor antigens. *Curr Opin Immunol.* 1997; 9(5):684-93.
96. Tumor and Vaccine Site With a Toll Like Receptor (TLR) Agonist: Bethesda (MD): National Library of Medicine (US); [updated 2009 Aug 17. Identifier NCT00960752]
97. Jurk, M.; Heil, F.; Vollmer, J.; Schetter, C.; Krieg, A. M.; Wagner, H.; Lipford, G.; Bauer, S. Human TLR7 or TLR8 independently confer responsiveness to the antiviral compound R-848. *Nat Immunol.* 2002; 3(6):499.
98. Cervantes, J. L.; Weinerman, B.; Basole, C.; Salazar, J. C. TLR8: the forgotten relative revindicated. *Cell Mol Immunol.* 2012; 9(6):434-8.
99. Bi, D.; Gao, Y.; Chu, Q.; Cui, J.; Xu, T. NOD1 is the innate immune receptor for iE-DAP and can activate NF-kappaB pathway in teleost fish. *Dev Comp Immunol.* 2017; 76:238-246.
100. Grimes, C. L.; Ariyananda, L. D. Z.; Melnyk, J. E.; O'shea, E. K. The Innate Immune Protein Nod2 Binds Directly to MDP, a Bacterial Cell Wall Fragment. *Journal of the American Chemical Society.* 2012; 134(33):13535-13537.
101. Wilmanski, J. M.; Petnicki-Ocwieja, T.; Kobayashi, K. S. NLR proteins: integral members of innate immunity and mediators of inflammatory diseases. *Journal of Leukocyte Biology.* 2008; 83(1):13-30.
102. Yamamoto, S.; Ma, X. Role of Nod2 in the development of Crohn's disease. *Microbes and infection / Institut Pasteur.* 2009; 11(12):912-918.
103. Kim, Y. K.; Shin, J.-S.; Nahm, M. H. NOD-Like Receptors in Infection, Immunity, and Diseases. *Yonsei Medical Journal.* 2016; 57(1):5-14.
104. Traub, S.; Von Aulock, S.; Hartung, T.; Hermann, C. MDP and other muopeptides-direct and synergistic effects on the immune system. *J Endotoxin Res.* 2006; 12(2):69-85.

## REFERENCES

105. Ellouz, F.; Adam, A.; Ciorbaru, R.; Lederer, E. Minimal structural requirements for adjuvant activity of bacterial peptidoglycan derivatives. *Biochem Biophys Res Commun.* 1974; 59(4):1317-25.
106. Warger, T.; Osterloh, P.; Rechtsteiner, G.; Fassbender, M.; Heib, V.; Schmid, B.; Schmitt, E.; Schild, H.; Radsak, M. P. Synergistic activation of dendritic cells by combined Toll-like receptor ligation induces superior CTL responses in vivo. *Blood.* 2006; 108(2):544-50.
107. Zhu, Q.; Egelston, C.; Vivekanandhan, A.; Uematsu, S.; Akira, S.; Klinman, D. M.; Belyakov, I. M.; Berzofsky, J. A. Toll-like receptor ligands synergize through distinct dendritic cell pathways to induce T cell responses: Implications for vaccines. *Proceedings of the National Academy of Sciences.* 2008; 105(42):16260-16265.
108. Underhill, D. M. Collaboration between the innate immune receptors dectin-1, TLRs, and Nods. *Immunol Rev.* 2007; 219:75-87.
109. Blum, J. S.; Wearsch, P. A.; Cresswell, P. Pathways of Antigen Processing. *Annual Review of Immunology.* 2013; 31:443-473.
110. Kambayashi, T.; Laufer, T. M. Atypical MHC class II-expressing antigen-presenting cells: can anything replace a dendritic cell? *Nature Reviews Immunology.* 2014; 14:719.
111. Landsverk, O. J.; Bakke, O.; Gregers, T. F. MHC II and the endocytic pathway: regulation by invariant chain. *Scand J Immunol.* 2009; 70(3):184-93.
112. Pond, L.; Kuhn, L. A.; Teyton, L.; Schutze, M. P.; Tainer, J. A.; Jackson, M. R.; Peterson, P. A. A role for acidic residues in di-leucine motif-based targeting to the endocytic pathway. *J Biol Chem.* 1995; 270(34):19989-97.
113. Hewitt, E. W. The MHC class I antigen presentation pathway: strategies for viral immune evasion. *Immunology.* 2003; 110(2):163-169.
114. Ortmann, B.; Copeman, J.; Lehner, P. J.; Sadasivan, B.; Herberg, J. A.; Grandea, A. G.; Riddell, S. R.; Tampe, R.; Spies, T.; Trowsdale, J.; Cresswell, P. A critical role for tapasin in the assembly and function of multimeric MHC class I-TAP complexes. *Science.* 1997; 277(5330):1306-9.
115. Oancea, G.; O'mara, M. L.; Bennett, W. F.; Tieleman, D. P.; Abele, R.; Tampe, R. Structural arrangement of the transmission interface in the antigen ABC transport complex TAP. *Proc Natl Acad Sci U S A.* 2009; 106(14):5551-6.
116. Joffre, O. P.; Segura, E.; Savina, A.; Amigorena, S. Cross-presentation by dendritic cells. *Nat Rev Immunol.* 2012; 12(8):557-69.



## REFERENCES

117. Alloatti, A.; Kotsias, F.; Hoffmann, E.; Amigorena, S. Evaluation of Cross-presentation in Bone Marrow-derived Dendritic Cells in vitro and Splenic Dendritic Cells ex vivo Using Antigen-coated Beads. *Bio-protocol*. 2016; 6(22):e2015.
118. Flores-Romo, L. In vivo maturation and migration of dendritic cells. *Immunology*. 2001; 102(3):255-262.
119. Heath, W. R.; Carbone, F. R. Cross-presentation in viral immunity and self-tolerance. *Nature Reviews Immunology*. 2001; 1:126.
120. Fehres, C. M.; Unger, W. W. J.; Garcia-Vallejo, J. J.; Van Kooyk, Y. Understanding the Biology of Antigen Cross-Presentation for the Design of Vaccines Against Cancer. *Frontiers in Immunology*. 2014; 5:149.
121. Fontana, M. F.; Vance, R. E. Two signal models in innate immunity. *Immunol Rev*. 2011; 243(1):26-39.
122. Curtsinger, J. M.; Schmidt, C. S.; Mondino, A.; Lins, D. C.; Kedl, R. M.; Jenkins, M. K.; Mescher, M. F. Inflammatory cytokines provide a third signal for activation of naive CD4+ and CD8+ T cells. *J Immunol*. 1999; 162(6):3256-62.
123. Zinkernagel, R. M. Restriction by H-2 gene complex of transfer of cell-mediated immunity to *Listeria monocytogenes*. *Nature*. 1974; 251:230.
124. Artyomov, M. N.; Lis, M.; Devadas, S.; Davis, M. M.; Chakraborty, A. K. CD4 and CD8 binding to MHC molecules primarily acts to enhance Lck delivery. *Proceedings of the National Academy of Sciences*. 2010; 107(39):16916-16921.
125. Mittrucker, H. W.; Visekruna, A.; Huber, M. Heterogeneity in the differentiation and function of CD8(+) T cells. *Arch Immunol Ther Exp (Warsz)*. 2014; 62(6):449-58.
126. Lasalle, J. M.; Hafler, D. A. T cell anergy. *Faseb j*. 1994; 8(9):601-8.
127. Beyersdorf, N.; Kerkau, T.; Hünig, T. CD28 co-stimulation in T-cell homeostasis: a recent perspective. *Immunotargets and Therapy*. 2015; 4:111-122.
128. Scott, P. IL-12: initiation cytokine for cell-mediated immunity. *Science*. 1993; 260(5107):496-7.
129. Santarlasci, V.; Cosmi, L.; Maggi, L.; Liotta, F.; Annunziato, F. IL-1 and T Helper Immune Responses. *Frontiers in Immunology*. 2013; 4:182.
130. Shibuya, K.; Robinson, D.; Zonin, F.; Hartley, S. B.; Macatonia, S. E.; Somoza, C.; Hunter, C. A.; Murphy, K. M.; O'garra, A. IL-1 $\alpha$  and TNF- $\alpha$  Are Required for IL-12-Induced Development of Th1 Cells Producing High Levels of IFN- $\gamma$  in BALB/c But Not C57BL/6 Mice. *The Journal of Immunology*. 1998; 160(4):1708-1716.

## REFERENCES

131. Swain, S. L.; Weinberg, A. D.; English, M.; Huston, G. IL-4 directs the development of Th2-like helper effectors. *The Journal of Immunology*. 1990; 145(11):3796-3806.
132. Suzuki, J.; Isobe, M.; Izawa, A.; Takahashi, W.; Yamazaki, S.; Okubo, Y.; Amano, J.; Sekiguchi, M. Differential Th1 and Th2 cell regulation of murine cardiac allograft acceptance by blocking cell adhesion of ICAM-1/LFA-1 and VCAM-1/VLA-4. *Transpl Immunol*. 1999; 7(1):65-72.
133. Croft, M.; So, T.; Duan, W.; Soroosh, P. The Significance of OX40 and OX40L to T cell Biology and Immune Disease. *Immunological Reviews*. 2009; 229(1):173-191.
134. Corthay, A. A three-cell model for activation of naive T helper cells. *Scand J Immunol*. 2006; 64(2):93-6.
135. Qin, Z.; Richter, G.; Schuler, T.; Ibe, S.; Cao, X.; Blankenstein, T. B cells inhibit induction of T cell-dependent tumor immunity. *Nature Medicine*. 1998; 4(5):627-30.
136. Lundak, R. L.; Raidt, D. J. Cellular immune response against tumor cells. I. In vitro immunization of allogeneic and syngeneic mouse spleen cell suspensions against DBA mastocytoma cells. *Cell Immunol*. 1973; 9(1):60-6.
137. Vesely, M. D.; Kershaw, M. H.; Schreiber, R. D.; Smyth, M. J. Natural innate and adaptive immunity to cancer. *Annu Rev Immunol*. 2011; 29:235-71.
138. Aspod, C.; Pedroza-Gonzalez, A.; Gallegos, M.; Tindle, S.; Burton, E. C.; Su, D.; Marches, F.; Banchereau, J.; Palucka, A. K. Breast cancer instructs dendritic cells to prime interleukin 13-secreting CD4+ T cells that facilitate tumor development. *J Exp Med*. 2007; 204(5):1037-47.
139. De Visser, K. E.; Korets, L. V.; Coussens, L. M. De novo carcinogenesis promoted by chronic inflammation is B lymphocyte dependent. *Cancer Cell*. 2005; 7(5):411-23.
140. Andreu, P.; Johansson, M.; Affara, N. I.; Pucci, F.; Tan, T.; Junankar, S.; Korets, L.; Lam, J.; Tawfik, D.; Denardo, D. G.; Naldini, L.; De Visser, K. E.; De Palma, M.; Coussens, L. M. FcRgamma activation regulates inflammation-associated squamous carcinogenesis. *Cancer Cell*. 2010; 17(2):121-34.
141. Fenner, F. Smallpox, "the most dreadful scourge of the human species." Its global spread and recent eradication. *Med J Aust*. 1984; 141(12-13):841-6.
142. Shchelkunov, S. N. Emergence and reemergence of smallpox: The need for development of a new generation smallpox vaccine. *Vaccine*. 2011; 29:D49-D53.

## REFERENCES

143. National Advisory Committee On, I. An advisory committee statement (ACS). National Advisory Committee on Immunization (NACI). Statement on smallpox vaccination. *Can Commun Dis Rep.* 2002; 28(ACS-1):1-12.
144. Zepp, F. Principles of vaccine design-Lessons from nature. *Vaccine.* 2010; 28 Suppl 3:C14-24.
145. Delany, I.; Rappuoli, R.; De Gregorio, E. Vaccines for the 21st century. *EMBO Mol Med.* 2014; 6(6):708-20.
146. Geeraedts, F.; Goutagny, N.; Hornung, V.; Severa, M.; De Haan, A.; Pool, J.; Wilschut, J.; Fitzgerald, K. A.; Huckriede, A. Superior immunogenicity of inactivated whole virus H5N1 influenza vaccine is primarily controlled by Toll-like receptor signalling. *PLoS Pathog.* 2008; 4(8):e1000138.
147. Marrack, P.; Mckee, A. S.; Munks, M. W. Towards an understanding of the adjuvant action of aluminium. *Nature Reviews Immunology.* 2009; 9:287.
148. Stils, J. H. F. Adjuvants and Antibody Production: Dispelling the Myths Associated with Freund's Complete and Other Adjuvants. *ILAR Journal.* 2005; 46(3):280-293.
149. Di Pasquale, A.; Preiss, S.; Tavares Da Silva, F.; Garcon, N. Vaccine Adjuvants: from 1920 to 2015 and Beyond. *Vaccines (Basel).* 2015; 3(2):320-43.
150. Tsukahara, T.; Hirohashi, Y.; Kanaseki, T.; Nakatsugawa, M.; Kubo, T.; Sato, N.; Torigoe, T. Peptide vaccination therapy: Towards the next generation. *Pathol Int.* 2016; 66(10):547-553.
151. Harper, D. M.; Demars, L. R. HPV vaccines – A review of the first decade. *Gynecologic Oncology.* 2017; 146(1):196-204.
152. Lollini, P.-L.; Cavallo, F.; Nanni, P.; Quaglino, E. The Promise of Preventive Cancer Vaccines. *Vaccines.* 2015; 3(2):467-489.
153. Rabinovich, G. A.; Gabrilovich, D.; Sotomayor, E. M. Immunosuppressive strategies that are mediated by tumor cells. *Annu Rev Immunol.* 2007; 25:267-96.
154. Bobbala, S.; Hook, S. Is There an Optimal Formulation and Delivery Strategy for Subunit Vaccines? *Pharm Res.* 2016; 33(9):2078-97.
155. Rosenberg, S. A.; Restifo, N. P. Adoptive cell transfer as personalized immunotherapy for human cancer. *Science.* 2015; 348(6230):62-8.
156. Sharma, P.; Allison, J. P. The future of immune checkpoint therapy. *Science.* 2015; 348(6230):56-61.
157. De Jong, W. H.; Borm, P. J. A. Drug delivery and nanoparticles: Applications and hazards. *Int J Nanomedicine.* 2008; 3(2):133-149.

## REFERENCES

158. Jeevanandam, J.; Barhoum, A.; Chan, Y. S.; Dufresne, A.; Danquah, M. K. Review on nanoparticles and nanostructured materials: history, sources, toxicity and regulations. *Beilstein Journal of Nanotechnology*. 2018; 9:1050-1074.
159. Luo, M.; Samandi, L. Z.; Wang, Z.; Chen, Z. J.; Gao, J. Synthetic nanovaccines for immunotherapy. *J Control Release*. 2017; 263:200-210.
160. Marques Neto, L. M.; Kipnis, A.; Junqueira-Kipnis, A. P. Role of Metallic Nanoparticles in Vaccinology: Implications for Infectious Disease Vaccine Development. *Frontiers in Immunology*. 2017; 8:239.
161. Jiao, M.; Zhang, P.; Meng, J.; Li, Y.; Liu, C.; Luo, X.; Gao, M. Recent advancements in biocompatible inorganic nanoparticles towards biomedical applications. *Biomater Sci*. 2018; 6(4):726-745.
162. Ahn, S.; Lee, I. H.; Kang, S.; Kim, D.; Choi, M.; Saw, P. E.; Shin, E. C.; Jon, S. Gold nanoparticles displaying tumor-associated self-antigens as a potential vaccine for cancer immunotherapy. *Adv Healthc Mater*. 2014; 3(8):1194-9.
163. Soenen, S. J.; Rivera-Gil, P.; Montenegro, J.-M.; Parak, W. J.; De Smedt, S. C.; Braeckmans, K. Cellular toxicity of inorganic nanoparticles: Common aspects and guidelines for improved nanotoxicity evaluation. *Nano Today*. 2011; 6(5):446-465.
164. Dykman, L. A.; Khlebtsov, N. G. Gold Nanoparticles in Biology and Medicine: Recent Advances and Prospects. *Acta Naturae*. 2011; 3(2):34-55.
165. Giner-Casares, J. J.; Henriksen-Lacey, M.; Coronado-Puchau, M.; Liz-Marzán, L. M. Inorganic nanoparticles for biomedicine: where materials scientists meet medical research. *Materials Today*. 2016; 19(1):19-28.
166. Soema, P. C.; Willems, G.-J.; Jiskoot, W.; Amorij, J.-P.; Kersten, G. F. Predicting the influence of liposomal lipid composition on liposome size, zeta potential and liposome-induced dendritic cell maturation using a design of experiments approach. *European Journal of Pharmaceutics and Biopharmaceutics*. 2015; 94:427-435.
167. Anari, E. Liposome: Classification, Preparation, and Applications in Nanomedicine 2013.
168. Bozzuto, G.; Molinari, A. Liposomes as nanomedical devices. *Int J Nanomedicine*. 2015; 10:975-999.
169. Taneichi, M.; Ishida, H.; Kajino, K.; Ogasawara, K.; Tanaka, Y.; Kasai, M.; Mori, M.; Nishida, M.; Yamamura, H.; Mizuguchi, J.; Uchida, T. Antigen chemically coupled to the surface of liposomes are cross-presented to CD8<sup>+</sup> T cells and induce potent antitumor immunity. *J Immunol*. 2006; 177(4):2324-30.

## REFERENCES

170. Ignatius, R.; Mahnke, K.; Rivera, M.; Hong, K.; Isdell, F.; Steinman, R. M.; Pope, M.; Stamatatos, L. Presentation of proteins encapsulated in sterically stabilized liposomes by dendritic cells initiates CD8(+) T-cell responses in vivo. *Blood*. 2000; 96(10):3505-13.
171. Bulbake, U.; Doppalapudi, S.; Kommineni, N.; Khan, W. Liposomal Formulations in Clinical Use: An Updated Review. *Pharmaceutics*. 2017; 9(2).
172. Sah, H.; Thoma, L. A.; Desu, H. R.; Sah, E.; Wood, G. C. Concepts and practices used to develop functional PLGA-based nanoparticulate systems. *Int J Nanomedicine*. 2013; 8:747-65.
173. Kan, P.; Tsao, C. W.; Wang, A. J.; Su, W. C.; Liang, H. F. A liposomal formulation able to incorporate a high content of Paclitaxel and exert promising anticancer effect. *J Drug Deliv*. 2011; 2011:629234.
174. Rao, J. P.; Geckeler, K. E. Polymer nanoparticles: Preparation techniques and size-control parameters. *Progress in Polymer Science*. 2011; 36(7):887-913.
175. Zambaux, M. F.; Bonneaux, F.; Gref, R.; Maincent, P.; Dellacherie, E.; Alonso, M. J.; Labrude, P.; Vigneron, C. Influence of experimental parameters on the characteristics of poly(lactic acid) nanoparticles prepared by a double emulsion method. *Journal of Controlled Release*. 1998; 50(1):31-40.
176. Musyanovych, A.; Schmitz-Wienke, J.; Mailander, V.; Walther, P.; Landfester, K. Preparation of biodegradable polymer nanoparticles by miniemulsion technique and their cell interactions. *Macromol Biosci*. 2008; 8(2):127-39.
177. Holzapfel, V.; Musyanovych, A.; Landfester, K.; Lorenz Myriam, R.; Mailänder, V. Preparation of Fluorescent Carboxyl and Amino Functionalized Polystyrene Particles by Miniemulsion Polymerization as Markers for Cells. *Macromolecular Chemistry and Physics*. 2005; 206(24):2440-2449.
178. Ruizendaal, L.; Bhattacharjee, S.; Pournazari, K.; Rosso-Vasic, M.; De Haan, L.; Alink, G. M.; Marcelis, A. T. M.; Zuilhof, H. Synthesis and cytotoxicity of silicon nanoparticles with covalently attached organic monolayers 2009. 339-347 p.
179. Fröhlich, E. The role of surface charge in cellular uptake and cytotoxicity of medical nanoparticles. *Int J Nanomedicine*. 2012; 7:5577-5591.
180. Luo, X.; Feng, M.; Pan, S.; Wen, Y.; Zhang, W.; Wu, C. Charge shielding effects on gene delivery of polyethylenimine/DNA complexes: PEGylation and phospholipid coating. *J Mater Sci Mater Med*. 2012; 23(7):1685-95.
181. Irvine, D. J.; Hanson, M. C.; Rakhra, K.; Tokatlian, T. Synthetic Nanoparticles for Vaccines and Immunotherapy. *Chemical Reviews*. 2015; 115(19):11109-11146.

## REFERENCES

182. Ahsan, F.; Rivas, I. P.; Khan, M. A.; Torres Suarez, A. I. Targeting to macrophages: role of physicochemical properties of particulate carriers--liposomes and microspheres--on the phagocytosis by macrophages. *J Control Release*. 2002; 79(1-3):29-40.
183. Vyas, S. P.; Kannan, M. E.; Jain, S.; Mishra, V.; Singh, P. Design of liposomal aerosols for improved delivery of rifampicin to alveolar macrophages. *Int J Pharm*. 2004; 269(1):37-49.
184. Dreaden, E. C.; Austin, L. A.; Mackey, M. A.; El-Sayed, M. A. Size matters: gold nanoparticles in targeted cancer drug delivery. *Ther Deliv*. 2012; 3(4):457-78.
185. Kulkarni, S. A.; Feng, S. S. Effects of particle size and surface modification on cellular uptake and biodistribution of polymeric nanoparticles for drug delivery. *Pharm Res*. 2013; 30(10):2512-22.
186. Manolova, V.; Flace, A.; Bauer, M.; Schwarz, K.; Saudan, P.; Bachmann, M. F. Nanoparticles target distinct dendritic cell populations according to their size. *Eur J Immunol*. 2008; 38(5):1404-13.
187. Hu, Y.; Litwin, T.; Nagaraja, A. R.; Kwong, B.; Katz, J.; Watson, N.; Irvine, D. J. Cytosolic Delivery of Membrane-Impermeable Molecules in Dendritic Cells Using pH-Responsive Core-Shell Nanoparticles. *Nano Letters*. 2007; 7(10):3056-3064.
188. Keller, S.; Wilson, J. T.; Patilea, G. I.; Kern, H. B.; Convertine, A. J.; Stayton, P. S. Neutral polymer micelle carriers with pH-responsive, endosome-releasing activity modulate antigen trafficking to enhance CD8(+) T cell responses. *J Control Release*. 2014; 191:24-33.
189. Pusic, K.; Aguilar, Z.; Mcloughlin, J.; Kobuch, S.; Xu, H.; Tsang, M.; Wang, A.; Hui, G. Iron oxide nanoparticles as a clinically acceptable delivery platform for a recombinant blood-stage human malaria vaccine. *Faseb j*. 2013; 27(3):1153-66.
190. Afroz, S.; Medhi, H.; Maity, S.; Minhas, G.; Battu, S.; Giddaluru, J.; Kumar, K.; Paik, P.; Khan, N. Mesoporous ZnO nanocapsules for the induction of enhanced antigen-specific immunological responses. *Nanoscale*. 2017; 9(38):14641-14653.
191. Ilyinskii, P. O.; Roy, C. J.; O'neil, C. P.; Browning, E. A.; Pittet, L. A.; Altreuter, D. H.; Alexis, F.; Tonti, E.; Shi, J.; Basto, P. A.; Iannacone, M.; Radovic-Moreno, A. F.; Langer, R. S.; Farokhzad, O. C.; Von Andrian, U. H.; Johnston, L. P. M.; Kishimoto, T. K. Adjuvant-carrying synthetic vaccine particles augment the immune response to encapsulated antigen and exhibit strong local immune activation without inducing systemic cytokine release. *Vaccine*. 2014; 32(24):2882-2895.
192. Ebrahimian, M.; Hashemi, M.; Maleki, M.; Hashemitabar, G.; Abnous, K.; Ramezani, M.; Haghparast, A. Co-delivery of Dual Toll-Like Receptor Agonists

## REFERENCES

- and Antigen in Poly(Lactic-Co-Glycolic) Acid/Polyethylenimine Cationic Hybrid Nanoparticles Promote Efficient In Vivo Immune Responses. *Frontiers in Immunology*. 2017; 8:1077.
193. Widmer, J.; Thauvin, C.; Mottas, I.; Nguyen, V. N.; Delie, F.; Allémann, E.; Bourquin, C. Polymer-based nanoparticles loaded with a TLR7 ligand to target the lymph node for immunostimulation. *International Journal of Pharmaceutics*. 2018; 535(1):444-451.
  194. Sorensen, N. S.; Boas, U.; Heegaard, P. M. H. Enhancement of Muramyl dipeptide (MDP) Immunostimulatory Activity by Controlled Multimerization on Dendrimers. *Macromolecular Bioscience*. 2011; 11(11):1484-1490.
  195. Poecheim, J.; Barnier-Quer, C.; Collin, N.; Borchard, G. Ag85A DNA Vaccine Delivery by Nanoparticles: Influence of the Formulation Characteristics on Immune Responses. *Vaccines*. 2016; 4(3):32.
  196. Wang, J. E.; Jorgensen, P. F.; Ellingsen, E. A.; Almióf, M.; Thiemermann, C.; Foster, S. J.; Aasen, A. O.; Solberg, R. Peptidoglycan primes for LPS-induced release of proinflammatory cytokines in whole human blood. *Shock*. 2001; 16(3):178-82.
  197. Saba, T. M. Physiology and physiopathology of the reticuloendothelial system. *Arch Intern Med*. 1970; 126(6):1031-52.
  198. Alexis, F.; Pridgen, E.; Molnar, L. K.; Farokhzad, O. C. Factors affecting the clearance and biodistribution of polymeric nanoparticles. *Mol Pharm*. 2008; 5(4):505-15.
  199. Van Vlerken, L. E.; Vyas, T. K.; Amiji, M. M. Poly(ethylene glycol)-modified nanocarriers for tumor-targeted and intracellular delivery. *Pharm Res*. 2007; 24(8):1405-14.
  200. Zopes, D.; Stein, B.; Mathur, S.; Graf, C. Improved Stability of “Naked” Gold Nanoparticles Enabled by in Situ Coating with Mono and Multivalent Thiol PEG Ligands. *Langmuir*. 2013; 29(36):11217-11226.
  201. Gref, R.; Minamitake, Y.; Peracchia, M. T.; Trubetskoy, V.; Torchilin, V.; Langer, R. Biodegradable long-circulating polymeric nanospheres. *Science*. 1994; 263(5153):1600-3.
  202. Knop, K.; Hoogenboom, R.; Fischer, D.; Schubert, U. S. Poly(ethylene glycol) in drug delivery: pros and cons as well as potential alternatives. *Angew Chem Int Ed Engl*. 2010; 49(36):6288-308.
  203. Qi, Y.; Chilkoti, A. Protein-Polymer Conjugation—Moving Beyond PEGylation. *Current Opinion in Chemical Biology*. 2015; 28:181-193.

## REFERENCES

204. Zahr, A. S.; Davis, C. A.; Pishko, M. V. Macrophage uptake of core-shell nanoparticles surface modified with poly(ethylene glycol). *Langmuir*. 2006; 22(19):8178-85.
205. Kanaras, A. G.; Kamounah, F. S.; Schaumburg, K.; Kiely, C. J.; Brust, M. Thioalkylated tetraethylene glycol: a new ligand for water soluble monolayer protected gold clusters. *Chem Commun (Camb)*. 2002; (20):2294-5.
206. Kwon, G. S. Polymeric micelles for delivery of poorly water-soluble compounds. *Crit Rev Ther Drug Carrier Syst*. 2003; 20(5):357-403.
207. Bao, W.; Liu, R.; Wang, Y.; Wang, F.; Xia, G.; Zhang, H.; Li, X.; Yin, H.; Chen, B. PLGA-PLL-PEG-Tf-based targeted nanoparticles drug delivery system enhance antitumor efficacy via intrinsic apoptosis pathway. *Int J Nanomedicine*. 2015; 10:557-566.
208. Zhang, F.; Zhang, S.; Pollack, S. F.; Li, R.; Gonzalez, A. M.; Fan, J.; Zou, J.; Leininger, S. E.; Pavia-Sanders, A.; Johnson, R.; Nelson, L. D.; Raymond, J. E.; Elsabahy, M.; Hughes, D. M. P.; Lenox, M. W.; Gustafson, T. P.; Wooley, K. L. Improving Paclitaxel Delivery: In Vitro and In Vivo Characterization of PEGylated Polyphosphoester-Based Nanocarriers. *Journal of the American Chemical Society*. 2015; 137(5):2056-2066.
209. Cruz, L. J.; Tacke, P. J.; Fokkink, R.; Figdor, C. G. The influence of PEG chain length and targeting moiety on antibody-mediated delivery of nanoparticle vaccines to human dendritic cells. *Biomaterials*. 2011; 32(28):6791-803.
210. Vila, A.; Sanchez, A.; Evora, C.; Soriano, I.; Vila Jato, J. L.; Alonso, M. J. PEG-PLA nanoparticles as carriers for nasal vaccine delivery. *J Aerosol Med*. 2004; 17(2):174-85.
211. Carrillo-Conde, B.; Song, E.-H.; Chavez-Santoscoy, A.; Phanse, Y.; Ramer-Tait, A. E.; Pohl, N. L. B.; Wannemuehler, M. J.; Bellaire, B. H.; Narasimhan, B. Mannose-Functionalized "Pathogen-like" Polyanhydride Nanoparticles Target C-Type Lectin Receptors on Dendritic Cells. *Molecular Pharmaceutics*. 2011; 8(5):1877-1886.
212. Molino, N. M.; Neek, M.; Tucker, J. A.; Nelson, E. L.; Wang, S.-W. Display of DNA on Nanoparticles for Targeting Antigen Presenting Cells. *ACS biomaterials science & engineering*. 2017; 3(4):496-501.
213. Lahoud, M. H.; Ahmet, F.; Zhang, J. G.; Meuter, S.; Policheni, A. N.; Kitsoulis, S.; Lee, C. N.; O'keeffe, M.; Sullivan, L. C.; Brooks, A. G.; Berry, R.; Rossjohn, J.; Mintern, J. D.; Vega-Ramos, J.; Villadangos, J. A.; Nicola, N. A.; Nussenzweig, M. C.; Stacey, K. J.; Shortman, K.; Heath, W. R.; Caminschi, I. DEC-205 is a cell surface receptor for CpG oligonucleotides. *Proc Natl Acad Sci U S A*. 2012; 109(40):16270-5.



## REFERENCES

214. Saluja, S. S.; Hanlon, D. J.; Sharp, F. A.; Hong, E.; Khalil, D.; Robinson, E.; Tigelaar, R.; Fahmy, T. M.; Edelson, R. L. Targeting human dendritic cells via DEC-205 using PLGA nanoparticles leads to enhanced cross-presentation of a melanoma-associated antigen. *Int J Nanomedicine*. 2014; 9:5231-5246.
215. Cruz, L. J.; Rosalia, R. A.; Kleinovink, J. W.; Rueda, F.; Lowik, C. W.; Ossendorp, F. Targeting nanoparticles to CD40, DEC-205 or CD11c molecules on dendritic cells for efficient CD8(+) T cell response: a comparative study. *J Control Release*. 2014; 192:209-18.
216. Cruz, L. J.; Tacke, P. J.; Fokkink, R.; Joosten, B.; Stuart, M. C.; Albericio, F.; Torensma, R.; Figdor, C. G. Targeted PLGA nano- but not microparticles specifically deliver antigen to human dendritic cells via DC-SIGN in vitro. *Journal of Controlled Release*. 2010; 144(2):118-126.
217. Macri, C.; Dumont, C.; Johnston, A. P. R.; Mintern, J. D. Targeting dendritic cells: a promising strategy to improve vaccine effectiveness. *Clinical & Translational Immunology*. 2016; 5(3):e66.
218. Luo, Z.; Wang, C.; Yi, H.; Li, P.; Pan, H.; Liu, L.; Cai, L.; Ma, Y. Nanovaccine loaded with poly I:C and STAT3 siRNA robustly elicits anti-tumor immune responses through modulating tumor-associated dendritic cells in vivo. *Biomaterials*. 2015; 38:50-60.
219. Hoffman, A. S. Stimuli-responsive polymers: biomedical applications and challenges for clinical translation. *Adv Drug Deliv Rev*. 2013; 65(1):10-6.
220. Couvreur, P. Nanoparticles in drug delivery: past, present and future. *Adv Drug Deliv Rev*. 2013; 65(1):21-3.
221. Elzoghby, A. O.; Samy, W. M.; Elgindy, N. A. Protein-based nanocarriers as promising drug and gene delivery systems. *J Control Release*. 2012; 161(1):38-49.
222. Ge, J.; Neofytou, E.; Lei, J.; Beygui, R. E.; Zare, R. N. Protein-polymer hybrid nanoparticles for drug delivery. *Small*. 2012; 8(23):3573-8.
223. Yoo, J. W.; Irvine, D. J.; Discher, D. E.; Mitragotri, S. Bio-inspired, bioengineered and biomimetic drug delivery carriers. *Nat Rev Drug Discov*. 2011; 10(7):521-35.
224. Goszczynski, T. M.; Filip-Psurska, B.; Kempinska, K.; Wietrzyk, J.; Boratynski, J. Hydroxyethyl starch as an effective methotrexate carrier in anticancer therapy. *Pharmacol Res Perspect*. 2014; 2(3):e00047.
225. Shen, L.; Higuchi, T.; Tubbe, I.; Voltz, N.; Krummen, M.; Pektor, S.; Montermann, E.; Rausch, K.; Schmidt, M.; Schild, H.; Grabbe, S.; Bros, M. A trifunctional dextran-based nanovaccine targets and activates murine dendritic cells, and induces

## REFERENCES

- potent cellular and humoral immune responses in vivo. *PLoS One*. 2013; 8(12):e80904.
226. Fleige, E.; Quadir, M. A.; Haag, R. Stimuli-responsive polymeric nanocarriers for the controlled transport of active compounds: concepts and applications. *Adv Drug Deliv Rev*. 2012; 64(9):866-84.
227. Mura, S.; Nicolas, J.; Couvreur, P. Stimuli-responsive nanocarriers for drug delivery. *Nat Mater*. 2013; 12(11):991-1003.
228. Nicolas, J.; Mura, S.; Brambilla, D.; Mackiewicz, N.; Couvreur, P. Design, functionalization strategies and biomedical applications of targeted biodegradable/biocompatible polymer-based nanocarriers for drug delivery. *Chem Soc Rev*. 2013; 42(3):1147-235.
229. Pan, Y. J.; Chen, Y. Y.; Wang, D. R.; Wei, C.; Guo, J.; Lu, D. R.; Chu, C. C.; Wang, C. C. Redox/pH dual stimuli-responsive biodegradable nanohydrogels with varying responses to dithiothreitol and glutathione for controlled drug release. *Biomaterials*. 2012; 33(27):6570-9.
230. Zhang, Z. Y.; Xu, Y. D.; Ma, Y. Y.; Qiu, L. L.; Wang, Y.; Kong, J. L.; Xiong, H. M. Biodegradable ZnO@polymer core-shell nanocarriers: pH-triggered release of doxorubicin in vitro. *Angew Chem Int Ed Engl*. 2013; 52(15):4127-31.
231. Piradashvili, K.; Alexandrino, E. M.; Wurm, F. R.; Landfester, K. Reactions and Polymerizations at the Liquid-Liquid Interface. *Chem Rev*. 2016; 116(4):2141-69.
232. Suketaka, I.; Yumo, T.; Akikazu, K.; Ken-Ichi, K. A Facile Synthesis of 2,5-Disubstituted Tetrazoles by the Reaction of Phenylsulfonylhydrazones with Arenediazonium Salts. *Bulletin of the Chemical Society of Japan*. 1976; 49(7):1920-1923.
233. Fan, Y.; Deng, C.; Cheng, R.; Meng, F.; Zhong, Z. In situ forming hydrogels via catalyst-free and bioorthogonal "tetrazole-alkene" photo-click chemistry. *Biomacromolecules*. 2013; 14(8):2814-21.
234. Schlaad, H.; Kukula, H.; Rudloff, J.; Below, I. Synthesis of  $\alpha,\omega$ -Heterobifunctional Poly(ethylene glycol)s by Metal-Free Anionic Ring-Opening Polymerization. *Macromolecules*. 2001; 34(13):4302-4304.
235. Zal, T.; Volkmann, A.; Stockinger, B. Mechanisms of tolerance induction in major histocompatibility complex class II-restricted T cells specific for a blood-borne self-antigen. *J Exp Med*. 1994; 180(6):2089-99.
236. Cohen, J. L.; Schubert, S.; Wich, P. R.; Cui, L.; Cohen, J. A.; Mynar, J. L.; Frechet, J. M. Acid-degradable cationic dextran particles for the delivery of siRNA therapeutics. *Bioconjug Chem*. 2011; 22(6):1056-65.

## REFERENCES

237. Piradashvili, K.; Fichter, M.; Mohr, K.; Gehring, S.; Wurm, F. R.; Landfester, K. Biodegradable protein nanocontainers. *Biomacromolecules*. 2015; 16(3):815-21.
238. Piradashvili, K.; Simon, J.; Paßlick, D.; Hohner, J. R.; Mailander, V.; Wurm, F. R.; Landfester, K. Fully degradable protein nanocarriers by orthogonal photoclick tetrazole-ene chemistry for the encapsulation and release. *Nanoscale Horizons*. 2017; 2(5):297-302.
239. Kang, B. Carbohydrate nanocarriers in biomedical applications: Construction and surface modification [Doctoral thesis]. Mainz: Johannes Gutenberg University; 2015.
240. Didierlaurent, A. M.; Collignon, C.; Bourguignon, P.; Wouters, S.; Fierens, K.; Fochesato, M.; Dendouga, N.; Langlet, C.; Malissen, B.; Lambrecht, B. N.; Garçon, N.; Van Mechelen, M.; Morel, S. Enhancement of adaptive immunity by the human vaccine adjuvant AS01 depends on activated dendritic cells. *J Immunol*. 2014; 193(4):1920-30.
241. Bros, M.; Montermann, E.; Cholaszczynska, A.; Reske-Kunz, A. B. The phosphodiesterase 4 inhibitor roflumilast augments the Th17-promoting capability of dendritic cells by enhancing IL-23 production, and impairs their T cell stimulatory activity due to elevated IL-10. *Int Immunopharmacol*. 2016; 35:174-184.
242. Graham, F. L.; Smiley, J.; Russell, W. C.; Nairn, R. Characteristics of a human cell line transformed by DNA from human adenovirus type 5. *J Gen Virol*. 1977; 36(1):59-74.
243. He, T.; Tang, C.; Xu, S.; Moyana, T.; Xiang, J. Interferon gamma stimulates cellular maturation of dendritic cell line DC2.4 leading to induction of efficient cytotoxic T cell responses and antitumor immunity. *Cell Mol Immunol*. 2007; 4(2):105-11.
244. Besche, V.; Wiechmann, N.; Castor, T.; Trojandt, S.; Hohn, Y.; Kunkel, H.; Grez, M.; Grabbe, S.; Reske-Kunz, A. B.; Bros, M. Dendritic cells lentivirally engineered to overexpress interleukin-10 inhibit contact hypersensitivity responses, despite their partial activation induced by transduction-associated physical stress. *J Gene Med*. 2010; 12(3):231-43.
245. Steinman, R. M.; Mellman, I. S.; Muller, W. A.; Cohn, Z. A. Endocytosis and the recycling of plasma membrane. *J Cell Biol*. 1983; 96(1):1-27.
246. FDA. Guidance for Industry: Pyrogen and Endotoxins Testing. *U.S. Department of Health and Human Services*. 2012.
247. Wang, Z.; Gerstein, M.; Snyder, M. RNA-Seq: a revolutionary tool for transcriptomics. *Nature Reviews Genetics*. 2009; 10:57.

## REFERENCES

248. Livak, K. J.; Schmittgen, T. D. Analysis of relative gene expression data using real-time quantitative PCR and the 2(-Delta Delta C(T)) Method. *Methods*. 2001; 25(4):402-8.
249. Paßlick, D.; Piradashvili, K.; Bamberger, D.; Li, M.; Jiang, S.; Strand, D.; P, R. W.; Landfester, K.; Bros, M.; Grabbe, S.; Mailander, V. Delivering all in one: Antigen-nanocapsule loaded with dual adjuvant yields superadditive effects by DC-directed T cell stimulation. *J Control Release*. 2018; 289:23-34.
250. Tacke, P. J.; De Vries, I. J.; Torensma, R.; Figdor, C. G. Dendritic-cell immunotherapy: from ex vivo loading to in vivo targeting. *Nat Rev Immunol*. 2007; 7(10):790-802.
251. Steichen, S. D.; Caldorera-Moore, M.; Peppas, N. A. A review of current nanoparticle and targeting moieties for the delivery of cancer therapeutics. *European journal of pharmaceutical sciences : official journal of the European Federation for Pharmaceutical Sciences*. 2013; 48(3):416-427.
252. Whitmore, M. M.; Devere, M. J.; Edling, A.; Oates, R. K.; Simons, B.; Lindner, D.; Williams, B. R. Synergistic activation of innate immunity by double-stranded RNA and CpG DNA promotes enhanced antitumor activity. *Cancer Res*. 2004; 64(16):5850-60.
253. Roelofs, M. F.; Joosten, L. A.; Abdollahi-Roodsaz, S.; Van Lieshout, A. W.; Sprong, T.; Van Den Hoogen, F. H.; Van Den Berg, W. B.; Radstake, T. R. The expression of toll-like receptors 3 and 7 in rheumatoid arthritis synovium is increased and costimulation of toll-like receptors 3, 4, and 7/8 results in synergistic cytokine production by dendritic cells. *Arthritis Rheum*. 2005; 52(8):2313-22.
254. Krummen, M.; Balkow, S.; Shen, L.; Heinz, S.; Loquai, C.; Probst, H. C.; Grabbe, S. Release of IL-12 by dendritic cells activated by TLR ligation is dependent on MyD88 signaling, whereas TRIF signaling is indispensable for TLR synergy. *J Leukoc Biol*. 2010; 88(1):189-99.
255. Theiner, G.; Rossner, S.; Dalpke, A.; Bode, K.; Berger, T.; Gessner, A.; Lutz, M. B. TLR9 cooperates with TLR4 to increase IL-12 release by murine dendritic cells. *Mol Immunol*. 2008; 45(1):244-52.
256. Surendran, N.; Simmons, A.; Pichichero, M. E. TLR agonist combinations that stimulate Th type I polarizing responses from human neonates. *Innate Immun*. 2018; 24(4):240-251.
257. Fritz, J. H.; Girardin, S. E.; Fitting, C.; Werts, C.; Mengin-Lecreulx, D.; Caroff, M.; Cavaillon, J. M.; Philpott, D. J.; Adib-Conquy, M. Synergistic stimulation of human monocytes and dendritic cells by Toll-like receptor 4 and NOD1- and NOD2-activating agonists. *Eur J Immunol*. 2005; 35(8):2459-70.

## REFERENCES

258. Uehara, A.; Yang, S.; Fujimoto, Y.; Fukase, K.; Kusumoto, S.; Shibata, K.; Sugawara, S.; Takada, H. Muramyl dipeptide and diaminopimelic acid-containing desmuramylpeptides in combination with chemically synthesized Toll-like receptor agonists synergistically induced production of interleukin-8 in a NOD2- and NOD1-dependent manner, respectively, in human monocytic cells in culture. *Cell Microbiol.* 2005; 7(1):53-61.
259. Tikhvatulin, A. I.; Dzharullaeva, A. S.; Tikhvatulina, N. M.; Shcheblyakov, D. V.; Shmarov, M. M.; Dolzhikova, I. V.; Stanhope-Baker, P.; Naroditsky, B. S.; Gudkov, A. V.; Logunov, D. Y.; Gintsburg, A. L. Powerful Complex Immunoadjuvant Based on Synergistic Effect of Combined TLR4 and NOD2 Activation Significantly Enhances Magnitude of Humoral and Cellular Adaptive Immune Responses. *PLoS One.* 2016; 11(5):e0155650.
260. Ni, K.; O'Neill, H. C. The role of dendritic cells in T cell activation. *Immunology And Cell Biology.* 1997; 75:223.
261. Del Giudice, G.; Podda, A.; Rappuoli, R. What are the limits of adjuvanticity? *Vaccine.* 2001; 20:S38-S41.
262. Graham, B. S.; Keefer, M. C.; Mcelrath, M.; Et Al. Safety and immunogenicity of a candidate hiv-1 vaccine in healthy adults: Recombinant glycoprotein (rgp) 120: a randomized, double-blind trial. *Annals of Internal Medicine.* 1996; 125(4):270-279.
263. Verschoor, E. J.; Mooij, P.; Oostermeijer, H.; Van Der Kolk, M.; Ten Haaf, P.; Verstrepen, B.; Sun, Y.; Morein, B.; Åkerblom, L.; Fuller, D. H.; Barnett, S. W.; Heeney, J. L. Comparison of Immunity Generated by Nucleic Acid-, MF59-, and ISCOM-Formulated Human Immunodeficiency Virus Type 1 Vaccines in Rhesus Macaques: Evidence for Viral Clearance. *Journal of Virology.* 1999; 73(4):3292-3300.
264. Geddes, K.; Magalhaes, J. G.; Girardin, S. E. Unleashing the therapeutic potential of NOD-like receptors. *Nat Rev Drug Discov.* 2009; 8(6):465-79.
265. Shaw, P. J.; Lamkanfi, M.; Kanneganti, T. D. NOD-like receptor (NLR) signaling beyond the inflammasome. *Eur J Immunol.* 2010; 40(3):624-7.
266. Maisonneuve, C.; Bertholet, S.; Philpott, D. J.; De Gregorio, E. Unleashing the potential of NOD- and Toll-like agonists as vaccine adjuvants. *Proceedings of the National Academy of Sciences.* 2014; 111(34):12294-12299.
267. Timmermans, K.; Plantinga, T. S.; Kox, M.; Vaneker, M.; Scheffer, G. J.; Adema, G. J.; Joosten, L. A.; Netea, M. G. Blueprints of signaling interactions between pattern recognition receptors: implications for the design of vaccine adjuvants. *Clin Vaccine Immunol.* 2013; 20(3):427-32.

## REFERENCES

268. Knotigova, P.; Zyka, D.; Mašek, J.; Kovalová, A.; Krupka, M.; Bartheldyová, E.; Kulich, P.; Koudelka, Š.; Lukáč, R.; Kauerová, Z.; Vacek, A.; Stuchlova Horynova, M.; Kozubík, A.; Miller, A.; Fekete, L.; Kratochvilová, I.; Ježek, J.; Ledvina, M.; Raska, M.; Turanek, J. Molecular Adjuvants Based on Nonpyrogenic Lipophilic Derivatives of norAbuMDP/GMDP Formulated in Nanoliposomes: Stimulation of Innate and Adaptive Immunity 2015.
269. Ishida, H.; Saiki, I.; Saito, S.; Hasegawa, A.; Kiso, M.; Azuma, I. Regression of line-10 hepatocellular carcinoma by a less toxic cord factor analogue combined with L18-MDP or synthetic lipid A analogues. *Vaccine*. 1988; 6(5):440-4.
270. Ishihara, C.; Hamada, N.; Yamamoto, K.; Iida, J.; Azuma, I.; Yamamura, Y. Effect of muramyl dipeptide and its stearyl derivatives on resistance to Sendai virus infection in mice. *Vaccine*. 1985; 3(5):370-4.
271. Osada, Y.; Mitsuyama, M.; Une, T.; Matsumoto, K.; Otani, T.; Satoh, M.; Ogawa, H.; Nomoto, K. Effect of L18-MDP(Ala), a synthetic derivative of muramyl dipeptide, on nonspecific resistance of mice to microbial infections. *Infect Immun*. 1982; 37(1):292-300.
272. Sato, T.; Shikama, Y.; Shimauchi, H.; Endo, Y.; Takada, H. Analgesic effects of chemically synthesized NOD1 and NOD2 agonists in mice. *Innate Immun*. 2011; 17(1):54-9.
273. Sosnowska, D.; Mysliwski, A.; Dzierzbicka, K.; Kolodziejczyk, A. M. The in vitro effect of new muramyl peptide derivatives on cytotoxic activity of NK (natural killer) cells from hamsters bearing Ab Bomirski melanoma. *Biotherapy*. 1997; 10(2):161-8.
274. Israely, T.; Melamed, S.; Achdout, H.; Erez, N.; Politi, B.; Waner, T.; Lustig, S.; Paran, N. TLR3 and TLR9 agonists improve postexposure vaccination efficacy of live smallpox vaccines. *PLoS One*. 2014; 9(10):e110545.
275. Maurer, T.; Pournaras, C.; Aguilar-Pimentel, J. A.; Thalgott, M.; Horn, T.; Heck, M.; Heit, A.; Kuebler, H.; Gschwend, J. E.; Nawroth, R. Immunostimulatory CpG-DNA and PSA-peptide vaccination elicits profound cytotoxic T cell responses. *Urol Oncol*. 2013; 31(7):1395-401.
276. Jones, G. J.; Steinbach, S.; Clifford, D.; Baldwin, S. L.; Ireton, G. C.; Coler, R. N.; Reed, S. G.; Vordermeier, H. M. Immunisation with ID83 fusion protein induces antigen-specific cell mediated and humoral immune responses in cattle. *Vaccine*. 2013; 31(45):5250-5.
277. Duthie, M. S.; Windish, H. P.; Fox, C. B.; Reed, S. G. Use of defined TLR ligands as adjuvants within human vaccines. *Immunol Rev*. 2011; 239(1):178-96.

## REFERENCES

278. Dagenais, M.; Dupaul-Chicoine, J.; Saleh, M. Function of NOD-like receptors in immunity and disease. *Curr Opin Investig Drugs*. 2010; 11(11):1246-55.
279. Kawai, T.; Akira, S. Toll-like receptor and RIG-I-like receptor signaling. *Ann N Y Acad Sci*. 2008; 1143:1-20.
280. Green, J. M.; Noel, P. J.; Sperling, A. I.; Walunas, T. L.; Gray, G. S.; Bluestone, J. A.; Thompson, C. B. Absence of B7-dependent responses in CD28-deficient mice. *Immunity*. 1994; 1(6):501-8.
281. Sperling, A. I.; Auger, J. A.; Ehst, B. D.; Rulifson, I. C.; Thompson, C. B.; Bluestone, J. A. CD28/B7 interactions deliver a unique signal to naive T cells that regulates cell survival but not early proliferation. *J Immunol*. 1996; 157(9):3909-17.
282. Athie-Morales, V.; Smits, H. H.; Cantrell, D. A.; Hilkens, C. M. U. Sustained IL-12 Signaling Is Required for Th1 Development. *The Journal of Immunology*. 2004; 172(1):61-69.
283. Diehl, S.; Rincon, M. The two faces of IL-6 on Th1/Th2 differentiation. *Mol Immunol*. 2002; 39(9):531-6.
284. Van Heel, D. A.; Ghosh, S.; Butler, M.; Hunt, K. A.; Lundberg, A. M.; Ahmad, T.; McGovern, D. P.; Onnie, C.; Negoro, K.; Goldthorpe, S.; Foxwell, B. M.; Mathew, C. G.; Forbes, A.; Jewell, D. P.; Playford, R. J. Muramyl dipeptide and toll-like receptor sensitivity in NOD2-associated Crohn's disease. *Lancet*. 2005; 365(9473):1794-6.
285. Schwarz, H.; Posselt, G.; Wurm, P.; Ulbing, M.; Duschl, A.; Horejs-Hoeck, J. TLR8 and NOD signaling synergistically induce the production of IL-1beta and IL-23 in monocyte-derived DCs and enhance the expression of the feedback inhibitor SOCS2. *Immunobiology*. 2013; 218(4):533-42.
286. Tada, H.; Aiba, S.; Shibata, K.; Ohteki, T.; Takada, H. Synergistic effect of Nod1 and Nod2 agonists with toll-like receptor agonists on human dendritic cells to generate interleukin-12 and T helper type 1 cells. *Infect Immun*. 2005; 73(12):7967-76.
287. Shafique, M.; Wilschut, J.; De Haan, A. Induction of mucosal and systemic immunity against respiratory syncytial virus by inactivated virus supplemented with TLR9 and NOD2 ligands. *Vaccine*. 2012; 30(3):597-606.
288. Moore, K. W.; De Waal Malefyt, R.; Coffman, R. L.; O'garra, A. Interleukin-10 and the interleukin-10 receptor. *Annu Rev Immunol*. 2001; 19:683-765.
289. Demangel, C.; Bertolino, P.; Britton, W. J. Autocrine IL-10 impairs dendritic cell (DC)-derived immune responses to mycobacterial infection by suppressing DC

## REFERENCES

- trafficking to draining lymph nodes and local IL-12 production. *Eur J Immunol.* 2002; 32(4):994-1002.
290. Fukao, T.; Frucht, D. M.; Yap, G.; Gadina, M.; O'shea, J. J.; Koyasu, S. Inducible expression of Stat4 in dendritic cells and macrophages and its critical role in innate and adaptive immune responses. *J Immunol.* 2001; 166(7):4446-55.
291. Corinti, S.; Albanesi, C.; La Sala, A.; Pastore, S.; Girolomoni, G. Regulatory activity of autocrine IL-10 on dendritic cell functions. *J Immunol.* 2001; 166(7):4312-8.
292. De Smedt, T.; Van Mechelen, M.; De Becker, G.; Urbain, J.; Leo, O.; Moser, M. Effect of interleukin-10 on dendritic cell maturation and function. *Eur J Immunol.* 1997; 27(5):1229-35.
293. Bachelder, E. M.; Beaudette, T. T.; Broaders, K. E.; Frechet, J. M.; Albrecht, M. T.; Mateczun, A. J.; Ainslie, K. M.; Pesce, J. T.; Keane-Myers, A. M. In vitro analysis of acetalated dextran microparticles as a potent delivery platform for vaccine adjuvants. *Mol Pharm.* 2010; 7(3):826-35.
294. Almeida, J. P. M.; Lin, A. Y.; Figueroa, E. R.; Foster, A. E.; Drezek, R. A. In vivo gold nanoparticle delivery of peptide vaccine induces anti-tumor immune response in prophylactic and therapeutic tumor models. *Small.* 2015; 11(12):1453-1459.
295. Singh, S. M.; Alkie, T. N.; Nagy, E.; Kulkarni, R. R.; Hodgins, D. C.; Sharif, S. Delivery of an inactivated avian influenza virus vaccine adjuvanted with poly(D,L-lactic-co-glycolic acid) encapsulated CpG ODN induces protective immune responses in chickens. *Vaccine.* 2016; 34(40):4807-13.
296. Silva, J. M.; Zupancic, E.; Vandermeulen, G.; Oliveira, V. G.; Salgado, A.; Videira, M.; Gaspar, M.; Graca, L.; Preat, V.; Florindo, H. F. In vivo delivery of peptides and Toll-like receptor ligands by mannose-functionalized polymeric nanoparticles induces prophylactic and therapeutic anti-tumor immune responses in a melanoma model. *J Control Release.* 2015; 198:91-103.
297. Goldinger, S. M.; Dummer, R.; Baumgaertner, P.; Mihic-Probst, D.; Schwarz, K.; Hammann-Haenni, A.; Willers, J.; Geldhof, C.; Prior, J. O.; Kundig, T. M.; Michielin, O.; Bachmann, M. F.; Speiser, D. E. Nano-particle vaccination combined with TLR-7 and -9 ligands triggers memory and effector CD8(+) T-cell responses in melanoma patients. *Eur J Immunol.* 2012; 42(11):3049-61.
298. Ornelas-Megiatto, C.; Shah, P. N.; Wich, P. R.; Cohen, J. L.; Tagaev, J. A.; Smolen, J. A.; Wright, B. D.; Panzner, M. J.; Youngs, W. J.; Frechet, J. M.; Cannon, C. L. Aerosolized antimicrobial agents based on degradable dextran nanoparticles loaded with silver carbene complexes. *Mol Pharm.* 2012; 9(11):3012-22.



## REFERENCES

299. Broaders, K. E.; Cohen, J. A.; Beaudette, T. T.; Bachelder, E. M.; Fréchet, J. M. J. Acetalated dextran is a chemically and biologically tunable material for particulate immunotherapy. *Proceedings of the National Academy of Sciences*. 2009; 106(14):5497-5502.
300. Foerster, F.; Bamberger, D.; Schupp, J.; Weilbacher, M.; Kaps, L.; Strobl, S.; Radi, L.; Diken, M.; Strand, D.; Tuettenberg, A.; Wich, P. R.; Schuppan, D. Dextran-based therapeutic nanoparticles for hepatic drug delivery. *Nanomedicine (Lond)*. 2016; 11(20):2663-2677.
301. Marina-Garcia, N.; Franchi, L.; Kim, Y. G.; Hu, Y.; Smith, D. E.; Boons, G. J.; Nunez, G. Clathrin- and dynamin-dependent endocytic pathway regulates muramyl dipeptide internalization and NOD2 activation. *J Immunol*. 2009; 182(7):4321-7.
302. Parant, M. A.; Audibert, F. M.; Chedid, L. A.; Level, M. R.; Lefrancier, P. L.; Choay, J. P.; Lederer, E. Immunostimulant activities of a lipophilic muramyl dipeptide derivative and of desmuramyl peptidolipid analogs. *Infect Immun*. 1980; 27(3):826-31.
303. Akinc, A.; Battaglia, G. Exploiting endocytosis for nanomedicines. *Cold Spring Harb Perspect Biol*. 2013; 5(11):a016980.
304. El-Sayed, A.; Harashima, H. Endocytosis of gene delivery vectors: from clathrin-dependent to lipid raft-mediated endocytosis. *Mol Ther*. 2013; 21(6):1118-30.
305. Sahay, G.; Alakhova, D. Y.; Kabanov, A. V. Endocytosis of nanomedicines. *J Control Release*. 2010; 145(3):182-95.
306. Yameen, B.; Choi, W. I.; Vilos, C.; Swami, A.; Shi, J.; Farokhzad, O. C. Insight into nanoparticle cellular uptake and intracellular targeting. *J Control Release*. 2014; 190:485-99.
307. Kirchhausen, T. Clathrin. *Annual Review of Biochemistry*. 2000; 69(1):699-727.
308. Sandvig, K.; Torgersen, M. L.; Raa, H. A.; Van Deurs, B. Clathrin-independent endocytosis: from nonexisting to an extreme degree of complexity. *Histochemistry and Cell Biology*. 2008; 129(3):267-276.
309. Falcone, S.; Cocucci, E.; Podini, P.; Kirchhausen, T.; Clementi, E.; Meldolesi, J. Macropinocytosis: regulated coordination of endocytic and exocytic membrane traffic events. *J Cell Sci*. 2006; 119(22):4758-4769.
310. Gratton, S. E. A.; Ropp, P. A.; Pohlhaus, P. D.; Luft, J. C.; Madden, V. J.; Napier, M. E.; Desimone, J. M. The effect of particle design on cellular internalization pathways. *Proceedings of the National Academy of Sciences*. 2008; 105(33):11613-11618.

## REFERENCES

311. Zhang, L.; Zhang, S.; Ruan, S.-B.; Zhang, Q.-Y.; He, Q.; Gao, H.-L. Lapatinib-incorporated lipoprotein-like nanoparticles: preparation and a proposed breast cancer-targeting mechanism. *Acta Pharmacologica Sinica*. 2014; 35:846.
312. Langston Suen, W. L.; Chau, Y. Size-dependent internalisation of folate-decorated nanoparticles via the pathways of clathrin and caveolae-mediated endocytosis in ARPE-19 cells. *J Pharm Pharmacol*. 2014; 66(4):564-73.
313. Zhang, S.; Li, J.; Lykotrafitis, G.; Bao, G.; Suresh, S. Size-Dependent Endocytosis of Nanoparticles. *Adv Mater*. 2009; 21:419-424.
314. Florez, L.; Herrmann, C.; Cramer, J. M.; Hauser, C. P.; Koynov, K.; Landfester, K.; Crespy, D.; Mailander, V. How shape influences uptake: interactions of anisotropic polymer nanoparticles and human mesenchymal stem cells. *Small*. 2012; 8(14):2222-30.
315. Shen, H.; Tesar, B. M.; Walker, W. E.; Goldstein, D. R. Dual Signaling of MyD88 and TRIF are Critical for Maximal TLR4-Induced Dendritic Cell Maturation. *Journal of immunology (Baltimore, Md : 1950)*. 2008; 181(3):1849-1858.
316. Lim, T. S.; Goh, J. K.; Mortellaro, A.; Lim, C. T.; Hammerling, G. J.; Ricciardi-Castagnoli, P. CD80 and CD86 differentially regulate mechanical interactions of T-cells with antigen-presenting dendritic cells and B-cells. *PLoS One*. 2012; 7(9):e45185.
317. Thiel, M.; Wolfs, M. J.; Bauer, S.; Wenning, A. S.; Burckhart, T.; Schwarz, E. C.; Scott, A. M.; Renner, C.; Hoth, M. Efficiency of T-cell costimulation by CD80 and CD86 cross-linking correlates with calcium entry. *Immunology*. 2010; 129(1):28-40.
318. Bal, S. M.; Slutter, B.; Verheul, R.; Bouwstra, J. A.; Jiskoot, W. Adjuvanted, antigen loaded N-trimethyl chitosan nanoparticles for nasal and intradermal vaccination: adjuvant- and site-dependent immunogenicity in mice. *Eur J Pharm Sci*. 2012; 45(4):475-81.
319. Poecheim, J.; Heuking, S.; Brunner, L.; Barnier-Quer, C.; Collin, N.; Borchard, G. Nanocarriers for DNA Vaccines: Co-Delivery of TLR-9 and NLR-2 Ligands Leads to Synergistic Enhancement of Proinflammatory Cytokine Release. *Nanomaterials*. 2015; 5(4):2317-2334.
320. Pavot, V.; Rochereau, N.; Resseguier, J.; Gutjahr, A.; Genin, C.; Tiraby, G.; Perouzel, E.; Lioux, T.; Vernejoul, F.; Verrier, B.; Paul, S. Cutting edge: New chimeric NOD2/TLR2 adjuvant drastically increases vaccine immunogenicity. *J Immunol*. 2014; 193(12):5781-5.
321. Savina, A.; Amigorena, S. Phagocytosis and antigen presentation in dendritic cells. *Immunol Rev*. 2007; 219:143-56.

## REFERENCES

322. Pietrzak-Nguyen, A.; Piradashvili, K.; Fichter, M.; Pretsch, L.; Zepp, F.; Wurm, F. R.; Landfester, K.; Gehring, S. MPLA-coated hepatitis B virus surface antigen (HBsAg) nanocapsules induce vigorous T cell responses in cord blood derived human T cells. *Nanomedicine*. 2016; 12(8):2383-2394.
323. Fichter, M.; Piradashvili, K.; Pietrzak-Nguyen, A.; Pretsch, L.; Kuhn, G.; Strand, S.; Knuf, M.; Zepp, F.; Wurm, F. R.; Mailander, V.; Landfester, K.; Gehring, S. Polymeric hepatitis C virus non-structural protein 5A nanocapsules induce intrahepatic antigen-specific immune responses. *Biomaterials*. 2016; 108:1-12.
324. Trombetta, E. S.; Mellman, I. Cell biology of antigen processing in vitro and in vivo. *Annu Rev Immunol*. 2005; 23:975-1028.
325. Foged, C.; Brodin, B.; Frokjaer, S.; Sundblad, A. Particle size and surface charge affect particle uptake by human dendritic cells in an in vitro model. *International Journal of Pharmaceutics*. 2005; 298(2):315-322.
326. Swanson, J. A. Shaping cups into phagosomes and macropinosomes. *Nat Rev Mol Cell Biol*. 2008; 9(8):639-49.
327. Steinman, R. M.; Swanson, J. The endocytic activity of dendritic cells. *The Journal of Experimental Medicine*. 1995; 182(2):283-288.
328. Sallusto, F.; Cella, M.; Danieli, C.; Lanzavecchia, A. Dendritic cells use macropinocytosis and the mannose receptor to concentrate macromolecules in the major histocompatibility complex class II compartment: downregulation by cytokines and bacterial products. *The Journal of Experimental Medicine*. 1995; 182(2):389-400.
329. Pardoll, D. M.; Topalian, S. L. The role of CD4+ T cell responses in antitumor immunity. *Current Opinion in Immunology*. 1998; 10(5):588-594.
330. Golubovskaya, V.; Wu, L. Different Subsets of T Cells, Memory, Effector Functions, and CAR-T Immunotherapy. *Cancers (Basel)*. 2016; 8(3).
331. Bourgeois, C.; Tanchot, C. Mini-review CD4 T cells are required for CD8 T cell memory generation. *Eur J Immunol*. 2003; 33(12):3225-31.
332. Janssen, E. M.; Lemmens, E. E.; Wolfe, T.; Christen, U.; Von Herrath, M. G.; Schoenberger, S. P. CD4+ T cells are required for secondary expansion and memory in CD8+ T lymphocytes. *Nature*. 2003; 421:852.
333. Zhao, M.; Liu, Y.; Hsieh, R. S.; Wang, N.; Tai, W.; Joo, K.-I.; Wang, P.; Gu, Z.; Tang, Y. Clickable Protein Nanocapsules for Targeted Delivery of Recombinant p53 Protein. *Journal of the American Chemical Society*. 2014; 136(43):15319-15325.

## REFERENCES

334. Toita, R.; Murata, M.; Abe, K.; Narahara, S.; Piao, J. S.; Kang, J.-H.; Ohuchida, K.; Hashizume, M. Biological evaluation of protein nanocapsules containing doxorubicin. *Int J Nanomedicine*. 2013; 8:1989-1999.
335. Ren, D.; Kratz, F.; Wang, S. W. Protein nanocapsules containing doxorubicin as a pH-responsive delivery system. *Small*. 2011; 7(8):1051-60.
336. Schoenborn, J. R.; Wilson, C. B. Regulation of interferon-gamma during innate and adaptive immune responses. *Adv Immunol*. 2007; 96:41-101.
337. Bhat, P.; Leggatt, G.; Waterhouse, N.; Frazer, I. H. Interferon- $\gamma$  derived from cytotoxic lymphocytes directly enhances their motility and cytotoxicity. *Cell Death & Disease*. 2017; 8:e2836.
338. Gagliani, N.; Huber, S. Basic Aspects of T Helper Cell Differentiation. *Methods Mol Biol*. 2017; 1514:19-30.
339. Oriss, T. B.; Mccarthy, S. A.; Morel, B. F.; Campana, M. A.; Morel, P. A. Crossregulation between T helper cell (Th)1 and Th2: inhibition of Th2 proliferation by IFN-gamma involves interference with IL-1. *J Immunol*. 1997; 158(8):3666-72.
340. Dykman, L. A.; Staroverov, S. A.; Fomin, A. S.; Khanadeev, V. A.; Khlebtsov, B. N.; Bogatyrev, V. A. Gold nanoparticles as an adjuvant: Influence of size, shape, and technique of combination with CpG on antibody production. *Int Immunopharmacol*. 2018; 54:163-168.
341. Francica, J. R.; Lynn, G. M.; Laga, R.; Joyce, M. G.; Ruckwardt, T. J.; Morabito, K. M.; Chen, M.; Chaudhuri, R.; Zhang, B.; Sastry, M.; Druz, A.; Ko, K.; Choe, M.; Pechar, M.; Georgiev, I. S.; Kueltzo, L. A.; Seymour, L. W.; Mascola, J. R.; Kwong, P. D.; Graham, B. S.; Seder, R. A. Thermoresponsive Polymer Nanoparticles Co-deliver RSV F Trimers with a TLR-7/8 Adjuvant. *Bioconjug Chem*. 2016; 27(10):2372-2385.
342. Shen, L.; Krauthauser, S.; Fischer, K.; Hobernik, D.; Abassi, Y.; Dzionek, A.; Nikolaev, A.; Voltz, N.; Diken, M.; Krummen, M.; Montermann, E.; Tubbe, I.; Lorenz, S.; Strand, D.; Schild, H.; Grabbe, S.; Bros, M. Vaccination with trifunctional nanoparticles that address CD8(+) dendritic cells inhibits growth of established melanoma. *Nanomedicine (Lond)*. 2016; 11(20):2647-2662.
343. Shen, L.; Tenzer, S.; Storck, W.; Hobernik, D.; Raker, V. K.; Fischer, K.; Decker, S.; Dzionek, A.; Krauthauser, S.; Diken, M.; Nikolaev, A.; Maxeiner, J.; Schuster, P.; Kappel, C.; Verschoor, A.; Schild, H.; Grabbe, S.; Bros, M. Protein corona-mediated targeting of nanocarriers to B cells allows redirection of allergic immune responses. *J Allergy Clin Immunol*. 2018.

## REFERENCES

344. Wang, C.; Zhu, W.; Luo, Y.; Wang, B. Z. Gold nanoparticles conjugating recombinant influenza hemagglutinin trimers and flagellin enhanced mucosal cellular immunity. *Nanomedicine*. 2018; 14(4):1349-1360.
345. Liu, K. C.; Yeo, Y. Extracellular stability of nanoparticulate drug carriers. *Arch Pharm Res*. 2014; 37(1):16-23.
346. Garrett, W. S.; Chen, L. M.; Kroschewski, R.; Ebersold, M.; Turley, S.; Trombetta, S.; Galan, J. E.; Mellman, I. Developmental control of endocytosis in dendritic cells by Cdc42. *Cell*. 2000; 102(3):325-34.
347. Hickman-Miller, H. D.; Yewdell, J. W. Youth has its privileges: maturation inhibits DC cross-priming. *Nat Immunol*. 2006; 7(2):125-6.
348. Reis E Sousa, C. Dendritic cells in a mature age. *Nat Rev Immunol*. 2006; 6(6):476-83.
349. Liu, Z.; Jiao, Y.; Wang, Y.; Zhou, C.; Zhang, Z. Polysaccharides-based nanoparticles as drug delivery systems. *Adv Drug Deliv Rev*. 2008; 60(15):1650-62.
350. Vogel, C.; Marcotte, E. M. Insights into the regulation of protein abundance from proteomic and transcriptomic analyses. *Nat Rev Genet*. 2012; 13(4):227-32.
351. Chatel, A.; Lievre, C.; Barrick, A.; Bruneau, M.; Mouneyrac, C. Transcriptomic approach: A promising tool for rapid screening nanomaterial-mediated toxicity in the marine bivalve *Mytilus edulis*-Application to copper oxide nanoparticles. *Comp Biochem Physiol C Toxicol Pharmacol*. 2018; 205:26-33.
352. Gliga, A. R.; Di Bucchianico, S.; Lindvall, J.; Fadeel, B.; Karlsson, H. L. RNA-sequencing reveals long-term effects of silver nanoparticles on human lung cells. *Sci Rep*. 2018; 8(1):6668.
353. Hu, H.; Li, L.; Guo, Q.; Zong, H.; Yan, Y.; Yin, Y.; Wang, Y.; Oh, Y.; Feng, Y.; Wu, Q.; Gu, N. RNA sequencing analysis shows that titanium dioxide nanoparticles induce endoplasmic reticulum stress, which has a central role in mediating plasma glucose in mice. *Nanotoxicology*. 2018; 12(4):341-356.
354. Zheng, M.; Lu, J.; Zhao, D. Toxicity and Transcriptome Sequencing (RNA-seq) Analyses of Adult Zebrafish in Response to Exposure Carboxymethyl Cellulose Stabilized Iron Sulfide Nanoparticles. *Sci Rep*. 2018; 8(1):8083.
355. Mathan, T. S. M.; Textor, J.; Sköld, A. E.; Reinieren-Beeren, I.; Van Oorschot, T.; Brüning, M.; Figdor, C. G.; Buschow, S. I.; Bakdash, G.; De Vries, I. J. M. Harnessing RNA sequencing for global, unbiased evaluation of two new adjuvants for dendritic-cell immunotherapy. *Oncotarget*. 2017; 8(12):19879-19893.

## REFERENCES

356. Bult, C. J.; Eppig, J. T.; Blake, J. A.; Kadin, J. A.; Richardson, J. E.; The Mouse Genome Database, G. Mouse genome database 2016. *Nucleic Acids Research*. 2016; 44(Database issue):D840-D847.
357. Ten Brinke, A.; Karsten, M. L.; Dieker, M. C.; Zwaginga, J. J.; Van Ham, S. M. The clinical grade maturation cocktail monophosphoryl lipid A plus IFN $\gamma$  generates monocyte-derived dendritic cells with the capacity to migrate and induce Th1 polarization. *Vaccine*. 2007; 25(41):7145-52.
358. Massa, C.; Thomas, C.; Wang, E.; Marincola, F.; Seliger, B. Different maturation cocktails provide dendritic cells with different chemoattractive properties. *J Transl Med*. 2015; 13:175.
359. Zhu, M.; Xu, W.; Su, H.; Huang, Q.; Wang, B. Addition of CpG ODN and Poly (I:C) to a standard maturation cocktail generates monocyte-derived dendritic cells and induces a potent Th1 polarization with migratory capacity. *Hum Vaccin Immunother*. 2015; 11(7):1596-605.
360. Hotz, C.; Treinies, M.; Mottas, I.; C. Rötzer, L.; Oberson, A.; Spagnuolo, L.; Perdicchio, M.; Spinetti, T.; Herbst, T.; Bourquin, C. Reprogramming of TLR7 signaling enhances anti-tumor NK and cytotoxic T cell responses 2016.
361. Griffith, J. W.; Sokol, C. L.; Luster, A. D. Chemokines and chemokine receptors: positioning cells for host defense and immunity. *Annu Rev Immunol*. 2014; 32:659-702.
362. Proietto, A. I.; O'keeffe, M.; Gartlan, K.; Wright, M. D.; Shortman, K.; Wu, L.; Lahoud, M. H. Differential production of inflammatory chemokines by murine dendritic cell subsets. *Immunobiology*. 2004; 209(1-2):163-72.
363. Sallusto, F.; Palermo, B.; Lenig, D.; Miettinen, M.; Matikainen, S.; Julkunen, I.; Forster, R.; Burgstahler, R.; Lipp, M.; Lanzavecchia, A. Distinct patterns and kinetics of chemokine production regulate dendritic cell function. *Eur J Immunol*. 1999; 29(5):1617-25.
364. Vissers, J. L. M.; Hartgers, F. C.; Lindhout, E.; Teunissen, M. B. M.; Figdor, C. G.; Adema, G. J. Quantitative analysis of chemokine expression by dendritic cell subsets in vitro and in vivo. *Journal of Leukocyte Biology*. 2001; 69(5):785-793.
365. Fujita, H.; Asahina, A.; Gao, P.; Fujiwara, H.; Tamaki, K. Expression and regulation of RANTES/CCL5, MIP-1 $\alpha$ /CCL3, and MIP-1 $\beta$ /CCL4 in mouse Langerhans cells. *J Invest Dermatol*. 2004; 122(5):1331-3.
366. Ross, R.; Ross, X. L.; Ghadially, H.; Lahr, T.; Schwing, J.; Knop, J.; Reske-Kunz, A. B. Mouse langerhans cells differentially express an activated T cell-attracting CC chemokine. *J Invest Dermatol*. 1999; 113(6):991-8.

## REFERENCES

367. Piqueras, B.; Connolly, J.; Freitas, H.; Palucka, A. K.; Banchereau, J. Upon viral exposure, myeloid and plasmacytoid dendritic cells produce 3 waves of distinct chemokines to recruit immune effectors. *Blood*. 2006; 107(7):2613-2618.
368. Yoneyama, H.; Narumi, S.; Zhang, Y.; Murai, M.; Baggiolini, M.; Lanzavecchia, A.; Ichida, T.; Asakura, H.; Matsushima, K. Pivotal Role of Dendritic Cell-derived CXCL10 in the Retention of T Helper Cell 1 Lymphocytes in Secondary Lymph Nodes. *The Journal of Experimental Medicine*. 2002; 195(10):1257-1266.
369. Sallusto, F.; Schaerli, P.; Loetscher, P.; Schaniel, C.; Lenig, D.; Mackay, C. R.; Qin, S.; Lanzavecchia, A. Rapid and coordinated switch in chemokine receptor expression during dendritic cell maturation. *Eur J Immunol*. 1998; 28(9):2760-9.
370. Helbig, K. J.; Beard, M. R. The role of viperin in the innate antiviral response. *J Mol Biol*. 2014; 426(6):1210-9.
371. Skaug, B.; Chen, Z. J. Emerging Role of ISG15 in Antiviral Immunity. *Cell*. 2010; 143(2):187-190.
372. Singh-Jasuja, H.; Thiolat, A.; Ribon, M.; Boissier, M. C.; Bessis, N.; Rammensee, H. G.; Decker, P. The mouse dendritic cell marker CD11c is down-regulated upon cell activation through Toll-like receptor triggering. *Immunobiology*. 2013; 218(1):28-39.
373. Sun, X.; Zhang, M.; El-Zataari, M.; Owyang, S. Y.; Eaton, K. A.; Liu, M.; Chang, Y. M.; Zou, W.; Kao, J. Y. TLR2 mediates Helicobacter pylori-induced tolerogenic immune response in mice. *PLoS One*. 2013; 8(9):e74595.
374. Mahnke, K.; Becher, E.; Ricciardi-Castagnoli, P.; Luger, T. A.; Schwarz, T.; Grabbe, S. CD14 is expressed by subsets of murine dendritic cells and upregulated by lipopolysaccharide. *Adv Exp Med Biol*. 1997; 417:145-59.
375. Kissick, H. T.; Dunn, L. K.; Ghosh, S.; Nechama, M.; Kobzik, L.; Arredouani, M. S. The Scavenger Receptor MARCO Modulates TLR-Induced Responses in Dendritic Cells. *PLoS One*. 2014; 9(8):e104148.
376. Brutkiewicz, R. R. Cell Signaling Pathways That Regulate Antigen Presentation. *J Immunol*. 2016; 197(8):2971-2979.
377. Hanada, T.; Yoshimura, A. Regulation of cytokine signaling and inflammation. *Cytokine Growth Factor Rev*. 2002; 13(4-5):413-21.
378. Ivashkiv, L. B. Jak-STAT signaling pathways in cells of the immune system. *Rev Immunogenet*. 2000; 2(2):220-30.
379. Kawai, T.; Akira, S. The roles of TLRs, RLRs and NLRs in pathogen recognition. *Int Immunol*. 2009; 21(4):317-37.

## REFERENCES

380. Lawrence, T. The Nuclear Factor NF- $\kappa$ B Pathway in Inflammation. *Cold Spring Harbor Perspectives in Biology*. 2009; 1(6):a001651.
381. Milner, C. M.; Campbell, R. D. Structure and expression of the three MHC-linked HSP70 genes. *Immunogenetics*. 1990; 32(4):242-51.
382. Schiffer, R.; Baron, J.; Dagtekin, G.; Jahnen-Dechent, W.; Zwadlo-Klarwasser, G. Differential regulation of the expression of transporters associated with antigen processing, TAP1 and TAP2, by cytokines and lipopolysaccharide in primary human macrophages. *Inflamm Res*. 2002; 51(8):403-8.
383. Gao, J.; Wu, H.; Shi, X.; Huo, Z.; Zhang, J.; Liang, Z. Comparison of Next-Generation Sequencing, Quantitative PCR, and Sanger Sequencing for Mutation Profiling of EGFR, KRAS, PIK3CA and BRAF in Clinical Lung Tumors. *Clin Lab*. 2016; 62(4):689-96.
384. Pombo, M. A.; Zheng, Y.; Fei, Z.; Martin, G. B.; Rosli, H. G. Use of RNA-seq data to identify and validate RT-qPCR reference genes for studying the tomato-Pseudomonas pathosystem. *Scientific Reports*. 2017; 7:44905.
385. Van Goor, A.; Slawinska, A.; Schmidt, C. J.; Lamont, S. J. Distinct functional responses to stressors of bone marrow derived dendritic cells from diverse inbred chicken lines. *Dev Comp Immunol*. 2016; 63:96-110.
386. Miller, J. C.; Brown, B. D.; Shay, T.; Gautier, E. L.; Jovic, V.; Cohain, A.; Pandey, G.; Leboeuf, M.; Elpek, K. G.; Helft, J.; Hashimoto, D.; Chow, A.; Price, J.; Greter, M.; Bogunovic, M.; Bellemare-Pelletier, A.; Frenette, P. S.; Randolph, G. J.; Turley, S. J.; Merad, M.; The Immunological Genome, C. Deciphering the transcriptional network of the DC lineage. *Nature Immunology*. 2012; 13(9):888-899.
387. Levine, T. P.; Chain, B. M. Endocytosis by antigen presenting cells: dendritic cells are as endocytically active as other antigen presenting cells. *Proceedings of the National Academy of Sciences of the United States of America*. 1992; 89(17):8342-8346.
388. Cassell, D. J.; Schwartz, R. H. A quantitative analysis of antigen-presenting cell function: activated B cells stimulate naive CD4 T cells but are inferior to dendritic cells in providing costimulation. *J Exp Med*. 1994; 180(5):1829-40.
389. Corinti, S.; Medaglini, D.; Prezzi, C.; Cavani, A.; Pozzi, G.; Girolomoni, G. Human Dendritic Cells Are Superior to B Cells at Presenting a Major Histocompatibility Complex Class II-Restricted Heterologous Antigen Expressed on Recombinant *Streptococcus gordonii*. *Infection and Immunity*. 2000; 68(4):1879-1883.
390. Paulis, L. E.; Mandal, S.; Kreutz, M.; Figdor, C. G. Dendritic cell-based nanovaccines for cancer immunotherapy. *Curr Opin Immunol*. 2013; 25(3):389-95.



## REFERENCES

391. Reddy, S. T.; Van Der Vlies, A. J.; Simeoni, E.; Angeli, V.; Randolph, G. J.; O'neil, C. P.; Lee, L. K.; Swartz, M. A.; Hubbell, J. A. Exploiting lymphatic transport and complement activation in nanoparticle vaccines. *Nature Biotechnology*. 2007; 25:1159.
392. Moon, J. J.; Suh, H.; Li, A. V.; Ockenhouse, C. F.; Yadava, A.; Irvine, D. J. Enhancing humoral responses to a malaria antigen with nanoparticle vaccines that expand Tfh cells and promote germinal center induction. *Proc Natl Acad Sci U S A*. 2012; 109(4):1080-5.
393. Taheri, S.; Baier, G.; Majewski, P.; Barton, M.; Forch, R.; Landfester, K.; Vasilev, K. Synthesis and antibacterial properties of a hybrid of silver-potato starch nanocapsules by miniemulsion/polyaddition polymerization. *Journal of Materials Chemistry B*. 2014; 2(13):1838-1845.
394. Crespy, D.; Stark, M.; Hoffmann-Richter, C.; Ziener, U.; Landfester, K. Polymeric Nanoreactors for Hydrophilic Reagents Synthesized by Interfacial Polycondensation on Miniemulsion Droplets. *Macromolecules*. 2007; 40(9):3122-3135.
395. Collins, M. A. Toxicology of toluene diisocyanate. *Appl Occup Environ Hyg*. 2002; 17(12):846-55.
396. Mueller, J. O.; Voll, D.; Schmidt, F. G.; Delaittre, G.; Barner-Kowollik, C. Fluorescent polymers from non-fluorescent photoreactive monomers. *Chem Commun (Camb)*. 2014; 50(99):15681-4.
397. Tenzer, S.; Docter, D.; Kuharev, J.; Musyanovych, A.; Fetz, V.; Hecht, R.; Schlenk, F.; Fischer, D.; Kiouptsi, K.; Reinhardt, C.; Landfester, K.; Schild, H.; Maskos, M.; Knauer, S. K.; Stauber, R. H. Rapid formation of plasma protein corona critically affects nanoparticle pathophysiology. *Nat Nanotechnol*. 2013; 8(10):772-81.
398. Monopoli, M. P.; Aberg, C.; Salvati, A.; Dawson, K. A. Biomolecular coronas provide the biological identity of nanosized materials. *Nat Nanotechnol*. 2012; 7(12):779-86.
399. Salvati, A.; Pitek, A. S.; Monopoli, M. P.; Prapainop, K.; Bombelli, F. B.; Hristov, D. R.; Kelly, P. M.; Aberg, C.; Mahon, E.; Dawson, K. A. Transferrin-functionalized nanoparticles lose their targeting capabilities when a biomolecule corona adsorbs on the surface. *Nat Nanotechnol*. 2013; 8(2):137-43.
400. Nienhaus, G. U.; Maffre, P.; Nienhaus, K. Studying the protein corona on nanoparticles by FCS. *Methods Enzymol*. 2013; 519:115-37.
401. Walkey, C. D.; Olsen, J. B.; Guo, H.; Emili, A.; Chan, W. C. W. Nanoparticle Size and Surface Chemistry Determine Serum Protein Adsorption and Macrophage Uptake. *Journal of the American Chemical Society*. 2012; 134(4):2139-2147.

## REFERENCES

402. Suk, J. S.; Xu, Q.; Kim, N.; Hanes, J.; Ensign, L. M. PEGylation as a strategy for improving nanoparticle-based drug and gene delivery. *Advanced drug delivery reviews*. 2016; 99(Pt A):28-51.
403. Lachmann, P. J.; Thompson, R. A. Reactive lysis: The complement-mediated lysis of unsensitized cells : II. The characterization of activated reactor as C56 and the participation of C8 and C9. *The Journal of Experimental Medicine*. 1970; 131(4):643-657.
404. Degn, S. E.; Thiel, S. Humoral pattern recognition and the complement system. *Scand J Immunol*. 2013; 78(2):181-93.
405. Ratelade, J.; Verkman, A. S. Inhibitor(s) of the classical complement pathway in mouse serum limit the utility of mice as experimental models of neuromyelitis optica. *Molecular immunology*. 2014; 62(1):104-113.
406. Lesniak, A.; Campbell, A.; Monopoli, M. P.; Lynch, I.; Salvati, A.; Dawson, K. A. Serum heat inactivation affects protein corona composition and nanoparticle uptake. *Biomaterials*. 2010; 31(36):9511-9518.
407. Miteva, M.; Kirkbride, K. C.; Kilchrist, K. V.; Werfel, T. A.; Li, H.; Nelson, C. E.; Gupta, M. K.; Giorgio, T. D.; Duvall, C. L. Tuning PEGylation of mixed micelles to overcome intracellular and systemic siRNA delivery barriers. *Biomaterials*. 2015; 38:97-107.
408. Mori, A.; Klibanov, A. L.; Torchilin, V. P.; Huang, L. Influence of the steric barrier activity of amphipathic poly(ethyleneglycol) and ganglioside GM1 on the circulation time of liposomes and on the target binding of immunoliposomes in vivo. *FEBS Lett*. 1991; 284(2):263-266.
409. Gref, R.; Luck, M.; Quellec, P.; Marchand, M.; Dellacherie, E.; Harnisch, S.; Blunk, T.; Muller, R. H. 'Stealth' corona-core nanoparticles surface modified by polyethylene glycol (PEG): influences of the corona (PEG chain length and surface density) and of the core composition on phagocytic uptake and plasma protein adsorption. *Colloids and Surfaces B-Biointerfaces*. 2000; 18(3-4):301-313.
410. Owens, D. E., 3rd; Peppas, N. A. Opsonization, biodistribution, and pharmacokinetics of polymeric nanoparticles. *Int J Pharm*. 2006; 307(1):93-102.
411. Peracchia, M. T. Stealth nanoparticles for intravenous administration. *STP Pharma Sciences*. 2003; 13:155-161.
412. Vonarbourg, A.; Passirani, C.; Saulnier, P.; Benoit, J. P. Parameters influencing the stealthiness of colloidal drug delivery systems. *Biomaterials*. 2006; 27(24):4356-73.
413. Braeckmans, K.; Buyens, K.; Bouquet, W.; Vervaet, C.; Joye, P.; Vos, F. D.; Plawinski, L.; Dœuvre, L.; Angles-Cano, E.; Sanders, N. N.; Demeester, J.; Smedt,

## REFERENCES

- S. C. D. Sizing Nanomatter in Biological Fluids by Fluorescence Single Particle Tracking. *Nano Letters*. 2010; 10(11):4435-4442.
414. Peracchia, M. T.; Fattal, E.; Desmaele, D.; Besnard, M.; Noel, J. P.; Gomis, J. M.; Appel, M.; D'angelo, J.; Couvreur, P. Stealth PEGylated polycyanoacrylate nanoparticles for intravenous administration and splenic targeting. *J Control Release*. 1999; 60(1):121-8.
415. Polyak, B.; Cordovez, B. How can we predict behavior of nanoparticles in vivo? *Nanomedicine (Lond)*. 2016; 11(3):189-92.
416. Gustafson, H. H.; Holt-Casper, D.; Grainger, D. W.; Ghandehari, H. Nanoparticle Uptake: The Phagocyte Problem. *Nano Today*. 2015; 10(4):487-510.
417. Verhoef, J. J. F.; Anchordoquy, T. J. Questioning the Use of PEGylation for Drug Delivery. *Drug delivery and translational research*. 2013; 3(6):499-503.
418. Moghimi, S. M.; Szebeni, J. Stealth liposomes and long circulating nanoparticles: critical issues in pharmacokinetics, opsonization and protein-binding properties. *Prog Lipid Res*. 2003; 42(6):463-78.
419. Zhang, P.; Sun, F.; Liu, S.; Jiang, S. Anti-PEG antibodies in the clinic: Current issues and beyond PEGylation. *J Control Release*. 2016; 244(Pt B):184-193.
420. Hadjesfandiari, N.; Parambath, A. 13 - Stealth coatings for nanoparticles: Polyethylene glycol alternatives. In: Parambath, A., editor. *Engineering of Biomaterials for Drug Delivery Systems*: Woodhead Publishing; 2018. p. 345-361.
421. Ecker, J. R.; Davis, R. W. Inhibition of gene expression in plant cells by expression of antisense RNA. *Proceedings of the National Academy of Sciences*. 1986; 83(15):5372-5376.
422. Fire, A.; Xu, S.; Montgomery, M. K.; Kostas, S. A.; Driver, S. E.; Mello, C. C. Potent and specific genetic interference by double-stranded RNA in *Caenorhabditis elegans*. *Nature*. 1998; 391:806.
423. Jana, S.; Chakraborty, C.; Nandi, S.; Deb, J. K. RNA interference: potential therapeutic targets. *Appl Microbiol Biotechnol*. 2004; 65(6):649-57.
424. Chakraborty, C.; Sharma, A. R.; Sharma, G.; Doss, C. G. P.; Lee, S.-S. Therapeutic miRNA and siRNA: Moving from Bench to Clinic as Next Generation Medicine. *Molecular Therapy Nucleic Acids*. 2017; 8:132-143.
425. Cheng, S.; Coffey, G.; Zhang, X. H.; Shaknovich, R.; Song, Z.; Lu, P.; Pandey, A.; Melnick, A. M.; Sinha, U.; Wang, Y. L. SYK inhibition and response prediction in diffuse large B-cell lymphoma. *Blood*. 2011; 118(24):6342-52.

## REFERENCES

426. Ahn, Y. H.; Hong, S. O.; Kim, J. H.; Noh, K. H.; Song, K. H.; Lee, Y. H.; Jeon, J. H.; Kim, D. W.; Seo, J. H.; Kim, T. W. The siRNA cocktail targeting interleukin 10 receptor and transforming growth factor-beta receptor on dendritic cells potentiates tumour antigen-specific CD8(+) T cell immunity. *Clin Exp Immunol.* 2015; 181(1):164-78.
427. Kim, T. K.; Eberwine, J. H. Mammalian cell transfection: the present and the future. *Analytical and Bioanalytical Chemistry.* 2010; 397(8):3173-3178.
428. Larsson, E.; Sander, C.; Marks, D. mRNA turnover rate limits siRNA and microRNA efficacy. *Molecular Systems Biology.* 2010; 6:433-433.
429. Guzman-Villanueva, D.; El-Sherbiny, I. M.; Herrera-Ruiz, D.; Vlassov, A. V.; Smyth, H. D. Formulation approaches to short interfering RNA and MicroRNA: challenges and implications. *J Pharm Sci.* 2012; 101(11):4046-66.
430. Hickerson, R. P.; Vlassov, A. V.; Wang, Q.; Leake, D.; Ilves, H.; Gonzalez-Gonzalez, E.; Contag, C. H.; Johnston, B. H.; Kaspar, R. L. Stability Study of Unmodified siRNA and Relevance to Clinical Use. *Oligonucleotides.* 2008; 18(4):345-354.
431. Wang, J.; Lu, Z.; Wientjes, M. G.; Au, J. L. S. Delivery of siRNA Therapeutics: Barriers and Carriers. *The AAPS Journal.* 2010; 12(4):492-503.
432. Robbins, M.; Judge, A.; Maclachlan, I. siRNA and innate immunity. *Oligonucleotides.* 2009; 19(2):89-102.
433. Dolina, J.; J Sung, S.-S.; I Novobrantseva, T.; M Nguyen, T.; Hahn, Y. Lipidoid Nanoparticles Containing PD-L1 siRNA Delivered In Vivo Enter Kupffer Cells and Enhance NK and CD8&plus; T Cell-mediated Hepatic Antiviral Immunity2013. e72 p.
434. Bochicchio, S.; Dalmoro, A.; Barba, A. A.; Grassi, G.; Lamberti, G. Liposomes as siRNA delivery vectors. *Curr Drug Metab.* 2014; 15(9):882-92.
435. Hughes, J.; Yadava, P.; Mesaros, R. Liposomal siRNA delivery. *Methods Mol Biol.* 2010; 605:445-59.
436. Resnier, P.; Montier, T.; Mathieu, V.; Benoit, J. P.; Passirani, C. A review of the current status of siRNA nanomedicines in the treatment of cancer. *Biomaterials.* 2013; 34(27):6429-43.
437. Szebeni, J.; Moghimi, S. M. Liposome triggering of innate immune responses: a perspective on benefits and adverse reactions. *J Liposome Res.* 2009; 19(2):85-90.

## REFERENCES

438. Sercombe, L.; Veerati, T.; Moheimani, F.; Wu, S. Y.; Sood, A. K.; Hua, S. Advances and Challenges of Liposome Assisted Drug Delivery. *Frontiers in Pharmacology*. 2015; 6:286.
439. Fichter, M.; Dedters, M.; Pietrzak-Nguyen, A.; Pretsch, L.; Meyer, C. U.; Strand, S.; Zepp, F.; Baier, G.; Landfester, K.; Gehring, S. Monophosphoryl lipid A coating of hydroxyethyl starch nanocapsules drastically increases uptake and maturation by dendritic cells while minimizing the adjuvant dosage. *Vaccine*. 2015; 33(7):838-46.
440. Noga, M.; Edinger, D.; Rödl, W.; Wagner, E.; Winter, G.; Besheer, A. Controlled shielding and deshielding of gene delivery polyplexes using hydroxyethyl starch (HES) and alpha-amylase. *Journal of Controlled Release*. 2012; 159(1):92-103.
441. Noga, M.; Edinger, D.; Kläger, R.; Wegner, S. V.; Spatz, J. P.; Wagner, E.; Winter, G.; Besheer, A. The effect of molar mass and degree of hydroxyethylation on the controlled shielding and deshielding of hydroxyethyl starch-coated polyplexes. *Biomaterials*. 2013; 34(10):2530-2538.
442. Kang, B.; Okwieka, P.; Schottler, S.; Seifert, O.; Kontermann, R. E.; Pfizenmaier, K.; Musyanovych, A.; Meyer, R.; Diken, M.; Sahin, U.; Mailander, V.; Wurm, F. R.; Landfester, K. Tailoring the stealth properties of biocompatible polysaccharide nanocontainers. *Biomaterials*. 2015; 49:125-34.
443. Kang, B.; Okwieka, P.; Schottler, S.; Winzen, S.; Langhanki, J.; Mohr, K.; Opatz, T.; Mailander, V.; Landfester, K.; Wurm, F. R. Carbohydrate-Based Nanocarriers Exhibiting Specific Cell Targeting with Minimum Influence from the Protein Corona. *Angew Chem Int Ed Engl*. 2015; 54(25):7436-40.
444. Baier, G.; Baumann, D.; Siebert, J. M.; Musyanovych, A.; Mailander, V.; Landfester, K. Suppressing unspecific cell uptake for targeted delivery using hydroxyethyl starch nanocapsules. *Biomacromolecules*. 2012; 13(9):2704-15.
445. Winzen, S.; Schoettler, S.; Baier, G.; Rosenauer, C.; Mailaender, V.; Landfester, K.; Mohr, K. Complementary analysis of the hard and soft protein corona: sample preparation critically effects corona composition. *Nanoscale*. 2015; 7(7):2992-3001.
446. Narayanan, D.; Nair, S.; Menon, D. A systematic evaluation of hydroxyethyl starch as a potential nanocarrier for parenteral drug delivery. *Int J Biol Macromol*. 2015; 74:575-84.
447. Frick, S. U.; Domogalla, M. P.; Baier, G.; Wurm, F. R.; Mailaender, V.; Landfester, K.; Steinbrink, K. Interleukin-2 Functionalized Nanocapsules for T Cell-Based Immunotherapy. *ACS Nano*. 2016.
448. Hartog, C. S.; Natanson, C.; Sun, J.; Klein, H. G.; Reinhart, K. Concerns over use of hydroxyethyl starch solutions. *The BMJ*. 2014; 349:g5981.

## REFERENCES

449. Brunkhorst, F. M.; Engel, C.; Bloos, F.; Meier-Hellmann, A.; Ragaller, M.; Weiler, N.; Moerer, O.; Gruendling, M.; Oppert, M.; Grond, S.; Olthoff, D.; Jaschinski, U.; John, S.; Rossaint, R.; Welte, T.; Schaefer, M.; Kern, P.; Kuhnt, E.; Kiehntopf, M.; Hartog, C.; Natanson, C.; Loeffler, M.; Reinhart, K. Intensive insulin therapy and pentastarch resuscitation in severe sepsis. *N Engl J Med.* 2008; 358(2):125-39.
450. Myburgh, J. A.; Finfer, S.; Bellomo, R.; Billot, L.; Cass, A.; Gattas, D.; Glass, P.; Lipman, J.; Liu, B.; McArthur, C.; McGuinness, S.; Rajbhandari, D.; Taylor, C. B.; Webb, S. A. Hydroxyethyl starch or saline for fluid resuscitation in intensive care. *N Engl J Med.* 2012; 367(20):1901-11.
451. Perner, A.; Haase, N.; Guttormsen, A. B.; Tenhunen, J.; Klemenzson, G.; Aneman, A.; Madsen, K. R.; Moller, M. H.; Elkjaer, J. M.; Poulsen, L. M.; Bendtsen, A.; Winding, R.; Steensen, M.; Berezowicz, P.; Soe-Jensen, P.; Bestle, M.; Strand, K.; Wiis, J.; White, J. O.; Thornberg, K. J.; Quist, L.; Nielsen, J.; Andersen, L. H.; Holst, L. B.; Thormar, K.; Kjaeldgaard, A. L.; Fabritius, M. L.; Mondrup, F.; Pott, F. C.; Moller, T. P.; Winkel, P.; Wetterslev, J. Hydroxyethyl starch 130/0.42 versus Ringer's acetate in severe sepsis. *N Engl J Med.* 2012; 367(2):124-34.
452. Tseng, Y. C.; Mozumdar, S.; Huang, L. Lipid-based systemic delivery of siRNA. *Adv Drug Deliv Rev.* 2009; 61(9):721-31.
453. Besheer, A.; Vogel, J.; Glanz, D.; Kressler, J.; Groth, T.; Mader, K. Characterization of PLGA nanospheres stabilized with amphiphilic polymers: hydrophobically modified hydroxyethyl starch vs pluronics. *Mol Pharm.* 2009; 6(2):407-15.
454. Sakhtianchi, R.; Minchin, R. F.; Lee, K. B.; Alkilany, A. M.; Serpooshan, V.; Mahmoudi, M. Exocytosis of nanoparticles from cells: role in cellular retention and toxicity. *Adv Colloid Interface Sci.* 2013; 201-202:18-29.
455. Wang, C. T.; Lu, J. C.; Bai, J.; Chang, P. Y.; Martin, T. F.; Chapman, E. R.; Jackson, M. B. Different domains of synaptotagmin control the choice between kiss-and-run and full fusion. *Nature.* 2003; 424(6951):943-7.
456. Nakamura, T.; Fujiwara, Y.; Warashina, S.; Harashima, H. The intracellular pharmacodynamics of siRNA is responsible for the low gene silencing activity of siRNA-loaded nanoparticles in dendritic cells. *Int J Pharm.* 2015; 494(1):271-7.
457. Hilgenbrink, A. R.; Low, P. S. Folate receptor-mediated drug targeting: from therapeutics to diagnostics. *J Pharm Sci.* 2005; 94(10):2135-46.
458. Sudimack, J.; Lee, R. J. Targeted drug delivery via the folate receptor. *Adv Drug Deliv Rev.* 2000; 41(2):147-62.

## REFERENCES

459. Stella, B.; Arpicco, S.; Peracchia, M. T.; Desmaele, D.; Hoebeke, J.; Renoir, M.; D'angelo, J.; Cattel, L.; Couvreur, P. Design of folic acid-conjugated nanoparticles for drug targeting. *J Pharm Sci.* 2000; 89(11):1452-64.
460. Yoo, H. S.; Park, T. G. Folate receptor targeted biodegradable polymeric doxorubicin micelles. *J Control Release.* 2004; 96(2):273-83.
461. Lu, J.; Zhao, W.; Huang, Y.; Liu, H.; Marquez, R.; Gibbs, R. B.; Li, J.; Venkataramanan, R.; Xu, L.; Li, S.; Li, S. Targeted Delivery of Doxorubicin by Folic Acid-Decorated Dual Functional Nanocarrier. *Molecular Pharmaceutics.* 2014; 11(11):4164-4178.
462. Scomparin, A.; Salmaso, S.; Eldar-Boock, A.; Ben-Shushan, D.; Ferber, S.; Tiram, G.; Shmeeda, H.; Landa-Rouben, N.; Leor, J.; Caliceti, P.; Gabizon, A.; Satchi-Fainaro, R. A comparative study of folate receptor-targeted doxorubicin delivery systems: Dosing regimens and therapeutic index. *Journal of Controlled Release.* 2015; 208:106-120.
463. Brown, G. D.; Willment, J. A.; Whitehead, L. C-type lectins in immunity and homeostasis. *Nature Reviews Immunology.* 2018; 18(6):374-389.
464. Shrimpton, R. E.; Butler, M.; Morel, A. S.; Eren, E.; Hue, S. S.; Ritter, M. A. CD205 (DEC-205): a recognition receptor for apoptotic and necrotic self. *Mol Immunol.* 2009; 46(6):1229-39.
465. Wollenberg, A.; Mommaas, M.; Oppel, T.; Schottdorf, E. M.; Gunther, S.; Moderer, M. Expression and function of the mannose receptor CD206 on epidermal dendritic cells in inflammatory skin diseases. *J Invest Dermatol.* 2002; 118(2):327-34.
466. Caminschi, I.; Proietto, A. I.; Ahmet, F.; Kitsoulis, S.; Shin Teh, J.; Lo, J. C. Y.; Rizzitelli, A.; Wu, L.; Vremec, D.; Van Dommelen, S. L. H.; Campbell, I. K.; Maraskovsky, E.; Braley, H.; Davey, G. M.; Mottram, P.; Van De Velde, N.; Jensen, K.; Lew, A. M.; Wright, M. D.; Heath, W. R.; Shortman, K.; Lahoud, M. H. The dendritic cell subtype-restricted C-type lectin Clec9A is a target for vaccine enhancement. *Blood.* 2008; 112(8):3264-3273.
467. Soilleux, E. J.; Morris, L. S.; Leslie, G.; Chehimi, J.; Luo, Q.; Levroney, E.; Trowsdale, J.; Montaner, L. J.; Doms, R. W.; Weissman, D.; Coleman, N.; Lee, B. Constitutive and induced expression of DC-SIGN on dendritic cell and macrophage subpopulations in situ and in vitro. *J Leukoc Biol.* 2002; 71(3):445-57.
468. Arnáiz, B.; Martínez-Ávila, O.; Falcon-Perez, J. M.; Penadés, S. Cellular Uptake of Gold Nanoparticles Bearing HIV gp120 Oligomannosides. *Bioconjugate Chemistry.* 2012; 23(4):814-825.
469. Arosio, D.; Chiodo, F.; Reina, J. J.; Marelli, M.; Penades, S.; Van Kooyk, Y.; Garcia-Vallejo, J. J.; Bernardi, A. Effective targeting of DC-SIGN by alpha-

## REFERENCES

- fucosylamide functionalized gold nanoparticles. *Bioconjug Chem.* 2014; 25(12):2244-51.
470. Chiodo, F.; Marradi, M.; Park, J.; Ram, A. F.; Penades, S.; Van Die, I.; Tefsen, B. Galactofuranose-coated gold nanoparticles elicit a pro-inflammatory response in human monocyte-derived dendritic cells and are recognized by DC-SIGN. *ACS Chem Biol.* 2014; 9(2):383-9.
471. Stead, S. O.; Mcinnes, S. J. P.; Kireta, S.; Rose, P. D.; Jesudason, S.; Rojas-Canales, D.; Warther, D.; Cunin, F.; Durand, J. O.; Drogemuller, C. J.; Carroll, R. P.; Coates, P. T.; Voelcker, N. H. Manipulating human dendritic cell phenotype and function with targeted porous silicon nanoparticles. *Biomaterials.* 2018; 155:92-102.
472. Geijtenbeek, T. B.; Krooshoop, D. J.; Bleijs, D. A.; Van Vliet, S. J.; Van Duijnhoven, G. C.; Grabovsky, V.; Alon, R.; Figdor, C. G.; Van Kooyk, Y. DC-SIGN-ICAM-2 interaction mediates dendritic cell trafficking. *Nat Immunol.* 2000; 1(4):353-7.
473. Geijtenbeek, T. B.; Torensma, R.; Van Vliet, S. J.; Van Duijnhoven, G. C.; Adema, G. J.; Van Kooyk, Y.; Figdor, C. G. Identification of DC-SIGN, a novel dendritic cell-specific ICAM-3 receptor that supports primary immune responses. *Cell.* 2000; 100(5):575-85.
474. Engering, A.; Geijtenbeek, T. B.; Van Vliet, S. J.; Wijers, M.; Van Liempt, E.; Demarex, N.; Lanzavecchia, A.; Fransen, J.; Figdor, C. G.; Piguët, V.; Van Kooyk, Y. The dendritic cell-specific adhesion receptor DC-SIGN internalizes antigen for presentation to T cells. *J Immunol.* 2002; 168(5):2118-26.
475. Svajger, U.; Anderluh, M.; Jeras, M.; Obermajer, N. C-type lectin DC-SIGN: an adhesion, signalling and antigen-uptake molecule that guides dendritic cells in immunity. *Cell Signal.* 2010; 22(10):1397-405.
476. Cambi, A.; Beeren, I.; Joosten, B.; Fransen, J. A.; Figdor, C. G. The C-type lectin DC-SIGN internalizes soluble antigens and HIV-1 virions via a clathrin-dependent mechanism. *Eur J Immunol.* 2009; 39(7):1923-8.



# 8. Appendix

## 8.1 Supplementary data

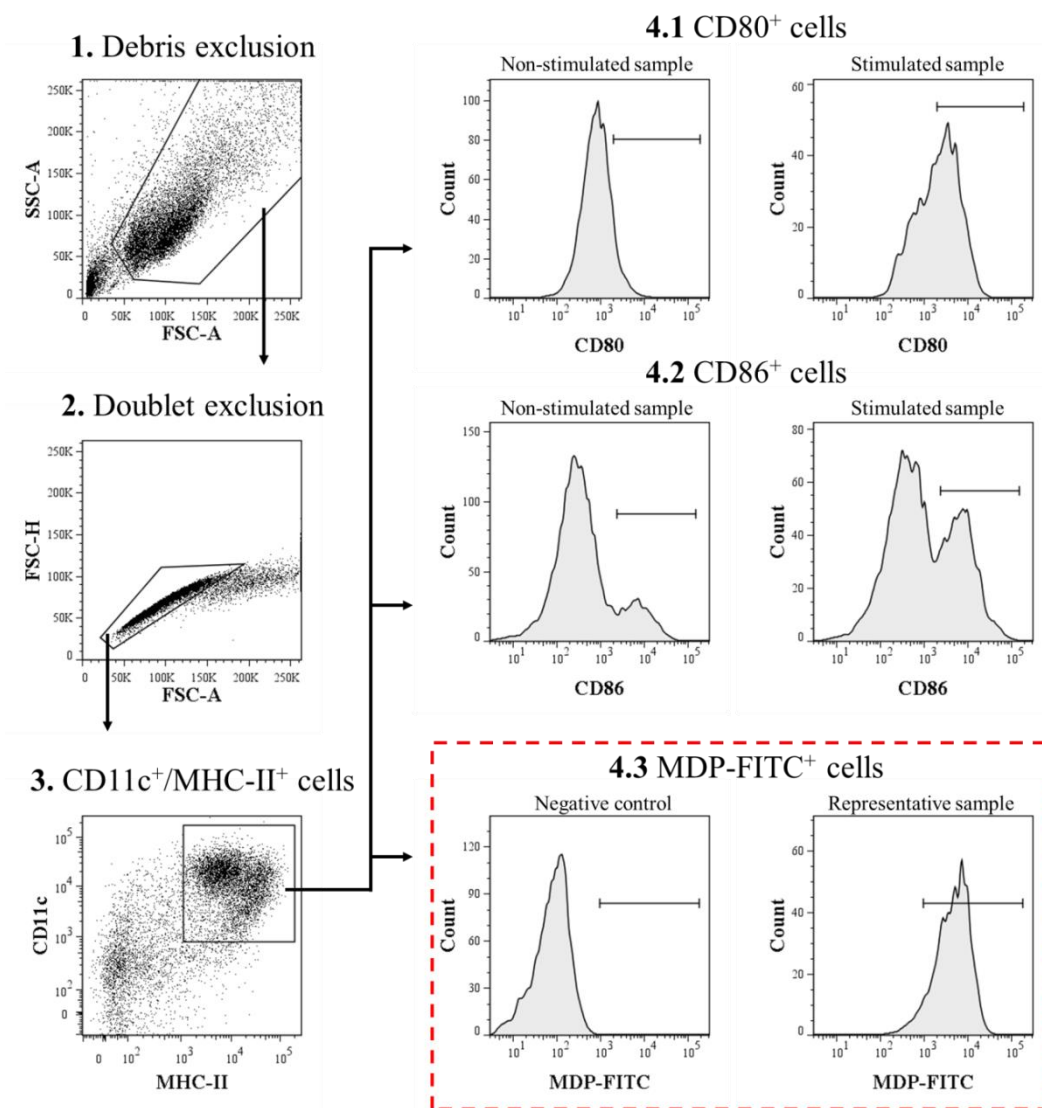


**Figure S 1** Gating strategy for soluble adjuvants and adjuvant-loaded nanocarriers

BMDCs stimulated with soluble adjuvants or adjuvant-loaded nanocarriers were analyzed by (1) debris exclusion, (2) doublet exclusion, (3) gating on CD11c<sup>+</sup>/MHC-II<sup>+</sup> BMDCs and subsequent measurement of (4.1) CD80 and (4.2) CD86 expression. To measure association with MDP-loaded Dex-NPs, (4.3) MDP-FITC<sup>+</sup> BMDCs were assessed. The red framed gating was merely used for Dex-NP experiments. Figure published in the Journal of Controlled Release in a modified version [249].

APPENDIX

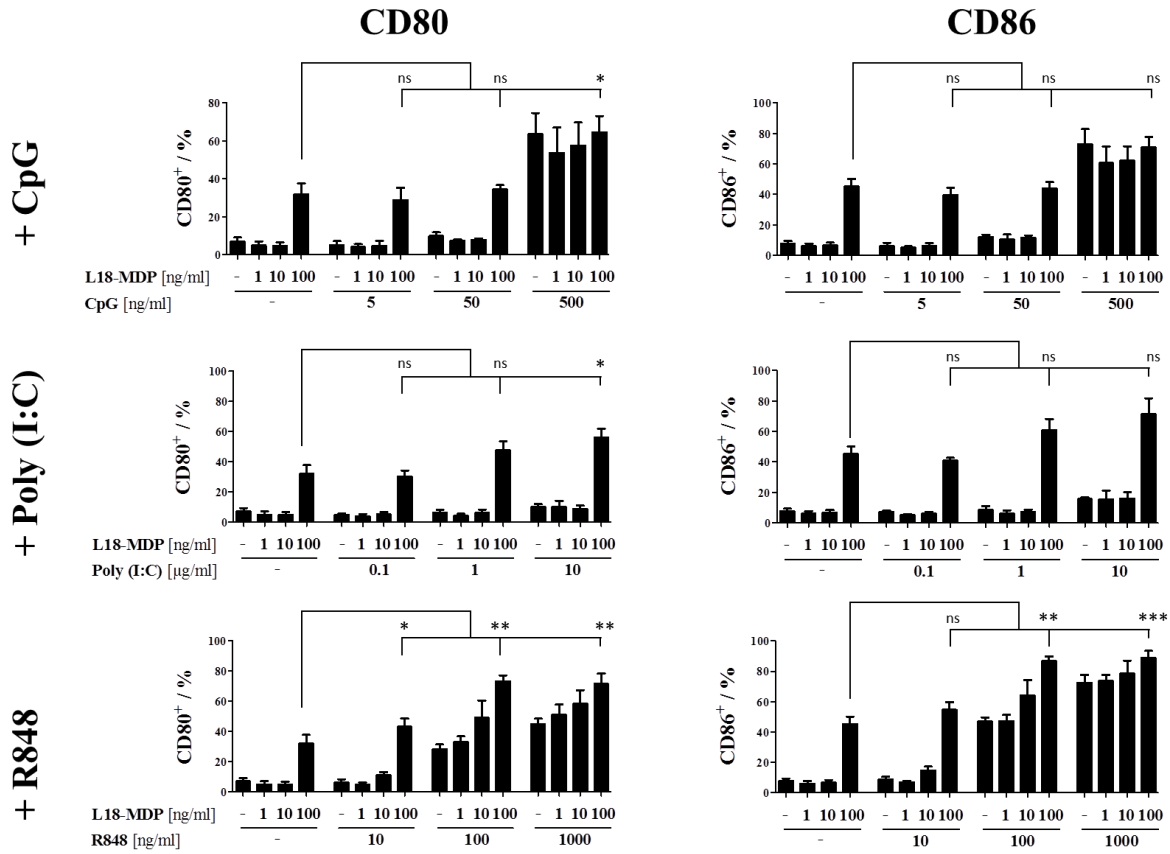


**Figure S 2** Identification of superadditive TLR/NLR ligand combinations by frequency

BMDCs ( $2 \times 10^5$  cells/ml) were analyzed for CD80 and CD86 expression after 24 h treatment with different TLR ligands and L18-MDP, alone or in combination as indicated, via flow cytometry. CpG (5-500 ng/ml), Poly I:C (0.1-10 μg/ml) and R848 (10-1000 ng/ml) were applied simultaneously to L18-MDP (1-100 ng/ml). Identification of possible superadditive effects was done on the basis of CD80/CD86 frequencies (mean ± SD; n=3). \*p < 0.05, \*\*p < 0.01, \*\*\*p < 0.001. Data and figure published in the Journal of Controlled Release [249].

## APPENDIX

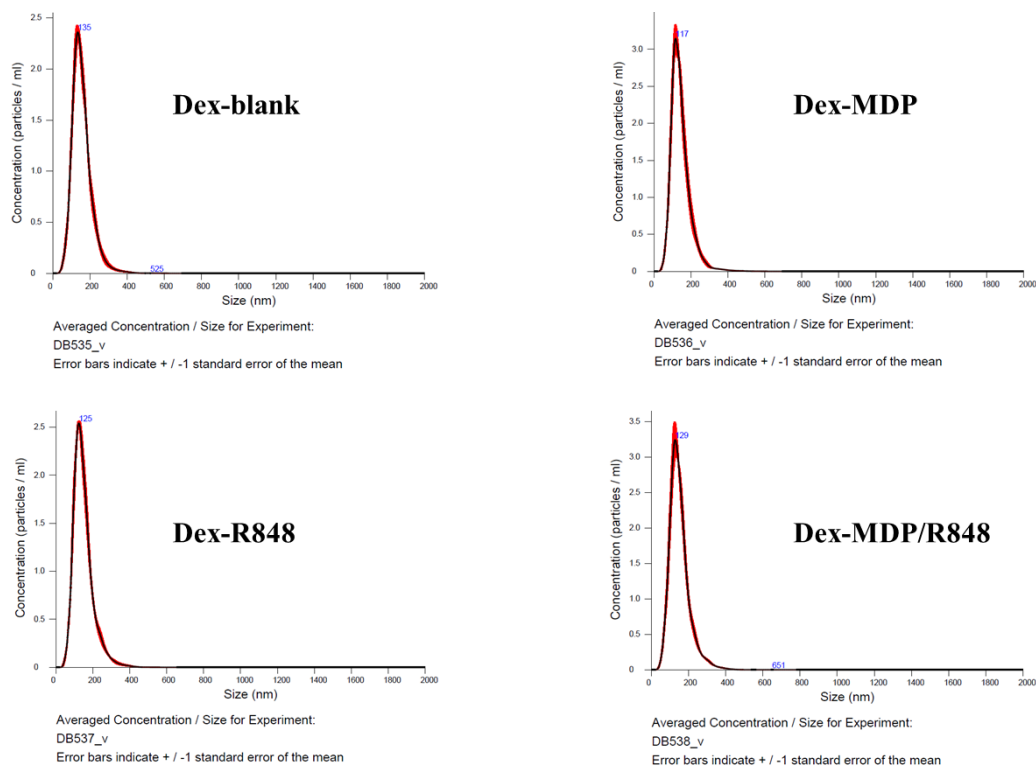


**Figure S 3** Exemplary NTA primary data

Primary data for size determination of adjuvant-loaded Dex-NPs was generated by NTA. Shown are the data for empty Dex-NPs as well as for MDP-, R848- and MDP/R848-loaded ones. Data and figure published in the Journal of Controlled Release [249].

Particle type	Ø Mean / nm	Ø Mode / nm	SD Value / nm
<b>Dex-blank</b>	156.1 ± 2.4	134.5 ± 3.2	52.8 ± 3.2
<b>Dex-MDP</b>	143.9 ± 2.5	122.4 ± 5.7	53.2 ± 1.1
<b>Dex-R848</b>	148.1 ± 0.8	125.5 ± 3.5	53.5 ± 2.0
<b>Dex-MDP/R848</b>	151.5 ± 2.0	131.6 ± 4.5	54.0 ± 0.9

**Table S 1** Size determination of Dex-NPs via NTA

Particle size (diameter Ø) of the Dex-NP formulations was determined with five individual measurements per samples. Mean size and SD correspond to the arithmetic values calculated based on the sizes of all particles detected in NTA measurement. Mode values describe the average size of the main particle population. Data published in the Journal of Controlled Release [249].

APPENDIX

Particle type	nmol MDP/ mg NP	µg MDP/ mg NP	nmol R848/ mg NP	µg R848/ mg NP
<b>Dex-blank</b>	-	-	-	-
<b>Dex-MDP</b>	1.34	0.66	-	-
<b>Dex-R848</b>	-	-	1.26	0.44
<b>Dex-MDP/R848</b>	1.38	0.68	1.29	0.45

**Table S 2** Quantification of encapsulated MDP-FITC and R848 in Dex-NPs

The particulation of MDP and R848 in Dex-NPs was analyzed by means of fluorescent MDP-FITC and the fluorescent properties of R848 itself. To do so, MDP-FITC and R848 fluorescence in four Dex-NP types (Dex-blank, Dex-MDP-FITC, Dex-R848, and Dex-MDP-FITC/R848) was measured by fluorescence spectroscopy. Based on these results, the actual MDP/R848 contents in Dex-NP formulations used for stimulation assays (including Dex-MDP and Dex-MDP/R848 with non-labeled MDP) were calculated with a calibration curve in the range of 0.0625 µg/ml to 10 µg/ml. Data published in the Journal of Controlled Release [249].

Capsule type	Ø / nm in cyclohexane	Ø / nm in water	ζ / mV
<b>OVA-blank-NC</b>	256	348	-26
<b>OVA-MDP-NC</b>	268	404	-27
<b>OVA-R848-NC</b>	331	335	-32
<b>OVA-MDP/R848-NC</b>	302	338	-31

**Table S 3** Size and charge determination of OVA-NCs via DLS

The diameters of the experimentally used OVA-NCs in cyclohexane and water as well as the zeta potential (ζ) were measured via DLS. Data published in the Journal of Controlled Release [249].

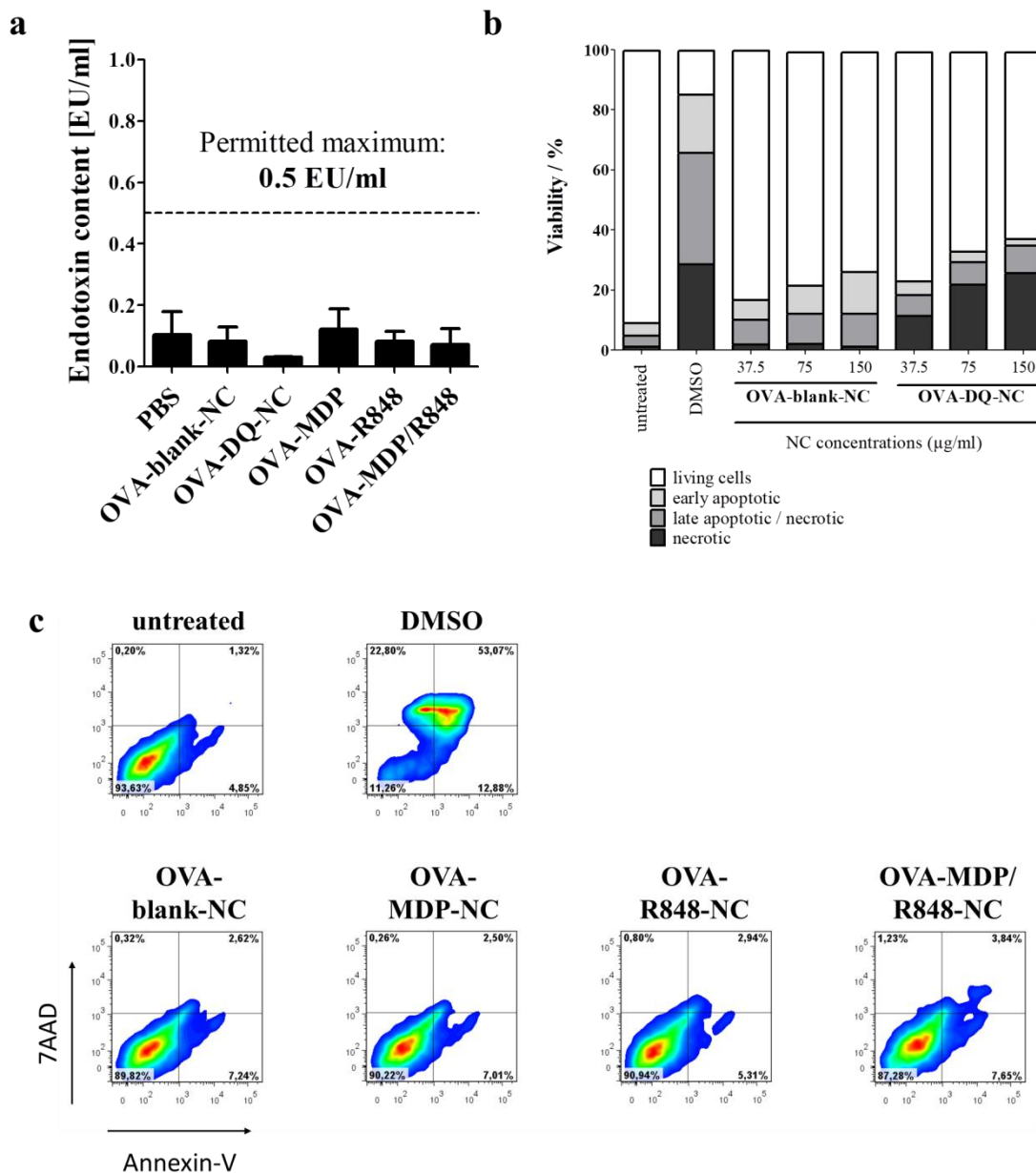


**Figure S 4** Quality tests for OVA-NC formulations

OVA-NCs were tested to exclude endotoxin contaminations and cytotoxic effects on BMDCs. (a) Endotoxin concentrations in OVA-NC formulations were assessed by LAL assay (mean  $\pm$  SD; n=2, two independent NC batches). (b) Cytotoxicity of OVA-blank- and OVA-DQ-NC was measured. Therefore, BMDCs ( $1 \times 10^6$  cells/ml) were incubated with increasing concentrations (37.5-150  $\mu$ g/ml) for 24 h. Viability was determined by 7AAD/Annexin V staining. 10 vol-% DMSO was used as positive control. (c) BMDC viability after treatment with adjuvant-loaded OVA-NCs (100  $\mu$ g/ml) for 24 h. Plots are representative of two experiments. Figure S 4c as well as corresponding data published in the Journal of Controlled Release [249].

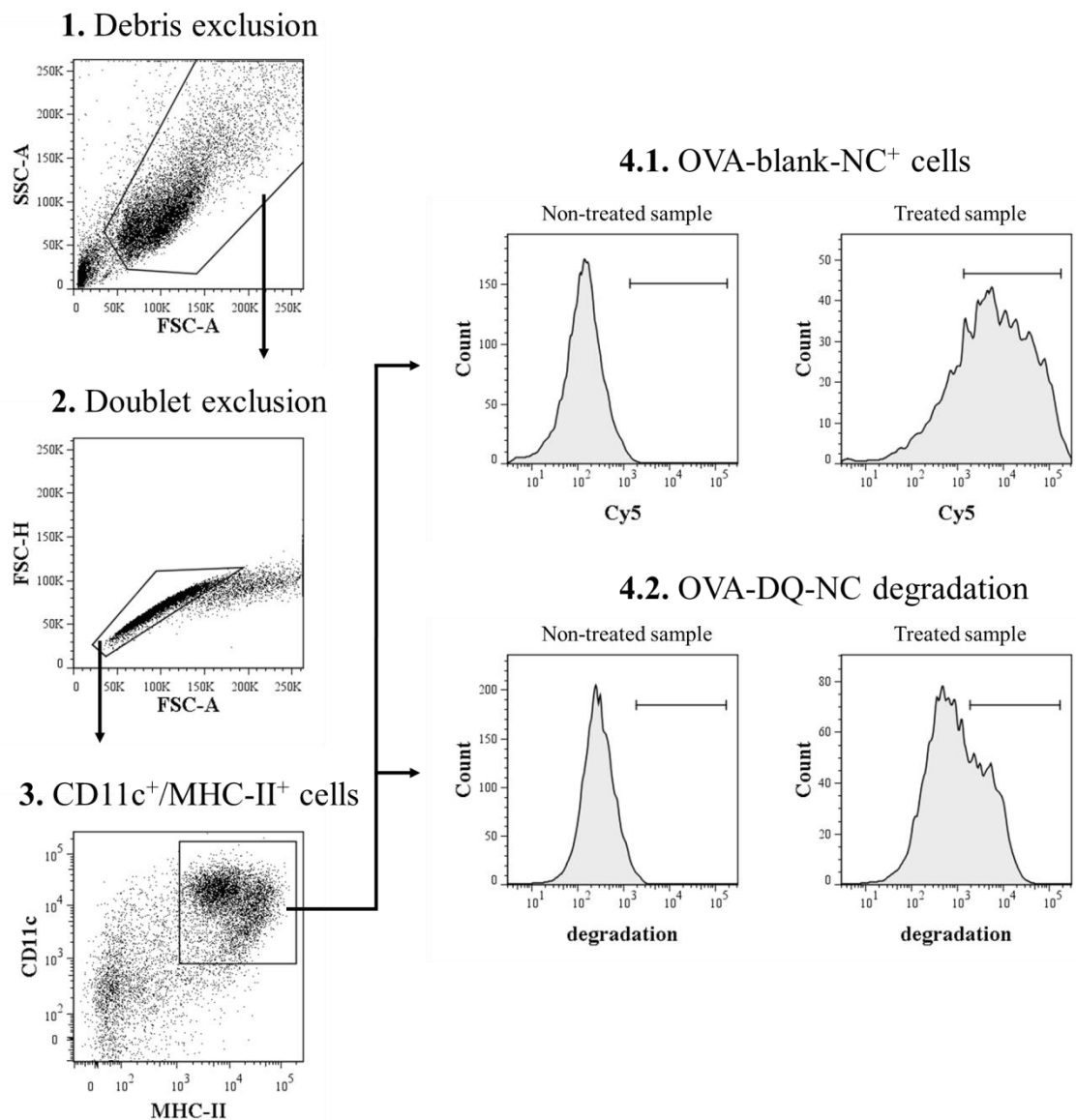


**Figure S 5** Gating strategy for OVA-blank- and OVA-DQ-NCs

BMDCs stimulated with OVA-blank- and OVA-DQ-NC were analyzed by (1) debris exclusion, (2) doublet exclusion, (3) gating on CD11c<sup>+</sup>/MHC-II<sup>+</sup> BMDCs and subsequent measurement of (4.1) OVA-blank-NC<sup>+</sup> cells (based on Cy5 signal) and (4.2) OVA-DQ-NC degradation by degradation-derived emission. Figure published in the Journal of Controlled Release in a modified version [249].

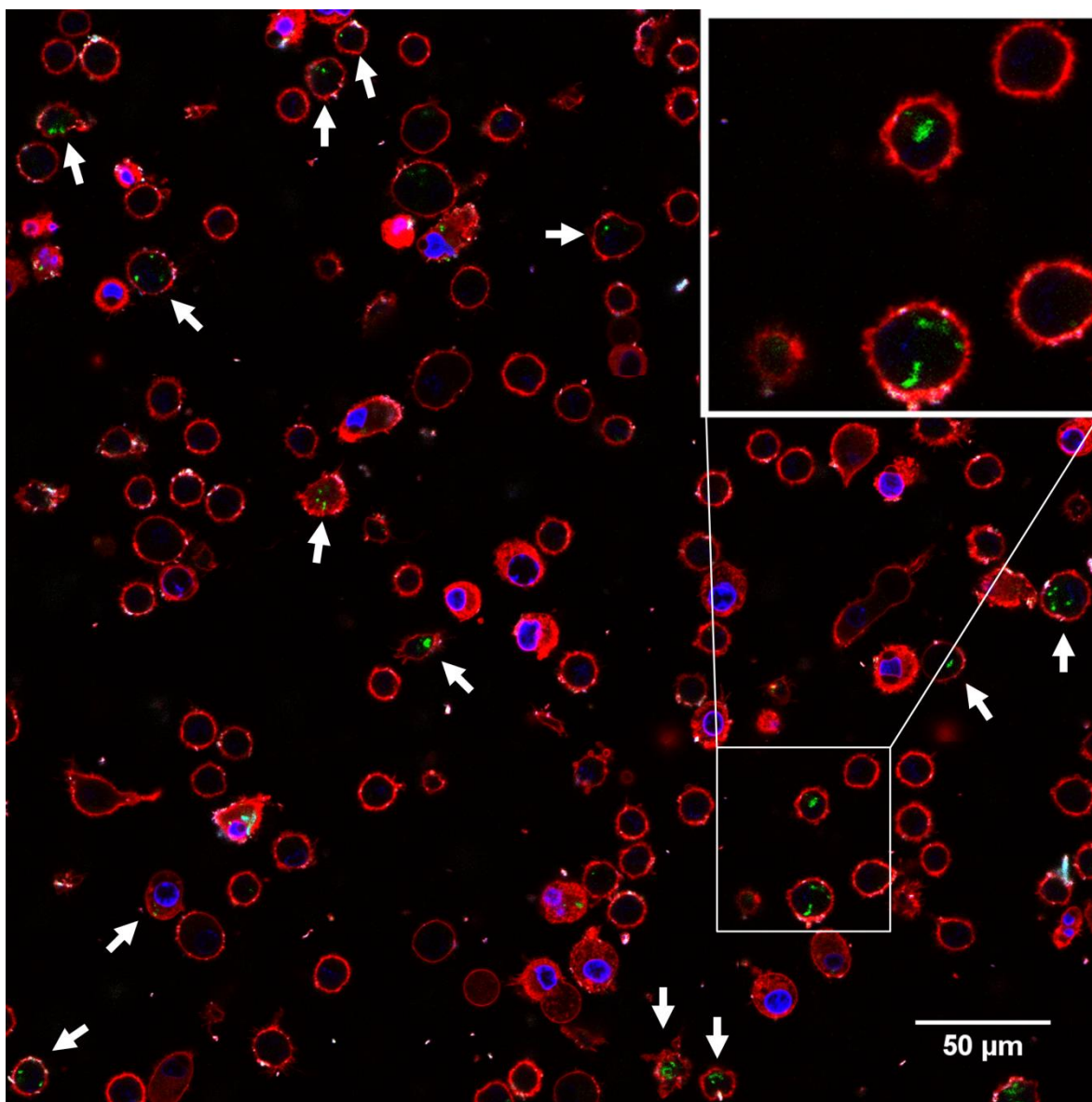


**Figure S 6** Confocal image of OVA-DQ-NC degradation

The representative CLSM tile scan image shows BMDCs ( $7.5 \times 10^5$  cells/ml) that were treated with OVA-DQ-NC (100 µg/ml) for 3 h at 37 °C. OVA-DQ degradation is indicated by green signals inside the cells (white arrows). Membranes were stained with CellMask Orange (red), and cell nuclei with DAPI (blue). Figure published in the Journal of Controlled Release [249].

APPENDIX

Capsule type	nmol MDP/ mg NP	µg MDP/ mg NP	nmol R848/ mg NP	µg R848/ mg NP	Enc <sub>eff</sub> / % (MDP/R848)
OVA-blank-NC	-	-	-	-	-
OVA-MDP-NC	7.78	3.83	-	-	(80.2 / -----)
OVA-R848-NC	-	-	3.16	1.11	(----- / 69.6)
OVA-MDP/R848-NC	7.14	3.52	2.85	1.00	(73.6 / 65.9)

**Table S 4** Quantification of encapsulated MDP-Alexa 488 and R848 in OVA-NCs

Encapsulation of MDP and R848 in OVA-NPs was analyzed by means of fluorescent MDP-Alexa 488 and the fluorescent properties of R848 itself. MDP-Alexa 488 and R848 fluorescence in four OVA-NC types (OVA-blank-NC, OVA-MDP-Alexa 488-NC, OVA-R848-NC, and OVA-MDP-Alexa 488/R848-NC) was measured by fluorescence spectroscopy. Based on these results, the actual MDP/R848 contents in OVA-NC formulations used for stimulation assays (including OVA-MDP-NCs and OVA-MDP/R848-NCs with non-labeled MDP) were calculated with a calibration curve in the range of 20 µg/ml to 135 µg/ml. Encapsulation efficiency (Enc<sub>eff</sub>) was determined by comparison of applied and remaining adjuvant fluorescence. Data published in the Journal of Controlled Release [249].

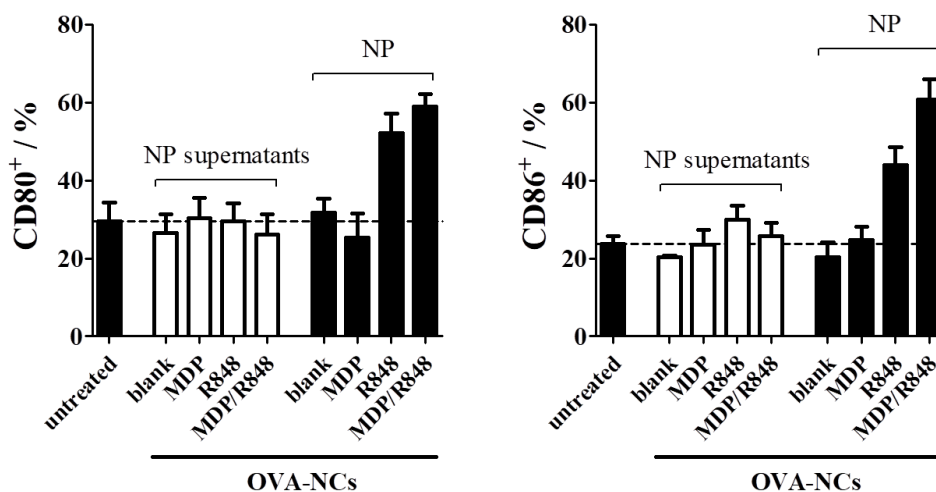


**Figure S 7** Biological activity of OVA-NCs' supernatants

To detect potential free adjuvants (MDP, R848) in the OVA-NC formulations, BMDCs ( $2 \times 10^5$  cells/ml) were treated with the different types of OVA-NCs (100 µg/ml) or with the corresponding volumes of their supernatants for 24 h. Afterwards, the frequencies of CD80- and CD86-positive BMDCs were measured by flow cytometry. The results are displayed relative to the untreated control (dashed line, mean  $\pm$  SD; n=2). Data and figure published in the Journal of Controlled Release [249].



## APPENDIX

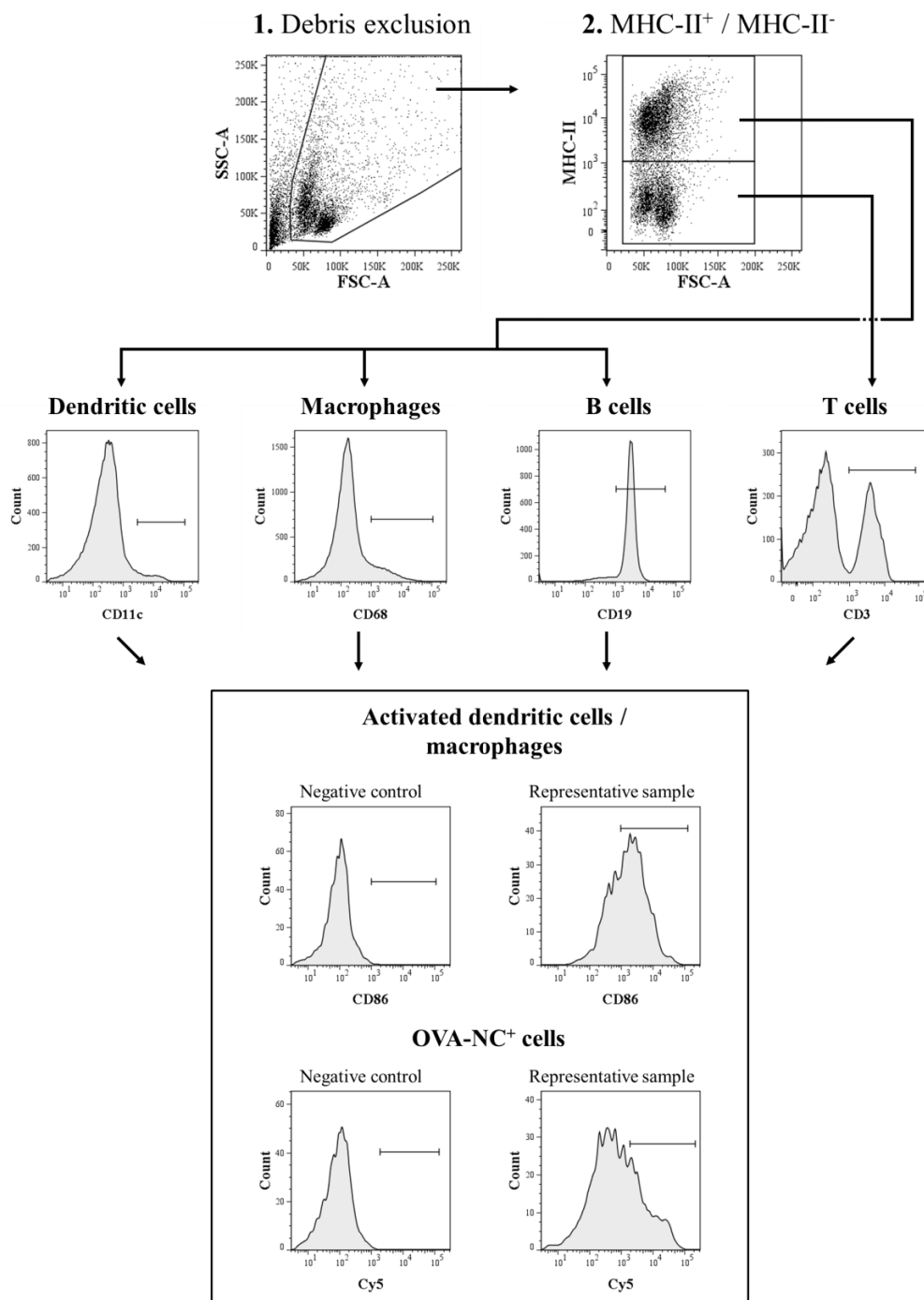


**Figure S 8** Gating strategy for spleen cell interaction analysis

(1) Exclusion of cell debris and unbound nanocapsules. (2) Exclusion of cell doublets. (3) Distinction between MHC-II<sup>+</sup> and MHC-II<sup>-</sup> cells. MHC-II<sup>+</sup>/CD11c<sup>+</sup> (dendritic cells), MHC-II<sup>+</sup>/CD68<sup>+</sup> (macrophages), MHC-II<sup>+</sup>/CD19<sup>+</sup> (B cells) and MHC-II<sup>+</sup>/CD3<sup>+</sup> (T cells) populations were analyzed separately. Activated DCs and macrophages were identified via CD86 expression, OVA-NC<sup>+</sup> cells by the encapsulated Cy5-Oligo. Gates were defined based on unstained BMDCs. Figure published in the Journal of Controlled Release in a modified version [249].

APPENDIX

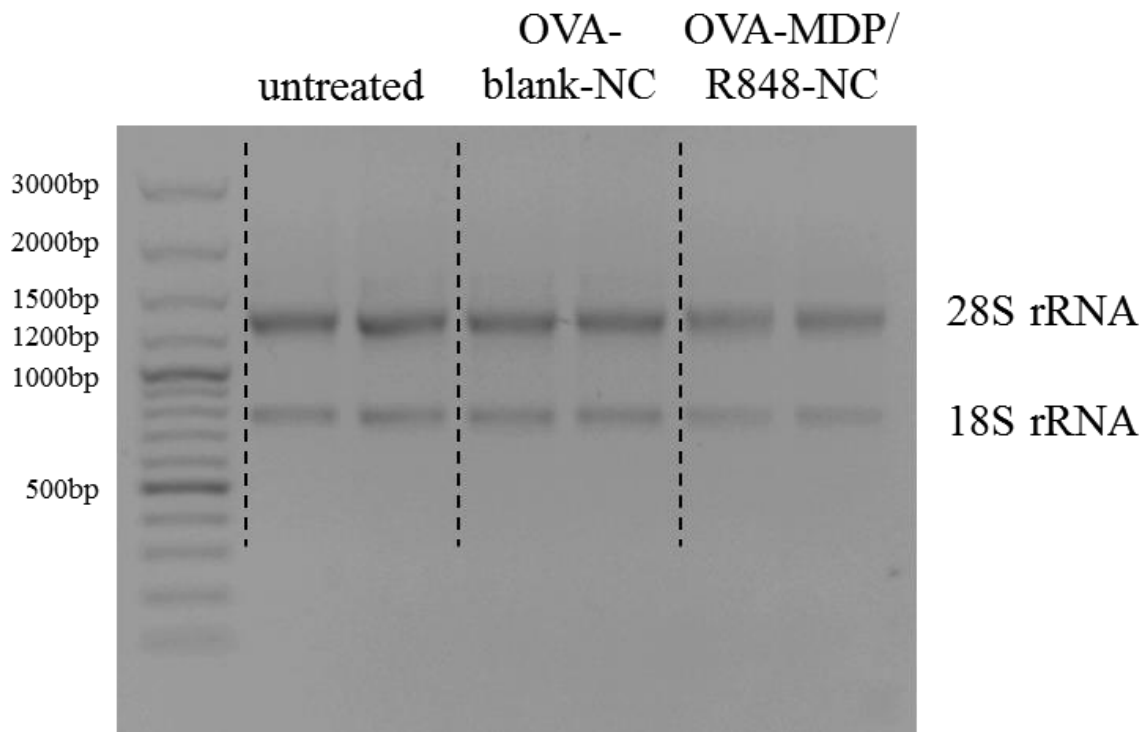


**Figure S 9** Total RNA quality control by gel electrophoresis

RNA samples of BMDCs treated with OVA-blank-NCs or OVA-MDP/R848-NCs (each 75  $\mu\text{g/ml}$ ) were checked for purity by agarose gel electrophoresis. Bands for 28S and 18S rRNA are indicated. A DNA ladder from 100 to 3000 bp was used as size orientation.

APPENDIX

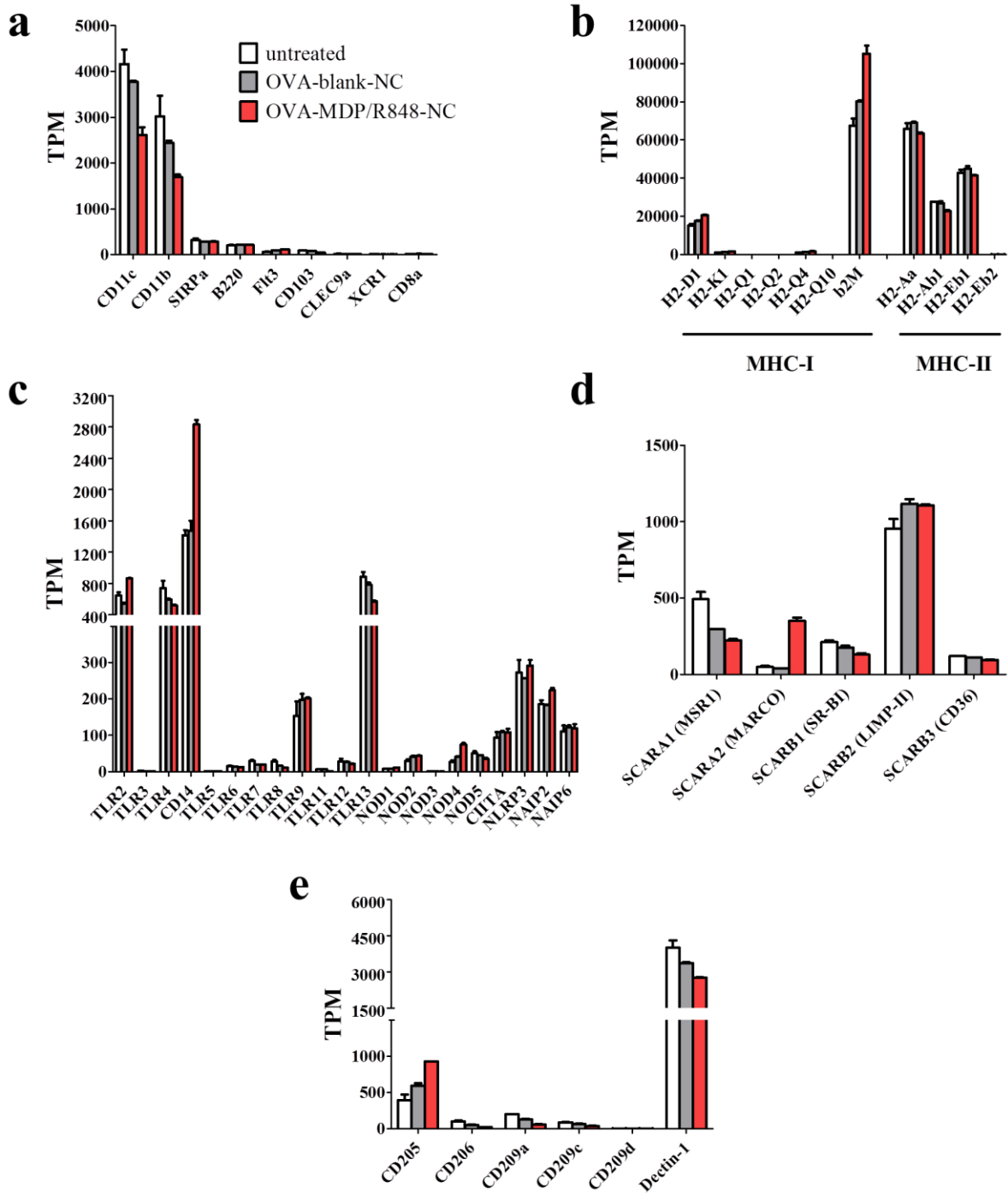


**Figure S 10** mRNA expression of PRRs and DC markers in stimulated BMDCs

BMDCs ( $2 \times 10^6$  cells/ml) were treated with OVA-blank- or OVA-MDP/R848-NCs (both 75  $\mu$ g/ml) for 1, 2 and 4 h. Untreated BMDCs were used as negative control. The three time points of each sample were pooled, mRNA was isolated and RNA-Seq performed. TPM values for (a) DC markers, (b) MHC components, (c) TLRs/NLRs, (d) scavenger receptors and (e) C-type lectins were calculated (mean  $\pm$  SD; n=2).

APPENDIX

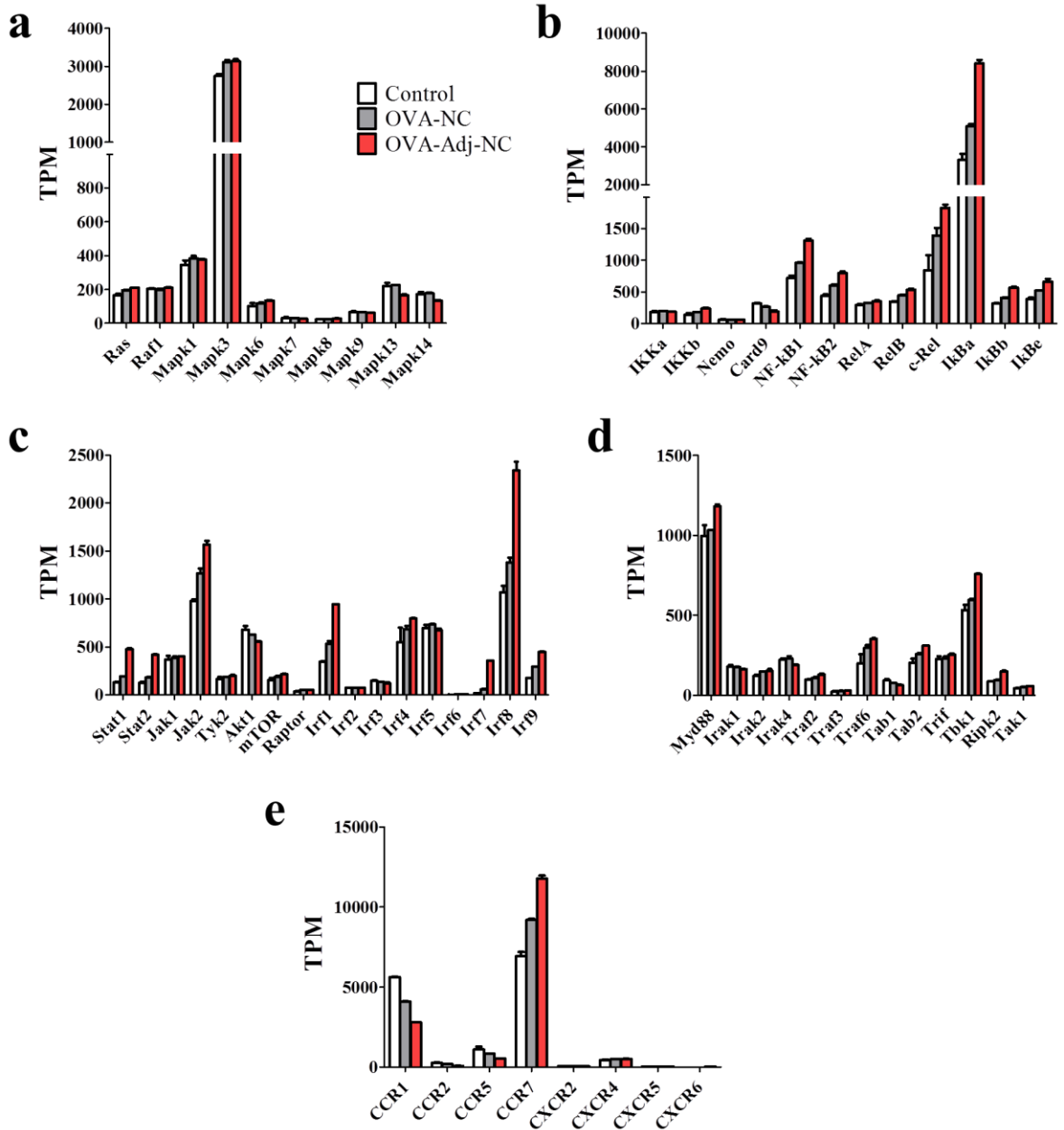


**Figure S 11** mRNA expression of signaling components in stimulated BMDCs

BMDCs ( $2 \times 10^6$  cells/ml) were treated with OVA-blank- or OVA-MDP/R848-NCs (both 75  $\mu$ g/ml) for 1, 2 and 4 h. Untreated BMDCs were used as negative control. The three time points of each sample were pooled, mRNA was isolated and RNA-Seq performed. TPM values for (a) MAPK/ERK signaling, (b) NF-κB signaling (c), IFN signaling, (d) TLR/NLR signaling and (d) chemokine receptors were calculated (mean  $\pm$  SD; n=2).

APPENDIX

Capsule type	Ø / nm in cyclohexane	Ø / nm in water	ζ / mV
OT-DN-R848-NC	290	291	-37
HT-DN-R848-NC	285	315	-30

**Table S 5** Size and charge determination of alternative protein nanocapsules via DLS

The diameters of protein nanocapsules, cross-linked by bioorthogonal tetrazole-ene cycloaddition, in cyclohexane and water as well as the zeta potential (ζ) were measured via DLS. Data published in Nanoscale Horizons [238].

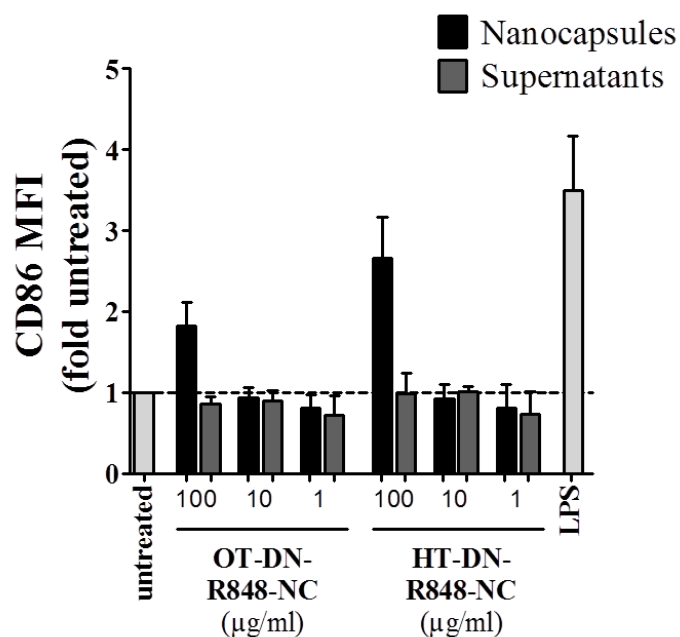


**Figure S 12** Biological activity of OT- and HT-DN-R848-NCs' supernatants

To detect potential free R848 in the OT- and HT-DN-R848-NC formulations, BMDCs ( $2 \times 10^5$  cells/ml) were treated with the different types of NCs (1-100 µg/ml) or with the corresponding volumes of their supernatants for 24 h. Untreated (dashed line) and LPS-treated (100 ng/ml) BMDCs were used as control. Afterwards, CD86 expression was measured by flow cytometry. Results were plotted as fold untreated (mean ± SD; n=2). Data and figure published in Nanoscale Horizons [238].

## APPENDIX

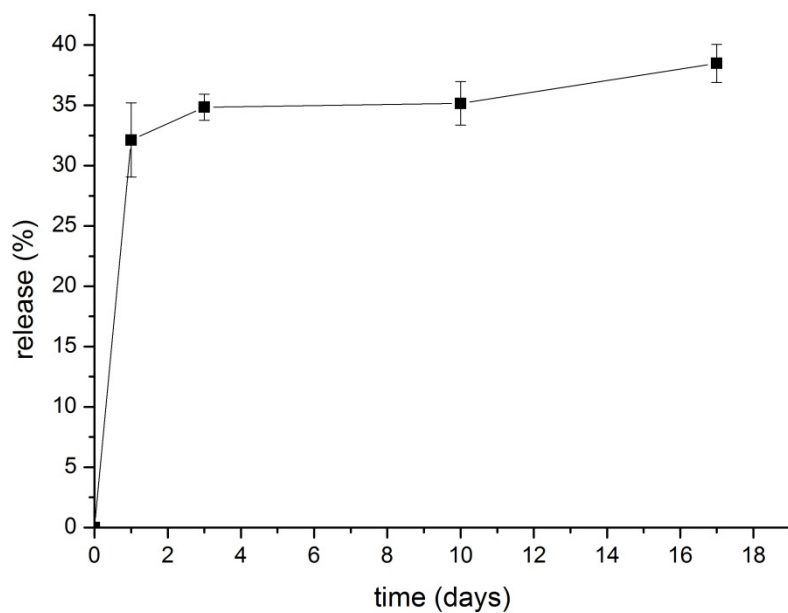


**Figure S 13** Encapsulation efficiency of HES-NCs

D-mannosamine release after transfer into water dispersion was used to assess the encapsulation efficiency of HES-NCs. The large initial release on day 1 results from free non-encapsulated D-mannosamine. The released D-mannosamine was detected by a fluorogenic reaction with fluorescamine.

## APPENDIX

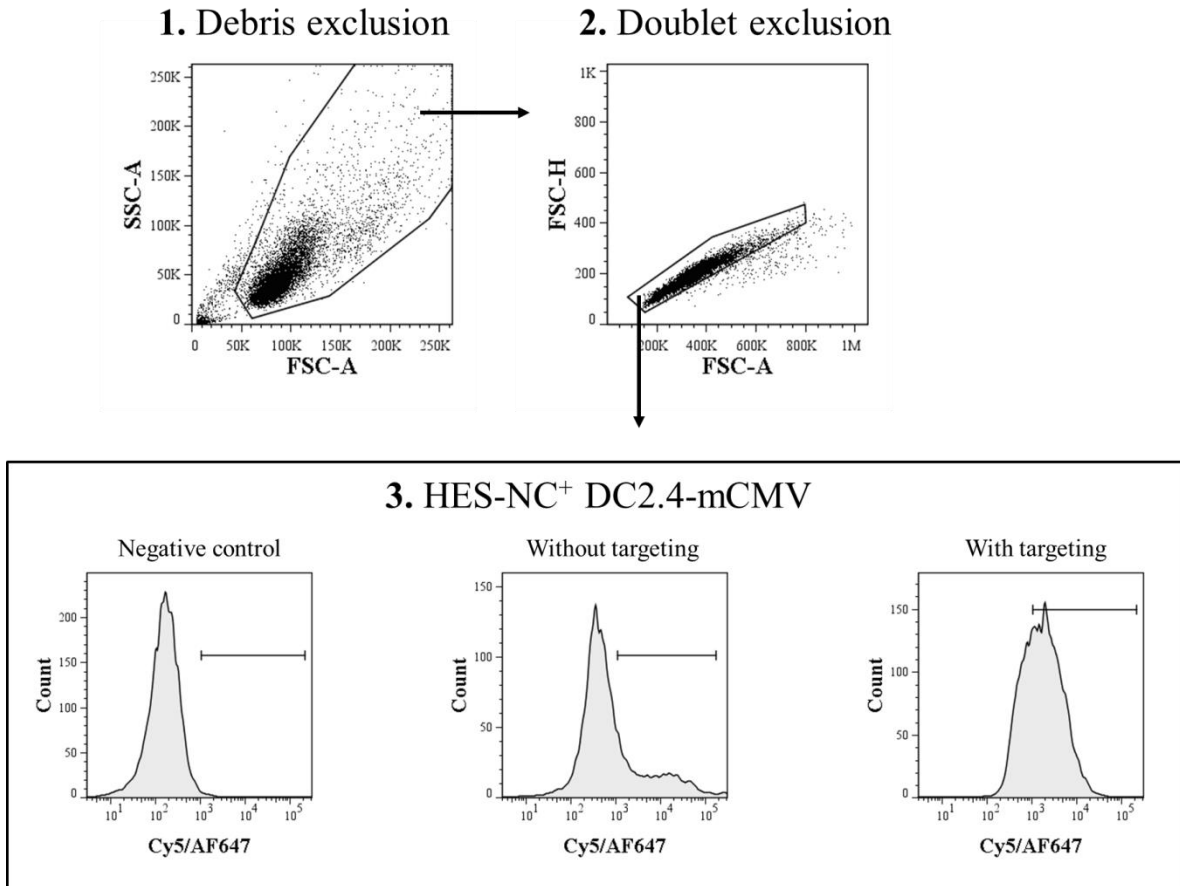


**Figure S 14** Gating strategy for HES-NCs

DC2.4-mCMV treated with siRNA-loaded HES-NCs were analyzed by flow cytometry by (1) debris exclusion, (2) doublet exclusion and (3) subsequent measurement of HES-NC<sup>+</sup> cells (based on Cy5/AF647 signal).

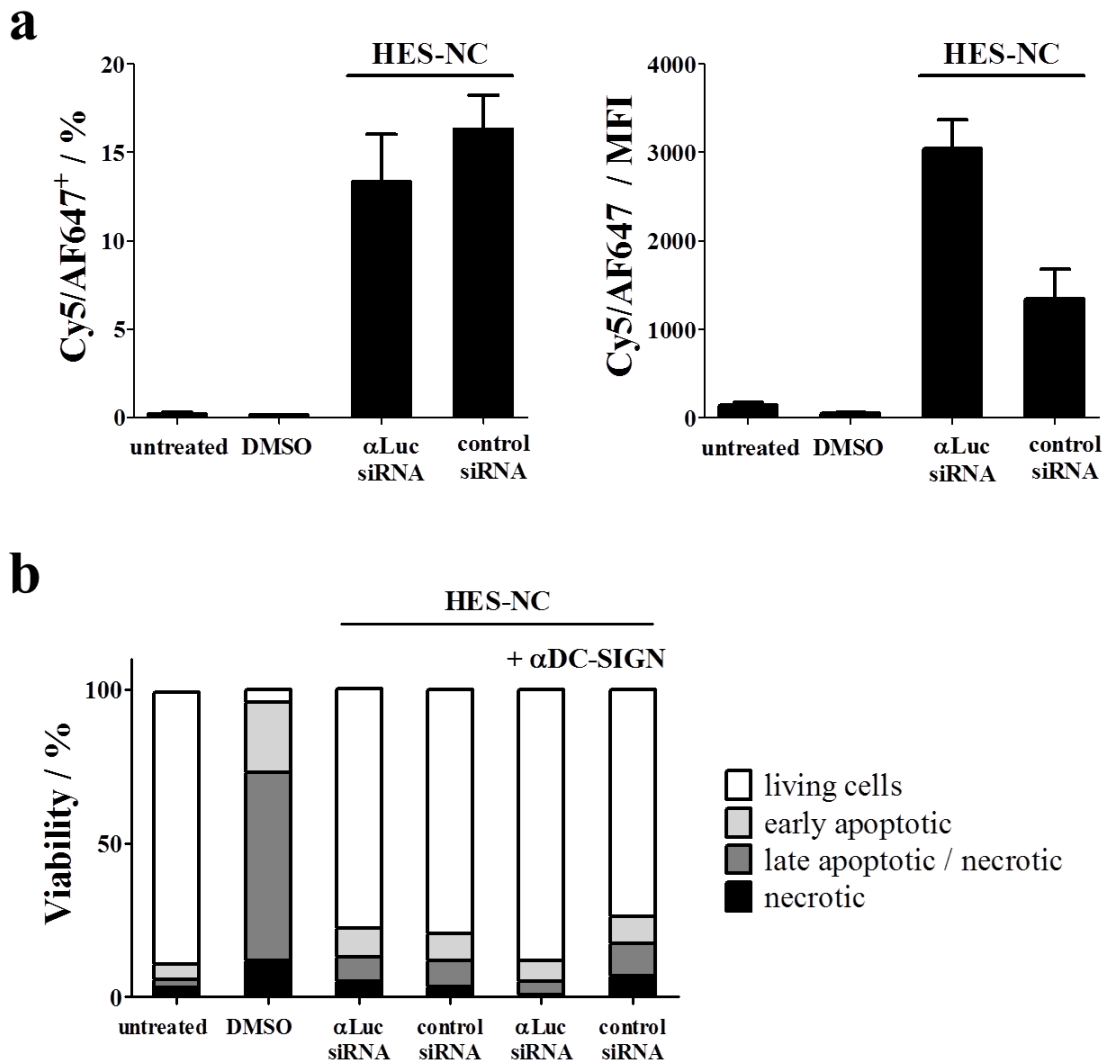


**Figure S 15** Quality tests for HES-NC formulations

To test to what extent siRNA-loaded HES-NCs were bound by DC2.4-mCMV and how far these capsules were cytotoxic for those cells, appropriate tests were performed. (a) HES-NC<sup>+</sup> DC2.4-mCMV were measured based on encapsulated Cy5 (in case of αLuc siRNA) and Alexa647-label (in case of control siRNA) respectively. For this purpose, cells ( $1 \times 10^5$  cells/ml, seeded 24 h before) were treated with 300 μg/ml NCs for 24 h and the resulting frequencies and MFIs were determined by flow cytometry (mean ± SD; n=3). (b) Cytotoxicity of siRNA-loaded HES-NCs (± αDC-SIGN) was measured. Therefore, DC2.4-mCMV ( $1 \times 10^5$  cells/ml, seeded 24 h before) were incubated with 300 μg/ml of the indicated HES-NC formulations for 24 h. Resulting viability was determined by 7AAD/Annexin V staining. 10 vol-% DMSO was used as positive control (n=3).



## 8.2 List of Figures

Figure 1 DC development .....	5
Figure 2 TLR and NLR signaling.....	9
Figure 3 Project-relevant PRRs and adjuvants .....	12
Figure 4 Cross-presentation.....	14
Figure 5 Antibody-modification of HES-NCs .....	44
Figure 6 Schematic illustration of a flow cytometer .....	51
Figure 7 Viability measurement via 7AAD/Annexin V double staining .....	54
Figure 8 Light path in a confocal laser scanning microscope .....	57
Figure 9 Stimulatory effects of NLR ligands on CD80 and CD86 expression in BMDC ...	65
Figure 10 Identification of superadditive TLR/NLR ligand combinations by MFIs .....	67
Figure 11 Cytokine profiles after treatment with soluble TLR/NLR ligand combinations .	69
Figure 12 Superadditive BMDC stimulation with L18-MDP + R848 .....	70
Figure 13 Quality tests for Dex-NP formulations .....	73
Figure 14 BMDC stimulation with adjuvant-loaded Dex-NPs .....	75
Figure 15 Cytokine secretion triggered by adjuvant-loaded Dex-NPs.....	76
Figure 16 Biological activity of Dex-NPs' supernatants.....	77
Figure 17 Visualization of OVA-NC morphology .....	78
Figure 18 Cellular binding of OVA-NCs by BMDCs.....	80
Figure 19 Degradation of OVA-NCs by BMDCs .....	81
Figure 20 Temperature-dependent OVA-NC degradation .....	82
Figure 21 OVA-NC-mediated T cell proliferation .....	84
Figure 22 T cell proliferation triggered by nanocarrier combination.....	85
Figure 23 Cytokine secretion triggered by nanocarrier combination .....	86
Figure 24 BMDC stimulation with adjuvant-loaded OVA-NCs .....	89
Figure 25 Cytokine secretion triggered by adjuvant-loaded OVA-NCs .....	90
Figure 26 T cell stimulation induced by adjuvant-loaded OVA-NCs .....	92
Figure 27 mRNA expression of BMDCs treated with adjuvant-loaded OVA-NCs.....	94
Figure 28 Heat map based on mRNA mean enrichment scores (part 1) .....	98
Figure 29 Heat map based on mRNA mean enrichment scores (part 2) .....	99
Figure 30 Heat map based on mRNA mean enrichment scores (part 3) .....	100

## APPENDIX

Figure 31 qPCR and RNA-Seq results for exemplary upregulated genes.....	101
Figure 32 qPCR and RNA-Seq results for exemplary downregulated/balanced genes .....	102
Figure 33 Spleen cell interaction with adjuvant-loaded OVA-NCs.....	103
Figure 34 Comparison of TDI and TET-DN cross-linked nanocapsules .....	105
Figure 35 Cytotoxicity of different sera on murine BMDCs.....	107
Figure 36 NCs' stealth effect determined by PEG MW.....	108
Figure 37 NCs' stealth effect determined by PEGylation density .....	109
Figure 38 NCs' stealth effect determined by PEG mass density.....	111
Figure 39 Transduction and siRNA functionality check .....	113
Figure 40 Visualization of HES-NC morphology .....	114
Figure 41 Luciferase knockdown with siRNA-loaded HES-NCs .....	115
Figure 42 Luciferase expression upon treatment with targeting HES-NCs .....	118
Figure 43 DC2.4 targeting with $\alpha$ DC-SIGN-modified HES-NCs.....	119
Figure S 1 Gating strategy for soluble adjuvants and adjuvant-loaded nanocarriers .....	189
Figure S 2 Identification of superadditive TLR/NLR ligand combinations by frequency .	190
Figure S 3 Exemplary NTA primary data .....	191
Figure S 4 Quality tests for OVA-NC formulations.....	193
Figure S 5 Gating strategy for OVA-blank- and OVA-DQ-NCs .....	194
Figure S 6 Confocal image of OVA-DQ-NC degradation .....	195
Figure S 7 Biological activity of OVA-NCs' supernatants .....	196
Figure S 8 Gating strategy for spleen cell interaction analysis .....	197
Figure S 9 Total RNA quality control by gel electrophoresis .....	198
Figure S 10 mRNA expression of PRRs and DC markers in stimulated BMDCs .....	199
Figure S 11 mRNA expression of signaling components in stimulated BMDCs .....	200
Figure S 12 Biological activity of OT- and HT-DN-R848-NCs' supernatants.....	201
Figure S 13 Encapsulation efficiency of HES-NCs.....	202
Figure S 14 Gating strategy for HES-NCs .....	203
Figure S 15 Quality tests for HES-NC formulations.....	204

### 8.3 List of Tables

Table 1 Laboratory equipment .....	27
Table 2 Reagents and substances .....	29
Table 3 PRR ligands .....	30
Table 4 Buffers, solutions, media .....	32
Table 5 Consumables .....	33
Table 6 Antibodies .....	34
Table 7 Dextran-based NPs used for experiments.....	35
Table 8 Protein-based NCs used for stimulation experiments .....	35
Table 9 PEGylated and antibody-modified OVA-NCs used for experiments .....	35
Table 10 HES-NC used for experiments .....	36
Table 11 Commercial kits .....	37
Table 12 Software.....	37
Table 13 Identification of cell populations in flow cytometry .....	53
Table 14 Cytokines quantified via cytometric bead array .....	56
Table 15 Settings for RNA-Seq quantification with the Geneious software.....	61
Table 16 Composition of the qPCR mixture .....	62
Table 17 qPCR protocol .....	62
Table 18 KEGG-annotated pathway analysis.....	96
Table 19 Translational vs. transcriptional effects of OVA-MDP/R848-NCs in BMDCs..	102
Table S 1 Size determination of Dex-NPs via NTA.....	191
Table S 2 Quantification of encapsulated MDP-FITC and R848 in Dex-NPs.....	192
Table S 3 Size and charge determination of OVA-NCs via DLS .....	192
Table S 4 Quantification of encapsulated MDP-Alexa 488 and R848 in OVA-NCs.....	196
Table S 5 Size and charge determination of alternative protein nanocapsules via DLS ....	201

## 8.4 List of Abbreviations

(P((E/B)-b-EO))	<i>Poly((ethylene-co-butylene)-b-(ethylene oxide))</i>
7AAD	<i>7-Aminoactinomycin D</i>
AF647	<i>Alexa Fluor 647</i>
alum	<i>Aluminum salts</i>
AP-1	<i>Activator protein 1</i>
APC <sub>f</sub>	<i>Allophycocyanin</i>
APC <sub>f</sub> -Cy7	<i>APC<sub>f</sub>/cyanine 7</i>
APCs	<i>Antigen-presenting cells</i>
Azido-PEG-amine	<i>O-(2-aminoethyl)-O'-(2-azidoethyl)pentaethylene glycol</i>
bp	<i>Base pairs</i>
C12-iE-DAP	<i>Lauroyl-modified iE-DAP</i>
CARD	<i>Caspase recruitment domain</i>
CBA	<i>Cytometric bead array</i>
cDCs	<i>Conventional DCs</i>
CLP	<i>Common lymphoid progenitor</i>
CLSM	<i>Confocal laser scanning microscopy</i>
CMP	<i>Common myeloid progenitor</i>
copGFP	<i>GFP 2 from the copepod Pontellina plumata</i>
CpG	<i>CpG ODN 1826</i>
cpm	<i>Counts per minute</i>
CRT	<i>Calreticulin</i>
Cy5-Oligo	<i>Cy5-CCA CTC CTT TCC AGA AAA CT-3'</i>
Da	<i>Dalton</i>
DAMPs	<i>Damage-associated molecular patterns</i>
DAPI	<i>4',6-diamidino-2-phenylindole</i>
DAVID	<i>Database for Annotation, Visualization and Integrated Discovery</i>
DBCO-PEG4-NHS	<i>Dibenzocyclooctyne-PEG4-N-hydroxysuccinimidyl ester</i>
DCM	<i>Dichloromethane</i>
DCs	<i>Dendritic cells</i>
Dex	<i>Dextran</i>
Dex-blank	<i>Empty Dex-NP</i>
Dex-MDP	<i>MDP-loaded Dex-NP</i>
Dex-MDP/R848	<i>MDP/R848-loaded Dex-NP</i>
Dex-MDP-FITC	<i>MDP-FITC-loaded Dex-NP</i>
Dex-MDP-FITC/R848	<i>MDP-FITC/R848-loaded Dex-NP</i>
Dex-NPs	<i>Dex-based NPs</i>
Dex-R848	<i>R848-loaded Dex-NP</i>
DLS	<i>Dynamic light scattering</i>
DMSO	<i>Dimethyl sulfoxide</i>
DN	<i>Dinorbornene</i>
DOPE	<i>1,2-dioleoyl-sn-glycero-3-phosphoethanolamine</i>
DOTAP	<i>N-(2,3-dioleoyloxy-1-propyl)trimethylammonium methyl sulfate</i>
EDTA-Na <sub>2</sub>	<i>Ethylenediaminetetraacetic acid disodium salt hydrate</i>
EMEM	<i>Eagle's Minimum Essential Medium</i>
ERK	<i>Extracellular signal-regulated kinases</i>

## APPENDIX

ERp57 .....	<i>ER-resident protein 57</i>
FCS .....	<i>Fetal calf serum</i>
FDA .....	<i>Food and Drug Administration</i>
FITC .....	<i>Fluorescein</i>
Gbp .....	<i>Giga base pairs</i>
GFP .....	<i>Green fluorescent protein</i>
gp100 .....	<i>Glycoprotein 100</i>
HBSS .....	<i>Hank's Balanced Salt Solution</i>
HDDP .....	<i>1,6-hexanediol dipropiolate</i>
HES .....	<i>Hydroxyethyl starch</i>
HI .....	<i>Heat-inactivated</i>
hP .....	<i>Human plasma</i>
HPV .....	<i>Human papillomavirus</i>
hS .....	<i>Human serum</i>
HSA .....	<i>Human serum albumin</i>
HSC .....	<i>Hematopoietic stem cells</i>
HT-DN-R848-NCs .....	<i>HSA-based R848-loaded TET-NCs</i>
iE-DAP .....	<i><math>\gamma</math>-D-glutamyl-meso-diaminopimelic acid</i>
Ii .....	<i>Invariant chain</i>
IKK .....	<i>I<math>\kappa</math>B kinase</i>
IMDM .....	<i>Iscove's Modified Dulbecco's Medium</i>
iNOS .....	<i>Inducible nitric oxide synthase</i>
IR .....	<i>Infrared spectroscopy</i>
IRF3 .....	<i>Interferon regulatory factor 3</i>
iTreg .....	<i>Induced regulatory T cells</i>
JNKs .....	<i>c-Jun N-terminal kinases</i>
kDa .....	<i>Kilodalton</i>
L18-MDP .....	<i>Stearoyl group-modified MDP</i>
lipo .....	<i>Lipofectamine</i>
LPS .....	<i>Lipopolysaccharide</i>
MAGE-A3 .....	<i>Melanoma-associated antigen 3</i>
MAPK .....	<i>Mitogen-activated protein kinases</i>
MDP .....	<i>Muramyl dipeptide</i>
MDP-Alexa 488 .....	<i>MDP modified with Alexa Fluor 488 5-SDP ester</i>
MDP-FITC .....	<i>FITC-labeled MDP</i>
MFI .....	<i>Mean fluorescence intensities</i>
MHC .....	<i>Major histocompatibility complex</i>
MHC-I .....	<i>MHC type I</i>
MHC-II .....	<i>MHC type II</i>
MO .....	<i>Monocytes</i>
moDCs .....	<i>Monocyte-derived DCs</i>
MoDP .....	<i>Monocyte and dendritic cell progenitor</i>
MPS .....	<i>Mononuclear phagocyte system</i>
MR .....	<i>Mannose receptor</i>
mS .....	<i>Murine serum</i>
MW .....	<i>Molecular weight</i>
MYD88 .....	<i>Myeloid differentiation primary response 88</i>

## APPENDIX

NCs	Nanocapsules
NLRs	NOD-like receptors
NP	Nanoparticle
ns	Non-significant
nt	Nucleotides
OT-DN-R848-NCs	OVA-based R848-loaded TET-NCs
OVA	Ovalbumin
OVA-blank-NC	empty OVA-NCs
OVA-DQ	DQ OVA
OVA-DQ-NC	OVA-DQ-containing OVA-NC
OVA-MDP/R848-NCs	MDP/R848-loaded OVA-NCs
OVA-MDP-Alexa 488/R848-NCs	MDP-Alexa 488/R848-loaded OVA-NCs
OVA-MDP-Alexa 488-NCs	MDP-Alexa 488-loaded OVA-NCs
OVA-MDP-NCs	MDP-loaded OVA-NCs
OVA-NCs	OVA-based NCs
OVA-R848-NCs	R848-loaded OVA-NCs
PAMPs	Pathogen-associated molecular patterns
PBS	Phosphate-buffered Saline
PC	Phosphatidylcholine
PE	Phycocerythrin
PE-Cy7	PE/cyanine 7
PEG	Polyethylene glycol
PFA	Paraformaldehyde
PLA	Poly lactic acid
PLGA	Poly lactic-co-glycolic acid
Poly I:C	Polyinosinic:polycytidylic acid
PRRs	Pattern recognition receptors
PS	Polystyrene
PVA	Polyvinyl alcohol
qPCR	Quantitative real-time polymerase chain reaction
R848	Resiquimod
RIP2	Receptor-interacting serine/threonine-protein kinase 2
RISC	RNA-induced silencing complex
RLU	Relative light units
RNAi	RNA interference
ROS	Reactive oxygen species
rpm	Revolutions per minute
rRNA	Ribosomal RNA
SD	Standard deviation
SDP	Sulphodichlorophenol
SDS	Sodium dodecyl sulfate
SEM	Scanning electron microscopy
sMDP	Soluble MDP
Sp-Ac-Dex	Spermine-functionalized and acetalated Dex
sR848	Soluble R848
TAK1	TGF- $\beta$ -activated kinase 1
TAP	Transporter associated with antigen processing

APPENDIX

TBK1 .....	<i>TANK binding kinase 1</i>
Tc .....	<i>Cytotoxic T cells</i>
Tc1 .....	<i>Tc type 1</i>
Tc17 .....	<i>Tc type 17</i>
Tc2 .....	<i>Tc type 2</i>
TDI .....	<i>2,4-toluene diisocyanate</i>
TEA .....	<i>Triethylamine</i>
TEM .....	<i>Transmission electron microscopy</i>
TET .....	<i>4-(2-phenyl-2H-tetrazol-5-yl)benzoic acid</i>
Th .....	<i>T helper cells</i>
Th1 .....	<i>Th type 1</i>
Th17 .....	<i>Th type 17</i>
Th2 .....	<i>Th type 2</i>
TIR .....	<i>Toll/IL-1 receptor</i>
TLRs .....	<i>Toll-like receptors</i>
TPM .....	<i>Transcripts per kilobase million</i>
TRAF6 .....	<i>TNF receptor-associated factor 6</i>
Tri-DAP .....	<i>L-Alanine-modified iE-DAP</i>
TRIF .....	<i>TIR-domain-containing adapter-inducing interferon-<math>\beta</math></i>
TS .....	<i>Tapasin</i>
vs .....	<i>versus</i>
WHO .....	<i>World Health Organization</i>
$\beta$ 2m .....	<i><math>\beta</math>2-microglobulin</i>

## 9. Acknowledgments

Ich möchte mich sehr herzlich bei allen bedanken, die mich durch diese sehr aufregende und ereignisreiche Zeit der Doktorarbeit begleitet haben – wengleich ich auch froh bin, dass sie nun zu einem Abschluss kommt. Ich kann mich glücklich schätzen so viel Unterstützung und Aufmunterung von allen Seiten erfahren zu haben.

Ein großer Dank gilt ..., dass er es mir ermöglicht hat meine Doktorarbeit in seiner Arbeitsgruppe anfertigen zu können. Ich danke Ihnen für Ihr großes Interesse an meinem Projekt, die sehr gute Betreuung und, dass Sie immer ein offenes Ohr für mich hatten.

Ebenso danke ich ... für die Bereitschaft mich in ... zu integrieren und für die Möglichkeit, die Labor- und Seminarstrukturen der ... nutzen zu dürfen. Ich habe mich stets willkommen gefühlt.

Danken möchte ich ..., dass er mir beratend zur Seite stand, wann immer ich Fragen hatte, waren sie auch noch so banal. Und immer hatte er eine sinnvolle Antwort oder einen guten Ratschlag!

Vielen Dank an ... für die tolle Unterstützung von Seiten des .... Sie haben mir gezeigt, dass interdisziplinäre Kooperationsprojekte gut zu bewältigen sind und sehr fruchtbar sein können, wenn man viel miteinander redet, Rücksicht nimmt und jede Seite versucht ihren Teil des Projektes der anderen näher zu bringen.

Ich danke ... und ... für ihre technische Expertise sowie ihre unendliche Geduld, wenn man mal wieder nervige Fragen zu einer bestimmten Methode hatte.

Ohne die anderen Doktoranden der ... / ... wäre meine Zeit hier nicht so schön gewesen. Ich danke ... für eine unvergessliche Zeit mit viel Spaß, Verrücktheit, Lachkrämpfen, Filmzitate und schlechten Witzen.

Danke an alle Kooperationspartner, die tatkräftig an meinem Projekt mitgearbeitet haben:  
....



## *ACKNOWLEDGMENTS*

Ich danke dem Max Planck Graduate Center für die finanzielle Unterstützung, die vielen hilfreichen Seminare und die Möglichkeit internationale Konferenzen besuchen zu können.

Auch möchte ich mich bei meinen Eltern bedanken. Ihr wart mir stets eine starke Stütze und habt mir Sicherheit in jeder Lebenslage gegeben.

Zuletzt möchte ich mich bei ... bedanken. Ohne dich wäre das Ganze nicht möglich gewesen. Ich bin dir unendlich dankbar, dass du mich immer und überall bedingungslos unterstützt, mich sinnvoll kritisiert, meine Launen ertragen und in der Spur gehalten hast.

# Lebenslauf

**Name:** David Paßlick  
**Geburtsdatum:** 12.10.1987  
**Geburtsort:** Ochtrup  
**Adresse:** Kaiser-Wilhelm-Ring 19, 55118 Mainz

## Arbeitserfahrung

Seit 01/15      Wissenschaftlicher Mitarbeiter, Max-Planck-Institut für Polymerforschung, Mainz /  
Hautklinik, Universitätsmedizin Mainz  
02/13 – 09/14    Disponent im Hausnotruf, Deutsches Rotes Kreuz, Mainz  
08/10 – 04/12    Wissenschaftliche Hilfskraft, Humangenetik, LADR MVZ Recklinghausen  
04/08 – 05/08    Praktikant, Wessling Laboratorien, Altenberge  
04/07 – 02/08    Zivildienst, Sana-Kliniken Ostholstein, Fehmarn

## Ausbildung

01/15 – 11/18    Doktorand, Max-Planck-Institut für Polymerforschung, Mainz / Hautklinik,  
Universitätsmedizin Mainz  
04/12 – 12/14    Studium der Biomedizin, Johannes Gutenberg-Universität Mainz  
Abschluss: M.Sc. (1.3)  
02/12 – 03/12    Ausbildung zum Rettungssanitäter, Akademie für Gesundheitsberufe, Rheine  
10/08 – 12/11    Studium der Molekularbiologie, Westfälische Hochschule, Recklinghausen  
Abschluss: B.Sc (1.9)  
02/99 – 03/07    Allgemeine Hochschulreife, Städtisches Gymnasium Ochtrup  
Abschluss: Abitur (2.1)